Technical Report Documentation Page

1. Report No. FHWA/TX-06/0-4176-1	2. Government Accession No.	3. Recipient's Catalog No.
4. Title and Subtitle **Anchorage Requirements for Grouted Vertical-Duct Connectors in Precast Bent Cap Systems**		5. Report Date May 2006 6. Performing Organization Code
7. Author(s) **Francisco J. Brenes, Sharon L. Wood, and Michael E. Kreger**		8. Performing Organization Report No. 4176-1
9. Performing Organization Name and Address Center for Transportation Research The University of Texas at Austin 3208 Red River, Suite 200 Austin, TX 78705-2650		10. Work Unit No. (TRAIS) 11. Contract or Grant No. Research Project 0-4176
12. Sponsoring Agency Name and Address Texas Department of Transportation Research and Technology Implementation Office P.O. Box 5080 Austin, TX 78763-5080		13. Type of Report and Period Covered Technical Report (9/2001 - 8/2005) 14. Sponsoring Agency Code

15. Supplementary Notes

Project performed in cooperation with the Texas Department of Transportation and the Federal Highway Administration.

16. Abstract

Bridge projects constructed in Texas which utilize precast bent caps typically employ grouted vertical ducts in the cap-to-column connections. This type of connection is preferred due to the simple geometry and because the volume of grout needed to complete the connections is minimized. A number of questions related to the sensitivity of the behavior of the grouted vertical-duct connectors to design parameters were identified during the design and construction of these bridges.

Thirty-two, large-scale pullout tests of connectors grouted in galvanized steel and plastic ducts were conducted to investigate the response of this type of connector. The results indicate that the tensile capacity is sensitive to the type of duct, the embedded length of the connector, the number of connectors tested simultaneously in tension, and the placement of the connector within the duct. However, the results were not sensitive to epoxy coating on the connector or to the presence of spiral transverse reinforcement around the group of connectors.

Design equations are proposed for the minimum embedded length of all connectors to satisfy serviceability concerns and for the development length necessary to resist the calculated tensile stresses in the connectors under the design load combinations.

17. Key Words bent caps, bridge substructures, concrete bridges, development length, connections, ducts, grout, precast concrete	18. Distribution Statement No restrictions. This document is available to the public through the National Technical Information Service, Springfield, Virginia 22161; www.ntis.gov.

19. Security Classif. (of report) Unclassified	20. Security Classif. (of this page) Unclassified	21. No. of pages 252	22. Price

Form DOT F 1700.7 (8-72) Reproduction of completed page authorized

Center for Transportation Research
The University of Texas at Austin

ANCHORAGE REQUIREMENTS FOR GROUTED VERTICAL-DUCT CONNECTORS IN PRECAST BENT CAP SYSTEMS

Francisco J. Brenes
Sharon L. Wood
Michael E. Kreger

CTR Research Report:	4176-1
Report Date:	May 2006
Research Project:	0-4176
Research Project Title:	Development of Precast Bridge Construction Systems
Sponsoring Agency:	Texas Department of Transportation
Performing Agency:	Center for Transportation Research at the University of Texas at Austin

Project performed in cooperation with the Texas Department of Transportation and the Federal Highway Administration.

Center for Transportation Research
The University of Texas at Austin
3208 Red River
Austin, TX 78705

www.utexas.edu/research/ctr

Disclaimers

Author's Disclaimer: The contents of this report reflect the views of the authors, who are responsible for the facts and the accuracy of the data presented herein. The contents do not necessarily reflect the official view or policies of the Federal Highway Administration or the Texas Department of Transportation (TxDOT). This report does not constitute a standard, specification, or regulation.

Patent Disclaimer: There was no invention or discovery conceived or first actually reduced to practice in the course of or under this contract, including any art, method, process, machine manufacture, design or composition of matter, or any new useful improvement thereof, or any variety of plant, which is or may be patentable under the patent laws of the United States of America or any foreign country.

Notice: The United States Government and the State of Texas do not endorse products or manufacturers. If trade or manufacturers' names appear herein, it is solely because they are considered essential to the object of this report.

Engineering Disclaimer

THIS REPORT IS NOT INTENDED FOR CONSTRUCTION, BIDDING,
OR PERMIT PURPOSES.

Sharon L. Wood, Texas P.E. #83804
Research Supervisor

Acknowledgments

This research project was funded by the Texas Department of Transportation (TxDOT) under Project No. 0-4176. The support of the project director, Lloyd M. Wolf (BRG), and program coordinator, Randy Cox (BRG), are greatly appreciated. The contributions of the Project Monitoring Committee members, Ralph Browne (BRG), Eric Ingamells (BRG), Karl Janak (SCT), and John L. Vogel (HOU), are also gratefully acknowledged. Special thanks are extended to Michael Hyzak (BRG) for assistance in developing the design recommendations.

Products

Research Product P1, draft specifications for grouted vertical-duct connectors, is included as Chapter 9 of this research report.

TABLE OF CONTENTS

LIST OF FIGURES

LIST OF TABLES

CHAPTER 1
Introduction

A significant number of the nation's bridges are approaching the end of their service life. According to the FHWA (2003), approximately 30% of bridges in the U.S. are obsolete and need to be replaced. Moreover, urban congestion is increasing due to growing population. Therefore, the need for new bridge construction is expected to be high for the foreseeable future. Direct and indirect costs related to traffic control and disruption, work-zone safety, and environmental impact have become major concerns. Efficient bridge designs and new construction methods that address these concerns are needed. Improved efficiency in design and construction can reduce the total costs and produce bridges with a lower life-cycle cost.

The use of prefabricated concrete elements in bridge construction has the potential to reduce construction time and life-cycle costs while improving long-term bridge performance. This report focuses on the details needed to connect precast bent caps to the supporting columns using grouted vertical connectors.

1.1 PRECAST BRIDGE CONSTRUCTION IN TEXAS

Bridge construction involves many steps, but may be summarized in the following stages: construction of foundations, construction of the bridge substructure (generally columns and bent caps), and construction of the superstructure (girders and deck). The construction process consists of many time-consuming tasks such as erection and removal of formwork, placement of steel reinforcement cages and concrete, and time for concrete curing. Using prefabricated elements and systems allows time-consuming tasks, such as fabrication of components (including girders and bent caps), to be moved away from the construction site and the associated traffic. The obvious result is a shorter construction schedule in the field. Accelerated bridge construction translates into reduced congestion and delay time for motorists driving through or around the work site, which also reduces the possibility of injuries and fatalities due to vehicular accidents.

At most bridge construction sites, workers spend long periods of time in potentially dangerous locations, such as close to moving traffic, over water, near power lines, or at high elevations. Prefabrication of concrete members allows workers to shift many tasks off-site to a safer and controlled environment. The prefabricated elements can then be transported to the bridge site and quickly erected. The quality of the prefabricated elements is typically higher than that achieved by conventional cast-in-

place construction because the off-site environment is more conducive to better quality control, more thorough inspection, and improved monitoring of concrete curing.

The Texas Department of Transportation (TxDOT) has used prefabricated bridge elements for many years. Pretensioned girders have long been used in bridge construction, as have precast concrete partial-depth deck panels. In recent years, the need to reduce traffic disruption at work sites has lead to additional prefabricated bridge innovations. Most of these recent innovations have involved prefabrication of the substructure elements. In the 1990s, TxDOT constructed three bridges using precast bent caps: the Red Fish Bay Project in Port Aransas (Figure 1.1), the US 290 Ramp E-3 Project in Austin (Figure 1.2), and the Pierce Elevated Project in downtown Houston (Figure 1.3).

The contractor suggested using precast bent caps on the Redfish Bay Project to minimize concrete operations over water (Wolf and Friedman 1994, Medlock et al. 2002). Connections involved large voids or pockets preformed into the caps to house connectors (Figure 1.1). U-shaped, epoxy-coated #9 dowels were grouted into embedded sleeves that were cast in trestle piles. Precast caps were then lowered over the dowels, and concrete was cast inside the voids to complete the connections. Construction time for the project was reduced by one third compared with the estimated construction time for cast-in-place bent caps.

The US 290 Ramp E-3 Project in Austin (Figure 1.2) was originally conceptualized as cast-in-place construction. The bent cap design for this ramp was changed to precast when it was found that estimated closure time of the ramp to traffic due to construction would be reduced from weeks to only hours (Medlock et al. 2002). The cap was cast adjacent to the erection site. Two vertical sleeves made of corrugated steel duct were formed on each end of the cap. Dywidag threaded bars that protruded from the columns below passed through the entire cross section and post-tensioned at the top. Grout was then poured into the sleeves to complete the connection.

The use of prefabricated bent caps on the Pierce Elevated Project in downtown Houston allowed the project to be completed in 95 days instead of the estimated 548 days needed for conventional cast-in-place construction (Medlock et al. 2002, Wigington 1997). This replacement project used the existing foundations and columns and only replaced the bent caps, girders, and bridge deck. After removal of the original deteriorated superstructure and bent caps, post-tensioning bars were epoxied into the top of the columns. The new precast caps, which contained preformed sleeves made of corrugated steel duct, were then lowered into position (Figure 1.3). Bars were anchored through plates at the top of the cap, and sleeves were filled with grout.

Recognizing the benefits of precast bent caps, TxDOT initiated research project 1748, "Development of a Precast Bent Cap System," (Matsumoto et al. 2001) with the University of Texas at

Austin. This research was completed in 2001 and produced a series of connection types, a design methodology, and constructible connection details for the different connection types.

Figure 1.1 Red Fish Bay Project

Figure 1.2 US 290 Ramp E-3 Project

Figure 1.3 Pierce Elevated Project

Since the completion of research project 1748, TxDOT has initiated new bridge projects that incorporate precast bent caps. Grouted vertical ducts were used in the cap-to-column connections of these bridges. Contractors and TxDOT engineers prefer this type of precast connection because the volume of grout needed to complete the connections is minimized. Many uncertainties regarding the details and configuration of the connections were recognized during the design and construction of these bridges. Concern among TxDOT engineers involved in the design of the new bridge projects led to this investigation on the behavior of grouted vertical duct connections.

1.2 PREVIOUS RESEARCH AT THE UNIVERSITY OF TEXAS AT AUSTIN

The success of the Red Fish Bay and Pierce Elevated projects prompted TxDOT engineers to initiate formal development of precast bent cap systems and sponsor research project 1748. Three types of connections, grout pockets, grouted vertical ducts, and bolted connections, were studied in this project (Figure 1.4). Grout pocket connections incorporate precast voids or pockets formed in the bent cap to accommodate connectors. Grouted vertical duct connections incorporate corrugated ducts which serve as sleeves to house the connectors. Bolted connections are similar to grouted vertical duct connections, but the connectors run through the entire depth of the cap and are anchored by bearing at the top. In all connection types, pockets or sleeves are filled with grout. Advantages and disadvantages of these connection types were identified (Table 1.1).

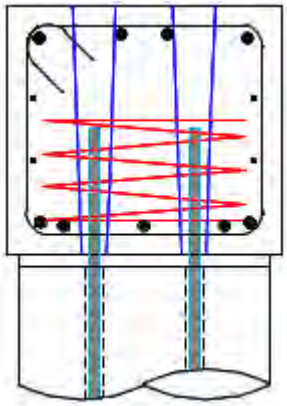

a. Grout Pocket Connection

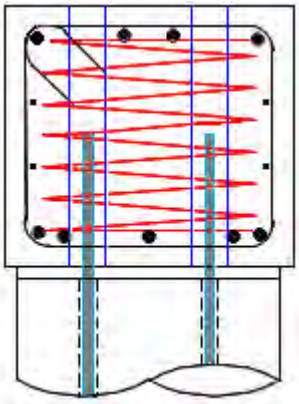

b. Grouted Vertical Duct Connection

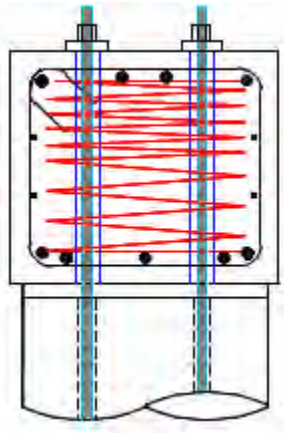

c. Bolted Connection

Figure 1.4 Connection Types Developed during TxDOT Project 1748 (Matsumoto et al. 2001)

Table 1.1 Advantages and Disadvantages of Bent Cap Connection Types (Matsumoto et al. 2001)

Grout Pockets	Grouted Vertical Ducts	Bolted Connection
+ simple grouting operations	+ stay-in-place ducts	+ stay-in-place ducts
+ large construction tolerances	+ smaller volume of grout needed	+ optional post-tensioning
- potential congestion of cap reinforcement	+ minimal interference with cap reinforcement	+ minimal interference with cap reinforcement
- large exposed top surface	+ more limited exposed top surface	- exposed cap top anchorage needs to be protected

A three-phase experimental program was conducted to investigate and refine the connection details. The first phase of testing consisted of 32 pull-out tests of headed and straight bars embedded in grout pockets and grouted vertical ducts. Of the 32 tests, 24 involved reinforcing bars embedded in grouted pockets (14 single-bar tests and 10 double-bar tests). The remaining tests were single-bar tests embedded in grouted vertical ducts. All tests of grouted vertical ducts used #11 epoxy-coated bars and corrugated galvanized steel ducts. Experimental parameters included embedment depth, grout type, and connector type (straight and headed connectors). A photograph of one of the grouted vertical duct tests is shown in Figure 1.5. Results from the first phase of testing were used to develop anchorage design provisions for straight and headed bars embedded in grout pockets and ducts. Information about grout performance and placement techniques was also obtained. The recommended development lengths in tension were recommended:

grout pocket connections: $$\ell_d = \frac{0.022 d_b f_y}{\sqrt{f_c'}} \quad (1.1)$$

grouted vertical-duct connections, $$\ell_d = \frac{0.024 d_b f_y}{\sqrt{f_c'}} \quad (1.2)$$

where ℓ_d is the development length in tension (in.), d_b is the nominal diameter of the connector (in.), f_y is the specified yield strength of the connector (psi), and f_c' is the specified compressive strength of the concrete (psi).

Full-scale single column and bent cap specimens were tested during the second phase of the research (Figure 1.6). Grouted vertical-duct connectors were constructed using #9 bars. The full-scale tests confirmed the adequacy of the anchorage design.

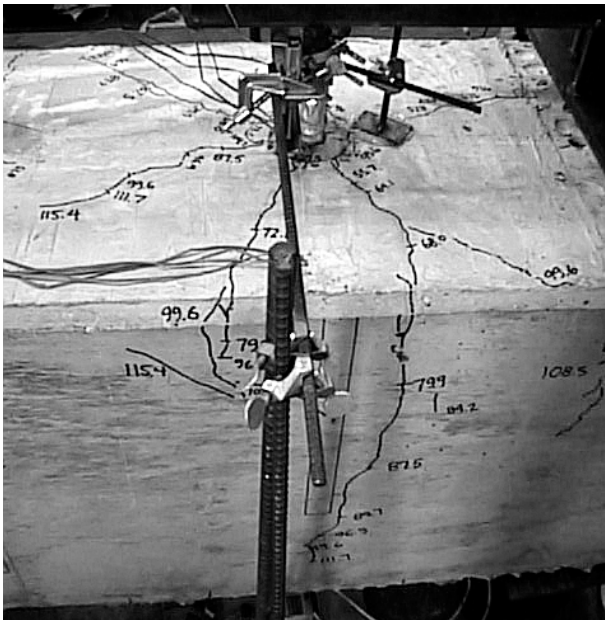

Figure 1.5 Test of Single Bar Embedded in Grouted Vertical Duct (Matsumoto et al. 2001)

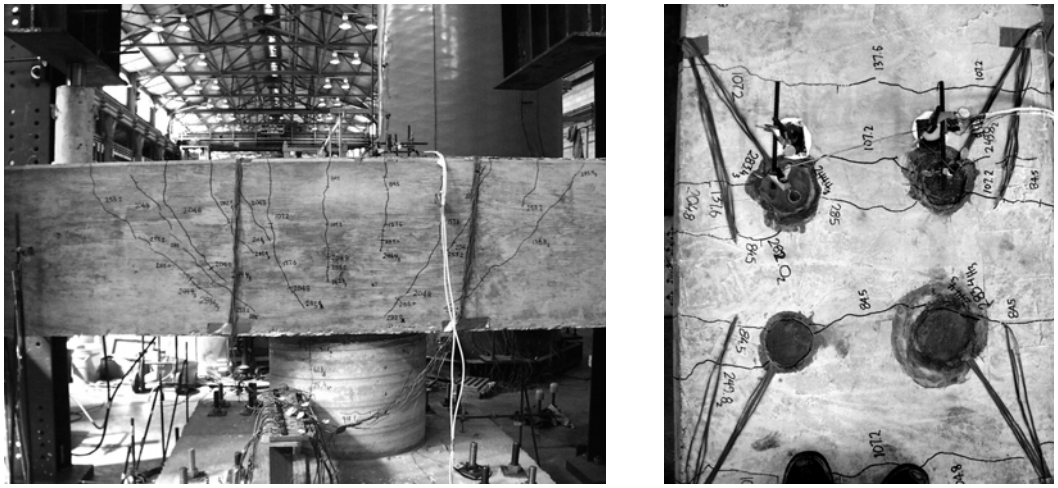

Figure 1.6 Test of Column-Bent Cap Specimen with Grouted Vertical Ducts (Matsumoto et al. 2001)

Two multi-column bents were constructed in the field by a contractor (Figure 1.7) during the third phase of the project. The main purpose of this phase was to assess the constructability of the different connection types in the field. Behavior of connections was also examined. The researchers made observations on use of plans by the contractor, construction tolerances, setting of the caps, and grouting practices.

A grout performance specification and a comprehensive design methodology for precast bent cap systems were developed during this project. The design methodology is summarized in Chapter 3. The investigation concluded that the three connection types studied were acceptable connection alternatives for a precast bent cap system.

Figure 1.7 Full-Scale Multi-Column Bent (Matsumoto et al. 2001)

1.3 CHALLENGES AND NEEDS

Following the completion of research project 1748, TxDOT initiated the design of three bridge construction projects that incorporated precast bent caps. The Lake Ray Hubbard Bridge, the Lake Belton Bridge, and the Dallas High Five projects are discussed in more detail in Chapter 3. Grouted vertical duct connections were used in all three of these projects. This type of connection was selected by contractors and TxDOT engineers primarily because the volume of grout needed to complete the connections is significantly less that that required for grout pockets.

TxDOT engineers involved in the design and construction of these projects were concerned about the precast bent cap connection details being used. Many uncertainties about the behavior of grouted vertical duct connections arose because the design engineers used large numbers of closely-spaced #11 bars in the connections. In addition, contractor-driven construction modifications intending to increase bridge durability, such as replacing galvanized steel ducts with plastic ducts in the connections, raised additional concerns regarding the performance of the connections.

Very limited information was available regarding connectors embedded in grouted vertical ducts. TxDOT research project 1748 (Matsumoto et al. 2001) mainly addressed the behavior of grout pocket connections, and the small number of tests involving grouted vertical ducts were mostly limited to single-connector tests, and connectors housed inside galvanized steel ducts. The full-scale column-bent cap specimens, which comprised multiple-connectors, contained widely-spaced #9 bars. Information available elsewhere regarding the behavior of grouted vertical duct connections is scarce. The evolution of grouted vertical duct connections as the preferred connection type in precast bent cap systems, demonstrated by the new TxDOT bridges, has revealed the need for additional research on the behavior of these connections.

1.4 RESEARCH OBJECTIVES

Conscious of the continuing need for efficient bridge construction systems, the Texas Department of Transportation initiated research project 0-4176, "Development of Precast Bridge Construction Systems," at the University of Texas at Austin. The initial problem statement for this project contemplated the development of a largely precast bridge system that could be assembled and open to traffic in days or weeks instead of the months or years required for conventional cast-in-place construction. The start of project 0-4176 coincided with a TxDOT implementation study on precast bent cap connections. The implementation study, related to finalized research project 1748, was following closely the construction of the Lake Ray Hubbard Bridge. It became very clear at the inception of project 0-4176 that uncertainties in behavior of grouted vertical duct connections, which arose during the construction of the Lake Ray Hubbard Bridge, needed to be addressed and resolved through laboratory testing. Moreover, the design of the Lake Belton Bridge was almost complete, and additional uncertainties about the behavior of the conceived bent cap connections were emerging.

The demonstrated need for broad laboratory testing of grouted vertical duct connections prompted TxDOT engineers and the researchers participating in this investigation to pursue this matter. As a result, the research direction of project 0-4176 concentrated on examining the behavior of precast bent cap connections constructed using grouted vertical ducts in the laboratory. The main objectives of this research project were: (1) understand the behavior of grouted vertical duct connections constructed using galvanized steel and plastic ducts, (2) develop simple models to represent the measured connector behavior, and (3) develop appropriate design expressions for grouted vertical connectors.

1.5 SCOPE

The research conducted during Project 0-4176 is documented in this report and in the dissertation by Brenes (2005). Chapter 2 summarizes the available literature related to grouted vertical duct connections, precast bent caps, and anchorage of reinforcing bars. The current design and construction practices used by TxDOT for precast bent cap connections with grouted vertical ducts are presented in Chapter 3. Uncertainties that evolved during the construction of the new bridge projects are also described.

Chapter 4 presents an overview of the experimental program developed to examine the behavior of grouted vertical duct connections. Main parameters that affect the behavior of these connections, such as bar coating, duct material, embedment depth, and connector group effects are described. The design and fabrication processes of the test specimens are also detailed. The experimental setup and instrumentation used during the tests are then described in Chapter 5.

In Chapter 6, the presentation of the test results is divided into groups, based on the duct material used in the test specimens. The measured response is presented in terms of observed crack patterns, stress-displacement behavior of the connectors, stress distribution along the connectors, and duct response during loading. Pull-out failure modes are also identified. The pull-out modes of failure of the connection specimens are verified through forensic examination. Chapter 7 summarizes the analyses of the measured data. The observed effects of the parameters that influence connection behavior are discussed.

Recommendations for the embedded length of grouted vertical connectors are developed in Chapter 8. Development lengths in tension are based on the measured capacity of the connectors and minimum embedded depths are based on serviceability levels. A complete set of design provisions is presented in Chapter 9. Chapter 10 provides a summary and conclusions of the research, as well as suggestions for further research.

There are limitations on the scope of research of this project that deserve to be mentioned. All of the connections in this investigation were tested monotonically; consequently, the design recommendations are not intended to apply to seismic or dynamic applications. Additional tests taking this into consideration should determine if the results contained within this document can be extended to such cases. It is also possible that the design recommendations developed in this study may not be applicable to bent caps of unusual proportions or with connection configurations very different than those contemplated in this research.

CHAPTER 2
Literature Survey

The literature survey conducted for this investigation covers three main areas: (1) grouted vertical-duct connections, (2) precast bent caps, and (3) anchorage of reinforcing bars. The limited literature found regarding behavior and design of grouted vertical-duct connections is summarized in Section 2.1. Some of the available information is related to building applications. Bridge projects that have used precast bent caps are described in Section 2.2. Special attention is paid to the use of grouted vertical ducts. Section 2.3 reviews anchorage of reinforcing bars focuses on the mechanics of bond, results from experimental studies on bar anchorage in concrete and in grout, and code provisions for development length.

2.1 GROUTED VERTICAL-DUCT CONNECTIONS

Precast connections identified in this investigation as grouted vertical-duct connections incorporate ducts made of steel or plastic, such as those used in post-tensioning applications. Ducts serve as sleeves to house connectors, which are then filled with grout. There is limited information available regarding the use of this type of precast connection in the literature.

As is typical in precast construction, the primary objective when designing and detailing grouted vertical-duct connections is to obtain a precast connection that emulates the behavior of a cast-in-place connection. The differences between an emulative precast structure and a cast-in-place structure lie in the areas of field connections and assembly of prefabricated elements, while the analysis and design procedures remain the same for both. ACI Committee 550 (2001) has prepared a report that serves as a practical guide to detail connections between precast elements to emulate the behavior of cast-in-place structures. This document provides advice regarding detailing of joints and splices between precast building components, including wall systems, frame systems, and floor diaphragms. The report provides a series of connection details that generally involve the use of mechanical splices, such as proprietary threaded couplers. Details for joining wall panels using lapped splices inside a large conduit or duct are also presented; the conduit is filled with grout to complete the connection. One of these details is shown in Figure 2.1. The length of the lap splice shown must satisfy the provisions in ACI 318-05.

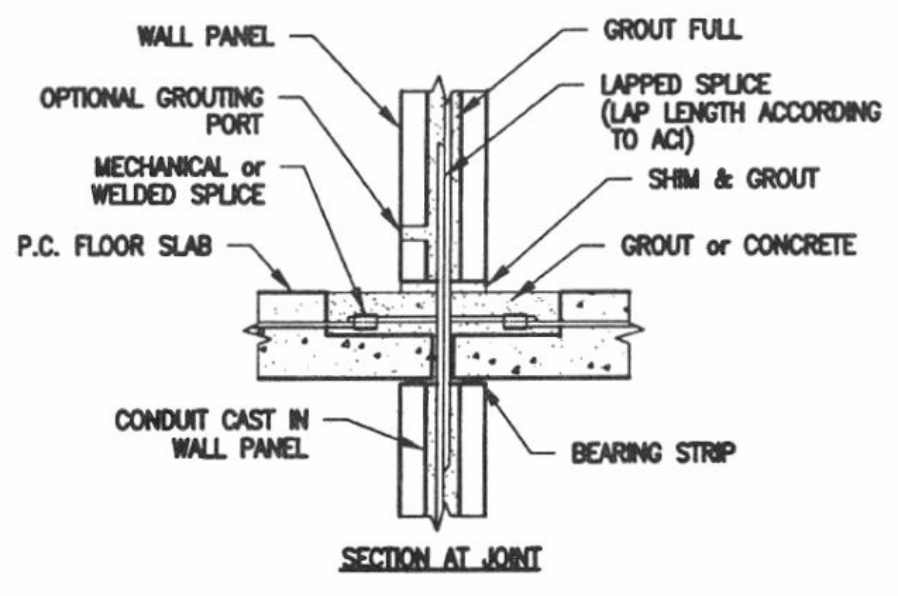

Figure 2.1 Detail to Join Wall Panels Vertically Using Large Conduit (ACI 550, 2001)

Park (1995) presented a perspective on the design and construction of buildings in New Zealand incorporating precast concrete elements in floors, moment resisting frames, and structural walls. Multi-story buildings have been built using a framing system where the precast beams pass through the columns. The longitudinal column bars from the column below pass through vertical holes in the precast beams and protrude above. The voids in the precast beam are formed using corrugated steel ducts, which are later filled with grout to anchor the column bars.

Figure 2.2 shows the construction of beam-column connections using this framing system. Columns can be precast or cast-in-place. If the columns are precast, mechanical splices or corrugated metal ducts are incorporated in the column end section. Tests of subassemblies of this construction system conducted by Restrepo et al. (1993) exhibited excellent ductility and stiffness. No significant differences in behavior were reported when the precast connections were compared with monolithic construction.

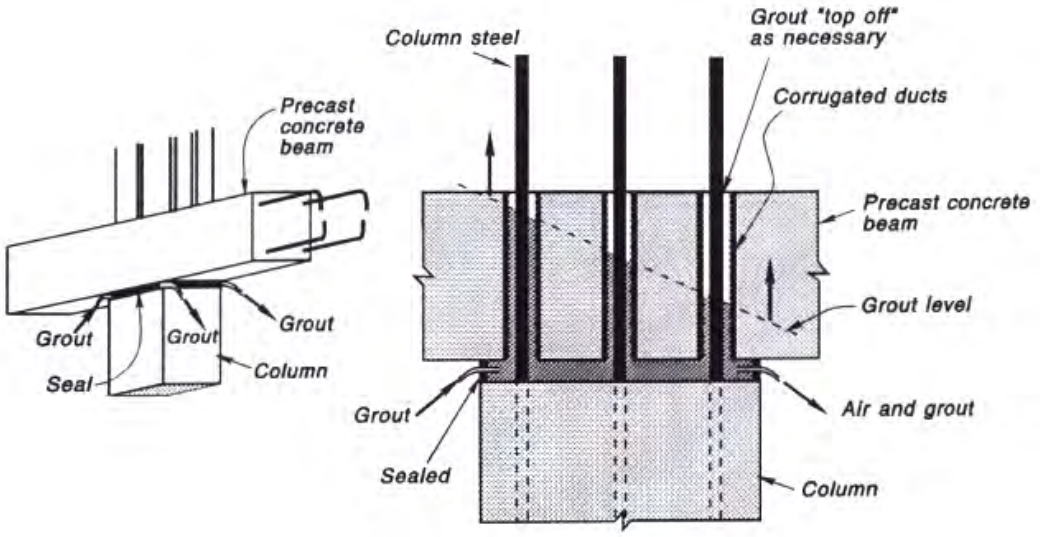

Figure 2.2 Precast Beam-Column Connections Used in New Zealand (Restrepo et al. 1993)

Stanton et al. (1986) reported test results and a design methodology for eight moment resisting precast beam-column connections. Two of the connection specimens used #6 dowel bars that were either partially or fully grouted in ducts. In both connection tests, bars yielded and very ductile behavior was observed. Debonding of the bars did not lead to any noticeable improvement in performance. Figure 2.3 shows flexural failure mechanisms for the type of connection tested: (1) yielding of the beam top reinforcement, (2) yielding of the dowels at the joint, (3) crushing of concrete at edge of column, (4) bond failure leading to pull-out before yielding of the connector, and (5) yielding of the dowel along the debonded length. To obtain ductile system behavior, mechanism (1) is the preferred failure mode, followed by mechanisms (2) and (5).

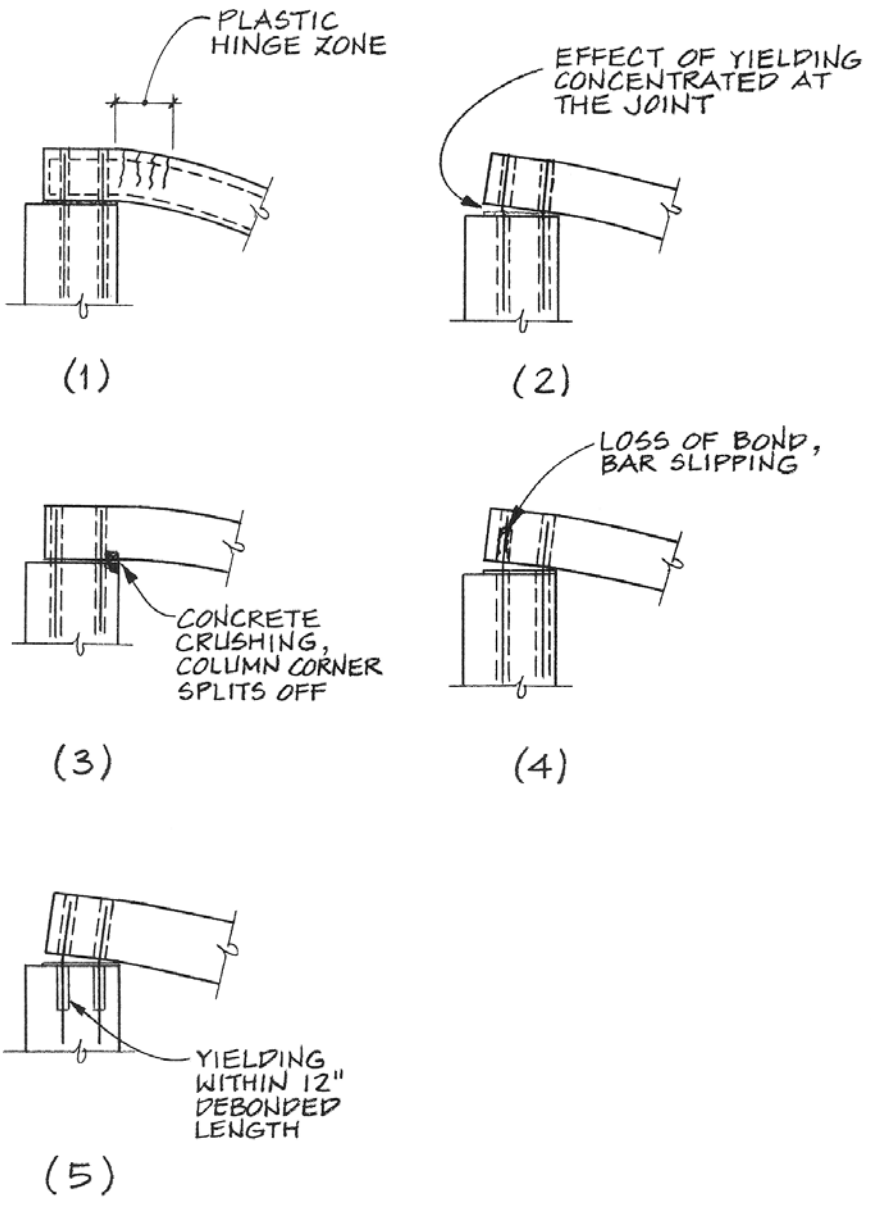

Figure 2.3 Flexural Failure Mechanisms for Precast Connection Using Grouted Ducts (Stanton et al. 1986)

The 5th edition of the *PCI Design Handbook* (1999) presents design provisions for reinforcing bars embedded in grout-filled metallic conduit. The conduit must have a minimum cover of 3 in. Additional requirements include: (1) minimum duct thickness of 0.023 in., (2) minimum clearance around the bar of 0.375 in., and (3) strength of the grout equal or higher than concrete strength, with a minimum strength of 5000 psi. Development length information is provided in a tabular form for different bar sizes. Values in the table were obtained from a design equation that appeared in the 4th edition of the *PCI Design Handbook* (1992). The embedment depth needed to develop yielding of the connector is given in Eq. (2.1):

$$\ell_e = \frac{0.04 A_b f_y}{\sqrt{f_c'}} \geq 12 \text{ in.} \qquad (2.1)$$

where ℓ_e is the required embedment length (in.), A_b is the area of the bar (in.^{2}), f_y is the specified yield strength of the bar (psi), and f_c' is the specified compressive strength of the concrete (psi). The use of Eq. (2.1) is restricted to #8 and smaller uncoated bars. The basis of the design equation and test data supporting its development are not stated in the source, but it is likely that the equation was based on the development length provisions in ACI 318-71.

Tests underway at California State University in Sacramento are investigating the seismic response of precast bent caps with grouted vertical-duct connectors. The first phases of testing have examined the cyclic behavior of single epoxy-coated #9 bars embedded in galvanized steel ducts (Mandawe et al. 2002, Matsumoto 2003). Connectors embedded $10d_b$ achieved yielding before failure by pull-out, while connectors embedded $16d_b$ failed by fracture. Figure 2.4 shows a photograph of a test involving a connector embedded $10d_b$. No significant bond degradation due to tension cycles was reported when bars were anchored to achieve yield and the strength of the grout was at least 1000 psi greater than the strength of the concrete. The preliminary results indicate that grouted vertical-duct connections are a viable alternative for use in precast bent cap systems in seismic regions.

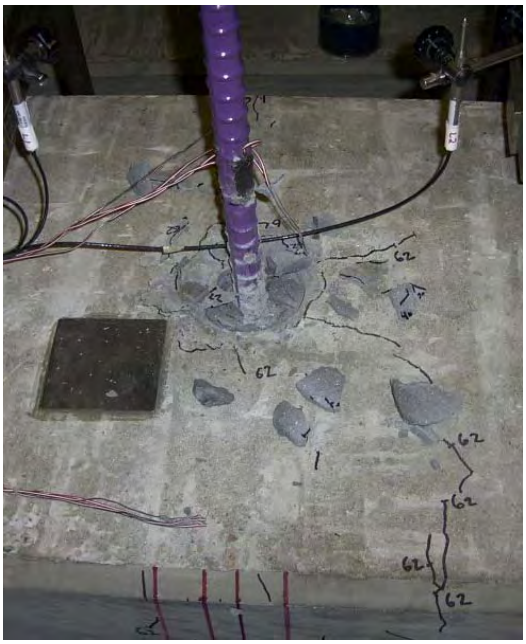

Figure 2.4 Test of Connector Embedded $10d_b$ (Mandawe et al. 2002)

VSL International Ltd. has conducted a series of investigations (Ganz 1991, Marti 1993) to compare the bond characteristics of tendons grouted in corrugated galvanized steel duct and PT-PLUS plastic ducts. Although tendons would not be used in grouted vertical-duct connections as the connectors, the research has some relevance with regard to the bond properties of post-tensioning ducts. Results of tendon pull-out tests on shallow slab-like concrete specimens (Ganz 1991) indicated that multi-strand tendons placed inside plastic ducts exhibited reductions in capacity and stiffness, compared with specimens constructed using corrugated steel ducts. Based on test data, development lengths on the order of 30 to 40 duct diameters were estimated for plastic ducts used in stressing applications. In a subsequent study involving similar pull-out tests and accompanying bond-length tests (Marti 1993), reductions in stiffness and capacity were also observed for tendon specimens using plastic ducts. Bond-length tests indicated that the development length required for plastic ducts was approximately 50% longer than that required for corrugated steel ducts.

Einea et al. (1995) tested a series of generic grout-filled reinforcing bar splices monotonically in tension utilizing standard steel pipe as the sleeve material (Figure 2.5). Four different types of splice specimens were tested using both lap splice and butt splice arrangements, and with different steel pipe end details. Details included welding steel rings on the ends of pipes to mobilize confinement action in the grout. Tests involved #5, #6, and #9 bars with embedded lengths between 5 and $11d_b$. Most specimens failed at an axial stress higher than the specified yield strength of the reinforcement.

Figure 2.5 Pullout Failure of Generic Grout-Filled Splice Sleeve (Einea et al. 1995)

High bond strengths were obtained due to the confined grout around the bars. However, the tests did not evaluate the bond between the steel pipe sleeve and concrete.

2.2 PRECAST BENT CAPS

As discussed in Chapter 1, several bridges in Texas have been constructed using precast bent caps in the past fifteen years. The TxDOT projects that utilized grouted vertical ducts will be discussed in detail in Chapter 3 of this report. Other bridge projects that utilized precast bent caps are summarized in this section.

The Getty Center People-Mover System in Los Angeles was built using precast concrete crossheads with grouted vertical-duct connections (Josten et al. 1995). The precast crosshead elements provided an efficient construction system in an environmentally sensitive site along steep hillsides (Figure 2.6). The columns of the tram system were cast-in-place and included a double reinforcing bar template to ensure adequate alignment of the vertical reinforcement that projected above the tops of the columns into the precast crosshead elements. The connection configuration typically consisted of 16 reinforcing bars, as large as #11s, in a 3'-0" diameter circular pattern. The protruding column bars were housed inside 1.5-in. diameter corrugated sleeves cast into the crossheads. High-strength grout was then poured into the sleeves to complete the connections. The sleeve diameter was restricted to 1.5 in. so that it would not interfere with the crosshead reinforcing. Construction of the crosshead elements also made use of templates in the formwork that aligned and maintained the corrugated sleeves at the proper location. Although clearances were extremely tight, all crossheads aligned correctly when erected in the field.

Figure 2.6 Precast Crossheads Used in the Getty Center People-Mover System Project (Josten et al. 1995)

The use of precast substructure and superstructure elements in the replacement bridge on Route 57 over the Wolf River in Moscow, Tennessee, facilitated rapid construction and made possible erection of the bridge from the top down without putting any equipment on the surrounding wetlands (PCI 2005). The contractor worked closely with engineers at the Tennessee Department of Transportation to develop a prototype connection adequate for the high seismic demands of the site.

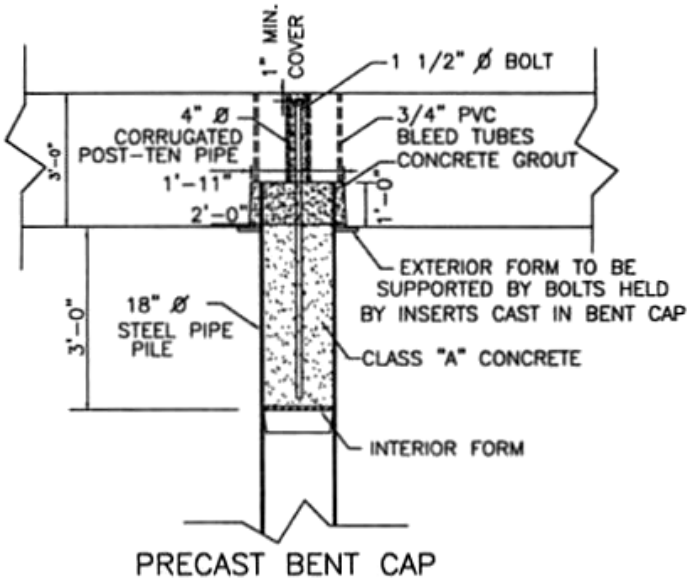

Figure 2.7 Wolf River Precast Bent Cap Connection (PCI 2005)

Bent cap connections consisted of grouted connectors placed inside corrugated metal ducts (Figure 2.7). A 24-in. diameter by 12-in. deep cylindrical recess was formed at the bottom of the precast caps. One 4-in. diameter corrugated duct was also provided in the cap to accommodate a 1.5-in. diameter high-strength connector that passed through the joint into the pipe section. The void surrounding the connector was filled with concrete (pipe section) and grout (cap section).

Precast bent caps were also used to construct the people-mover system at the Dallas/Fort Worth Airport People-Mover System (Nichols et al. 2001). The project incorporates precast segments of columns and inverted-T bent caps that are post-tensioned together. This structural system was selected by the owner because it reduced construction time substantially and minimized disruption to airport operations. Column segments and bent caps were fabricated at an adjacent precasting yard; they are then transported and erected during night operations. After each cap was in place, multi-strand post-tensioning tendons were threaded through ducts down the column around a bend that occurs in the base below grade. Tendons were then stressed and grout was placed inside the ducts.

Figure 2.8 Beaufort and Morehead Railroad Trestle Bridge Bent Caps (FHWA 2005a)

Precast bent caps were used in the Beaufort and Morehead Railroad Trestle Bridge Project in North Carolina. Pier caps were cast upside down with protruding top pile reinforcement (Figure 2.8). As caps were placed into position, top pile reinforcement was positioned inside steel pipe piles, and concrete was then pumped into the pipes to make the moment connections between caps and piles (FHWA 2005a). The use of precast bent caps improved constructability and minimized traffic disruption. Trestles were

replaced without rerouting rail traffic; individual spans were replaced between scheduled trains (FHWA 2005b).

The Florida Department of Transportation (FDOT) studied feasibility of using precast substructures in bridges (LoBuono et al. 1996). The impact of different column and bent cap arrangements on construction was considered by evaluating site requirements, speed of construction, methods of connection, and shape, weight, and size of precast elements. Multi-column and hammerhead caps were considered with both solid and voided cross sections. Proposed methods of connection between caps and columns included mechanical couplers, post-tensioning, and grouted pockets. An industry review board recommended using solid rectangle or inverted-U sections for bent caps over multiple columns or piles. For hammerhead caps, both precast cantilever sections joined by post-tensioning and voided sections were considered appropriate.

2.3 ANCHORAGE OF REINFORCING BARS

A brief overview of anchorage of reinforcing bars is presented in this section. Bond of straight, deformed reinforcing bars is emphasized. The mechanics of bond and how bond stresses are utilized to achieve development of reinforcement are discussed. Results from a suite of experimental studies on anchorage of bars in concrete and grout are also presented. Emphasis was given to tests of confined specimens due to their relevancy to grouted vertical-duct connections. The development length provisions in ACI 318-05 and the AASHTO LRFD Specifications (2004) are also reviewed.

2.3.1 Mechanics of Bond

Bond refers to the interaction between reinforcing steel and the surrounding concrete that allows transfer of tensile stresses between the steel and concrete. Lutz and Gergely (1967) demonstrated that bond between reinforcing bars and concrete is made up of three components: (1) chemical adhesion, (2) friction, and (3) mechanical interlocking of bar lugs (ribs) with the surrounding concrete. In the case of deformed bars, bond stresses are transferred mainly by mechanical interlock. The effect of chemical adhesion is small, and friction does not occur until there is slip between the reinforcing bar and the concrete.

The resultant force exerted by a steel rib on the concrete is inclined at an angle α to the axis of the bar (Figure 2.9b). This angle corresponds roughly to the angle of inclination of the face of the rib. The resultant force can be divided into a parallel component and a normal component, relative to the axis of the bar (Figure 2.9d). The parallel component is usually called the bond stress, while the normal or radial component is termed the splitting stress. Radial components of the bond forces are resisted by tensile

stress rings in the concrete surrounding the bar (Figure 2.9e). When a ring is stressed to rupture, it breaks and longitudinal (splitting) cracks appear on the concrete surface.

The formation of cracks around deformed bars acting in tension was studied by Goto (1971). Test specimens consisted of single deformed bars embedded concentrically in long concrete prisms. Cracking in the concrete was indicated by dye from special injecting holes provided in the specimens. Lateral cracks (called primary cracks) formed first at a few locations along the length of the specimens. Small internal cracks (such as those shown in Figure 2.9), which did not appear at the concrete surface, were seen around the bars along the entire length of the specimens. Cracks like these began to form shortly after the formation of primary cracks. The angles of these inclined cracks were in the range of 45 to 80 degrees relative to the bar axis. The inclination of these internal cracks matches the general orientation of the compressive forces exerted by the faces of the ribs on the concrete. Longitudinal cracks (in the direction of the bar axis) formed at higher stresses, and usually started at the locations of primary cracks.

Slip of a deformed bar occurs as a result of both the wedging action of the steel ribs pushing the concrete away (splitting), and due to the crushing of concrete keys by the ribs (pullout). In the absence of confinement, deformed bars fail in bond by splitting, which depends primarily on the force on the concrete and not so much on the bar stress and the bar perimeter (Figure 2.10a). If confinement is provided, usually by the use of stirrups and/or a large concrete cover, bond failure occurs by shear failure of the concrete keys between the steel ribs (Figure 2.10b), and the ultimate load per unit length depends increasingly on the bar perimeter (Lutz and Gergely 1967). After adhesion is lost and ribs begin to bear on the concrete, slip occurs by progressive crushing of the porous concrete paste structure in front of the rib. The compacted crushed concrete creates a wedge that becomes lodged in front of the rib and moves along with it. This, in effect produces a rib with a face angle of 30 to 40 degrees (Lutz and Gergely 1967). Thus, the angle at which the steel rib bears on the concrete, α, changes as load acting on the reinforcing bar increases. As a result, radial splitting stresses tend to increase at a rate greater than the parallel bond stresses as tensile load in the bar rises.

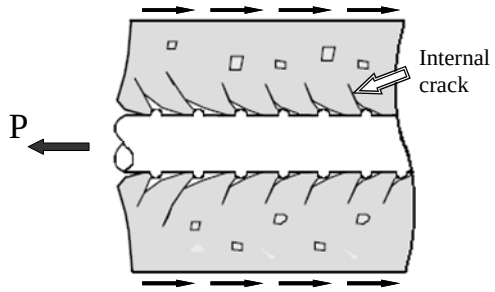

a. Tension acting on Reinforced Concrete

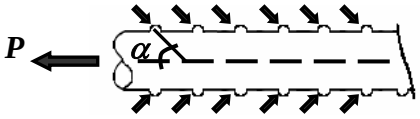

b. Bond Force on Bar

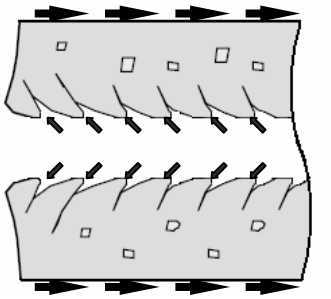

c. Reaction on Concrete

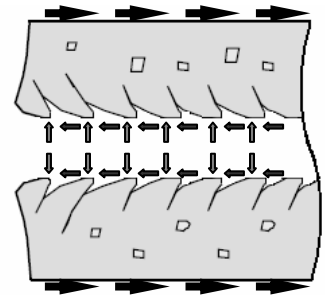

d. Parallel and Radial Components of Bond

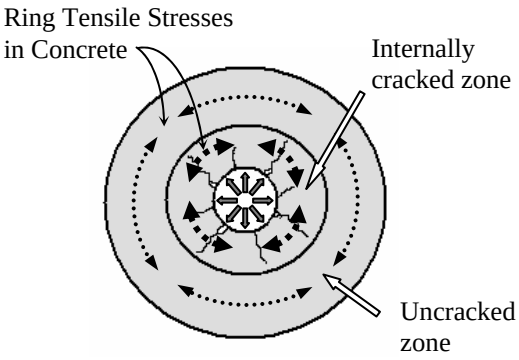

e. Cross Section

Figure 2.9 Forces between Deformed Bars and Surrounding Concrete

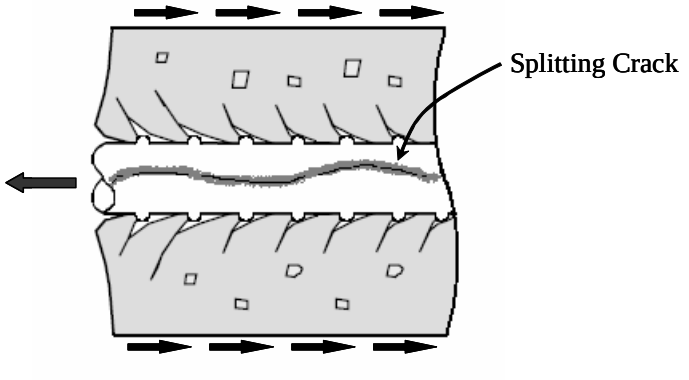

a. Bond Failure by Splitting

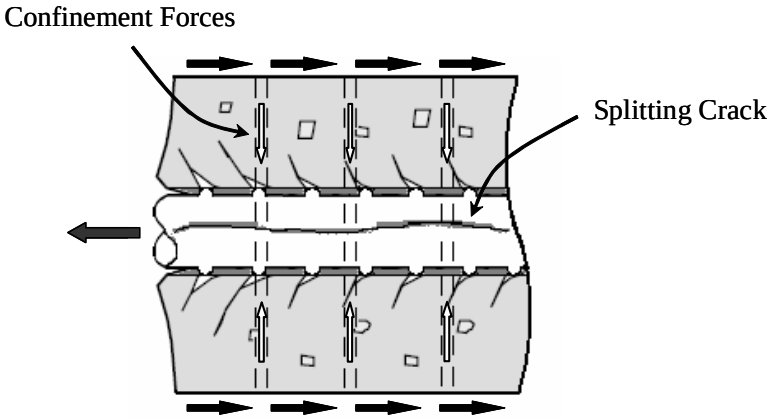

b. Bond Failure by Shearing of the Concrete Keys in Between Ribs (Pullout)

Figure 2.10 Effect of Confinement on Bond - Failure Modes

The splitting resistance of concrete can be enhanced if confinement stresses are superimposed onto the tensile ring stresses around the reinforcing bar. Confinement can be classified as either active or passive. Compressive stress fields induced by applied loads, reactions, and prestressing are considered to be active confinement. In contrast, passive confinement refers to compressive stress fields that are generated by forces in the mild reinforcement surrounding the anchorage zone of the bar. Surrounding reinforcement may involve spirals, stirrups, or straight bars perpendicular to the axis of the bar being anchored. Passive confinement is engaged only after crack deformations in the concrete ring develop that induce tension forces in the surrounding steel. Now acting as transverse reinforcement, the surrounding steel restricts the propagation and widening of splitting cracks that originate at the interface of the anchored bar and the concrete. Growth of splitting cracks is restrained more effectively when transverse reinforcement is placed close to the surface of the bar.

Eligehausen et al. (1983) tested both monotonically and cyclically a series of specimens built to represent the confined region of a beam-column joint. Single bars were embedded in concrete a short

length of $5d_b$. Different quantities and arrangements of transverse reinforcement, that included straight bars and stirrups, were used in most specimens. Alternately, transverse pressure was also applied to some specimens to represent the influence of column compressive forces on the joint. For specimens involving transverse reinforcement, test results showed small differences in bond behavior when the quantity or total area of transverse steel was varied (Figure 2.11). Pullout modes of failure were characteristic of these specimens; results indicated that there exists an upper limit on the quantity of transverse reinforcement after which there is no improvement in bond behavior. Improvement in bond resistance was observed as transverse pressure increased (Figure 2.12). The ratio between the added bond resistance and applied pressure decreased significantly with increasing pressure.

The influence of transverse reinforcement on bar anchorage was also investigated by Astrova et al. (1961). Spirals and an array of meshes of straight bars were used as the transverse reinforcement in rectangular concrete block specimens. Test results of specimens using mesh reinforcement showed an increase in bond strength; while specimens using spirals as transverse reinforcement did not produce a similar increase. As observed in the studies conducted by Eligehausen et al. (1983), increasing the quantity of transverse reinforcement beyond a certain point failed to yield any further increase in bond strength.

Tepfers (1973) conducted a series of tests on lapped splices in beam specimens with varying arrangements and quantities of transverse reinforcement. Confinement effects provided by stirrups and spirals were investigated. In the case of stirrups, the splice strength improved at an increasing rate as the stirrup diameter increased (Figure 2.13a). Similar data obtained for the specimens containing spiral reinforcement are shown in Figure 2.13b. Data points shown in this figure inside parenthesis indicate that failure of the splice had not been achieved when the test was stopped.

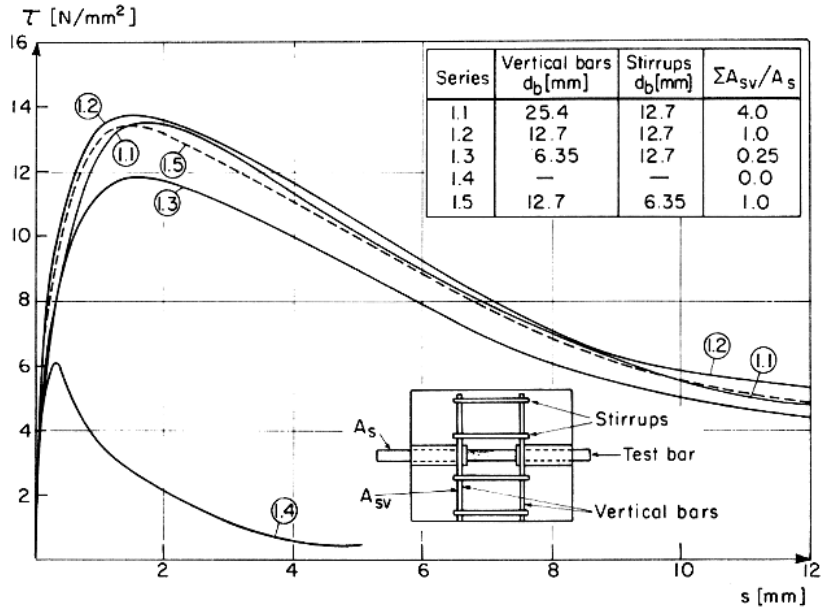

Figure 2.11 Influence of Transverse Reinforcement on Bond Stress-Slip Relationship (Goto 1971)

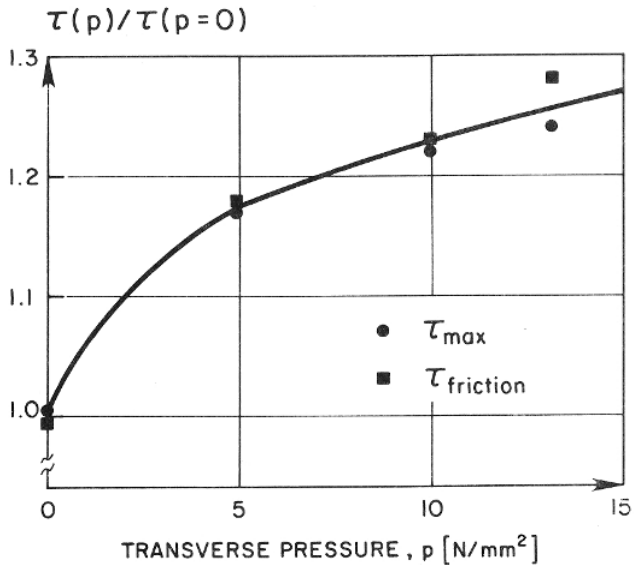

Figure 2.12 Influence of Transverse Pressure on Bond Resistance (Goto 1971)

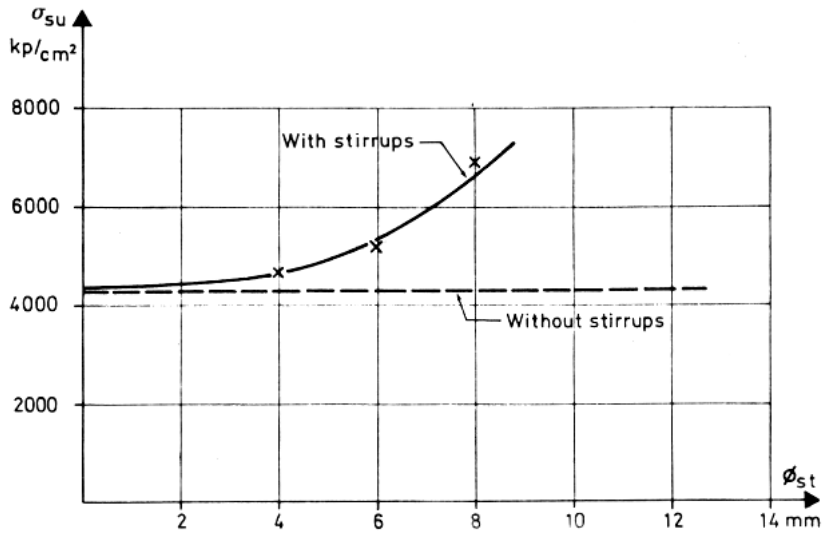

a. Splice Strength as a Function of Stirrup Diameter

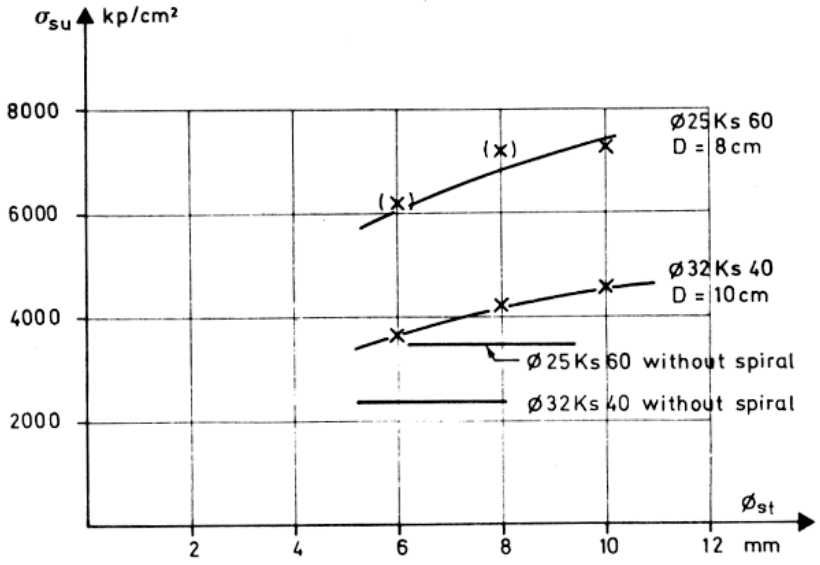

b. Splice Strength as a Function of Spiral Diameter

Figure 2.13 Effect of Transverse Reinforcement on Splice Strength (Astrova et al. 1961)

The influence of normal (transverse) pressure on bond strength has been studied by Untrauer and Henry (1965). Test specimens consisted of #6 and #9 bars embedded in 6-in. concrete cubes, and the lateral pressure applied ranged from 0 to 2370 psi. Results showed that bond strength increases approximately in proportion to the product of the square root of the normal pressure and the square root of the compressive strength of the concrete. The equation developed using regression analysis of test data is:

$$u_{ult} = \left(18.0 + 0.45\sqrt{f_n}\right)\sqrt{f_c'} \qquad (2.2)$$

where u_{ult} is the ultimate bond strength (psi), f_n is the applied normal pressure (psi), and f_c' is the specified compressive strength of the concrete (psi). The slip at ultimate bond stress was found to increase with corresponding increases in normal pressure. However, restraint provided to the test specimens by the loading plates was not evaluated and may have contributed to the observed improvement in bond strength.

2.3.2 Bond Stress

The distribution of bond stress along the length of a deformed bar embedded in concrete and subjected to axial tension is assumed to be similar to the diagram shown in Figure 2.14. At first, when the pull on the bar is small, high stresses develop near the loaded end of the bar; some slip of the bar occurs as adhesion between the bar and the concrete in this region breaks down and as steel ribs begin to crush part of the concrete between the ribs. Failure can occur at this early stage if concrete surrounding the bar is unconfined. If some degree of confinement is present, a rise in load tends to shift the bond stress diagram deeper along the bar engaging additional ribs to resist the additional load. In some instances, especially when the level of confinement is low around the loaded end of the bar, bond resistance near the surface can be reduced to zero due to extensive cracking and cone breakouts formed in the concrete. As load is increased to maximum levels, shifting of the bond stress diagram continues as bond stress peaks move deeper along the confined region of the bar. Failure occurs when there is no capacity left provided by the interlocking of the steel ribs and the concrete.

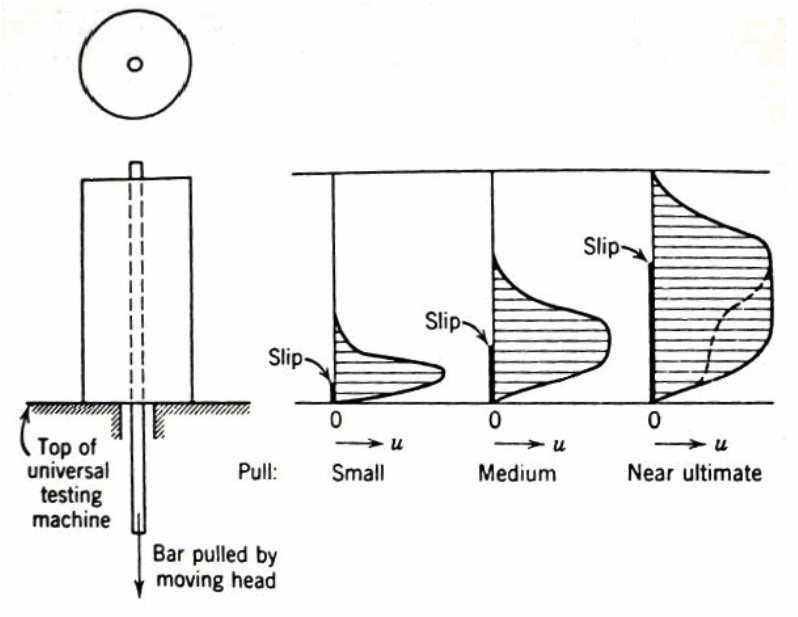

Figure 2.14 Bond Stress Distribution (Ferguson et al. 1988)

The distribution and magnitude of bond stresses along a bar are difficult to establish quantitatively. One problem is the progressive shifting of the bond distribution along the bar as bond deterioration occurs near the loaded end. Moreover, it is difficult to verify which ribs are actually transferring loads and what share of the load is being resisted by each rib. In spite of this, some assessment of bond stress is required in order to be able to estimate the length of embedment required to anchor bars effectively in concrete. As a way to deal with the complexities of actual bond stress conditions around reinforcing bars, investigators have resorted to the use of a nominal or average bond stress, *u*, determined by dividing the force in the bar, *P*, by the nominal bar perimeter ($\pi * d_b$), and the embedment length (ℓ_e). The equation follows:

$$u = \frac{P}{\pi d_b \ell_e} \tag{2.3}$$

Numerous experimental studies have been conducted to investigate the parameters that influence the anchorage of reinforcement. Conventional bond tests have consisted of a concrete block from which a reinforcing bar is pulled; in some test arrangements the block was modeled to be part of a beam or a joint. Orangun, Jirsa, and Breen (1977) evaluated the results of several studies on development length and lap splice length that were conducted in the United States and Europe. Variations in the average bond stress, *u*, obtained in the tests were plotted versus a set of test parameters that have been known to affect the strength of anchored bars. Studied parameters included the effect of embedment length, cover, bar spacing, bar diameter, concrete strength, and transverse reinforcement. Data from the tests were analyzed using a nonlinear regression analysis with the aim of developing a simple equation that could be

integrated into code design provisions. The resulting empirical equation was modified to determine development length rather than average bond strength for practical design purposes.

Viwathanatepa et al. (1979) investigated the bond deterioration of anchored bars. Specimens consisted of blocks of well-confined concrete constructed to represent a beam-column joint of a moment resisting frame. Concentrically placed single bars (with bonded lengths between 15 and $27d_b$) were tested monotonically and cyclically. Strain gages were installed along the bars at 1.5-in. spacing. The bond stress distribution along the bars was estimated by averaging calculated bond stress values between gage locations. Bond distribution diagrams similar to those shown in Figure 2.14 were observed. Three different concrete regions were identified and classified according to different bond behavior (Figure 2.15a). Ultimate peak bond strengths were found to be around 1.0, 2.1, and 4.0 ksi for unconfined, confined and pushed-end regions, respectively. The bond deterioration mechanism under monotonic loading is shown in Figure 2.15(b) and (c) for the unconfined and confined regions. In the unconfined region, the inclined internal cracks that form at the roots of the steel ribs propagate as load is applied until they reach the concrete surface; the failure mode is that of a cone-shaped concrete formation that breaks loose from the rest. The initial behavior exhibited by confined regions is similar to that of unconfined regions, but the presence of transverse reinforcement controls the propagation of inclined cracks. In the confined region, bond deterioration results from bearing failure, inelastic deformations of the concrete "strut" and reductions in the effective shearing area of the concrete (keys).

2.3.3 Anchorage of Bars in Grout

Grouted anchors are a type of adhesive anchor commonly used in repair and rehabilitation applications because they provide a practical and economical method for adding new concrete sections or steel members to an existing concrete structure. In spite of their frequent use, a very small number of studies were found in the literature that examined the anchorage of connectors in grout. Moreover, most of the literature concentrates on the behavior of headed connectors, and very limited information and test data are available regarding the anchorage of straight deformed bars.

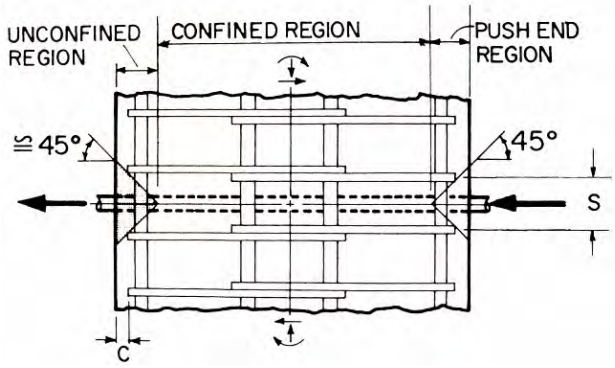

a. Regions in Concrete Block Specimen

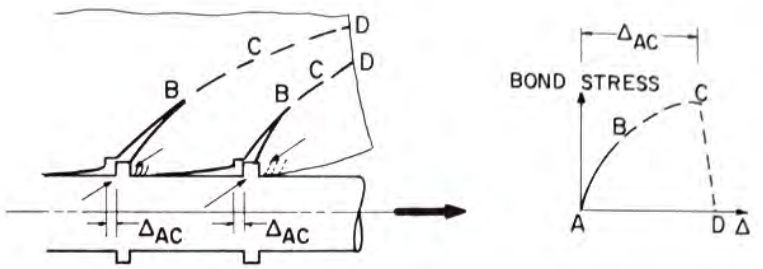

b. Mechanism of Bond Resistance in Unconfined Region

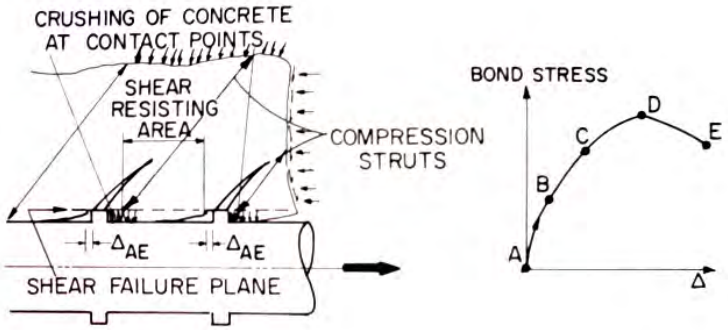

c. Mechanism of Bond Resistance in Confined Region

Figure 2.15 Bond Deterioration Mechanisms under Monotonic Loading (Viwathanatepa et al. 1979)

Darwin and Zavaregh (1996) examined the anchorage of reinforcing bars grouted into holes drilled in existing concrete. Tests involved #5 and #8 bars embedded in concrete blocks; most bars had a 3-in. cover. Epoxy-coated and uncoated bars were used. Embedment depths ranged between 6 and $19d_b$, and the drilled holes were typically 0.25 in. larger than the bar diameter. Six types of grout were examined, including two cement-based grouts. No transverse reinforcement was provided to aid in confinement. Most specimens exhibited a splitting failure, accompanied by the formation of a shallow angle concrete cone. Results showed that the bond strength provided by most grouts is not sensitive to

either hole diameter or drilling method. Bond strength improved with increases in embedment length, bar size, and cover. No significant differences in bond strength were observed due to epoxy-coating.

Cook et al. (1998) have reported on the behavior of single adhesive anchors under tensile load. Although the study concentrated on epoxy, polyester, and vinylester adhesives, results from the study are relevant to grouted anchors because methods of analysis and design are similar. Investigators analyzed data from a worldwide database using regression analysis; and then used the results to evaluate a series of design concepts and models. Design models were based on failure modes observed in tests and included concrete cone models, bond models, combined cone/concrete models, and two-interface bond models. Statistical analysis indicated that a model based on uniform bond stress provided the best fit to the data. Cook (1998) later reported on the applicability of the Uniform Bond Stress (UBS) model that was developed earlier Cook et al. (1998) for post-installed grouted anchors. Anchors included threaded rods with and without a hex nut at the end, and also straight #4 deformed bars. Embedment depths were typically between 6 and $7d_b$. All straight anchors exhibited bond failure at the grout-anchor interface, accompanied by a shallow concrete cone formation at the face. Performance of grouted anchors was considered comparable to that of cast-in-place anchors.

Miltenberger (2001) has proposed a rational procedure for strength design of grouted connectors (fasteners) that uses both the Concrete Capacity Design (CCD) model and the Uniform Bond Stress (UBS) model. Design equations that describe potential failure modes were developed along with modification factors that account for edge effects, group effects, and concrete cracking. The design of a group of connectors is limited by the strength of the connector that carries the largest load; structural analysis must be performed to identify that connector. After calculating the load demand or required capacity using the appropriate load factors, the nominal capacity of the connector is determined, plus applicable modification factors, for all potential failure modes. Basic tensile failure modes are shown in Figure 2.16.

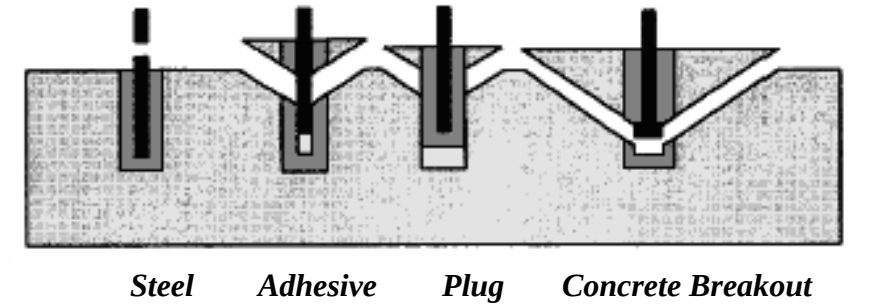

Figure 2.16 Basic Failure Modes for Grouted Connector (Miltenberger 2001)

Finally, a check on the interaction between tension and shear is performed. The mean bond strength and standard deviation determined from standardized tests on a specific grout anchor system are used to calculate the characteristic bond stress, τ', used for design. The characteristic bond stress corresponds to the 5% fractile, a statistical term meaning 90% confidence that there is 95% probability of the actual strength exceeding the nominal strength. For straight grouted connectors, the applicable nominal tensile strength equations corresponding to possible failure modes are:

connector yield:

$$N_s = f_y A_e \tag{2.4}$$

$$\phi N_n = \phi N_s \tag{2.5}$$

adhesive bond strength:

$$N_a = \tau'_a \pi d_b h_{ef} \tag{2.6}$$

$$\phi N_n = \phi \psi_g \psi_e \psi_{cr} N_a \tag{2.7}$$

plug bond strength:

$$N_o = \tau'_o \pi d_o h_{ef} \tag{2.8}$$

$$\phi N_n = \phi \psi_g \psi_e \psi_{cr} N_o \tag{2.9}$$

where

$$\psi_g = \frac{A_N}{nA_{No}} \leq 1.0 \tag{2.10}$$

$$\psi_e = 0.7 + 0.0375\frac{c}{d} \leq 1.0 \tag{2.11}$$

N_n = nominal tensile strength (lb)
N_s = basic anchor tensile strength (lb)
N_a = basic adhesive bond strength to steel (lb)
N_o = basic plug bond strength to steel (lb)
ϕ = capacity reduction factor, taken as 0.75
f_y = connector specified yield strength (psi)
A_e = effective connector area (in.^{2})
τ'_a = characteristic bond strength (psi)
τ'_o=characteristic bond strength calculated at grout-concrete interface (psi)
d_b = connector diameter (in.)
d_o = hole diameter (in.)
h_{ef} = embedment depth (in.)
ψ_g = modification factor for group effects
ψ_e = modification factor for side effects
ψ_{cr} = modification factor to account for cracking, taken as 0.5
A_N = projected failure surface for group of connectors (in.^{2})
A_{No} = projected failure surface for one connector (in.^{2}), (Figure 2.17)
n = number of connectors
c = shortest edge distance (in.)

The capacity of the connector groups is based on the smallest nominal capacity from Eq. (2.5), (2.7), and (2.9) for the most heavily loaded fastener.

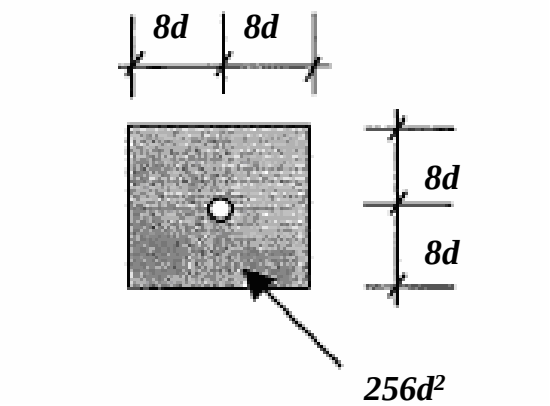

Figure 2.17 Influence Area for Single Straight Connector (Miltenberger 2001)

2.3.4 Code Provisions on Development Length

The ACI 318-05 Building Code Requirements for Structural Concrete contains design provisions for calculating the required development length of deformed straight bars. The equation follows:

$$\ell_d = \left(\frac{3}{40} \frac{f_y}{\sqrt{f'_c}} \frac{\psi_t \psi_e \psi_s}{\left(\frac{c + K_{tr}}{d_b} \right)} \right) \geq 12 \text{ in.} \tag{2.12}$$

where

$$\left(\frac{c + K_{tr}}{d_b} \right) \leq 2.5 \tag{2.13}$$

$$K_{tr} = \left(\frac{A_{tr} f_{yt}}{1500sn} \right) \tag{2.14}$$

ℓ_d = development length of bar in tension (in.)
d_b = bar diameter (in.)
f_y = specified yield strength of the connector (psi)
f'_c = specified compressive strength of concrete (psi)
ψ_t = reinforcement location factor
ψ_e = coating factor
ψ_s = reinforcement size factor (0.8 for #6 and smaller bars, 1.0 otherwise)
λ = lightweight aggregate concrete factor
c = spacing or cover dimension measured from center of connector (in.)
K_{tr} = transverse reinforcement index

A_{tr} = Area of transverse reinforcement (in.^{2})
f_{yt} = specified yield strength of transverse reinforcement (psi)
s = maximum spacing of transverse reinforcement within l_d (in.)
n = number of bars being developed along the plane of splitting

Equation (2.12) is based on the work performed by Orangun et al. (1977). A factor of 1.25 multiplying f_y is embedded in the equation to satisfy ductility requirements; the ACI equation also incorporates a strength reduction factor, ϕ, equal to 0.9 to account for deviations in material properties. The limit on the term $(c + K_{tr})/d_b$ is to safeguard against pullout type failures. For values above 2.5, ACI 318-05 states that a pullout failure is expected and an increase in cover or transverse reinforcement is unlikely to increase anchorage capacity.

In the AASHTO LRFD Bridge Design Specifications (2004), three design equations are provided for deformed bars developed in tension:

#11 and smaller bars, $$\ell_{db} = \left(\frac{1.25 A_b f_y}{\sqrt{f'_c}} \right) \geq \left\{ 0.4 A_b f_y, \text{ 12 in.} \right\} \quad (2.15)$$

#14 bars, $$\ell_{db} = \left(\frac{2.70 f_y}{\sqrt{f'_c}} \right) \geq 12 \text{ in.} \quad (2.16)$$

#18 bars, $$\ell_{db} = \left(\frac{3.50 f_y}{\sqrt{f'_c}} \right) \geq 12 \text{ in.} \quad (2.17)$$

where

ℓ_{db} = basic development length of bar in tension (in.)
A_b = area of reinforcing bar (in.^{2})
f_y = specified yield strength of steel reinforcement (ksi)
f'_c = specified concrete compressive strength (ksi)
d_b = diameter of bar (in.)

In order to obtain the required development length for design, ℓ_d, the basic development length, ℓ_{db}, obtained in Eq. (2.15) to (2.17), is multiplied by a series of modification factors:

Top bars with more than 12 in. of concrete below	1.4
Cover $\leq d_b$ or clear spacing $\leq 2d_b$	2.0
Lightweight aggregate, f_{ct} is specified	$0.22\sqrt{f'_c} / f_{ct} \geq 1.0$
For all-lightweight concrete, f_{ct} is not specified	1.3
For sand-lightweight concrete, f_{ct} is not specified	1.2
Epoxy-coated bars (cover less than 3db)	1.5
All other epoxy-coated bars	1.2
Bar spacing $\geq$ 6 in. and clear cover $\geq$ 3 in.	0.8
Spiral provided with diameter $\geq$ 0.25 in. and pitch $\leq$ 4 in.	0.75

Equation (2.15) is basically the same design equation provided in the ACI 318-71 Building Code for calculating development length. The differences lie in unit conversion from (psi) to (ksi) and minor rounding of coefficients. As in Eq. (2.12), a factor of 1.25 is embedded in the AASHTO equations.

CHAPTER 3
Current Use and Constraints

The advantages of precast bent cap systems compared with conventional construction were discussed in Chapter 1. Prefabrication has provided efficiency by accelerating the construction schedule for bridges, and has allowed workers to operate more safely over water and in congested urban areas. The fact that contractors have requested to use precast bent caps is also evidence that these systems enhance bridge constructability and economy.

Some of the connection details developed during research project 1748 (Matsumoto et al. 2001) are shown in Figure 3.1 through Figure 3.4. These details were important to the development of precast bent cap technology. Experimental results led to a systematic methodology for design of precast bent cap connections, which included design provisions for bars anchored in grouted ducts, grout pockets, and bolted connections. In addition, a comprehensive specification for precast bent cap connections was developed that addresses material properties, placement of caps, construction tolerances, and grouting methods. The design process for precast systems is summarized in Section 3.1.

In the last five years, a series of three important bridge projects in Texas have incorporated the recommendations from research project 1748. Precast bent caps proved to be a very efficient construction system in each of these projects. Grouted vertical ducts were used in the cap-to-column connections of these bridges. Design and construction aspects of these projects are summarized in Section 3.2.

However, many uncertainties about the behavior of grouted vertical duct connections arose during the design and construction of these bridges. Connection configurations and details used in practice were becoming more complex and had evolved beyond those developed by research project 1748 (Figure 3.3). Concern among TxDOT engineers involved in the design and construction of the new bridge projects, led to this investigation on the behavior of grouted vertical duct connections. Research needs are discussed in Section 3.3.

3.1 PRECAST BENT CAP ANALYSIS AND DESIGN PROCEDURES

A design methodology for a precast bent cap system was developed during research project 1748 (Matsumoto et al. 2001). This design procedure is summarized in Figure 3.5 and is currently used by TxDOT to design precast bent cap systems. The procedure is discussed in this section.

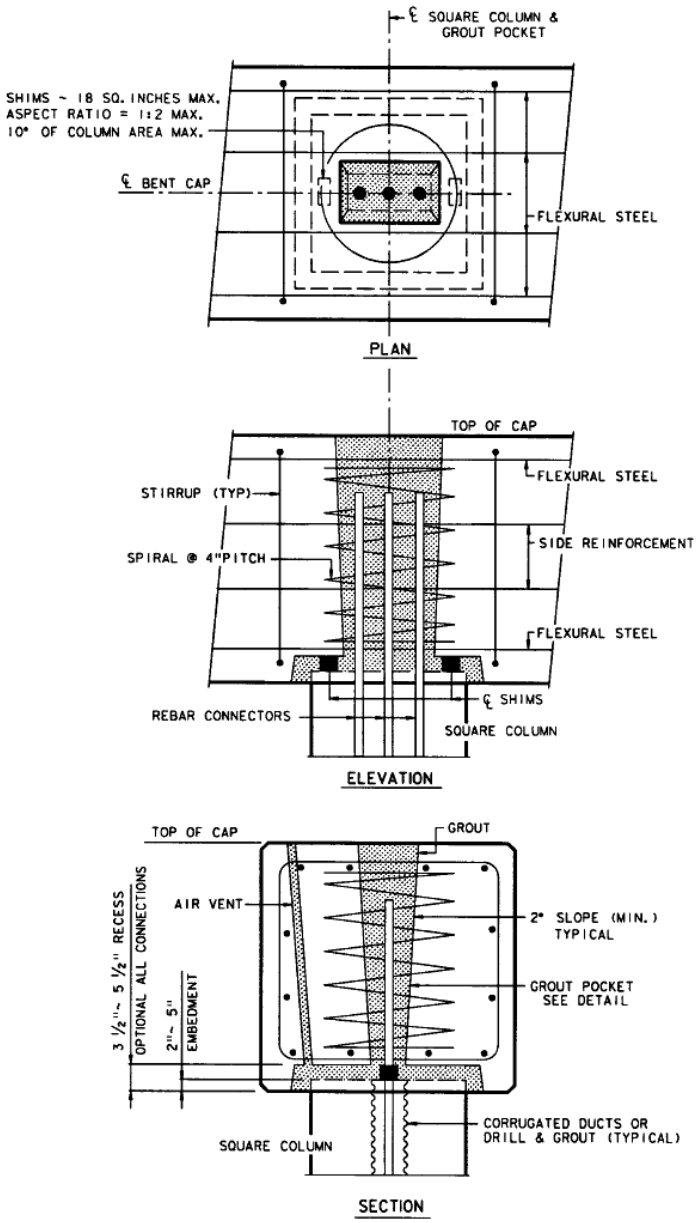

Figure 3.1 Connection Detail for Single-line Grout Pocket on Pile (Embedded Option) (Matsumoto et al. 2001)

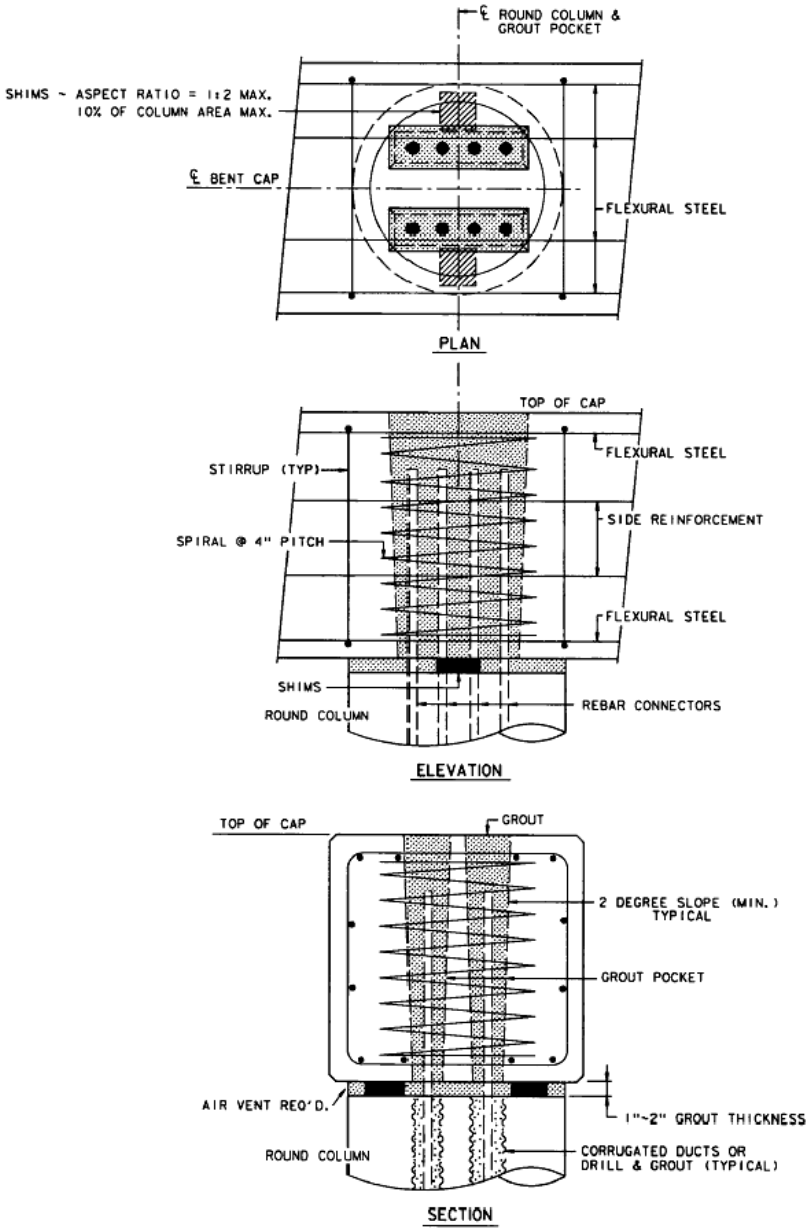

Figure 3.2 Connection Detail for Double-line Grout Pocket on Column (Surface-flush Option) (Matsumoto et al. 2001)

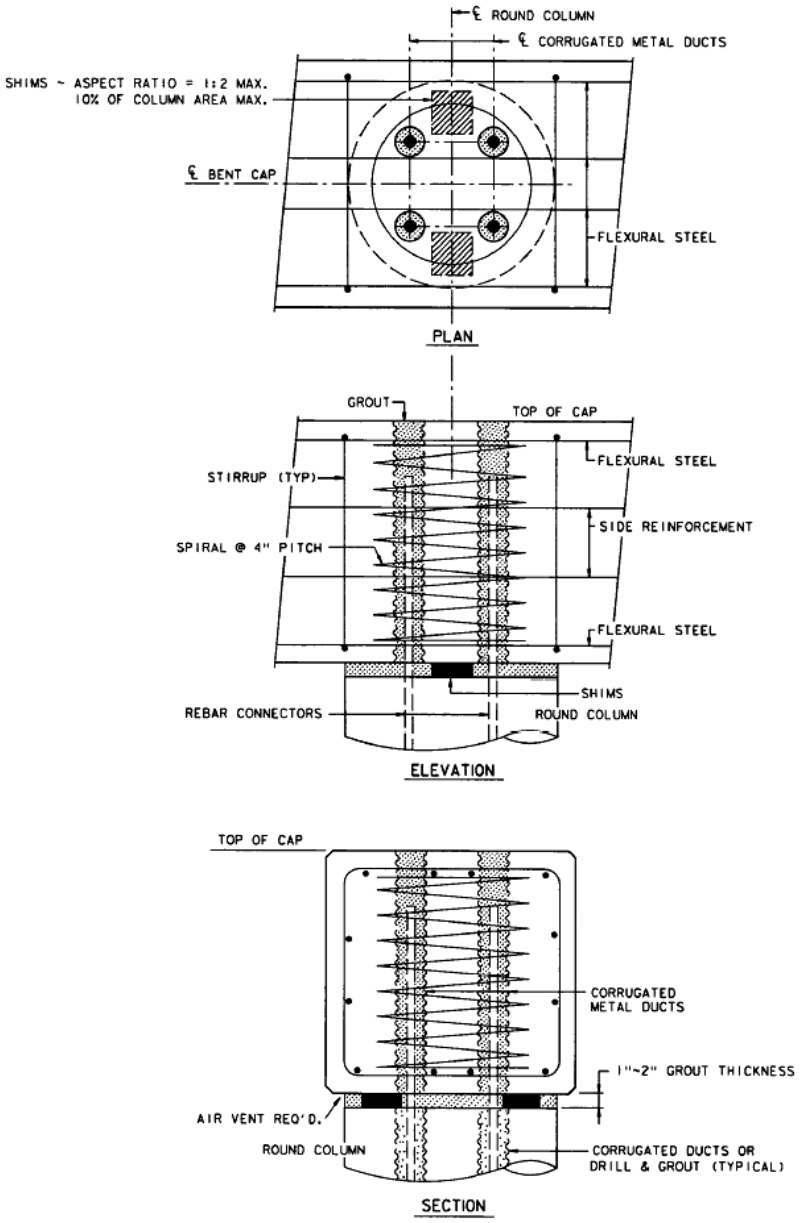

Figure 3.3 Connection Detail for Grouted Vertical Ducts on Column (Surface-flush Option) (Matsumoto et al. 2001)

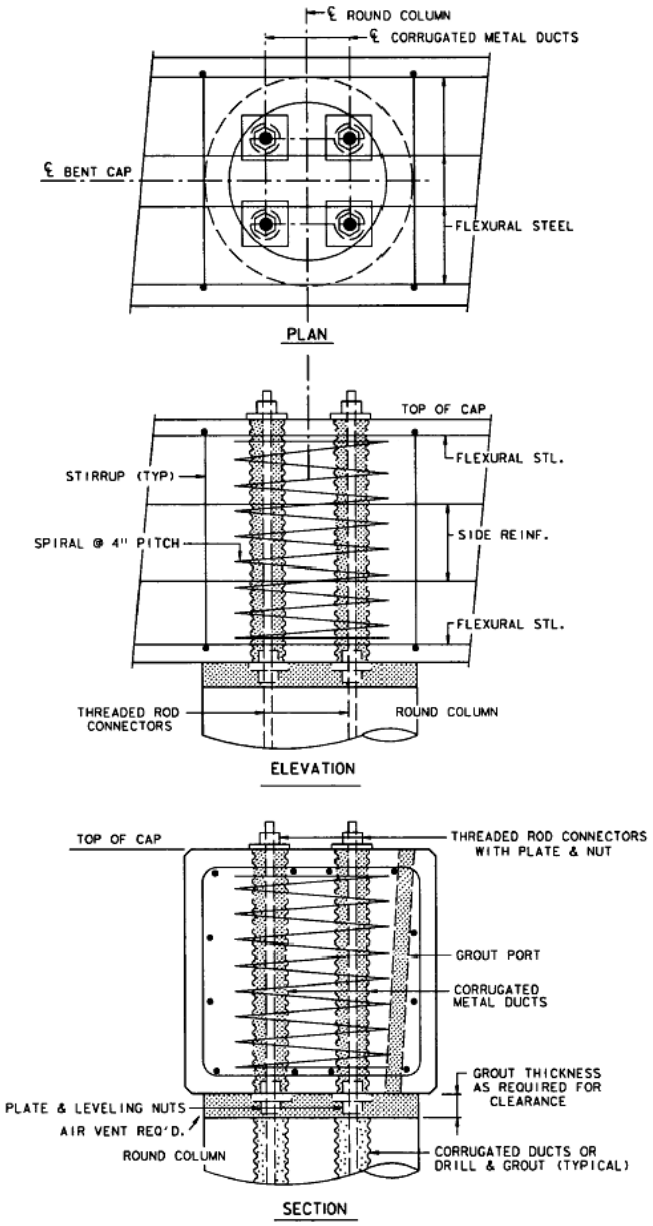

Figure 3.4 Connection Detail for Bolted Connection on Column (Surface-flush Option with Plate-and-Leveling Nut Option) (Matsumoto et al. 2001)

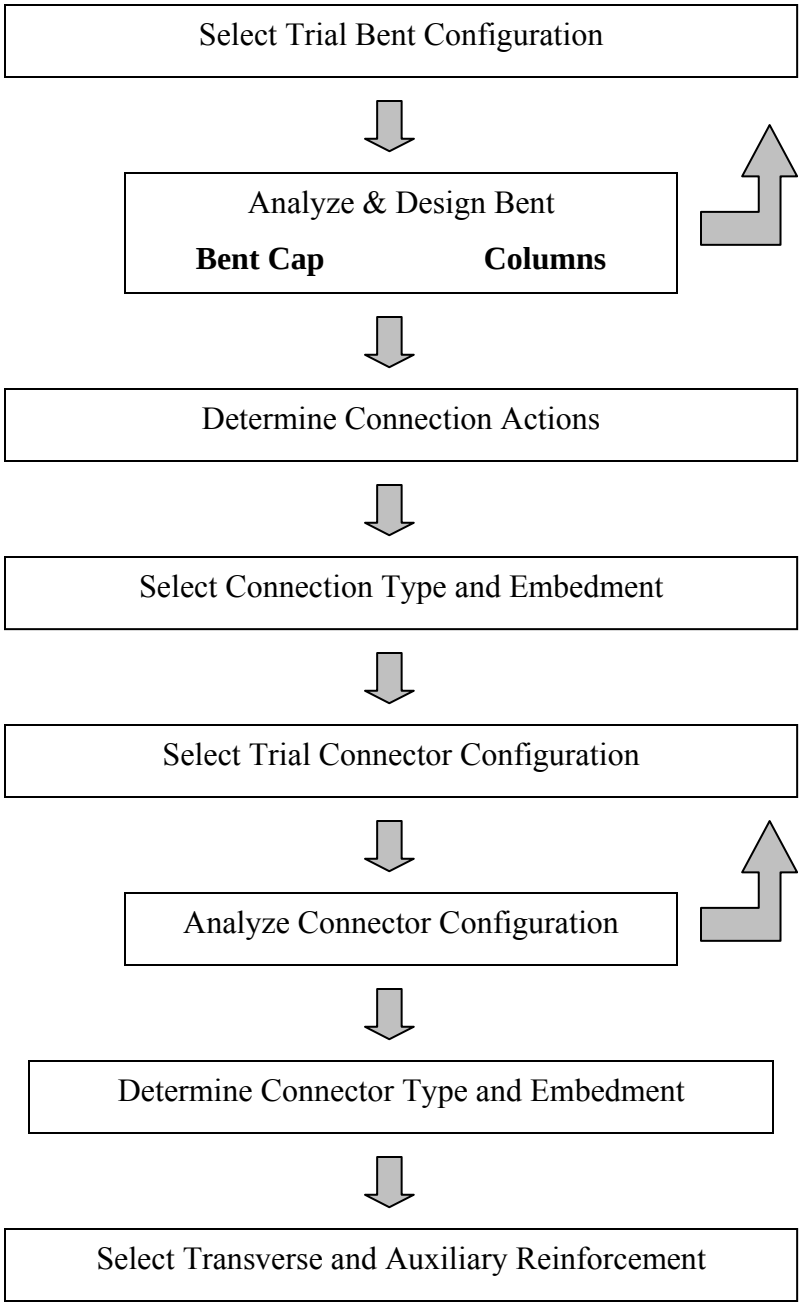

Figure 3.5 Design Flowchart for Precast Bent Cap System (Matsumoto et al. 2001)

3.1.1 Selection of Trial Bent Configuration

Short span bridges (spans less than 120 ft) comprise more than 90% of the bridges in Texas (Holt and Medlock 2004) and are ideal candidates for concrete construction. Following standard practice, TxDOT normally selects multi-column or trestle pile bents for short-span bridges. While these bent

configurations do not have a reputation for being the most visually attractive, they provide advantages such as structural redundancy and standardization. Typical bent caps used by TxDOT have rectangular or inverted-T cross-sections. Column sections may be round, rectangular, or square.

The majority of the bridges in Texas cross small streams in rural areas where aesthetics is not usually considered a priority. However, for bridges located in urban or recreational areas, TxDOT also considers aesthetics in the design. Recent projects have demonstrated that precast bent cap systems are versatile in that they can be integrated to very different bent configurations and do not limit the aesthetics of the bridge.

The process of selecting a trial bent configuration includes the selection of the cap type (cross-section), as well as the number, spacing, and size of columns or piles. Consideration is given to the characteristics of the superstructure, such as span lengths and girder type. The weight of the precast cap elements is usually high, and bent cap dimensions may be limited by crane capacities.

3.1.2 Analysis and Design of Bent

TxDOT currently designs bridges according to the AASHTO LRFD Bridge Design Specifications (2004). Dead and live loads, longitudinal forces (thermal effects, joint closing, braking), centrifugal forces, forces due to water flow (flood), wind and other lateral loads are considered at both the service and factored load levels. The design methodology does not consider seismic forces.

Differences in design for cast-in-place and precast bents concentrate on frame analysis and connection design. The effect of anchorage of connectors in a grouted connection, presence of a grouted bedding layer, and optional embedment of the column (or pile) in the cap were investigated (Matsumoto et al. 2001), and no significant differences in structural behavior versus that of a cast-in-place connection were noted. Connections of a precast bent cap system are considered to have a stiffness between that provided by a cast-in-place system (rigid) and a pinned (no rotational restraint) connection. The rotational stiffness of the connections is affected by the number and location of the connectors; a small number of connectors or a design configuration where connectors are located deep in the center of the joint results in a smaller rotational stiffness. Multi-column bents loaded in the transverse direction exhibited beam deflections within approximately 30 percent of a frame analysis assuming rigid connections (Matsumoto et al. 2001). Tests also showed that rotational stiffness depends not only on connector configuration, but also on the level of loading, and load history. The procedure suggests a simple approach where the bent is analyzed for the two limiting cases of pinned and rigid connection at the top of the column. The design of the connections is then based on the worst-case response of this frame analysis.

Caps and columns are usually considered separately in design. Bent caps are typically designed using in-house analysis programs that assume pinned connections at the top of the columns (Wolf and

Hyzak 2004). The forces in the columns in the transverse direction (relative to the bridge) are determined by the frame analysis that is also used to design the connections. In the longitudinal direction, columns are usually analyzed as having a pinned connection at the top.

3.1.3 Determination of Connection Actions

The forces acting on the connections are determined by frame analysis of the bent, considering the connection at the top of the columns to be capable of resisting moments. The load combination that controls the design consists of the most severe combination of simultaneous transverse and longitudinal actions. The factored loads acting on the connections are multiplied by a factor of 1.3, according to Section 1.3.3 of the AASHTO *LRFD Design Specifications* (2004).

3.1.4 Selection of Connection Type

The selection of the connection type is based on a series of factors, such as economics, constructability, and durability. Recent implementation of precast bent cap connections has demonstrated that grouted vertical ducts have evolved as the preferred connection type. The cost-savings offered by the reduced volume of grout used in grouted ducts compared with grout pockets, outweighs the benefits of having a simpler grouting operation. Bolted connections share the advantages provided by grouted vertical ducts and add the option of post-tensioning, which may be beneficial in some bridge applications that demand superior connection capacity to transfer large moments, or that demand a higher degree of redundancy in the connection.

The decision to embed columns (or piles) into the cap is also considered at this stage. Placing the cap surface-flush over the column simplifies the setting operations and allows for inspection of the bedding layer after the grouting operations. Embedment of the column in the cap enhances the durability of the connection by restricting the path of moisture, and also improves to some extent the rotational stiffness of the connection. Column embedment depths of 3 to 5 in. are recommended to accommodate vertical construction tolerances and to protect against corrosion in aggressive environments.

In the case of grouted vertical duct connections, the designer has the option of not continuing the ducts all the way to the top of the cap. This alleviates some of the concerns about exposure of the grout surface to the atmosphere leading to durability problems. However, in order to inspect that the grout has filled the entire height of the ducts, it may be necessary to extend a few of the ducts all the way to the top of the cap or have grout ports at the top.

3.1.5 Selection of Connector Configuration

A trial connector configuration is selected based on spacing and minimum connection reinforcement requirements. Connector and duct spacing are normally maximized to facilitate constructability and to limit splitting stresses in the concrete. Whenever possible, connectors are positioned away from the center of the joint for maximum eccentricity to resist moments.

The number, size, and yield strength of the connectors are determined by the magnitude of the loads to be resisted. As the number of connectors increase, spacing becomes more critical for construction and anchorage. Minimum clear connector spacing in grout pockets is $2d_b$. For grouted vertical ducts, a minimum clear spacing of one duct diameter is generally specified. The selection of the duct diameter must facilitate the placement of the bent cap in the field. It is recommended that duct diameters be 2 to 3 times the bar diameter and provide a horizontal tolerance of at least 1 in., although a horizontal tolerance of 1.5 in. is considered preferable.

Reinforcement crossing the joint must be at least 0.7% of the gross area of the column, or 1.0% of the gross area of the pile. To provide redundancy, a minimum of four connectors are provided in columns, while a minimum of three connectors are provided in trestle piles.

3.1.6 Analysis of Connector Configuration

The selected trial configuration is analyzed by evaluating strength and serviceability requirements. Checks at the strength limit state involve comparing the results obtained from the frame analysis (factored axial loads and moments acting in both the transverse and longitudinal directions) described in Section 3.1.3, with a design interaction diagram. Shear friction at the bedding layer and joint shear are also evaluated using the AASHTO *LRFD Design Specifications* (2004).

Checks at the service limit may include potential opening at the bedding layer, cracking in the connection region at the cap top, and deflections of the bent. The possibility of an opening at the bedding layer is conservatively estimated by establishing the location of the neutral axis for service-level load combinations; if the section analysis indicates that one or more connectors experience tension, then there is a potential for an opening to form. In cases where durability is a primary concern, such as in aggressive environments, the designer has the following options: (1) embedding the column (or pile) in the cap, (2) use of epoxy-coated connectors, (3) use of an external sealant, (4) use of water stops, and (5) post-tensioning if the connection is bolted. Control of concrete cracking in the connection area follows the provisions in Section 5.7.3.4 of the AASHTO *LRFD Design Specifications* (2004).

3.1.7 Determination of Connector Type and Embedment

Uncoated straight reinforcing bars are normally selected for bridges situated in non-corrosive environments (Wolf and Hyzak 2004); while epoxy-coated connectors are used in coastal and aggressive environments. The designer also has the option of using headed anchors to provide redundancy in the connection if the bond transfer mechanism is in question due to poor grouting operations, dynamic loads, or close connector spacing. However, constructability is impaired by the larger dimension of the head if the connectors are to be housed inside ducts. In the case of bolted connections, a large number of high-strength threaded rod systems are available that can be post-tensioned. Hooked bars or U-shaped bars can be used in grout pocket connections.

The embedment depth of connectors housed inside grout pockets and grouted vertical ducts is determined by design equations (Section 1.2), with the premise of ensuring a ductile mode of failure (yielding of the connector). There are also provisions for calculating the development length of headed bars in grout pockets. Results of this investigation will present new anchorage design provisions that take into account duct material and connector group effects.

3.1.8 Selection of Transverse Reinforcement

Transverse reinforcement in the form of spirals is specified around the connector group through the entire depth of the cap. Results of this investigation will show that the confining effect provided is insignificant in terms of improvements in strength and ductility. Spirals do however have the potential to control splitting cracks in the connection region and prevent deterioration of the joint; and designers are encouraged to use them.

3.2 CURRENT PRECAST BENT CAP CONSTRUCTION

A series of bridges have been completed in the last five years by TxDOT that have incorporated precast bent caps as part of their structure. In two of these bridges, the use of precast caps was requested by project contractors. The design and construction aspects of the Lake Ray Hubbard Bridge, the Lake Belton Bridge, and the Dallas High Five projects are described in Sections 3.2.1 to 3.2.3, respectively.

3.2.1 Lake Ray Hubbard Bridge Project

In 2000, TxDOT began replacement of the narrow two-lane crossing of SH 66 over Lake Ray Hubbard. The replacement of the 40 year-old bridge was necessary because it had become a congested route for commuters living in the suburbs east of Dallas (Medlock et al. 2002). The new crossing consists of a pair of bridges with conventional multi-column bents that support prestressed I-girders. Bridge lengths are 10,280 ft for the westbound structure, and 4,360 ft for the eastbound structure, and typical

span lengths are 100 ft. The project called for phased construction, which allowed the original structure to remain operational as the westbound replacement bridge was being built next to it. Traffic was then shifted to the completed westbound bridge, as construction of the eastbound bridge ensued following the removal of the original structure.

Three-column bents supported on drilled shaft foundations make up the substructure system of the replacement bridge. At the initial stages of the project, all substructure elements were constructed using cast-in-place concrete. However, before beginning construction of the westbound bridge, the contractor asked TxDOT for permission to use precast bent caps in order to accelerate construction, avoid the difficulties of handling formwork and materials over water, and to minimize exposure of the workers to power lines that were located very close to the site (Medlock et al. 2002, Freeby et al. 2003). Figure 3.6 shows a photograph of the construction site. The initial precast bent cap design by TxDOT involved a grout void connection detail. Although this detail facilitated construction tolerances, the amount of grout needed for completing the connections was cost prohibitive. TxDOT then designed a connection detail that would utilize grouted vertical ducts instead of grout pockets (Figure 3.7). This change in design led to a 60% reduction in the volume of grout needed (Freeby et al. 2003).

Figure 3.6 Lake Ray Hubbard Bridge Construction Site (Friggle 2002)

Figure 3.7 Lake Ray Hubbard Bridge Project

The final precast bent cap connection detail consisted of six #11 straight reinforcing bars, each housed inside a 4-in. diameter duct. Spiral reinforcement was provided around the connector group to control cracking and enhance ductility. Clear spacing between ducts was 4 in. (or one duct-diameter spacing) in the longitudinal direction of the cap. A photograph of a bent cap connection zone under construction is shown in Figure 3.8.

The contractor asked TxDOT for authorization to use plastic (polyethylene) ducts instead of the galvanized steel ducts that were specified in the design plans. The change in duct material was approved by TxDOT based on information supplied by the duct manufacturer regarding bond properties of the plastic ducts in prestressing applications. While there may be similarities between a reinforcing bar grouted in a duct and a grouted tendon, test data are required to assess the behavior of reinforcing bars grouted in plastic ducts. Because such test data were not available at the time, TxDOT designed the connections conservatively, assuming a reduced bond strength (Hyzak 2002).

The use of plastic ducts instead of galvanized steel ducts was considered beneficial to the bridge because of the enhanced durability. Constructability also improved because plastic is easier to cut in the field and is safer for workers to handle (no sharp edges).

Figure 3.8 Bent Cap Connection Zone under Construction

Drilled shaft and column construction were conducted while bent caps were being constructed at a casting yard setup at the eastern end of the bridge. Templates were used at the top of the columns during casting to position the connectors properly to match the sleeves formed in the bent cap element. Bent caps were loaded onto barges and transported for erection. Figure 3.9 shows a bent cap being hoisted for placement on top of the columns. Friction collars were placed on the columns to provide temporary support for the cap during the placement and grading operations. Grout was pumped from the bedding layer into each connection; three vents were provided in the forms of the bedding layer to ensure a successful grouting operation. Flow of grout up the ducts was monitored from the top.

The decision to precast the caps shortened the construction schedule by approximately six months. Most of the time saved was related to bent cap curing time, which was removed from the critical path (Friggle 2002). The safety of the workers was improved because most of the work associated with the construction of the caps was performed in a controlled environment on the ground instead of over water.

Figure 3.9 Bent Cap Placement Operations

3.2.2 Lake Belton Bridge Project

The replacement of the 50-year old two-lane crossing of SH 36 over Lake Belton began in the fall of 2002. The original 3,840 ft-long structure had numerous problems, including a deteriorated superstructure, a narrow width of only 26 ft, and railing damage. The new twin bridge structure incorporated two additional lanes of traffic, which increased the total roadway width to 84 ft. Prestressed U-beams make up the superstructure of the bridges; typical span lengths are 120 ft. The substructure of each bridge consists of twin, cast-in-place, round columns that support a massive hammerhead bent cap. Figure 3.10 shows a photograph of the bridge in an advanced stage of construction. A total of 62 identical caps were precast for this project.

Surface elevations fluctuate significantly in Lake Belton because it is a flood-control reservoir. The bridge needed to be constructed nearly 50 ft over the normal lake elevation to allow for these water level fluctuations (Freeby et al. 2003, Hyzak 2003). The lake is also a source of drinking water for the population of Waco, and environmental concerns favored precast instead of cast-in-place construction. TxDOT decided not to precast the columns of these bridges due to concerns about the performance of the column joints underwater. However, precasting of the bent caps was considered advantageous due to the large number of identical caps needed, the high construction elevations demanded by the site, and the higher quality control provided by prefabrication.

Figure 3.10 Construction of the Lake Belton Bridge

Lake Belton is a body of water that is used extensively for recreation. In the substructure design, the bridge incorporated aesthetics by emulating a single- pylon structure, with a stylized bent cap at the top. The caps vary in depth from 5'-6" at the middle to 3'-0" at the edge of the cantilevers. At the top, the caps measure 5'-6" in width, while at the bottom, the width reduces to 5'0". Figure 3.11 shows a cross section of the cap including the arrangement of reinforcement.

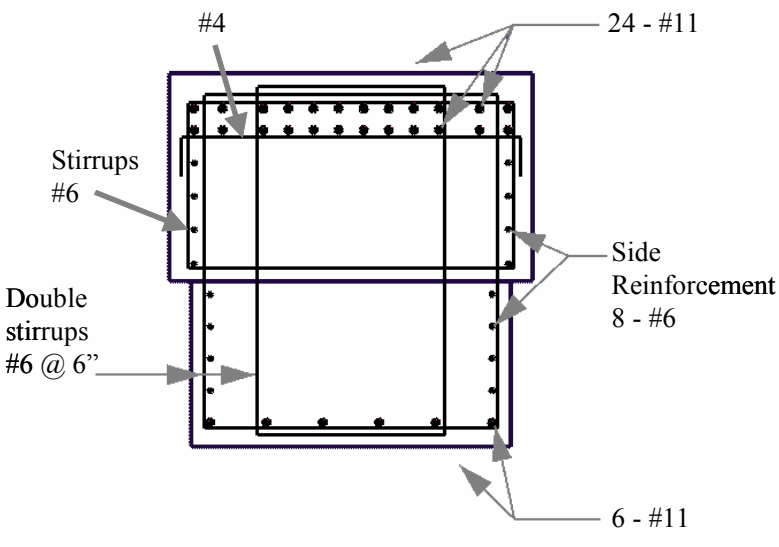

Figure 3.11 Bent Cap Reinforcement Scheme (Hyzak 2003)

Figure 3.12 Lake Belton Bridge Project

Each of the two connection zones (one for each column) involved the anchorage of fourteen #11 Grade 60 reinforcing bars in 4.5 in. diameter galvanized steel ducts (Figure 3.12). The connectors were embedded 4'-2" into the cap, and the ducts that housed them did not extend to the top of the cap. Discontinuing the ducts prevented interference with the negative moment reinforcement in the cap and also limited the area of grout that was exposed to the atmosphere.

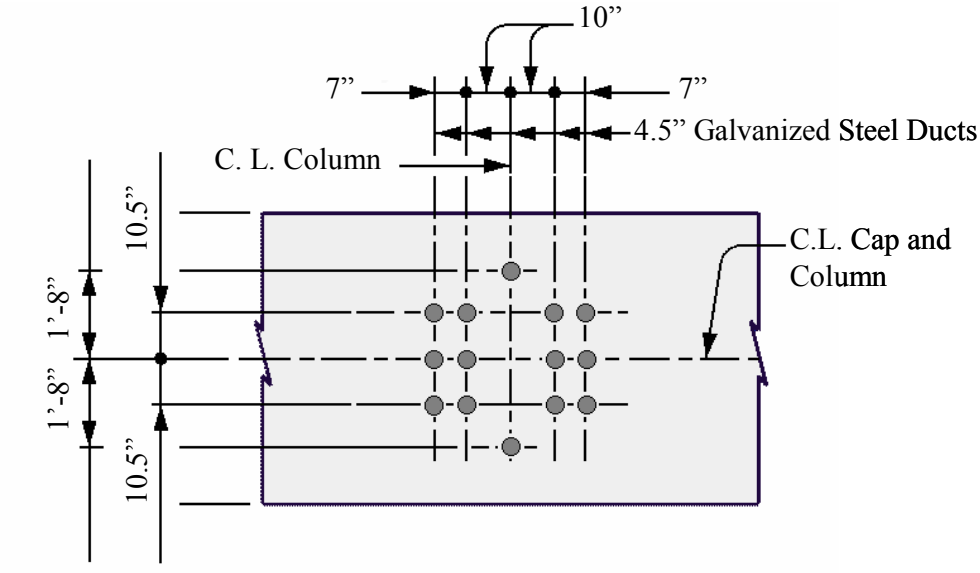

Figure 3.13 Bent Cap Connection Zone Detail (Hyzak 2003)

Two of the connectors (those closest to the sides of the cap) and their associated ducts extended all the way to the top of the cap (Figure 3.13). These connectors were plate anchored at the top to provide provisional support to the cap until grouting of the connections. The ducts that extended the full height of the cap aided in the inspection of the grout filling the ducts. Injection and vent ports for grout were provided in each duct to ensure adequate grouting and venting of the connections.

Each of the precast caps weighed approximately 75 kips. The caps were transported by truck from a precasting yard located 140 miles south of the construction site. After arriving at the site, caps were mounted on a barge with an integrated the crane used for lifting and placing the caps (Figure 3.14). A 2-in. thick bedding layer was formed between the cap and the columns that included dry-pack grout placed in the periphery of the connection zones. The bedding layer and the ducts were then filled with grout that was pumped at high pressure from below.

Figure 3.14 Bent Cap Placement Operation with Barge-mounted Crane

The final bent configuration posed many potential design problems for a precast bent cap connection. There was a question of how much tension would be developed in the connectors due to unbalanced moments. Although post-tensioning was an option, the top portion of the cap was congested with negative moment longitudinal reinforcement making it very difficult to provide suitable anchorage regions (Freeby et al. 2003). Analysis showed that the connectors could experience low levels of tension (around 7 ksi) under some load combinations, but not to the point where post-tensioning was considered necessary (Hyzak 2003).

3.2.3 Dallas High Five Project

The Dallas High Five Interchange project (Figure 3.15) at the intersection of Interstate Highway 635 and U.S. 75 was begun in 2001. The estimated cost of this project is $260 million and it represents the largest single contract ever awarded by TxDOT. The original design of the ramp structures involved cast-in-place construction, and included in the superstructure a combination of post-tensioned segmental trapezoidal beams and U-beams supported on single column bents. The giant interchange comprises five stacked levels of roadway and ramps, which required workers to erect formwork, and place steel rebar and concrete as high as 80 ft in the air (Figure 3.16). Shortly after the beginning of the project, the contractor requested using precast bent caps to accelerate construction and reduce lane closures. Precasting the caps on the ground allowed working crews to operate in a safe and controlled environment.

Caps were fabricated on the construction site (Figure 3.17). A typical detail of the inverted-T cap cross section is shown in Figure 3.18. A total of 18 - #11 bars (approximately 60% of the longitudinal reinforcing steel in the column) extended beyond the column and were grouted in the corrugated steel ducts provided in the caps. Ducts were located in the stem and in both ledges of each cap. Column bars that were anchored in the ledge regions of the cap had a short embedment length of around 18 in. ($13d_b$ for a #11 bar). Connections (bedding layer and ducts) were pressure grouted from the ground (Figure 3.19). Four threaded bars anchored at the top of the cap provided support during grouting operations. Except for those ducts housing the erection bolts, all other ducts were terminated before reaching the top surface of the cap.

Figure 3.15 Aerial View of Dallas High Five Interchange Construction Site

Figure 3.16 Tall Single Column Bent

Original estimates of construction time for the project indicated that completion would be achieved in 2007. At the time of this writing, the project seems to be ahead of schedule.

Figure 3.17 Placement of Bent Cap Reinforcement and Ducts

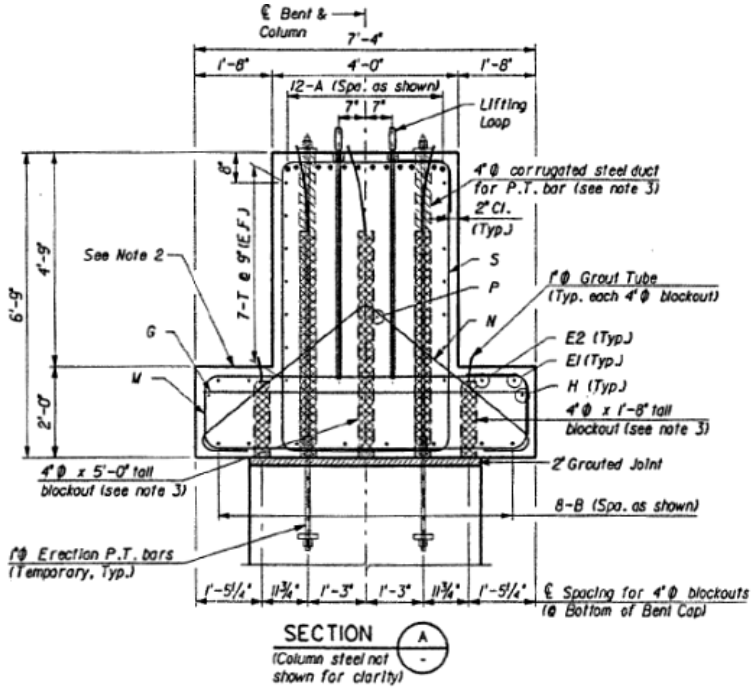

Figure 3.18 Detail of Bent Cap Cross Section

Figure 3.19 Dallas High Five Project

3.3 LIMITATIONS AND NEED FOR RESEARCH

Section 3.2 presented the design and construction aspects of three bridges in Texas that have incorporated precast bent caps with grouted vertical ducts. Many uncertainties arose regarding the behavior of grouted vertical duct connections during the design and construction of these bridges. The connection configurations and details that are currently being used have evolved from those developed by research project 1748 (Matsumoto et al. 2001). Original recommendations for design were based on the anchorage of single epoxy-coated connectors embedded in galvanized steel ducts. In light of recent construction experience, these recommendations need to be re-evaluated and extended to take into account the effects of multiple closely-spaced connectors and plastic duct material.

As a general trend, designers select large-diameter connectors, such as #11 bars, to minimize the number of connectors crossing the cap to column joint. Often, these connectors are placed very close to each other (duct clear spacing of one duct diameter or less) in order to avoid interference with cap reinforcement or due to restrictions imposed by the column section below on the embedment location of the connectors. Information about the interaction (group effects) among closely-spaced connectors is needed in order to evaluate anchorage strength.

Contractor-driven construction modifications aimed to increase bridge durability, such as replacing galvanized steel ducts with plastic ducts in the connections, raised additional concerns regarding the performance of the connections. Motivation for the use of plastic ducts stems in part from research conducted at the University of Texas at Austin (Salas et al. 2003). Long-term exposure tests of post-tensioned beams revealed serious durability problems associated with galvanized steel ducts. Forensic investigation of beams subjected to conditions representing aggressive environments indicated that the presence of grout voids was detrimental to the durability of the ducts; bleed water voids were observed in ducts even after high-quality grouting procedures. Use of galvanized steel ducts in aggressive environments was strongly discouraged. The use of plastic ducts instead of galvanized steel ducts requires investigation of the bond between the duct and the grout, and the concrete. The confinement provided by the duct to the grout is dependent on the stiffness of the duct material. Tests must be performed in order to establish required anchorage lengths for connectors embedded inside plastic ducts.

Demand for precast bent caps is expected to increase as TxDOT continues to incorporate rapid construction techniques as an option to conventional construction in upcoming projects. Precast bent cap technology is reaching the levels of maturity necessary for implementation in a standardized format in new bridge designs, and contractors now have an option of selecting a precast bent cap alternative over conventional cast-in-place construction. Design recommendations developed through experimental investigation and updated to reflect current construction practices are necessary to clarify the uncertainties that are causing concern to those involved in the design and construction of these systems.

CHAPTER 4
Overview of Experimental Program

An experimental program was developed to examine the behavior of precast bent cap connections constructed using grouted vertical ducts. A number of parameters that affect the behavior of these connections were identified and are described in Section 4.1. The limitation on the number of tests that could be performed did not allow for an experimental investigation of all parameters originally considered. Thus, the most important of these parameters were selected for investigation, based on their expected influence on behavior of the bent cap system and on current design configurations and probable future use.

The materials and dimensions of the test specimens were selected to represent those in prototype bent cap connections. The construction of the test specimens in discussed in Section 4.2 and the measured material properties are summarized in Section 4.3. The testing program is outlined in Section 4.4.

4.1 TEST PARAMETERS

The use of grouted vertical duct connections in precast bent cap systems provides a large number of options to the designer. Many connector configurations are possible, sometimes involving closely-spaced ducts. In order to obtain a connection that is more resistant to corrosion, the designer also has the option of using epoxy-coated connectors and/or plastic ducts. The design flexibility inherent in these connections led to a substantial number of parameters that were studied in the experimental program.

A testing program was developed to collect as much data as possible and obtain a better understanding about the behavior of these connections. Based on issues that were raised by TxDOT during construction of precast bent caps, a list of parameters to be studied was created. Due to the size of test specimens, the practical limitation on the number of tests that could be conducted during this investigation led to reducing the list of main parameters that were investigated experimentally. Identification of the main parameters was based on three considerations: the uncertainty associated with each parameter, the expected impact on behavior and durability of the bent cap, and the relation to current and future design practices.

Although none of the main parameters had been studied previously in the laboratory, some parameters were expected to have a greater influence on the bent cap behavior than others. For example, duct material and group effects were expected to impact connection behavior more than connector diameter and the ratio of duct diameter to connector diameter. Each of the main parameters is described

in the following sections. The parameters that were not selected to be evaluated experimentally are summarized in Section 4.1.7. Number 11 deformed reinforcing bars were used as the connectors in all test specimens.

4.1.1 Bar Coating

ACI 318 (2005) requires that the development length of epoxy-coated reinforcing bars be increased from 20 to 50 percent relative to uncoated bars due to a lack of adhesion and reduced friction between the bar and the concrete. The smaller increase of 20% can be used when the cover and spacing between bars is large, thereby precluding a splitting failure. The AASHTO LRFD Bridge Design Specifications (2004) uses the same modification factors. To explore the effect of coating on connector behavior, comparison tests were conducted using both epoxy-coated bars, and uncoated bars.

4.1.2 Duct Material

The duct material that is typically used in grouted vertical duct connections is the same as is used for post-tensioning applications. The ducts are inexpensive and readily available, they form a stay-in-place sleeve in the bent cap to house the connectors, and they come in a variety of sizes and corrugation patterns. Typically, these ducts are made of galvanized steel or from plastic materials like polyethylene or polypropylene. The main functions of the duct are to serve as a sleeve for the connector and to permit the transfer of forces within the connection. From a structural point of view, the galvanized steel duct was expected to perform better than the plastic ducts, due to adhesion and enhanced friction or mechanical interlock between the duct and both the surrounding concrete and the grout. Previous research by Matsumoto et al. (2001) investigated the performance of grouted vertical connectors in galvanized steel ducts. Since that research was conducted, there has been an increased interest in the use of plastic duct materials to inhibit corrosion in the connection.

A large portion of the testing program dealt with comparing the performance of connections configured with different duct materials. Three different duct types were selected for the investigation. The first type was made of a corrugated galvanized strip steel material conforming to ASTM A653 with a 26-gage thickness (Figure 4.1). The other two duct types were made from different plastic materials: one was made of high-density polyethylene (Figure 4.2), and the other was made of polypropylene (Figure 4.3). Because the bond transfer mechanism between the plastic duct and the concrete/grout depends mainly on friction and mechanical interlock, the influence of the rib pattern on behavior can be of great consequence. Only duct with a 4-in. nominal diameter was used in the tests. The geometric properties of each type of duct are summarized in Table 4.1.

Figure 4.1 Corrugated Galvanized Steel Duct

Figure 4.2 Corrugated High-Density Polyethylene Duct

Figure 4.3 Corrugated Polypropylene Duct

Table 4.1 Duct Dimensions

	Galvanized Steel	HD Polyethylene	Polypropylene
Internal Diameter (in.)	3.97	3.94	3.94
Wall Thickness (in.)	0.018	0.118	0.118
Corrugation Height (in.)	0.12	0.20	0.20
Rib Spacing (in.)	0.85	2.36	1.55

4.1.3 Embedment Depth

The capacity and failure mode of a connector are largely determined by the length of embedment. In general, deep embedment depths will produce a ductile mode of failure, while reduced ductility and lower capacities are expected from shallow embedment depths. A main objective of this investigation was to correlate connection performance with variation in the embedment depth of the connectors, given a particular connection configuration.

Initially, shallow embedment depths were explored in single-connector tests in order to establish the different failure modes characteristic of these types of connections. As testing progressed, and tests involved more than one connector, the embedment depth was increased, and other modes of failure were observed. The three different embedment depths selected were 8, 12, and 16 times the connector diameter ($8d_b$, $12d_b$, and $16d_b$).

4.1.4 Group Effects

Tests involving single connectors are acceptable to obtain general information about modes of failure, and for studying the effects of changes in parameters like bar coating or duct material. However, actual connections are constructed using more than one connector, and it is likely that in a precast bent cap connection at least two of the connectors could experience some level of tension at the same time. Moreover, the arrangement of connectors in actual connection designs is such that the spacing between them is relatively small, and some level of interaction is expected.

Tests consisting of multiple connectors had either two or three bars acting in tension simultaneously. Typically, the connectors were embedded $12d_b$ or $16d_b$ in these tests.

Precast bent cap connections are currently being designed in Texas using grouted vertical ducts with connectors positioned in close proximity to each other. The clear spacing between the ducts is often equal to the diameter of the duct. To explore the effect of connector spacing, duct clear spacing from one to two duct diameters was examined. For the 4-in. nominal diameter of the ducts used, this meant center-to-center distances between the connectors of 8 and 12 in.

Figure 4.4 Observed Alignment of Connectors – Lake Belton Bridge Project

4.1.5 Bar Eccentricity

The eccentric placement of connectors inside the duct was considered a main parameter for this investigation after observations of final bent cap placements in the field showed that connectors often made contact with the sides of the ducts. This issue caused concern to the engineers working on the Lake Belton Bridge Project. This situation can occur due to improper alignment of the connectors extending out of the column section, out-of-straightness of the reinforcing bars, or lack of a suitable connector template. A photograph of one of the connections at the Lake Belton Bridge (Figure 4.4) illustrates this situation.

4.1.6 Transverse Reinforcement

As discussed in Chapter 2, anchorage tests have shown that transverse reinforcement can increase the bond strength between reinforcing bars and surrounding concrete. In the case of a connector acting in tension, transverse reinforcement can increase bond strength by containing radial splitting and sustaining friction between the connector and the concrete. Confinement in a grouted vertical duct connection can have many sources. It can be a local passive form of confinement, like the type a duct provides to the connector and grout system, or it can be a global passive form of confinement like that provided by bent cap reinforcement. Active confinement can also be present in the form of a large compression field near the connection caused by a column or beam reaction. The effect of providing transverse reinforcement in the form of spirals around individual ducts was explored to study local confinement effects. In a similar fashion, the contrasting effect of providing a large spiral around the entire connection was also evaluated.

4.1.7 Other Parameters

Some parameters that were not considered in this experimental program but may influence the behavior of grouted vertical duct connections are described below.

4.1.7.1 Connector Type

The connector type may influence the behavior of a grouted vertical duct connection significantly. For example, a shallower embedment depth can be used with a headed connector compared with a straight connector. Headed connectors are seldom considered for use in these connections for two reasons: (1) unit costs are higher; and (2) the enlarged head reduces construction tolerances and may interfere with the inside surfaces of the ducts. Furthermore, although the use of headed connectors at a shallow embedment may increase the connection capacity substantially, tests by Matsumoto et al. (2001) indicated that their use at a deep embedment does not produce significant increases in capacity.

4.1.7.2 Connector Diameter

The connectors that are normally used in grouted vertical duct connections are large-diameter reinforcing bars, typically #11 bars. This is because the designer typically selects a reinforcement configuration that has a small number of connectors in order to minimize the amount of grout used in the connection and the interference of the vertical ducts with the reinforcement in the bent cap. It is expected that bars as small as #9 may be used in these connections, and it is possible that bars as large as #14 may be used for some large bridge applications. In this investigation, only #11 reinforcing bars were used as connectors.

Differences in bond behavior may be observed for connectors with different diameters, but given the small range of connector diameters that will probably be used in these connections; the differences in behavior are anticipated to be small.

4.1.7.3 Ratio of Duct Diameter to Connector Diameter

The selection of the diameter of the ducts used in a particular grouted vertical duct connection is controlled by construction tolerances and by interference with bent cap reinforcement. An efficient design would use the smallest-diameter duct that would accommodate the connector to reduce the amount of grout needed in the connection and minimize reinforcement congestion. However, the selection of the duct diameter must also allow for adequate tolerance to facilitate the placement of the bent cap in the field. Matsumoto et. al. (2001) recommended that duct diameters be 2 to 3 times the bar diameter and provide a horizontal tolerance of at least 1 in., although a horizontal tolerance of 1.5 in. was considered preferable.

Recent implementation of grouted vertical duct connections in the field has demonstrated that a clearance of at least 1 in. may be sufficient for jobs with a small number of connectors per connection, but that a 1.5-in. tolerance should be used when the number of connectors is large, such as the Lake Belton Bridge. Connections consisting of four or six connectors would be classified as having a small number of connectors.

Given the range of bar diameters used in grouted vertical duct connections, and with allowance for these minimal horizontal tolerances, it is expected that the ratio of duct diameter to connector diameter will vary between 2.66 and 3.15, as illustrated in Table 4.2. During this investigation, the value was maintained at 2.84, because only #11 reinforcing bars were used as connectors, and the duct size of 4 in. was used for all tests. Small differences in bond behavior are expected with variations of this parameter.

Table 4.2 Ideal Combinations of Connectors and Ducts

Bar Size	**#9**	**#10**	**#11**	**#14**
Bar Diameter (in.), d_b	1.128	1.270	1.410	1.693
Minimum duct diameter, d_b + 2”	3.128	3.270	3.410	3.693
Target duct diameter, d_b + 3”	4.128	4.270	4.410	4.693
Selected Duct Diameter, D	3.5″	4″	4″	4.5″
D/d_b	**3.10**	**3.15**	**2.84**	**2.66**

4.1.7.4 Grout Type

The choice of grout type could have a significant influence on the behavior of grouted vertical duct connections. However, the grouts that are typically specified by TxDOT for precast connections are based on the performance requirements developed during Project 1748 (Matsumoto et al. 2001). Only one type of grout was used during this experimental program, and this grout satisfies the performance requirements in Table 4.3.

4.1.7.5 Strength of Concrete

The construction of precast bent cap elements with high-strength concrete can be beneficial to the performance of grouted vertical duct connections. However, it is expected that the capacity of the connections would not increase substantially with an increase in the concrete compressive strength. One reason is that the formation of radial splitting cracks around the connectors, which limit the load transfer mechanism in these connections, depends not on the compressive properties, but on the tensile strength of the concrete. Because the tensile strength of concrete is related approximately to the square root of the compressive strength, the benefits of added strength are reduced. As a note of caution, to improve the

performance of the connection and avoid an undesired failure mode, any increase in concrete strength should be accompanied by a corresponding increase in grout strength.

Table 4.3 Grout Performance Specification (Matsumoto et al. 2001)

Property	**Values**	
Compressive strength (ASTM C-109, 2-in. cubes)	1 day 3 days 7 days 28 days	2500 psi 4000 psi 5000 psi 5800 psi
Expansion requirements (ASTM C 827 & ASTM C 1090)	Grade B or C – expansion per ASTM C 1107	
Modulus of elasticity (ASTM C-469)	$3.0\text{-}5.0 \times 10^6$ psi	
Coefficient of thermal expansion (ASTM C-531)	$3.0\text{-}10.0 \times 10^{-6}$ /ºF	
Flowability (ASTM C-939; CRD-C 611 Flow Cone)	Fluid consistency efflux time: 20-30 seconds	
Set Time (ASTM C-191)	Initial Final Work Time	3-5 hr 5-8 hr 30 min @ 80ºF
Freeze Thaw (ASTM C-666)	300 cycles, RDF 90%	
Sulfate Resistance (ASTM C-1012)	Expansion at 26 weeks < 0.1%	

4.2 SPECIMEN FABRICATION

The test specimens were designed with dimensions representative of actual dimensions within bent cap connection zones, and to provide an efficient means of testing connectors in tension. Because only the connection area of a typical bent cap was needed for the experiments, there was no need to build an entire bent cap. Instead, the test specimen consisted of a block beam that included a series of connection zones.

Specimens tested by Matsumoto et al. (2001) and bent cap elements designed for the Lake Ray Hubbard Bridge served as a benchmark for establishing the dimensions of the test specimens. The bent cap test specimens tested by Matsumoto, had a width of 2’-9” and a height of 2’-6”, with a side clear concrete cover to the ducts between 7.5 in. and 9 in. The bent caps used in the Lake Ray Hubbard Bridge (Figure 4.5) are a clear example of typical bent cap dimensions. In this case, the bent caps, which were supported on 3’-0” diameter columns, had a width of 3’-3”, and a height of 3’-3”. Based on the connection configuration, the clear cover between the side of the bent caps and the vertical ducts was 9.5 in.

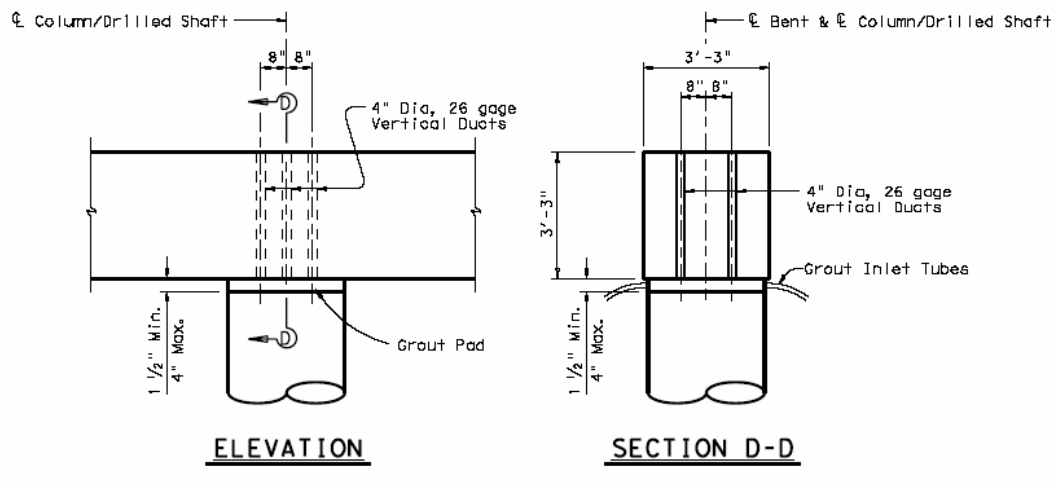

Figure 4.5 Lake Ray Hubbard Bridge Project – Connection Area Dimensions

The dimension of clear concrete side cover to the ducts is an important parameter for the design of the test specimens. A value for this side cover dimension corresponding to a lower bound for what could be expected in an actual connection was considered appropriate. The reasoning for this stemmed from the assumption that increases in side cover to the ducts would lead to enhanced bond strength due to better confinement of the connection and reduced potential for concrete splitting. The dimensions of the test specimens also needed to take into account the general connector configurations that were going to be examined during the tests. One aspect of connection details that was causing concern among designers was the close proximity of connectors in the field.

An example of this can be seen in the design of the Lake Ray Hubbard Bridge (Figure 4.6). Because this detail was typical of normal practice in current designs, the specimens were constructed with a clear spacing of one duct diameter between the ducts.

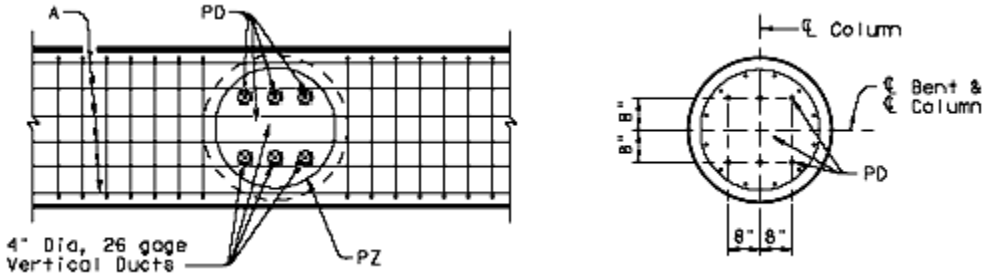

a. Connection Area (Plan) ***b. Pier/Column Section***

Figure 4.6 Lake Ray Hubbard Bridge Project – Placement of Connectors Relative to Pier Section

A square, four-duct pattern was selected as the standard for the experimental program, although a triangular arrangement was also used in the last series of tests. Constraints inherent in the test setup prevented the use of a clear spacing between the ducts in the transverse direction less than 5.5 in., which for a 4-in. diameter duct, meant that the clear spacing between ducts in the transverse direction could not be less than 1.375-duct diameters.

After processing and evaluating the requirements for dimensions of the test specimens, a square cross-section of 2'-6" was selected (Figure 4.7). This resulted in a clear concrete side cover to the ducts of 8.25 in., which is a realistic lower bound to what could be expected in an actual connection. A depth of 2'-6" was considered adequate because large-diameter connectors, like #11 reinforcing bars, could be embedded as deep as 18 d_b, which was considered sufficient during the initial planning of the testing program. The size of the connection area was somewhat smaller than that usually encountered in prototype bent caps, but deemed adequate for the purposes of the investigation.

The overall length of the beam specimens depended on the number of connection zones provided. Originally, the beam specimens were designed with three connection zones, but lifting limits on some laboratory equipment forced the specimens to have only two connection zones. The overall design length of the cap beam specimens was then 12'-0", and each had a weight of approximately 11 kip.

Reinforcement in the test specimens was designed to resist the anticipated loads during tests and prevent premature shear or bending failure of the concrete beam. Failure modes during the testing should only be related to anchorage failure or fracture of the connectors. Nonetheless, some consideration was also given to providing the connection regions of the specimens with a realistic reinforcement scheme, like that used in the Lake Ray Hubbard Bridge bent caps (Figure 4.8). To minimize the influence of the bent cap reinforcement on the connection behavior, stirrups were not placed in the immediate vicinity of the connection, and beam longitudinal reinforcement was not allowed to pass through the central portion of the connections.

The beam specimen reinforcement is shown in Figure 4.7. Longitudinal reinforcement consisted of 6-#8 reinforcing bars at both the top and bottom of the beam. Stirrups were #4 open stirrups at 6-in. spacing. Some specimens included transverse reinforcement around the ducts. Spiral reinforcement is shown in Figure 4.9. Large spirals, which surrounded groups of connectors, had a diameter of 24 in. and a pitch of 6 in.; whereas the small spirals, which surrounded individual ducts, had a diameter of 7.5 in. and a pitch of approximately 1.5 in. Bar diameters were 0.375 in. for the large spirals, and 0.25 in. for the small spirals.

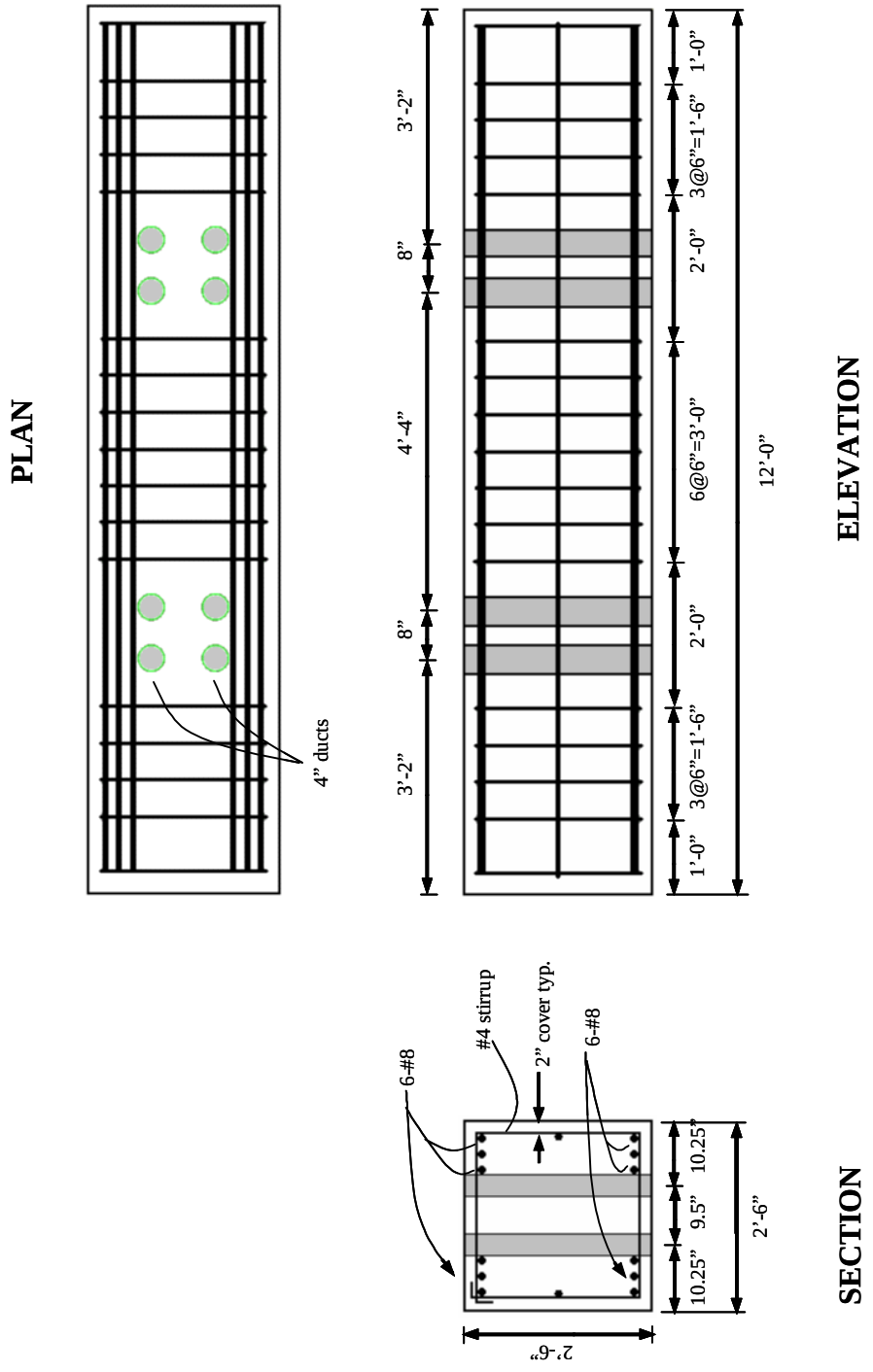

Figure 4.7 Geometry of Test Specimens

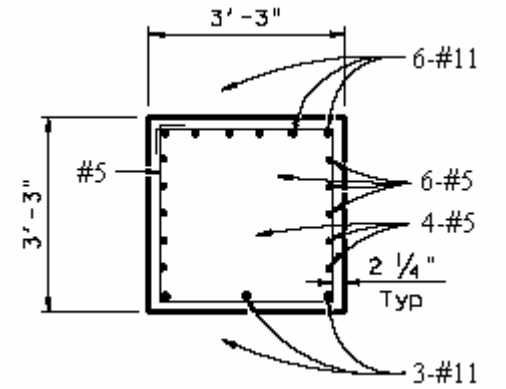

Figure 4.8 Lake Ray Hubbard Bridge Project – Bent Cap Reinforcement at Connection Zones

a. Individual Sprial ***b. Group Spiral***

Figure 4.9 Spirals Used as Transverse Reinforcement

Test specimens were constructed two at a time. After reinforcing cages were placed inside the formwork, ducts were ready to be placed. Ducts were sealed with duct tape at both ends to prevent penetration of concrete during casting. Duct locations were carefully laid out, and ducts were held in place by small, round, plywood block-outs at both ends to maintain proper alignment during concrete placement (Figure 4.10). Proper positioning and vertical alignment of ducts in the formwork was important because it ensured that the connector would be within tolerance to fit in the space allocated in the test setup.

Figure 4.10 Vertical Alignment of Ducts during Concrete Placement

The specimens were constructed using normal weight concrete. The maximum coarse aggregate size was ¾ in. A series of 6 in. by 12 in. concrete cylinders was prepared for each batch of concrete using standard procedures. Cylinders were cured in the lab in the same environment as the beam specimens. The entire concrete placement operation frequently lasted about one hour. Specimens were covered with large plastic sheets before initial set of the concrete. After initial set, wet burlap was placed between the concrete and plastic sheets and kept moist for three days.

Three or four days after concrete placement, the forms were removed, and the beams were left to gain strength for approximately two weeks (Figure 4.11). It is worth noting that at this point, a precast concrete bent cap in the field would be prepared to be hoisted and positioned into its final position on top of a bridge pier, followed by grouting operations to complete the connection. In contrast, the test specimens used in this investigation do not have accompanying piers to complete the connections. Instead, beams were moved to the testing area where they were set on neoprene pads and leveling shims on three concrete support blocks.

Individual connectors were then positioned within the ducts. The required embedment depth was measured from the top of the beam to the bottom of the connector and each connector was carefully aligned (Figure 4.12). The ducts were then filled with grout. Most of the connection zones had a square four-duct configuration, but usually, connectors were only placed in one or two of these ducts. However, all ducts were filled with grout.

Figure 4.11 Beam Specimens after Formwork Removal

The formwork required for filling the ducts with grout was simple. The bottom of the connection area was sealed with a square plywood panel, held firmly in position by a jacking device from below. At the top of the specimens, connectors were restrained and positioned using a combination of clamps, small shims, and wood blocks (Figure 4.13). Vertical alignment of the connectors was checked using surveying equipment.

Figure 4.12 Positioning and Vertical Alignment of Connectors in Preparation for Grouting Procedures

Figure 4.13 Formwork to Hold Connectors Aligned during Grouting

Only one beam was grouted at a time because the quantity of grout needed for two beams exceeded the volume capacity of the mechanical mortar mixer available in the laboratory. Grout was mixed for five minutes, and was then dumped through a 0.25-in. sieve into buckets, which were then taken to the top of the beam for placement of grout inside the ducts. Fluid consistency of the grout was also measured using a flow cone, and the temperatures of the mixing water, air, and grout after mixing were recorded.

Grout was placed using a gravity tremie-tube method. Grout was poured from buckets into large funnels, which had a 0.625 in. clear plastic hose that extended from the base of the funnel to the bottom of the duct (Figure 4.14). Ducts were thus filled from the bottom up, in a continuous, uninterrupted fashion to avoid the inclusion of air in the grout. A series of 2-in. grout cubes were also prepared. After the ducts were filled, and the grout was beginning to show signs of hardening, normally two to three hours after placement, a curing compound was applied on top of the grout surface, and wet cloth rags were then applied and kept moist for 24 hours.

Three days after grouting, grout formwork was removed and the specimen was brushed, and washed to remove dirt and grout chunks. At this point, fabrication of each specimen was complete. Generally, the grout achieved sufficient strength for testing of connections ten days after the grouting procedure.

Figure 4.14 Gravity Tremie-tube Technique to Fill Ducts with Grout

4.3 MATERIALS

The properties of the reinforcement, duct, concrete, and grout are summarized in the following sections.

4.3.1 Reinforcement

Grade 60 deformed bars, conforming to ASTM A615, were used for the connectors as well as reinforcement within the specimens. In the case of the connectors, both epoxy-coated and uncoated bars were used. The yield strength and deformation pattern differed for both types of bar. Moreover, after an initial set of tests, a discovery was made that there were two kinds of uncoated bars in the connector batch, which had different yield strengths. The deformation patterns of these two uncoated types were very similar, which lead to this fact going unnoticed at the start of the investigation. Still, in all cases it was possible to identify which type of uncoated bar was being used in each test. Measured yield and tensile stresses for the connectors are listed in Table 4.4.

Other kinds of steel reinforcement consisted of plain bars to form spirals. Grade 60 plain bars of 0.375-in. diameter were used for the large spirals that confined the entire four-duct connection zone, while smaller 0.25-in. diameter bars were used to confine individual ducts.

Table 4.4 Measured Properties of Connectors

Bar Type	Yield Stress (ksi)	Tensile Stress (ksi)
#11 Epoxy-Coated	68	102
#11 Uncoated Type I	75	106
#11 Uncoated Type II	59	95

4.3.2 Galvanized Duct

The corrugated galvanized strip steel duct used conformed to ASTM A653. All galvanized duct had a 26-gauge wall thickness (Table 4.1). Thicker duct was available, but due to the limitation on the number of tests, only the steel duct of 26-gauge wall thickness was used in the tests. It is expected that the use of steel ducts with thicker walls would lead to similar, if not better, behavior.

4.3.3 Plastic Duct

As mentioned in 4.1.2, the plastic duct material used in grouted vertical duct connections is that same material that is used in post-tensioning applications. The PTI Specification for Grouting of Post-Tensioned Structures (2001) requires that corrugated polyethylene and polypropylene ducts comply with fib technical bulletin 7: "Corrugated Plastic Ducts for Internal Bonded Post-Tensioning" (2000). Because corrugated plastic ducts are a recent innovation, products still differ widely in material properties and geometric patterns. As a result, they have not reached the level of standardization of corrugated galvanized steel ducts.

Two kinds of plastic duct were used in this investigation: one was made of high-density polyethylene, and the other was made of polypropylene. All ducts had a 4-in. nominal diameter. Corrugations for both types of ducts were circular and intermittent, as shown in Figure 4.2 and Figure 4.3. The duct made of polypropylene had an additional corrugation pattern in the longitudinal direction, designed to improve bond properties. Because the two plastic duct types have equal wall thickness, and because the tensile properties for both materials are similar, differences in behavior were expected to be due to variation in corrugation patterns. The geometric properties of the plastic ducts are summarized in Table 4.1.

4.3.4 Concrete

Concrete that was used to fabricate the test specimens was the standard TxDOT Class C mixture, with a specified compressive strength at 28 days of 3600 psi. Strength control was accomplished by testing standard 6 by 12 in. cylinders 3, 7, 14, and 28 days after casting. Cylinders were also tested on days that the specimens were tested. The average measured compressive strength of the concrete from all

batches at 28 days was 5100 psi. Additional information about the concrete is summarized in Appendix A.

4.3.5 Grout

All specimens were constructed using a high-precision, non-shrink, natural aggregate grout that meets the ASTM C 1107 Standard Specification for Grades B and C. More importantly, it also satisfies the TxDOT Grout Performance Specification (Table 4.3). The brand of grout selected for this project was also used by Matsumoto et al. (2001) in an investigation of precast bent cap systems and proved to be a very reliable material.

For the grouting operations, the water amounts used varied between 1.27 to 1.37 gallons (10.45 to 11.25 lb) of water per 55 lb bag of grout material, which were within the fluid consistency range provided by the manufacturer that would produce an efflux time of 25 to 35 sec using the ASTM C 939 flow cone standard test. Water amounts were adjusted depending on the temperature at the time of grouting. Efflux times measured using the flow cone were generally inconsistent, when compared with the amount of water in the mix or the air temperature, and were always higher than 35 sec. Table 4.6 summarizes temperature data and flow cone results for the grouting operations conducted. Even when the efflux times were high, no re-mixing or tempering of the grout was made. Strength control was accomplished by testing the ASTM C 109 standard 2-in. cubes ages of 1, 3, 7, and 28 days, as well as on test days. Following standard practice, strength data obtained from the cube tests were multiplied by a factor of 0.8 to obtain the modified grout compressive strength. The average compressive strength of the grout at 28 days was 6200 psi. Additional information about the grout is summarized in Appendix A.

4.4 OVERVIEW OF EXPERIMENTAL PROGRAM

As discussed in Chapter 1, the primary objective of the experimental program was to determine how different design parameters influenced the behavior of grouted vertical connectors. Although Matsumoto et al. (2001) had studied this type of connector, all tests were conducted using epoxy-coated connectors and galvanized steel ducts. The state of the practice in Texas has grown beyond the scope of this initial study, and additional tests were warranted.

A total of twelve beam specimens were constructed. Because the specimens were cast two at a time, the experimental program was divided into six series of tests. Each pair of specimens represented one series. An overview of the experimental program is summarized in Table 4.5. The results from each series were used to determine the experimental parameters in subsequent tests.

Table 4.5 Overview of Experimental Program

Test Parameters	Test Series					
	1	**2**	**3**	**4**	**5**	**6**
Bar Coating	X	X				
Duct Material	X	X	X	X	X	X
Embedment Depth	X		X	X	X	X
Group Effects						
Number of Connectors			X	X		X
Duct Clear Spacing					X	
Bar Eccentricity				X		
Transverse Reinforcement			X		X	

X – Parameter investigated in test series.

Three parameters were included in the first test series: connector coating, duct material, and embedded length. Only galvanized steel and high-density polyethylene ducts were used in this test series. Polypropylene duct was not introduced until the sixth series. Shallow embedded lengths of 8 and $12d_b$ were used to establish typical failure modes for the connectors. All connectors in the first series were tested individually. Multiple connectors were tested in subsequent series. Because the influence of bar coating seemed to decrease as the embedded length increased, bar coating was removed from the test matrix for subsequent test series.

The second test series focused on the influence of the duct material. All four specimens were constructed with an embedded depth of $12d_b$ and tested individually. Two of the four specimens were constructed without ducts. For these specimens, a split corrugated steel duct was cast in the beam and removed after initial set of the concrete. The grout was then poured into the void left by the duct and bonded directly to the concrete.

The third series was the first to explore the effect of multiple connectors. This series focused on double connectors embedded $16d_b$. Specimens were constructed with and without a single spiral that surrounded all four ducts in the connection zone.

The fourth and the fifth series, continued the investigation of group effects, and included respectively the parameters of bar eccentricity and local spiral reinforcement around individual plastic ducts.

Polypropylene duct was included in the sixth series. The inclusion of this third duct type resulted in a comparison of behavior between two types of plastic duct. This last series further explored the effect of multiple bars a step further by simultaneously testing three bars arranged in a triangular pattern.

The complete test matrix, including all 32 specimens, is summarized in Table 4.6. Number 11 bars were used as the connectors in all specimens.

Table 4.6 Complete Test Matrix

Connector Test	Test Series	Beam ID	Number of Connectors	Bar Coating	Duct Material	Embedded Length (d_b)	Transverse Reinforcement	Bar Eccentricity	Duct Clear Spacing (D)
1	1	1	1	Plain	Steel	8	Group	Centered	1
2	1	1	1	Epoxy	Steel	8	Group	Centered	1
3	1	1	1	Plain	Steel	12	Group	Centered	1
4	1	1	1	Epoxy	Steel	12	Group	Centered	1
5	1	2	1	Plain	PE	8	Group	Centered	1
6	1	2	1	Epoxy	PE	8	Group	Centered	1
7	1	2	1	Plain	PE	12	Group	Centered	1
8	1	2	1	Epoxy	PE	12	Group	Centered	1
9	2	3	1	Plain	PE	12	Group	Centered	1
10	2	3	1	Plain	Steel	12	Group	Centered	1
11	2	4	1	Epoxy	None	12	Group	Centered	1
12	2	4	1	Plain	None	12	Group	Centered	1
13	3	5	2	Plain	Steel	16	Group	Centered	1
14	3	5	2	Plain	PE	16	Group	Centered	1
15	3	6	2	Plain	Steel	16	None	Centered	1
16	3	6	2	Plain	PE	16	None	Centered	1
17	4	7	2	Plain	Steel	12	Group	Centered	1
18	4	7	2	Plain	PE	12	Group	Centered	1
19	4	8	1	Plain	Steel	8	Group	Eccentric	1
20	4	8	1	Plain	PE	8	Group	Eccentric	1
21	4	8	1	Plain	Steel	12	Group	Eccentric	1
22	4	8	1	Plain	PE	16	Group	Centered	1
23	5	9	2	Plain	Steel	12	Group	Centered	2
24	5	9	2	Plain	PE	16	Group	Centered	2
25	5	10	1	Plain	PE	8	Individual	Centered	1
26	5	10	2	Plain	PE	16	Individual	Centered	1
27	5	10	1	Plain	PE	12	Individual	Centered	1
28	6	11	2	Plain	PP	16	Group	Centered	1
29	6	11	1	Plain	PP	8	Group	Centered	1
30	6	11	1	Plain	PP	12	Group	Centered	1
31	6	12	3	Plain	Steel	16	None	Centered	1
32	6	12	3	Plain	PP	16	Group	Centered	1

CHAPTER 5
Experimental Setup

A precast bent cap must be designed to resist the axial forces, shears, and bending moments due to the applied loads (Figure 5.1). While it is possible to construct and test a bent cap in the laboratory under the design loads, it was decided to test the connectors under tensile loads to investigate the large number of parameters discussed in Chapter 4. The fundamental behavior of grouted vertical duct connections is centered on the bond transfer mechanism between the connector and the duct with the concrete. Thus, all of the actions that can occur simultaneously in a precast bent cap connection are resisted mainly by axial tension or compression in the connectors, and tension and compression in the surrounding concrete. Of these, the state of axial tension in the connectors is the one that is critical and warrants investigation.

A large number of tests were required to study the different combinations of the many variables considered for investigation, therefore a simple and inexpensive test setup that could be used to pull single or multiple connectors was considered appropriate for this investigation. The design of the test setup influenced the choice of instrumentation used to monitor the specimens.

The test setup is discussed in Section5.1, instrumentation is summarized in Section 5.2, and the test method is presented in Section 5.3.

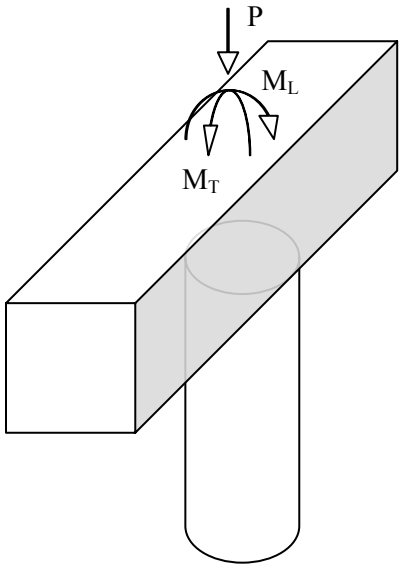

Figure 5.1 Expected Applied Loads on a Precast Bent Cap Connection

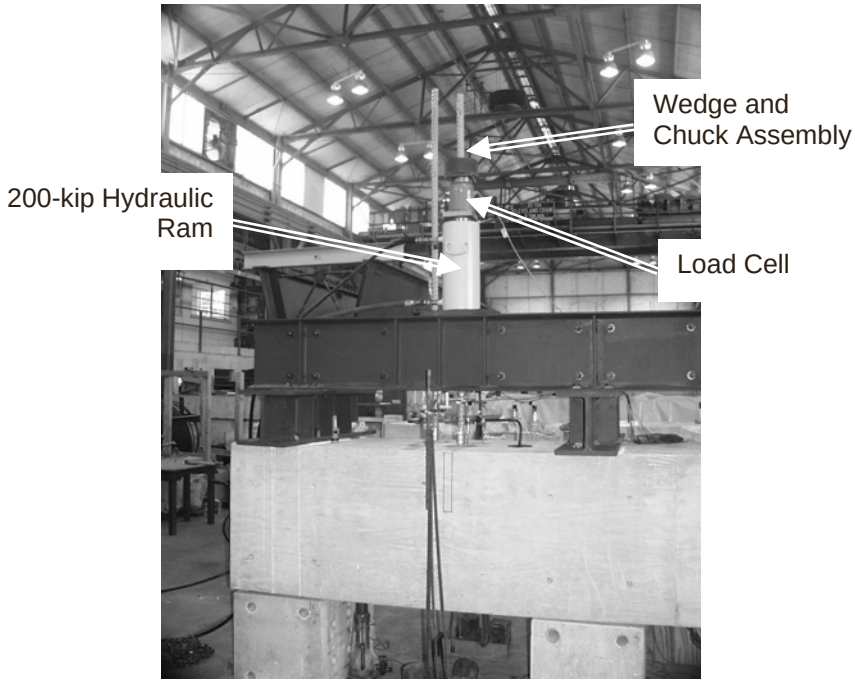

Figure 5.2 Test Setup

5.1 TEST SETUP

A photograph of the test setup selected is shown in Figure 5.2. The testing frame consisted of back-to-back C15X40 steel channels, which supported 200-kip capacity center-hole hydraulic rams, load cells, and wedge and chuck assemblies. The channels were bolted together with a 2-in. gap between them. The connectors, already embedded in the concrete specimens, extended between the channels. Three short wide-flange cross beams provided support for the channels, and transferred the loads to the concrete test specimen below. These crossbeams were bolted to both the back-to-back channels, and to the concrete beam for stability purposes. The concrete beam specimens rested on neoprene pads supported by three large concrete blocks, which provided space underneath the specimens for attaching the instrumentation needed to measure the connector end displacement and the beam deflection.

The test setup was arranged so that the bent cap connections were tested in an inverted position. Because the test specimens did not include a bridge pier element, forces acting in the connection were applied by pulling on the connectors. Tension forces in the connectors were then counteracted by reaction forces of the testing frame on the concrete beam specimens. A self-equilibrating force system was thus attained, which meant that attachment of the test setup to the laboratory floor was not required.

The test setup selected for conducting this investigation had these three main advantages: (1) it was simple and self-equilibrating, (2) it was versatile for testing various configurations of connectors with almost no modification, and (3) its testing frame was easy to mount and dismount from one test specimen

to the next providing test speed and efficiency. Furthermore, the test setup could be used with confidence, because similar test assemblies have been used successfully in the past for bar pullout tests.

As described in Chapter 4, every beam specimen had two connection zones. Typically, each connection zone accommodated four ducts in a square configuration. The initial series of testing involved many single connector tests with shallow embedment. In order to maximize the number of tests per beam specimen, two single connectors were tested within the same connection zone, with the test bars positioned in diagonally opposite corners. The results of these initial tests were later compared with the results of tests involving only a single connector per connection zone.

The interaction among multiple connectors was also an important experimental variable during the experiments. Connections containing two and three connectors were also tested. For tests involving two connectors, one set of back-to-back channels was used as the loading frame, because the connectors were oriented to represent a longitudinal moment (in the direction of the bridge) configuration. Double-connector tests representing a transverse moment configuration were not conducted because it was believed that the formation of splitting cracks for this configuration would cause smaller disturbances in the load transfer region than would the longitudinal moment arrangement. During the last phase of testing, three connectors were tested in a triangular configuration. A second set of back-to-back steel channels was used to apply load to the third bar. Figure 5.3 shows the configurations of the different connector arrangements used in the testing program.

The test setup proved to be a very efficient method of applying tensile loads during the experimental program. The only limitation was the minimum spacing of the connectors. The diameter of the hydraulic rams limited the minimum spacing of the connectors to 8 in., or a duct clear spacing of one duct diameter.

Although this test setup did not reproduce the typical state of stress expected in precast bent cap connections, it did produce a conservative load scenario where the connection experiences axial tension. In an actual connection, axial compression is expected to dominate. If tension is experienced by the connectors due to applied moments, the accompanying compression field in the connection provides a confinement effect, which would increase the capacity of the connector. Additionally, the pier would provide additional confinement that would increase the connector capacity further.

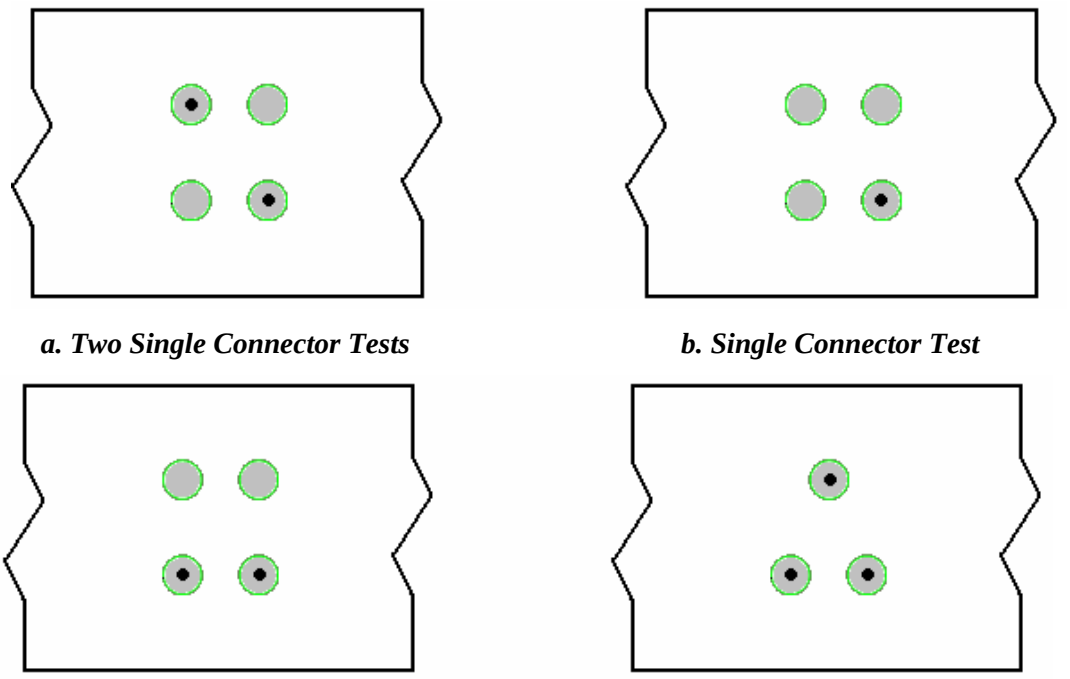

a. Two Single Connector Tests *b. Single Connector Test*

c. Double Connector Test *d. Triple Connector Test*

Figure 5.3 Test Connector Arrangements

5.2 INSTRUMENTATION

Three types of transducers were used during the tests: (1) load cells to measure applied load on the connectors, (2) strain gages to measure strains in the connectors, ducts, and spiral reinforcement, and (3) linear potentiometers to measure connector, grout, and beam displacements. It was important to obtain information about how load was distributed along the embedded portion of connectors and how much connectors slipped at different load stages. Measurements of strain in ducts and surrounding transverse reinforcement provided an indication of the degree of confinement provided at different load stages. Test data were acquired using a Hewlett Packard 3852A scanner and integrated LabView software, and all measuring devices were properly calibrated before the experiments began.

A 10,000-psi pressure transducer and two center-hole load cells were used to measure applied loads in the connectors. One load cell had a capacity of 200 kip, while the other had a capacity of 400 kip. The pressure transducer was used in all experiments, and load cells were used as needed, depending on the number of connectors. Correlation of data among these different load measuring devices was very good, with most discrepancies being smaller than 1 kip.

Two types of strain gages were used throughout the experiments. Strains in the connectors, transverse reinforcement, and galvanized steel ducts were measured using 5-mm strain gages. Strain

gages used to measure strains on the polyethylene and polypropylene ducts had a length of 6 mm. The techniques used to attach the strain gages to the surface of the structural components are described in Appendix B.

Strain gages were typically placed at 6-in. intervals along the embedded portion of each connector. Hence, the number of strain gages attached to each connector depended on the length of embedment. Figure 5.4 shows strain gage locations for a connector with an embedment depth of $12d_b$. Two diametrically-opposed strain gages were located at the lead end of the connector to monitor bar bending during tests. The stress distribution along the connector was determined based on the connector strain readings.

Strain gages were placed in two orientations on the galvanized metal ducts: in the circumferential direction and at an angle parallel to the seams of the duct (Figure 5.5). Strain gages were placed 4, 8, 13, and 18 in. from the top of the duct in the circumferential direction, and one gage was placed at 8 in. from the top of the duct parallel to the seams. On the plastic ducts all gages were placed in the circumferential direction at distances of 4, 8, 13, and 18 in. from the top of the duct. In a limited number of tests, one additional strain gage was placed 6 in. from the top of the duct to measure axial strain in the plastic duct. A polyethylene duct with complete strain gage installations is shown in Figure 5.6. The actual number of strain gages attached to a duct may be smaller if the embedment depth of the connector was shallow. Figure 5.7 shows a group of galvanized steel ducts with complete strain gage installations as they were being placed in the formwork.

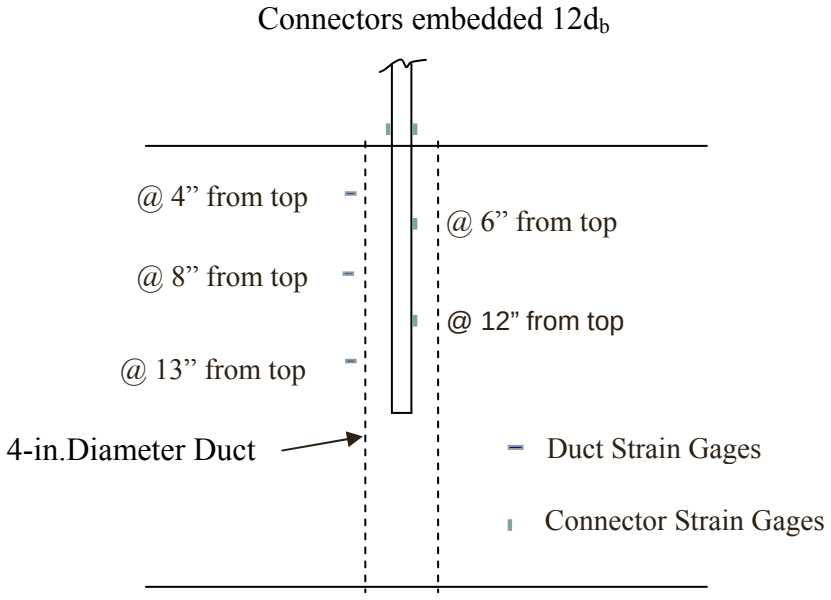

Figure 5.4 Typical Strain Gage Locations on Connectors and Ducts

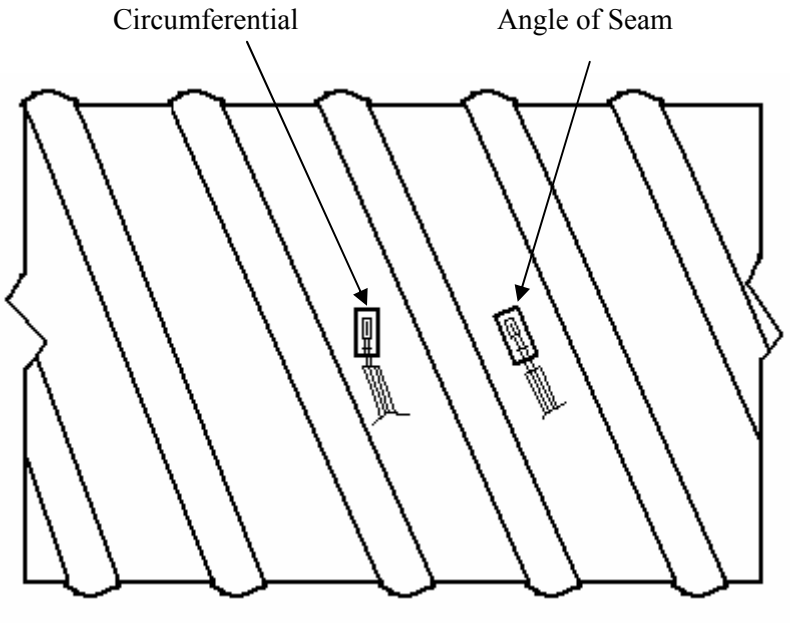

Figure 5.5 Strain Gage Orientations on Galvanized Steel Duct

Figure 5.6 Completed Gage Installations on HD Polyethylene Duct

Figure 5.7 Completed Strain Gage Installations on Galvanized Steel Ducts

Figure 5.8 illustrates the test setup with the instrumentation used to measure applied loads and displacements of the connectors, grout, and beam specimen. Load-displacement behavior of connectors was determined by measuring their lead and end displacements. The lead displacement was measured using two, 2-in. linear potentiometers placed on a stainless steel angle attached to the connector, as shown in Figure 5.9. Taking the average of the readings of two linear potentiometers would correct for any tilt experienced by the connector during testing. The connector end displacement was measured with the help of a threaded rod that extended through the bottom of the specimen and was screwed into the end of the connector, and to which was attached a string-type linear potentiometer. The threaded rod was protected from the grout by copper sheathing.

Displacement of the concrete beam was also measured using a string-type linear potentiometer. This beam deflection was then subtracted from the experimental connector lead and end displacement values during the data analyses to obtain the actual connector displacements. Figure 5.10 shows the instrumentation placed underneath the beam specimen.

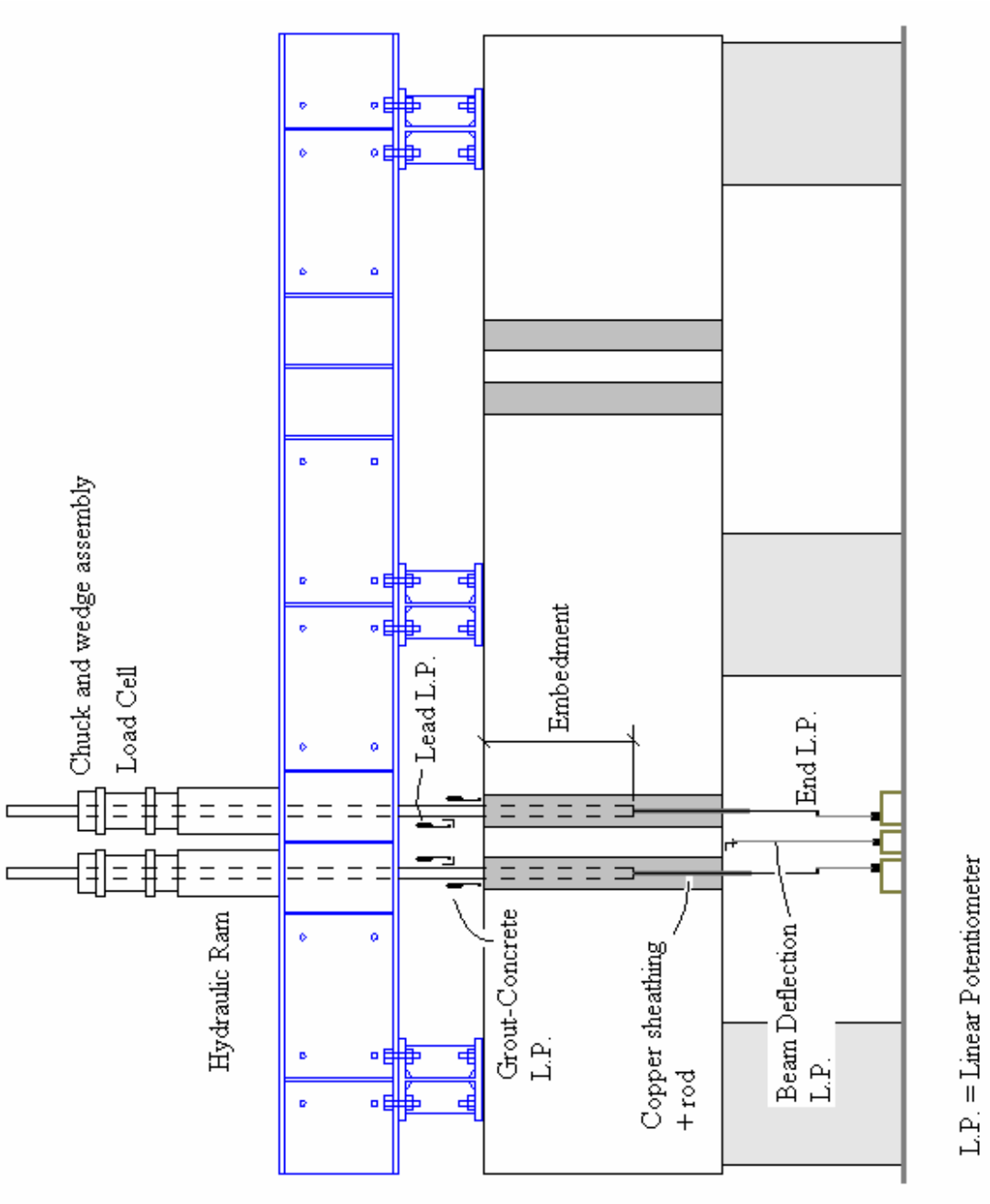

Figure 5.8 Schematic of Test Setup and Instrumentation

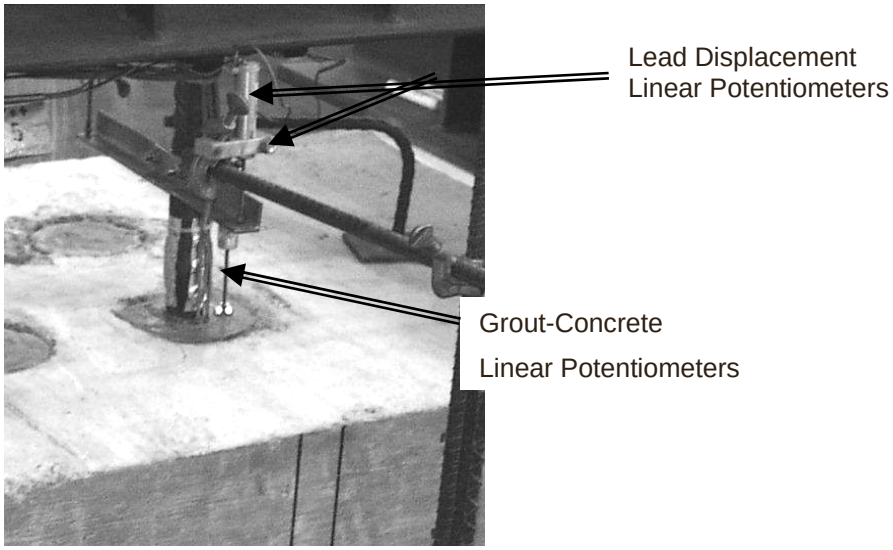

Figure 5.9 Instrumentation Used to Measure Lead Connector Displacement and Relative Displacement between Grout and Concrete

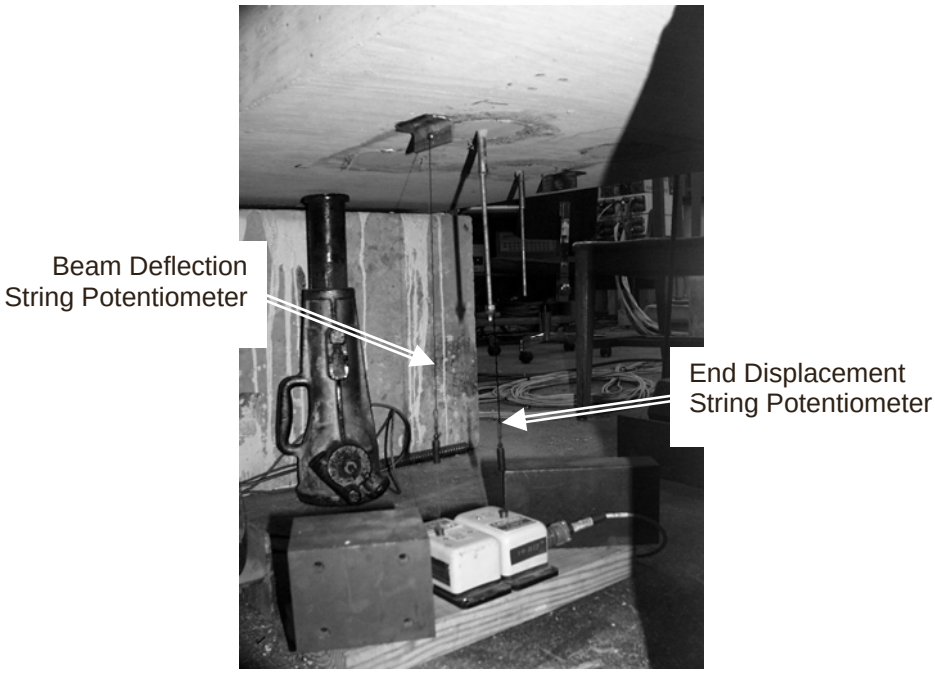

Figure 5.10 Instrumentation Used to Measure End Connector Displacement and Beam Deflection

Relative displacements between the grout and concrete were measured using a 2-in. linear potentiometer that was mounted on a small metal stand epoxy-glued to the top of the concrete beam (Figure 5.9). A small Plexiglas square was epoxy-glued to the top of the grout surface to serve as a smooth level surface for the tip of the linear potentiometers. Monitoring of the relative displacement between the grout and concrete was sometimes limited by the spreading and widening of radial cracks emanating from the ducts. However, the data were useful in acquiring information about slip of the connectors and about anchorage of the grout being confined by the duct.

5.3 TEST METHOD

After zeroing all electronic data channels, load was slowly applied to each connector using a 200-kip hydraulic ram located on top of the back-to-back channels. The hydraulic rams were actuated by a pneumatically-operated hydraulic pump. Application of pressure makes the piston of each ram move upward, which in turn presses upward on the chuck and wedge assembly causing the wedges to grip and lift the connector. Typically, a load cell was placed between the ram and wedge-chuck assembly to measure the applied load; a pressure transducer was also connected to the hydraulic pump to measure the applied load.

At the initial stages of testing, load was applied in 2-kip increments until the first signs of cracking were observed. Beam specimens were frequently monitored for the presence of cracks both in the grout and in the concrete. Data channels were scanned continuously every 3 sec during testing. The applied load and connector lead displacements were plotted in real-time during the experiments to aid in assessment of cracking and bar yield. At intermediate load stages, when cracking became significant, load was applied in 1-kip increments. Throughout each test, crack patterns were marked on the specimen with an indication of the load at which they appeared, until capacity of the connection was reached. Loads recorded on the specimens, and in further data analyses correspond to the forces acting on individual connectors, and not the summation of the group. Photographs of specimens were also taken at different stages of loading to serve as documentation for each test. Figure 5.11 shows cracks for one test at an intermediate load stage.

Load was applied until failure of the connection occurred. In cases where the test involved more than one connector, forces on each connector were kept approximately equal because the loading mechanism was force-controlled. Although the majority of these multiple-connector tests failed as a group, there were some instances where one connector failed before the others. In these cases, the failure load was taken as the load acting on the connection when the first connector failed, even though the remaining connectors sometimes reached a higher load when reloaded.

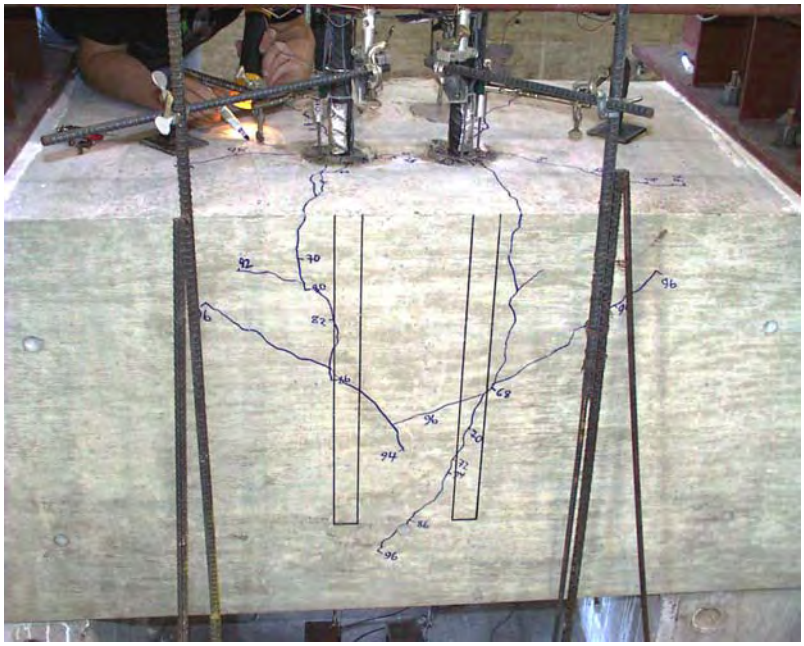

Figure 5.11 Marking of Crack Formations during a Test

The majority of the tests proceeded without any irregularity. Small noises were heard during some tests in the initial stages of loading, which corresponded to the wedge grip adjusting around the connector. Corresponding levels of slip were recorded. The application of load was interrupted during one test when a set of wedges was installed incorrectly and prevented the load from increasing beyond intermediate load levels. The specimen was immediately unloaded, and a new set of wedges was installed at a different location along the connector. Reloading proceeded until failure was achieved without any further irregularities.

CHAPTER 6
Measured Response

Key aspects of the measured response of the test specimens are summarized in this chapter. The measured capacity was most sensitive to the embedded length of the connector, the duct material, and the number of connectors. The influence of all parameters on the bond strength of the connectors is discussed in detail in Chapter 7.

All of the thirty-two connection specimens tested failed by pullout of the connectors. Fracture of the connectors was not observed due to the relatively shallow embedment depths tested in the experiments. A pure splitting type failure was not observed due to the presence of longitudinal, transverse, and confining reinforcement in the beams and the amount concrete cover around the ducts. However, radial splitting cracks did form around the ducts in most of the tests and concrete cone breakouts were common at failure.

The primary experimental parameters for each test series and key aspects of the measured response are summarized in Table 6.1 through Table 6.6. Observed crack patterns are discussed in Section 6.1 and the measured relationships between the applied stress and the slip at the end of the connector is summarized in Section 6.2. Observed modes of failure are discussed in Section 6.3. Because the measured response was sensitive to the duct material, specimens constructed using galvanized steel, polyethylene, and polypropylene ducts are discussed separately in each section.

Additional information about the response of the specimens, including the strain and stress distributions along the connector, the slip of the connector relative to the grout, and the strain in the duct, is presented in Appendix C.

6.1 OBSERVED CRACK PATTERNS

The test specimens were loaded monotonically to failure. During the tests, the specimens were monitored frequently for the formation of cracks in the grout and in the concrete. Cracks were marked on the surface of the specimens and the corresponding applied force level in the individual connector was indicated. Before the first cracks were observed, load was applied in 2-kip increments. After cracking, the loading increment was reduced to 1 kip.

Typically, radial cracks formed first in the grout. As loading continued, the radial cracks extended into the concrete. The axial stress in the connector corresponding to the formation of the radial cracks in the concrete is listed as f_{split} in Table 6.1 through Table 6.6. Radial cracks continued to form

until a widespread radial crack pattern in the concrete was observed. The corresponding axial stress is listed as f_{ws}. The formation of additional cracks in the concrete was sensitive to the duct material, and the observed patterns are discussed in the following sections.

Table 6.1 Overview of Test Series 1

Test	Bars	Duct	Coating	ℓ_e	Material Properties			Observed Response			
					f'_c	f_g	f_y	f_{split}	f_{ws}	f_{max}	δ_{max}
				(d_b)	(psi)	(psi)	(ksi)	(ksi)	(ksi)	(ksi)	(in.)
1	1-#11	Steel	Plain	8	5400	5000	75	46	48	58	0.20
2	1-#11	Steel	Epoxy	8	5400	6100	68	48	48	55	0.09
3	1-#11	Steel	Plain	12	5400	6400	75	47	72	87	0.19
4	1-#11	Steel	Epoxy	12	5400	6400	68	60	76	88	0.22
5	1-#11	PE	Plain	8	5400	4700	75	37	41	48	0.16
6	1-#11	PE	Epoxy	8	5400	5500	68	30	40	40	0.14
7	1-#11	PE	Plain	12	5400	5900	75	33	58	67	0.26
8	1-#11	PE	Epoxy	12	5400	5800	68	36	60	65	0.17

Table 6.2 Overview of Test Series 2

Test	Bars	Duct	Coating	ℓ_e	Material Properties			Observed Response			
					f'_c	f_g	f_y	f_{split}	f_{ws}	f_{max}	δ_{max}
				(d_b)	(psi)	(psi)	(ksi)	(ksi)	(ksi)	(ksi)	(in.)
9	1-#11	PE	Plain	12	4500	5100	75	42	50	54	0.22
10	1-#11	Steel	Plain	12	4500	5600	75	45	57	80	0.26
11	1-#11	None	Epoxy	12	4600	5100	68	45	56	68	0.13
12	1-#11	None	Plain	12	4600	5100	75	42	55	67	0.18

Table 6.3 Overview of Test Series 3

Test	Bars	Duct	Spiral	ℓ_e	Material Properties			Observed Response			
					f'_c	f_g	f_y	f_{split}	f_{ws}	f_{max}	δ_{max}
				(d_b)	(psi)	(psi)	(ksi)	(ksi)	(ksi)	(ksi)	(in.)
13	2-#11	Steel	Group	16	4700	5200	75	38	57	87	0.25
14	2-#11	PE	Group	16	4700	5300	75	42	49	64	0.27
15	2-#11	Steel	None	16	4700	5400	75	39	54	86	0.24
16	2-#11	PE	None	16	4700	5400	75	42	49	59	0.35

Table 6.4 Overview of Test Series 4

Test	Bars	Duct	Bar Location	ℓ_e	Material Properties			Observed Response			
					f'_c	f_g	f_y	f_{split}	f_{ws}	f_{max}	δ_{max}
				(d_b)	(psi)	(psi)	(ksi)	(ksi)	(ksi)	(ksi)	(in.)
17	2-#11	Steel	Centered	12	5200	4800	75	33	45	59	0.19
18	2-#11	PE	Centered	12	5300	4900	75	24	37	44	0.27
19	1-#11	Steel	Eccentric	8	5500	5100	59	41	46	49	0.14
20	1-#11	PE	Eccentric	8	5500	5100	59	31	40	40	0.19
21	1-#11	Steel	Eccentric	12	5500	5400	59	36	61	74	0.12
22	1-#11	PE	Centered	16	5500	5400	75	45	74	90	0.42

Table 6.5 Overview of Test Series 5

Test	Bars	Duct	Spiral	Duct Spacing (D)	ℓ_e (d_b)	Material Properties			Observed Response			
						f'_c (psi)	f_g (psi)	f_y (ksi)	f_{split} (ksi)	f_{ws} (ksi)	f_{max} (ksi)	δ_{max} (in.)
23	2-#11	Steel	Group	2	12	6100	6000	59	48	53	68	0.21
24	2-#11	PE	Group	2	16	6100	6300	75	43	52	65	0.18
25	1-#11	PE	Indiv.	1	8	6100	6500	75	34	34	34	0.12
26	2-#11	PE	Indiv.	1	16	6100	6500	75	39	48	62	0.18
27	1-#11	PE	Indiv.	1	12	6100	6500	75	49	54	63	0.15

Table 6.6 Overview of Test Series 6

Test	Bars	Duct	Spiral	ℓ_e (d_b)	Material Properties			Observed Response			
					f'_c (psi)	f_g (psi)	f_y (ksi)	f_{split} (ksi)	f_{ws} (ksi)	f_{max} (ksi)	δ_{max} (in.)
28	2-#11	PP	Group	16	6100	6800	59	44	53	85	0.20
29	1-#11	PP	Group	8	6100	7100	59	39	39	40	0.05
30	1-#11	PP	Group	12	6100	7100	59	32	60	68	0.08
31	3-#11	Steel	None	16	6100	5800	59	23	50	73	0.13
32	3-#11	PP	Group	16	6100	5800	59	20	47	67	0.21

6.1.1 Galvanized Steel Duct

Crack patterns in specimens constructed using galvanized steel duct are illustrated using Tests 10, 13, and 23. A single, plain bar with an embedded depth of $12d_b$ was loaded during Test 10. The first signs of cracking in the grout were observed at a load of 26 kip (17 ksi). As load increased, radial cracks were observed in the concrete at a load of approximately 68 kip (45 ksi). A widespread pattern of radial splitting (Figure 6.1) formed at a load of approximately 88 kip (57 ksi). The pattern of radial splitting in single connectors was generally axisymmetric, meaning cracks were usually spread equally in all directions. The cracks typically extended over a large portion of the top surface of the specimens.

Figure 6.1 Widespread Splitting in Test 10

Figure 6.2 shows the crack patter at failure (121 kip (80 ksi)). The V-shaped cracks that formed on the side of the specimen corresponding to the smallest cover indicate that the connector, grout, duct, and concrete were working together to resist the applied load. The orientations of these diagonal cracks indicate the presence of inclined compression struts in the concrete, which are a primary component of the resisting mechanism in the grouted vertical connections.

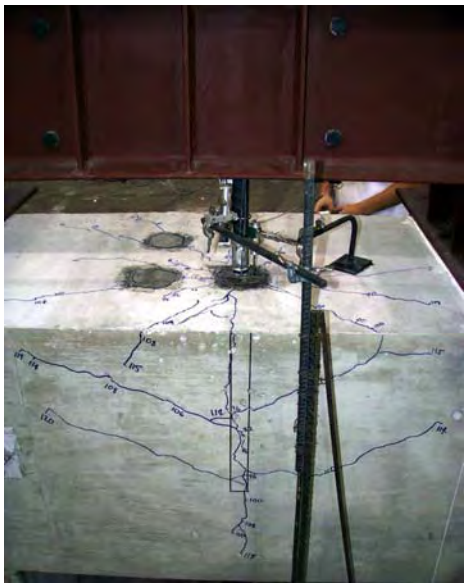

Figure 6.2 Crack Pattern at Failure – Test 10

The crack patterns at failure were similar for tests with multiple connectors. Two, plain bars with embedded depths of $16d_b$ were loaded during Test 13. The first signs of cracking in the grout were observed at a load of 24 kip (16 ksi), and radial cracks in the concrete were observed at a load of 86 kip (57 ksi). The crack patterns around the two connectors were similar throughout the test (Figure 6.3). The close proximity of connectors (clear spacing of 1*D* between ducts) caused extensive interaction between the connectors. Both connectors failed together as a unit at a load of approximately 132 kip (87 ksi) (Figure 6.4).

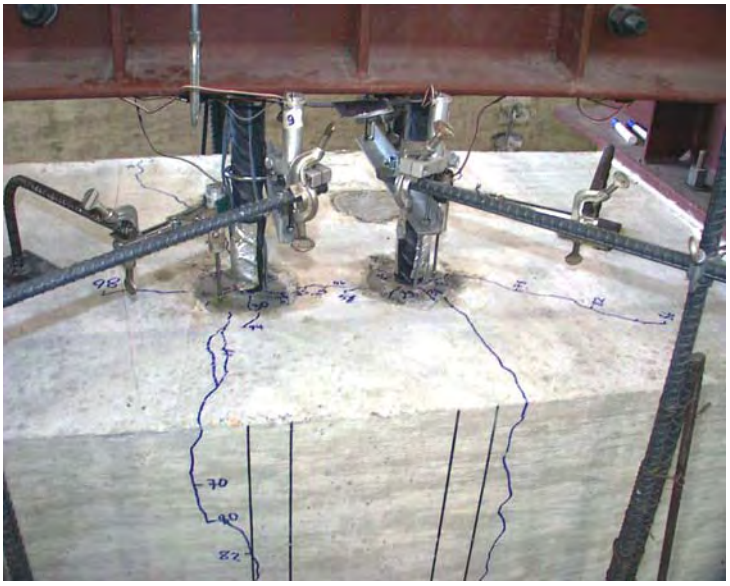

Figure 6.3 Widespread Splitting in Test 13

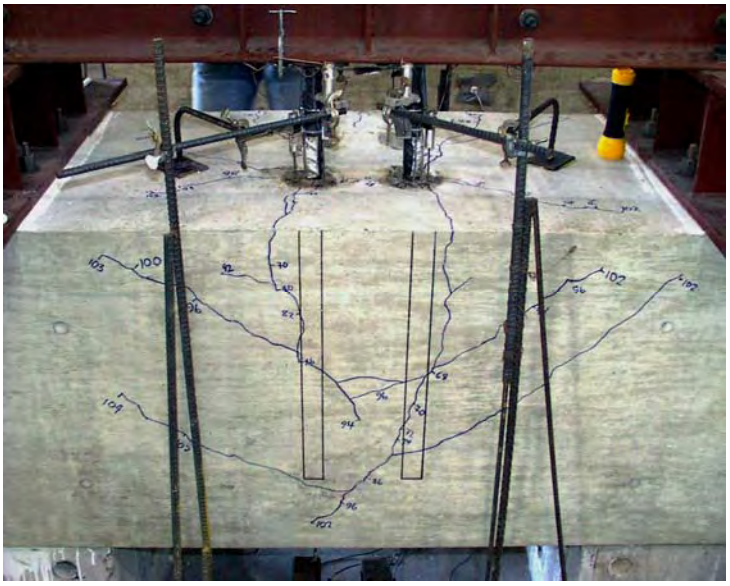

Figure 6.4 Crack Pattern at Failure – Test 13

Two connectors were also tested in Test 23. The connectors were embedded $12d_b$ and the clear spacing between ducts was $2D$. The increased duct clear spacing reduced the interaction between the connectors and different crack patterns were observed for each connector (Figure 6.5). In this test, cracks were first observed in the grout at a load of approximately 19 kip (13 ksi) and widespread splitting was observed at a load of 74 kip (49 ksi). As loading approached failure, the connectors acted as a unit. Figure 6.6 shows the crack pattern at failure, which included V-shaped cracks.

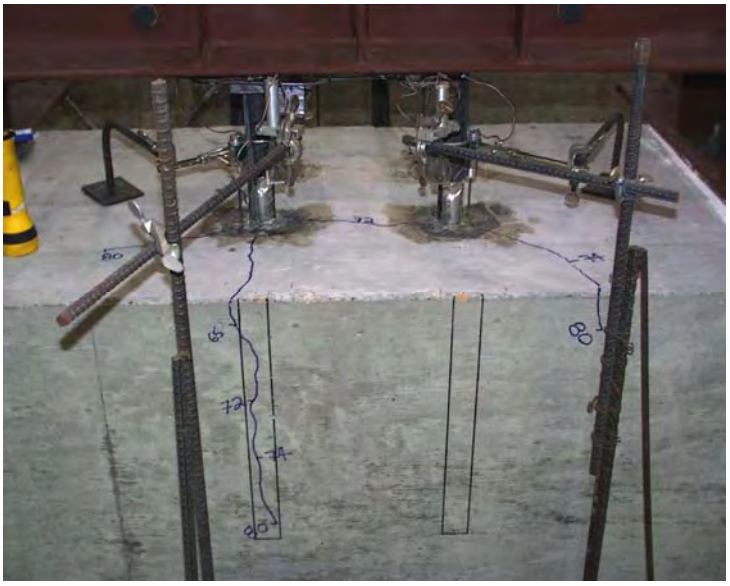

Figure 6.5 Widespread Splitting in Test 23

Figure 6.6 Crack Pattern at Failure – Test 23

6.1.2 Polyethylene Duct

Crack patterns in specimens constructed using polyethylene duct are illustrated using Tests 9 and 14. A single, plain bar with an embedded depth of $12d_b$ was loading during Test 9. The first signs of cracking in the grout were observed at a load of 20 kip (13 ksi). As load increased, radial cracks were observed in the concrete at a load of approximately 64 kip (42 ksi). Figure 6.7 shows the cracking pattern at a load of 78 kip (51 ksi). Fewer radial cracks were observed in this specimen compared with the specimens constructed using galvanized steel duct. In addition, the cracks occupied a much smaller area on the top surface of the beam. Figure 6.8 shows the crack pattern at failure (82 kip (54 ksi)). V-shaped crack formations did not form in this specimen.

Figure 6.7 Splitting Cracks in Test 9

Figure 6.8 Crack Pattern at Failure – Test 9

Two, plain bars with embedded depths of $16d_b$ were loaded during Test 14. The first signs of cracking in the grout were observed at a load of 27 kip (18 ksi). Unlike the single connector test with a shorter embedded depth, widespread cracking of the concrete was observed at a load of 75 kip (49 ksi) (Figure 6.9). The close proximity of connectors (clear spacing of 1*D* between ducts) caused extensive interaction between the connectors. V-shaped crack formations were seen on the side of the beam corresponding to the minimum cover as the connection approached failure. This meant that the force was being transferred effectively between the connector, grout, and polyethylene duct into the concrete. Both connectors failed together as a unit at a load of approximately 97 kip (64 ksi) (Figure 6.10). A horizontal crack formed on the side of the beam at failure. The depth of this crack corresponded to the depth of the top layer of longitudinal reinforcement in the beam.

Figure 6.9 Widespread Splitting in Test 14

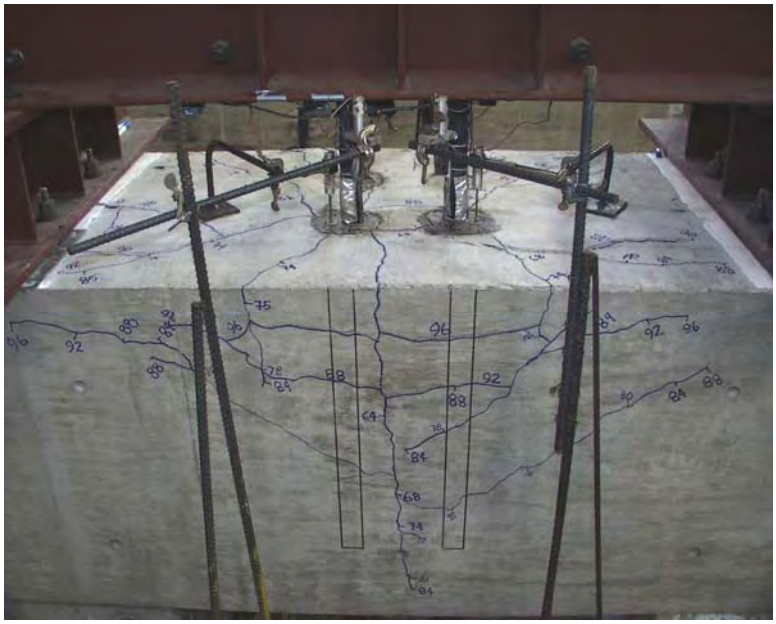

Figure 6.10 Crack Pattern at Failure – Test 14

6.1.3 Polypropylene Duct

Crack patterns in specimens constructed using polypropylene duct are illustrated using Tests 28 and 32. Two, plain bars with embedded depths of $16d_b$ were loaded during Test 28. The first signs of cracking in the grout were observed at a load of 18 kip (12 ksi), and radial cracks in the concrete were observed at a load of 66 kip (44 ksi). Widespread cracking of the concrete was observed at a load of 79 kip (49 ksi) (Figure 6.11). The crack patterns around the two connectors were similar throughout the test.

V-shaped crack formations were seen on the side of the beam corresponding to the minimum cover as the connection approached failure. This pattern indicated that the force was being transferred effectively between the connector, grout, and polpropylene duct into the concrete. Both connectors failed simultaneously by pullout at a load of approximately 128 kip (85 ksi) (Figure 6.12).

Three connectors, arranged in a triangular pattern and embedded $16d_b$, were loaded during Test 32. Cracking of the grout was observed at a load of 15 kip (10 ksi), while radial splitting cracks in the concrete started to develop at a load of 30 kip (20 ksi). V-shaped cracks, shown in Figure 6.13, formed at a load of 75 kip (50 ksi). Failure occurred at a load of 101 kip (67 ksi).

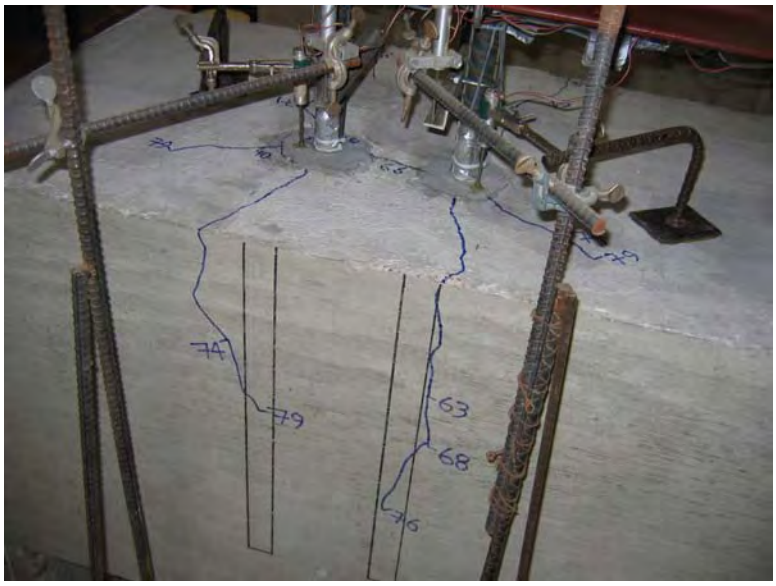

Figure 6.11 Widespread Splitting in Test 28

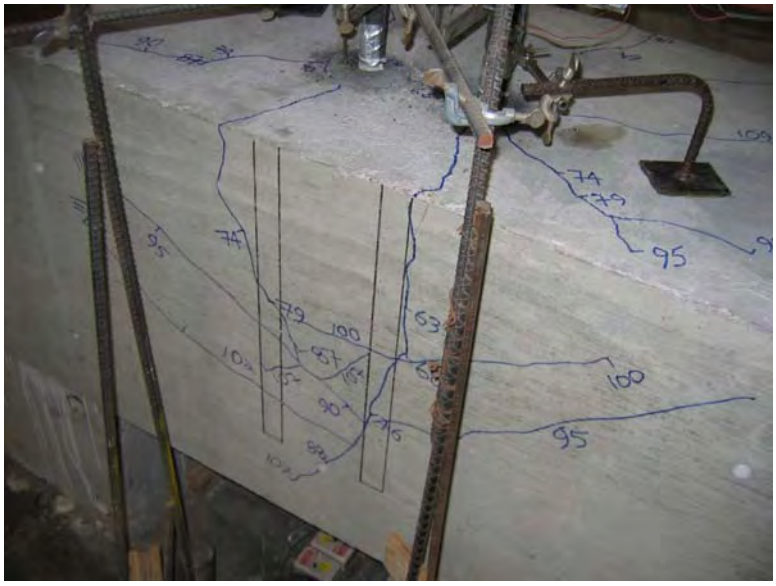

Figure 6.12 Formation of V-Shaped Cracks in Test 28

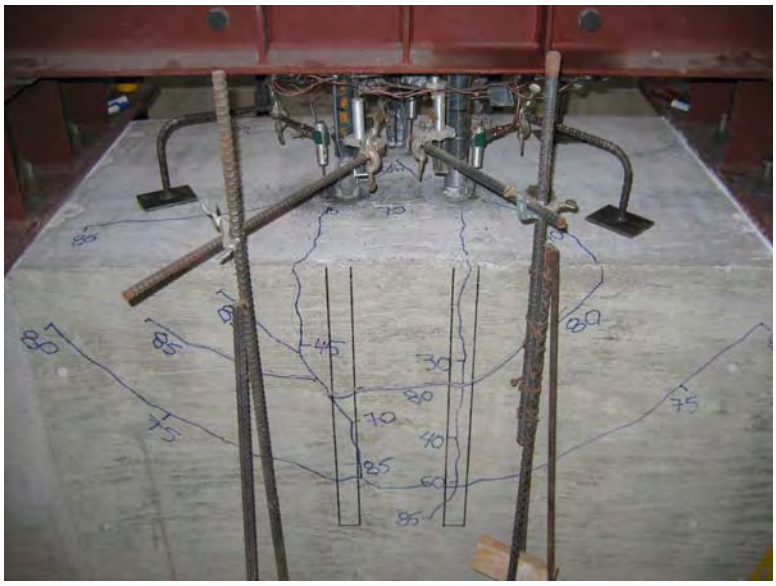

Figure 6.13 Formation of V-Shaped Cracks in Test 32

6.2 RELATIONSHIPS BETWEEN APPLIED TENSILE STRESS AND END SLIP

The overall response of the connectors is most easily evaluated from the load-displacement response. As discussed in Chapter 5, the loads applied to the connectors were measured using load cells and a pressure transducer, while the displacements at the free end and near the loaded end of the connector were measured using linear potentiometers.

Both the lead and end displacements provide valuable information about the response of the connector. As shown in Figure 6.14, the lead displacements were particularly useful for monitoring yielding of the connector during the tests. A yield plateau can be seen in the lead displacement curve. The displacements measured at the lead end of the connector consisted of two components: (1) slip of the connector relative to the beam, and (2) yielding of a portion of the connector near the lead end. In contrast, the free end displacements exhibited only the slip of the connector. While information from both sources was used to interpret the response of the specimens, the end displacement (also called end slip) is discussed in this section to investigate anchorage of connectors.

The load-displacement behavior of grouted vertical duct connections is presented by plotting the applied axial stress as a function of the end slip. Representative tests have been selected for each type of duct material. The general shape of the curves is similar for all specimens and characterized by a high initial stiffness and a gradual reduction in stiffness as cracks develop in the grout and concrete (Figure 6.14). The shape of the curves around the maximum stress depended if the connector yielded before pullout occurred.

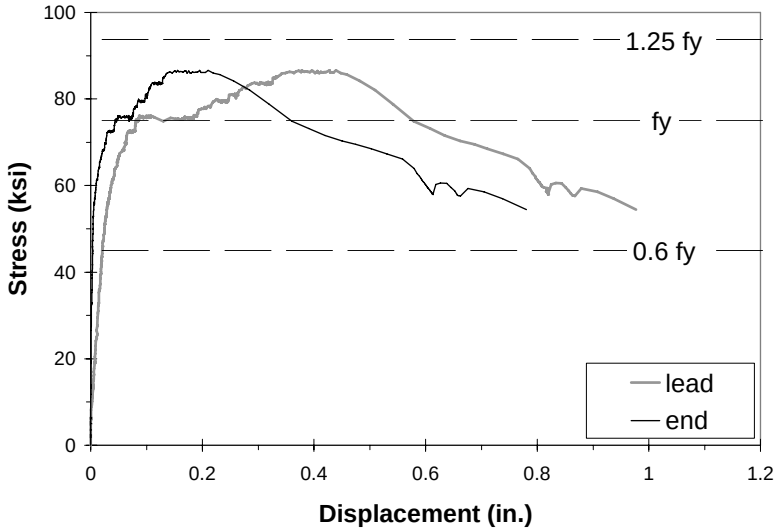

Figure 6.14 Measured Displacement Response during Test 3

To assist in interpreting the figures, lines corresponding to constant stress levels of the measured yield stress of the connectors, f_y; $0.6\,f_y$; and $1.25\,f_y$ are shown in the figures. Stress levels corresponding to the onset of cracking in the concrete, f_{split}; the development of a widespread radial crack pattern in the concrete, f_{ws}; and the maximum stress resisted by the connector, f_{max}, are listed in Table 6.1 through Table 6.6. The slip corresponding to the maximum stress, δ_{max}, is also reported.

6.2.1 Galvanized Steel Duct

The response of a single, yielding connector in galvanized steel duct is illustrated using Test 10 (Table 6.2 and Figure 6.15). Reductions in stiffness may be observed at the level of first cracking in the concrete (45 ksi) and the development of the widespread radial crack pattern (57 ksi). The maximum stress achieved by the connector (80 ksi) exceeded the measured yield stress of the connector (75 ksi). The slip at the maximum stress was 0.26 in.

The response of the two connectors loaded in Test 13 is shown in Figure 6.16 and critical values are listed in Table 6.3. As discussed in Section 6.1.1, the two connectors responded essentially identically up to the maximum stress. Due to the deeper embedded depth, the connectors were able to achieve a higher maximum stress (87 ksi) than the single connector in Test 10 (80 ksi), but otherwise, the response was very similar.

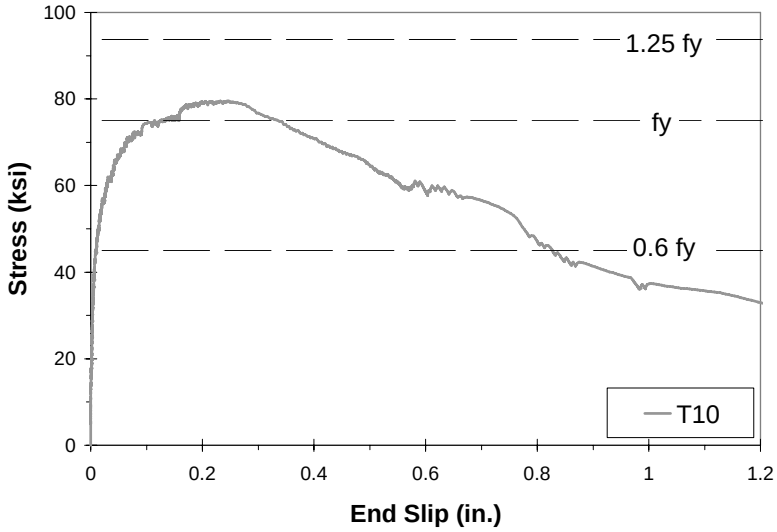

Figure 6.15 Slip Response during Test 10 (Single Plain Connector, Galvanized Steel Duct, Embedded $12d_b$)

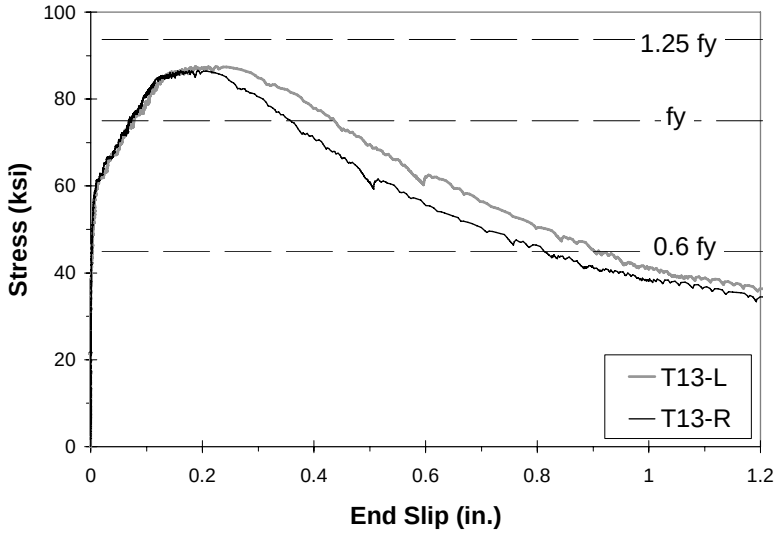

Figure 6.16 Slip Response during Test 13 (Double Plain Connector, Galvanized Steel Duct, Embedded $16d_b$)

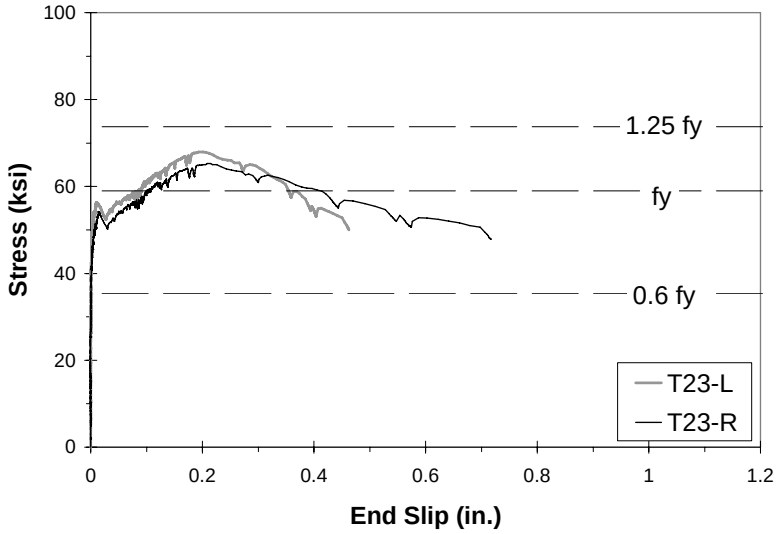

Figure 6.17 Slip Response during Test 23 (Double Plain Connector, Galvanized Steel Duct, Embedded $12d_b$)

Two connectors were also loaded during Test 23, but the embedded length was shorter than that in Test 13. Figure 6.17 indicates a drop in load and an increase in slip, when the connection reached a stress of 55 ksi, which corresponded to the development of widespread radial splitting cracks (Table 6.5). The shorter connector embedment used in Test 23 was not sufficient to anchor the bars as effectively as the deeper embedment in Test 13. When radial splitting cracks developed in the concrete, the forces in the connectors redistributed to maintain anchorage. The maximum load attained by the connectors in Test 23 was 68 ksi, which exceeded the yield stress of 59 ksi.

6.2.2 Polyethylene Duct

The response of single connectors in polyethylene duct is illustrated using Tests 5, 7, and 22 (Table 6.1, Table 6.4, and Figure 6.18). The connectors had embedded depths of $8d_b$, 12 d_b, and $16d_b$, respectively. Although the shapes of the curves are similar, only the connector with the deepest embedded length (Test 22) was able to develop the yield stress of the reinforcement.

The response of two connectors with embedded depths of $16d_b$ that were loaded during Test 14 is shown in Figure 6.19. The two connectors exhibited nearly identical response up to the maximum stress, but were only able to achieve a maximum stress of 64 ksi (Table 6.3), compared with a stress of 90 ksi in Test 22 for a single connector with the same embedded depth. After reaching the maximum load, the right connector began to pull out of the concrete. The test continued until failure of the right connector, then the left connector was reloaded individually to failure. The left connector achieved a maximum stress of 61 ksi after reloading.

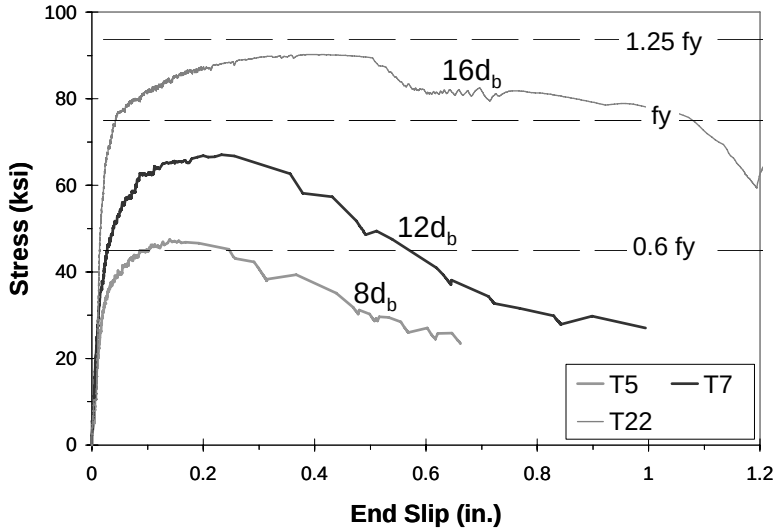

Figure 6.18 Slip Response during Tests 5, 7, and 22 (Single Plain Connectors, Polyethylene Duct)

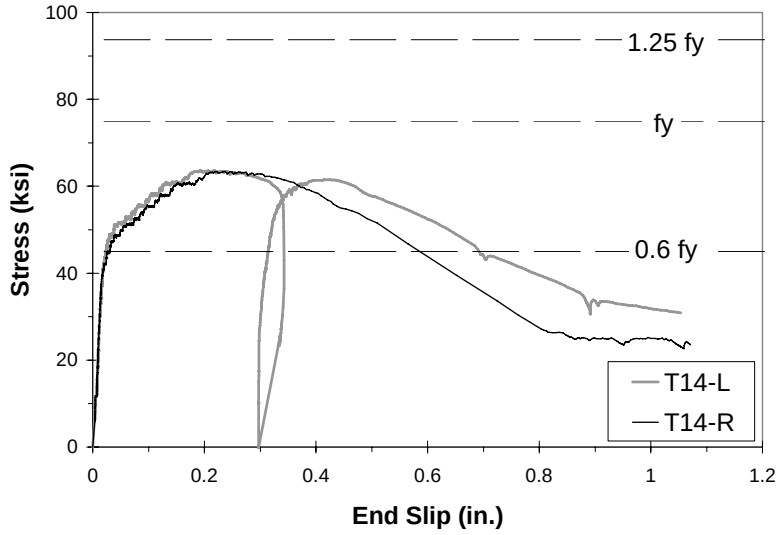

Figure 6.19 Slip Response during Test 14 (Double Plain Connectors, Polyethylene Duct, Embedded 16d_b, Duct Spacing D)

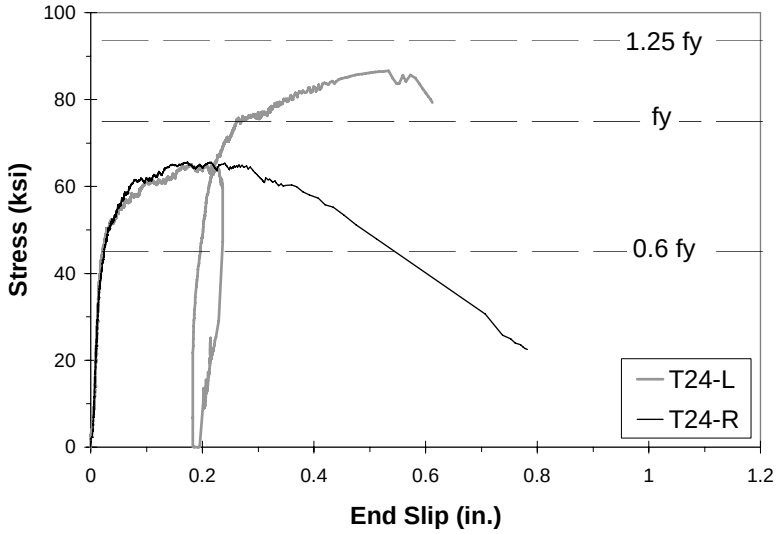

Figure 6.20 Slip Response during Test 24 (Double Plain Connectors, Polyethylene Duct, Embedded 16d_b, Duct Spacing 2D)

Two connectors were also loaded during Test 24, but the clear spacing of the duct was increased to 2D. The measured response is shown in Figure 6.20 and summarized in Table 6.5. The response was similar to that exhibited during Test 14. The right connector began to pull out of the concrete at an axial stress of 65 ksi. After failure of the right connector, the left connector was reloaded and achieved a stress of 87 ksi before pulling out of the concrete. This increase in capacity is attributed to the larger clear spacing between ducts, and the reduced interaction between the two connectors.

6.2.3 Polypropylene Duct

The response of single connectors in polypropylene duct is illustrated using Tests 29 and 30 (Table 6.6 and Figure 6.21). The connectors had embedded depths of 8d_b and 12 d_b, respectively. The shapes of the curves are similar, but the connector with the shallower embedded length (Test 29) was not able to develop the yield stress of the reinforcement. The noted jaggedness of the curves after the connections reached the maximum stress can be attributed to imperfections in the loading method.

The response of two connectors with embedded depths of 16d_b that were loaded during Test 28 is shown in Figure 6.22. The two connectors exhibited nearly identical response and achieved a maximum stress of 85 ksi (Table 6.6). A set of three connectors were tested in Test 32 (Figure 6.23). Again the connectors exhibited nearly identical response, but the maximum stress was only 67 ksi. This reduction in capacity is likely due to the group effect, as stress levels corresponding to cracking of the concrete and formation of widespread splitting cracks were also less in this test compared with Test 28.

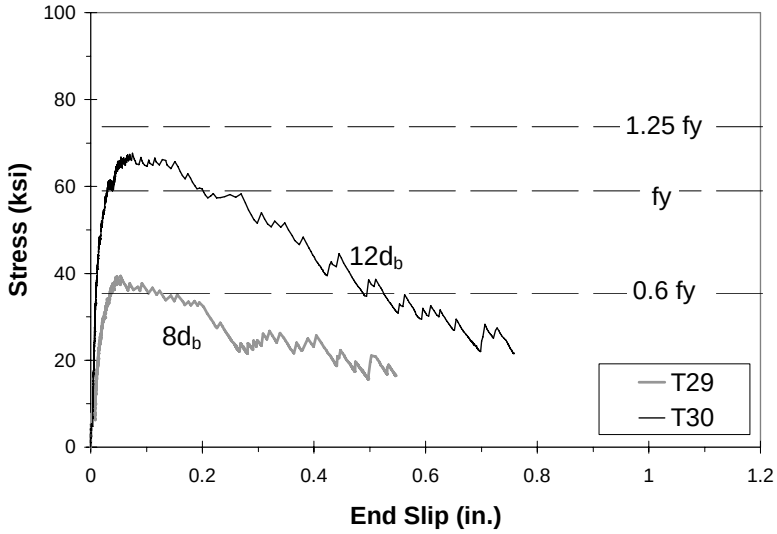

Figure 6.21 Slip Response during Tests 29 and 30 (Single Plain Connectors, Polypropylene Duct)

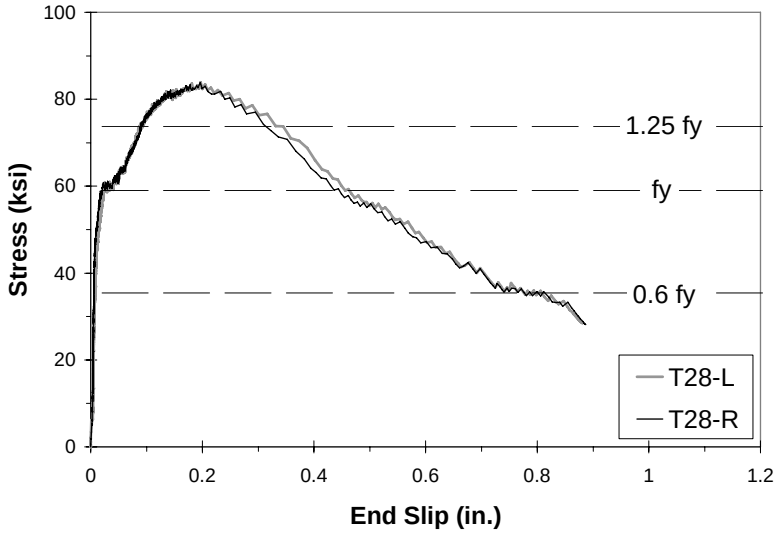

Figure 6.22 Slip Response during Test 28 (Double Plain Connectors, Polypropylene Duct, Embedded $16d_b$)

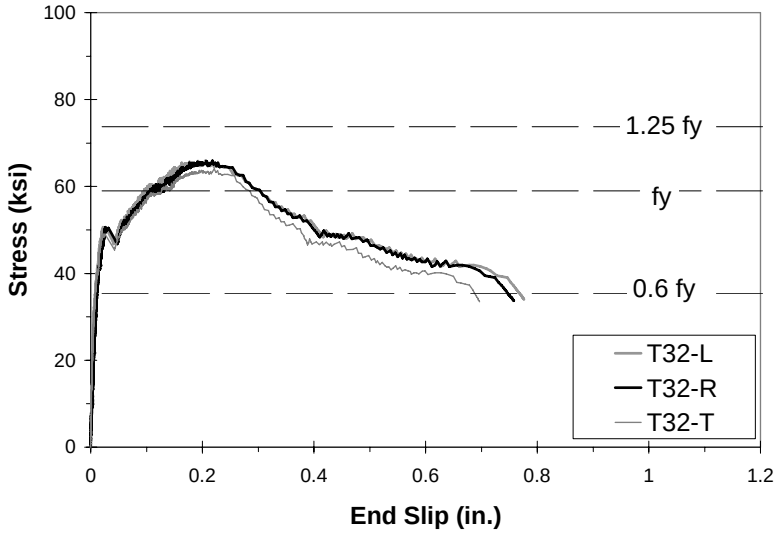

Figure 6.23 Slip Response during Test 32 (Triple Plain Connectors, Polypropylene Duct, Embedded 16d_b)

6.3 OBSERVED FAILURE MODES

As discussed, all specimens failed by pullout of the connectors; however, different modes of failure were observed. Before discussing the observed response of individual specimens, the modes of observed failure are generalized (Figure 6.24). In the following discussion, δ_e refers to the slip at the free end of the connector relative to the surrounding concrete and δ_g refers to the movement of the top surface of the grout relative to the top surface of the beam. A complete plug pullout failure (Figure 6.24b) occurs when the grout fractures at the free end of the connector and the grout and connector move together as a unit ($\delta_e = \delta_g$). The other extreme is a connector pullout failure (Figure 6.24d) where the connector moves almost independently of the grout ($\delta_e > \delta_g$). The most common mode of failure was a hybrid of these two modes (Figure 6.24c) where the grout fractured along the length of the connector and the top portion of the grout moved with the connector ($\delta_e < \delta_g$). This mode of failure is called a partial plug failure.

The observed failure modes were also complicated by the duct material. In some specimens, the duct remained embedded in the concrete, and the grout slipped relative to the duct. In other specimens, the duct remained in contact with the grout and slipped relative to the concrete. Visual and forensic investigations were conducted to determine the mode of failure for each specimen.

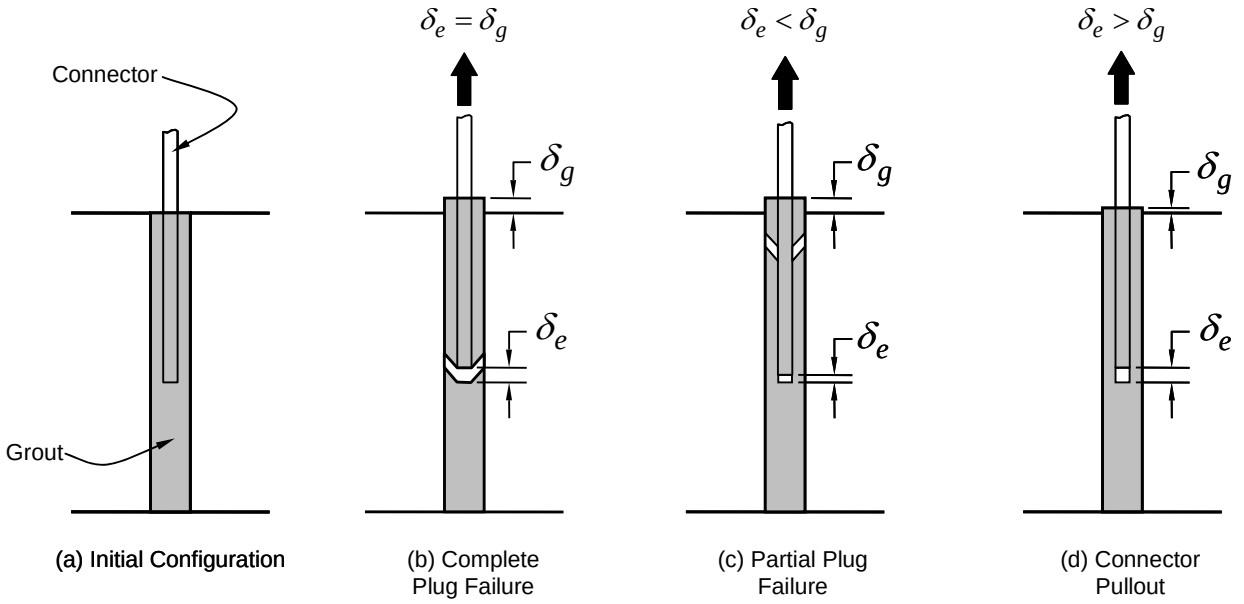

Figure 6.24 Idealized Pullout Modes of Failure

All connectors were loaded until the resistance was a small fraction of the capacity. At this time, significant slip between the connector/grout/duct and the concrete had occurred. Many times large portions of the connector were extracted from the concrete. In these cases, cracks in the grout and damage in the duct were visible and the mode of failure was established without further exploration. In other cases, chipping of the concrete was necessary to reach deeper sections of the connectors in order to identify the damage.

Considering the manner in which the connection specimens were loaded, it is possible that some of the observed damage occurred after the maximum load was achieved. Establishing the mode of failure for a particular connection was based on the forensic examinations and also after considering the duct strains and displacement of the connector relative to the grout.

6.3.1 Galvanized Steel Duct

The observed modes of failure for specimens with galvanized steel duct are summarized in Table 6.7. In all cases, the top segment of the galvanized steel duct remained bonded to the top portion of the grout and pulled out of the surrounding concrete. The length of the top segment of duct seemed to depend on the number of connections tested and depended on the depth of the cone-shaped concrete break-out zone that formed in the connection area at failure. The galvanized steel duct was effective at confining the grout and limiting slip of the grout. At failure, the seams in the duct opened at the locations where the grout had fractured. Photographs of the connectors in Test 4 and 23 are shown in Figure 6.25 and Figure 6.26, respectively.

Table 6.7 Observed Damage in Specimens with Galvanized Steel Duct

Test	Bars	Coating	ℓ_e (d_b)	f_{max} (ksi)	Observed Damage
1	1-#11	Plain	8	58	Duct seam opened 3 in. below surface
2	1-#11	Epoxy	8	55	Duct seam opened 4.5 in. below surface
19	1-#11	Plain	8	49	Duct seam opened 2.5 in. below surface
3	1-#11	Plain	12	87	Duct seams opened 4 and 5.5 in. below surface
4	1-#11	Epoxy	12	88	Duct seam opened 4 in. below surface
10	1-#11	Plain	12	80	Duct seams opened 3 and 4.5 in. below surface
21	1-#11	Plain	12	74	Duct fracture 4.5 in. below surface
17	2-#11	Plain	12	60	Left Bar: Duct seam opened 8.5 in. below surface Right Bar: Duct seam opened 8.5 in. below surface
23	2-#11	Plain	12	68	Left Bar: Duct seam opened 9.5 in. below surface Right Bar: Duct seam opened 8.5 in. below surface
13	2-#11	Plain	16	87	Insufficient data
15	2-#11	Plain	16	86	Left Bar: Duct seam opened 6.5 in. below surface Right Bar: Duct seam opened 8.5 in. below surface
31	3-#11	Plain	16	73	Left Bar: Duct seam opened 18 in. below surface Right Bar: Duct seam opened 14.5 in. below surface Third Bar: Duct seam opened 18 in. below surface

Figure 6.25 Observed Failure of Test 4 (Single Connector, Galvanized Steel Duct)

Figure 6.26 Observed Failure of Left Connector, Test 23 (Double Connector, Galvanized Steel Duct)

6.3.2 Polyethylene Duct

The failure modes observed in connections with polyethylene ducts were characterized by the fact that the grout was able to slip relative to the duct. Three different types of pullout failures were observed in these connections (Figure 6.27): (1) pullout of connector with a segment of the grout, (2) pullout of connector with a segment of the grout and the top portion of the duct, and (3) complete pullout of the connector and the grout from the duct (plug failure). In the third mode of failure, the ribs that formed in the grout at the locations of the duct corrugations were observed to shear off as the grout slipped out of the duct.

Connector embedment depth and the number of connectors per connection influenced the type of pullout failure (Table 6.8). Single connectors with shallow embedded depths tended to fail in the first mode, while single connectors with deeper embedded lengths and multiple connectors tended to fail in the third mode. In tests involving more than one connector, different pullout failure modes were sometimes observed. Figure 6.28 and Figure 6.29 show pictures of Tests 7 and 8, respectively, before and after the damaged duct was removed from the grout.

a. Mode 1 Partial Plug Failure without Duct

b. Mode 2 Partial Plug Failure with Duct

c.. Mode 3 Complete Plug Failure

Figure 6.27 Pullout Failure Modes for Polyethylene Duct Connections

Table 6.8 Observed Damage in Specimens with Polyethylene Duct

Test	**Bars**	**Coating**	ℓ_e **(d_b)**	f_{max} **(ksi)**	**Mode of Failure** (Fig. 6.27)	**Observed Damage**
5	1-#11	Plain	8	48	Mode 1	Partial plug failure – 2.5 in. of grout
6	1-#11	Epoxy	8	40	Mode 2	Partial plug failure – 4.5 in. of grout
20	1-#11	Plain	8	40	Mode 1	Partial plug failure – 1.0 in. of grout
25	1-#11	Plain	8	34	Mode 3	Complete plug failure
7	1-#11	Plain	12	67	Mode 1	Partial plug failure – 2.5 in. of grout
8	1-#11	Epoxy	12	65	Mode 3	Complete plug failure
9	1-#11	Plain	12	54	Mode 1	Partial plug failure – 2.5 in. of grout
27	1-#11	Plain	12	63	Mode 1	Partial plug failure – 4.5 in. of grout
18	2-#11	Plain	12	44	Mode 3	Complete plug failure
22	1-#11	Plain	16	90	Mode 3	Complete plug failure
14	2-#11	Plain	16	64	Modes 1/3	Left Bar: Partial plug failure – 4.5 in. of grout Right Bar: Complete plug failure
16	2-#11	Plain	16	59	Modes 2/3	Left Bar: Partial plug failure – 9 in. of grout Right Bar: Complete plug failure
24	2-#11	Plain	16	68	Modes 1/3	Left Bar: Complete plug failure Right Bar: Partial plug failure – 2.5 in. of grout
26	2-#11	Plain	16	62	Modes 2/3	Left Bar: Partial plug failure – 7.5 in. of grout Right Bar: Complete plug failure

Figure 6.28 Observed Failure of Test 7 (Single Connector, Polyethylene Duct)

Figure 6.29 Observed Failure of Test 8 (Single Connector, Polyethylene Duct)

6.3.3 Polypropylene Duct

All four specimens constructed with polypropylene ducts exhibited plug failures of the connector and grout with the top portion of the duct attached to the grout (Figure 6.30). Unlike the polyethylene duct, the polypropylene duct prevented the grout from slipping relative to the duct. The length of the top segment of the duct attached to the grout depended on the depth of the cone-shaped concrete breakout zone that formed in the connection area at failure. This top segment of the duct was intact in all cases. The remainder of the duct remained attached to the grout in some cases, with only the duct/grout ribs getting sheared off as the grout and connector pulled out. No differences were observed in modes of failure of the connections as a result of variation in embedment depth or in the number of connectors. The three connectors removed from Test 32 are shown in Figure 6.31 before and after the duct was removed.

Table 6.9 Observed Damage in Specimens with Polypropylene Duct

Test	Bars	Coating	ℓ_e (d_b)	f_{max} (ksi)	Observed Damage
29	1-#11	Plain	8	40	Complete plug failure with top portion of duct
30	1-#11	Plain	12	68	Complete plug failure with duct
28	2-#11	Plain	16	85	Complete plug failure with top portion of duct
32	3-#11	Plain	16	67	Left Bar: Partial plug failure with duct Right Bar: Partial plug failure with duct Third Bar: Partial plug failure with duct

Figure 6.30 Observed Failure of Tests 30 and 28 (Polypropylene Duct)

Figure 6.31 Connectors from Test 32 after Pullout (Polypropylene Duct)

6.4 SUMMARY

Thirty-two tests of grouted vertical-duct connectors were conducted during the experimental phase of this project to determine the sensitivity of the connector performance to common design parameters. The load-slip response of the connectors was similar. Initially, the connectors exhibited linear response. The stiffness decreased slight when the splitting cracks in the grout extended into the surrounding concrete. An appreciable decrease in stiffness was observed after the formation of a pattern of widespread radial cracks in the concrete. Each connector failed by pullout, but many achieved stresses well above the measured yield stress of the reinforcement. The capacity of the connectors tended to increase as the embedded depth increased and the capacity decreased as the number of connectors tested simultaneously in tension increased. Detailed comparisons of the response of the connectors are presented in Chapter 7.

CHAPTER 7
Sensitivity of Measured Response to Experimental Parameters

The measured response of grouted vertical connectors was presented in detail in Chapter 6 and Appendix C. In those discussions, test data were presented separately for specimens constructed with different duct materials. An attempt is made to evaluate the sensitivity of the response of the connectors to the primary experimental parameters in this chapter. As discussed in Chapter 4, the primary parameters in the experimental phase of this investigation were bar coating, duct material, embedment depth, number of connectors, clear spacing of ducts, bar eccentricity, and transverse reinforcement.

In the following sections, the influence of each the experimental parameter on the measured response of the grouted vertical connectors is evaluated. Sensitivity of connector response to bar coating is discussed in Section 7.2, to duct material is discussed in Section 7.3, to embedded depth is discussed in Section 7.4, to the number of connectors is discussed in Section 7.5, to the clear spacing of the ducts is discussed in Section 7.6, to bar eccentricity is discussed in Section 7.7, and to transverse reinforcement is discussed in Section 7.8. Before evaluating the response of the specimens, however, it is instructive to develop an idealized framework for interpreting the observed response of the grouted vertical connectors. This idealization is discussed in Section 7.1.

7.1 IDEALIZED BOND RESPONSE OF GROUTED VERTICAL CONNECTORS

The observed response of the grouted vertical connectors was similar to the bond response of reinforcing bars in confined concrete (Figure 2.9). After the adhesion between the grout and the connector is lost, the ribs in the connector begin to bear on the grout. Slip of the connector occurs by progressive crushing of the grout in from of the ribs and splitting cracks appear in the grout surrounding the connector (Figure 7.1a). Due to the confinement provided by the duct (both galvanized steel and plastic), these cracks had essentially no impact on the stiffness of the connectors (Figure 7.1d). Increasing the applied tensile load distributes the bond stresses deeper along the connector, which engages additional ribs. Additional splitting cracks form along the connector and the cracks extend into the surrounding concrete. The first observable change in stiffness (Point A in Figure 7.1d) was typically associated with the formation of splitting cracks in the concrete. At initial cracking of the concrete, the response was sensitive to the amount of confinement provided by the ducts.

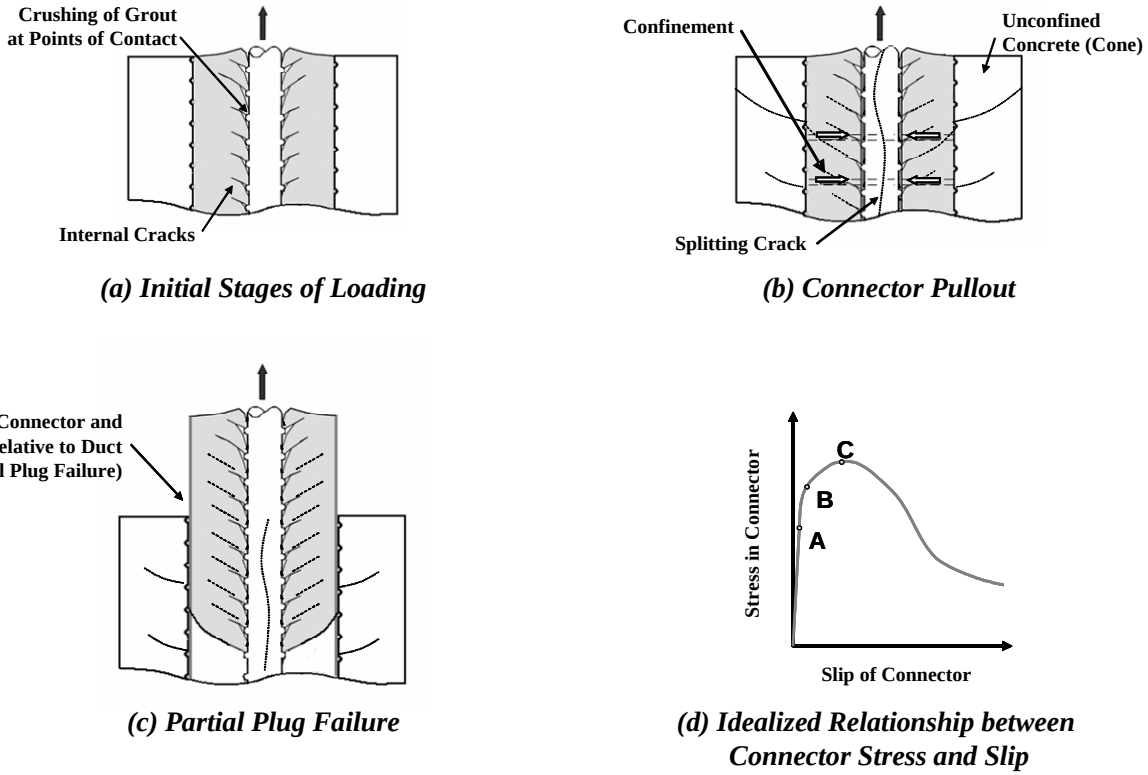

(a) Initial Stages of Loading

(b) Connector Pullout

(c) Partial Plug Failure

(d) Idealized Relationship between Connector Stress and Slip

Figure 7.1 Idealized Response of Grouted Vertical Connectors

The galvanized steel ducts acted as passive confinement that was engaged after the splitting cracks formed in the concrete (Figure 7.1b). After the formation of the widespread splitting cracks (Point B in Figure 7.1d), the stiffness of the connector decreased markedly. The resistance of the unconfined concrete near the surface was reduced by the formation of a concrete breakout cone. In the confined region below, the bond strength deteriorated due to bearing failure and reductions in the effective shearing area between the grout and the bar lugs. Pullout failures were most common.

In contrast, the polypropylene and polyethylene ducts did not confine the grout after the formation of widespread splitting cracks in the concrete. The plastic ducts tended to isolate the connector from the surrounding concrete in these specimens. In most of these tests, a large volume of grout slipped out of the duct with the connector (Figure 7.1c). In some cases, portions of the duct also pulled out with the plug of grout. In other cases, the grout ribs which correspond to the corrugations in the duct sheared off as the grout plug slipped relative to the duct.

In spite of the differences in the mode of failure, the shape of the stress-slip curves were similar. The comparisons discussed in this chapter are based on the maximum stress resisted by the connector (Point C in Figure 7.1d).

In comparing the response of the specimens, the average bond stress was used to evaluate the influence of the experimental parameters. Average bond stress, u, was calculated using Eq. (7.1):

$$u = \frac{f_s A_b}{\pi d_b \ell_e} \tag{7.1}$$

where f_s is the maximum tensile stress developed in the connector (psi), A_b is the area of the connector (in.^{2}), (π*d_b) is the perimeter of the connector (in.), and ℓ_e is the connector embedment depth (in.). Equation (7-1) is based on the assumption that bond stress is distributed uniformly along the connector, which is typically used to interpret the bond response of deformed reinforcement. This simplification was considered to be appropriate given the sparse information available regarding the actual bond stress distribution.

As discussed earlier in this section, the response of the connectors was sensitive to the formation of cracks in the concrete, but not sensitive to the formation of cracks in the grout. To facilitate comparisons among specimens with different strength concrete, the average bond stress has been divided by the square root of the compressive strength of the concrete in all comparisons. The square root of the compressive strength of the concrete was selected because this term is commonly assumed to be proportional to the tensile strength of the concrete. Because the observed response of the connectors was not sensitive to the formation of cracks in the grout, differences in grout strength were ignored in these comparisons.

7.2 INFLUENCE OF BAR COATING

The four pairs of specimens in Test Series 1 were used to evaluate the influence of bar coating. Single connectors were tested in all cases. The response of the four specimens with an embedded length of $8d_b$ is shown in Figure 7.2, and the four specimens with an embedded length of $12d_b$ are shown in Figure 7.3.

For the specimens with the shorter embedded lengths (Figure 7.2), the epoxy coating did not appear to influence the initial stiffness and had only a minor impact on behavior to the formation of widespread splitting cracks in the concrete. The maximum stress resisted by the epoxy-coated connectors was reduced by 17% for the specimens with polyethylene ducts (PE) and 6% for the specimens with galvanized steel ducts (GS). When the embedded length was increased, the differences between the response of the epoxy-coated and plain connectors were minimal (Figure 7.3).

Figure 7.4 shows the effect of bar coating on the axial stress distribution along the length of the bar. Data are shown for bars embedded $12d_b$. Although the bond-slip curves for plain and epoxy-coated bars were similar, some differences may be observed in the stress distributions along the connectors. As the load is increased from 40 to 80 ksi, stresses at a depth of 12 in. do not increase in the plain connector

as much as they do in the epoxy-coated connector. In a sense, the stresses are distributed more uniformly along the length of the epoxy-coated bar, and larger portions of the applied load are being carried by deeper sections of the connector. This difference in behavior can be attributed to the reduced frictional resistance of the epoxy coating.

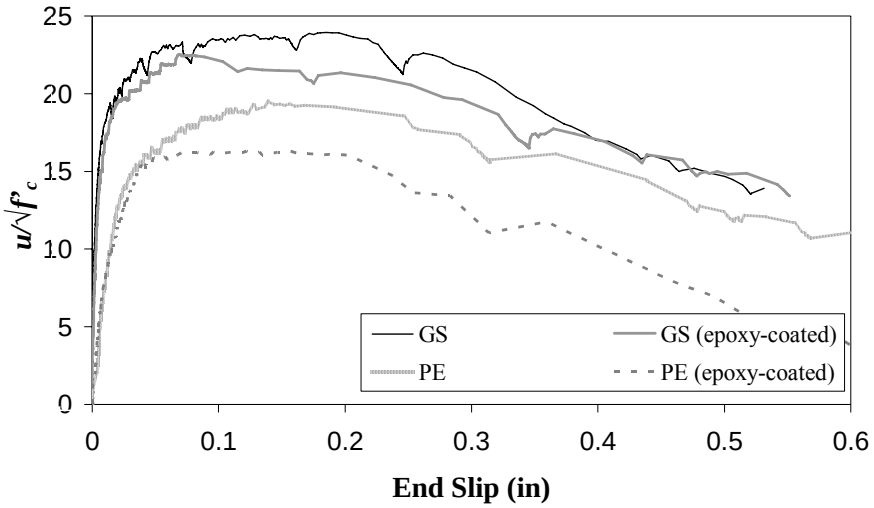

GS = Test 1 PE = Test 5
GS (epoxy-coated) = Test 2 PE (epoxy-coated) = Test 6

Figure 7.2 Influence of Bar Coating ($8d_b$ Embedment)

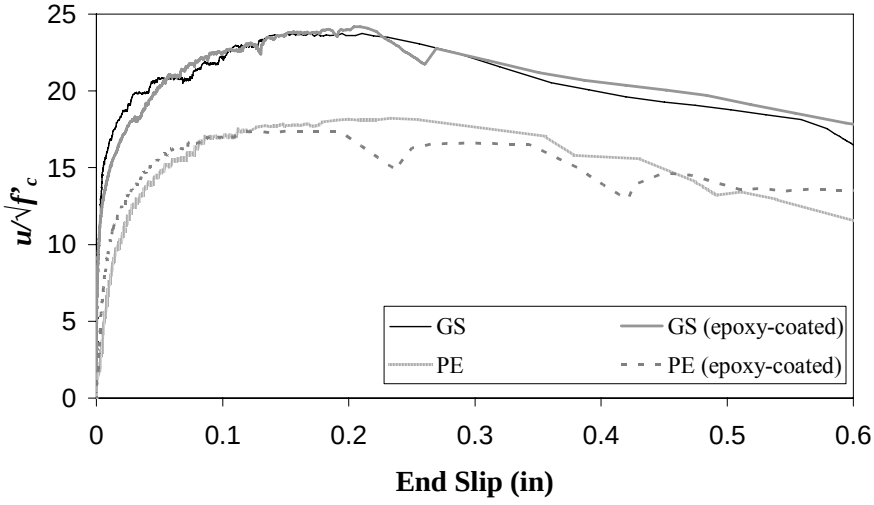

GS = Test 3 PE = Test 7
GS (epoxy-coated) = Test 4 PE (epoxy-coated) = Test 8

Figure 7.3 Influence of Bar Coating ($12d_b$ Embedment)

Bar coating was one of the first parameters investigated experimentally. Because data showed negligible effects on connector behavior at an embedment depth of $12d_b$, no further tests were conducted. In actual connections, the connector embedment depth will likely be much larger than $12d_b$. Thus, for practical purposes, the effect of bar coating on connection behavior is considered to be insignificant.

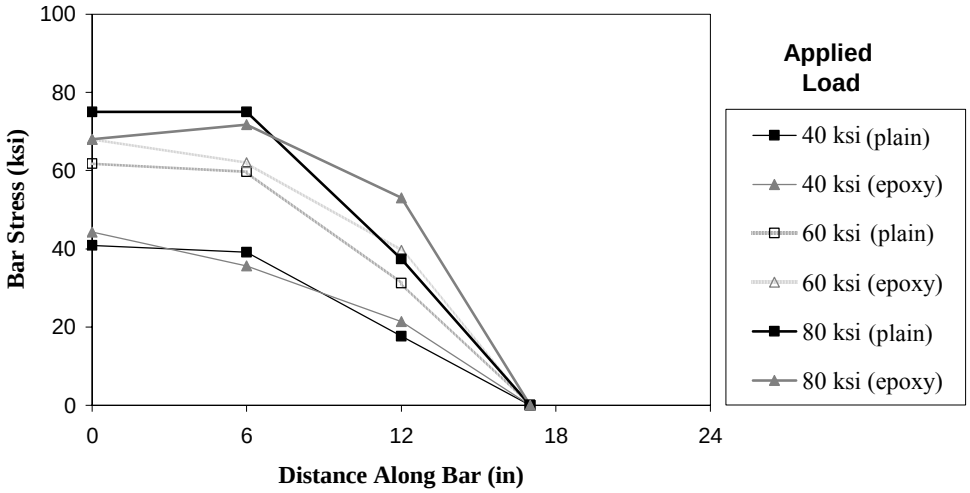

(plain) = Test 3 (epoxy) = Test 4

Figure 7.4 Sensitivity of Stress Distribution along Connector to Bar Coating (Galvanized Steel Duct, $12d_b$)

7.3 INFLUENCE OF DUCT MATERIAL

As discussed in Chapter 6, the connector response was sensitive to the choice of duct material. In particular, the observed modes of failure were closely tied to the duct material. The effect of duct material on behavior is evaluated by comparing the bond stress response of test specimens involving one, two, and three connectors. For tests with multiple connectors, the average response of the individual connectors is shown.

Specimens constructed with a single connector embedded $8d_b$ are compared in Figure 7.5. The initial stiffness and strength of the specimen with galvanized steel duct (GS) are greater than those for the two specimens with plastic ducts. Reductions in strength relative to the steel duct specimen are 18% and 37% for specimens with polyethylene (PE) and polypropylene (PP) ducts, respectively. The variation in stress distribution along the length of the connectors is shown in Figure 7.6. Stresses at a depth of 6 in. are consistently smaller for the specimen with galvanized steel duct. Polyethylene and polypropylene ducts are less effective at preventing slip of the connector, so high stresses propagate further down the connector.

Figure 7.7 shows the bond stress-slip response of single-connectors embedded $12d_b$. One of the specimens (ND) was constructed by removing a steel duct was removed from the beam prior to placement

of the connector and grout. The initial stiffness is again highest for the test specimen with galvanized steel ducts (GS). A slightly higher stiffness was observed for the specimen containing polypropylene (PP) with respect to the polyethylene (PE) duct. The curve corresponding to the specimen with no duct (ND) presents a small kink at the beginning of loading, possible caused by instrumentation error or by sudden adjustment of the wedges that gripped the connector. Consideration of the portion of the curve above the kink shows that the initial stiffness for the specimen with no duct is comparable to that of the polyethylene duct specimen. The initial slope of the bond stress-slip curve is related directly to the degree of confinement surrounding the connector.

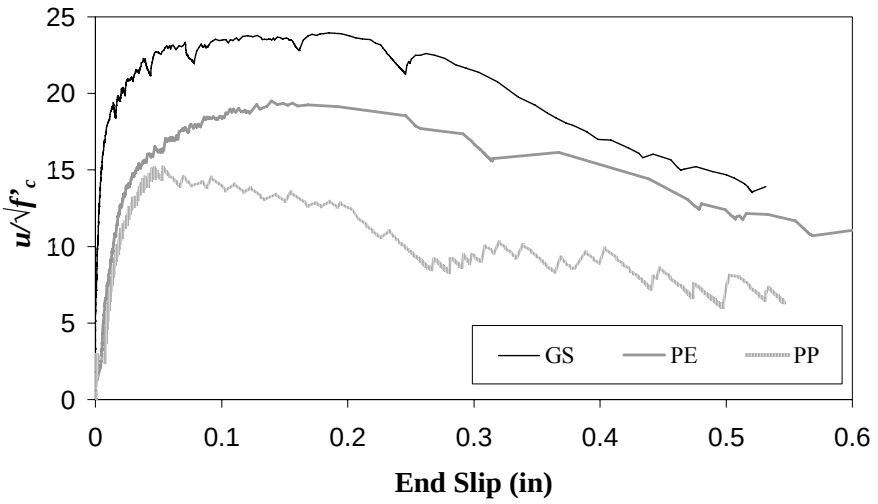

GS = Test 1 PE = Test 5 PP = Test 29

Figure 7.5 Influence of Duct Material (Single Connectors, $8d_b$ Embedment)

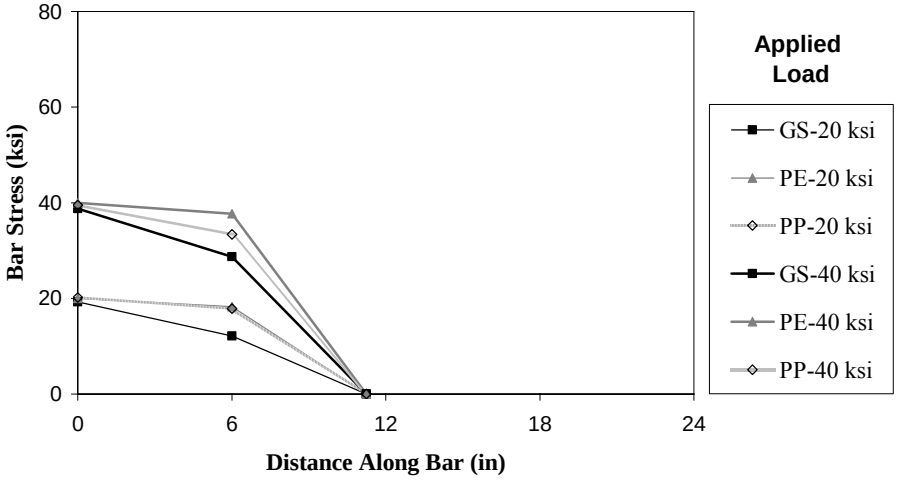

GS = Test 1 PE = Test 5 PP = Test 29

Figure 7.6 Influence of Duct Material on Stress Distribution along Connector (Single Connectors, $8d_b$ Embedment)

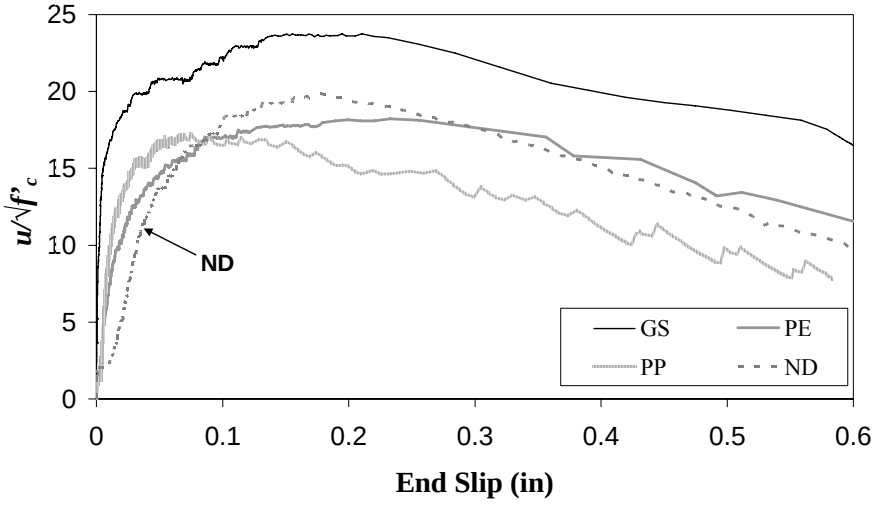

GS = Test 3 PE = Test 7 PP = Test 30 ND = Test 12

Figure 7.7 Influence of Duct Material (Single Connectors, 12d_b Embedment)

Comparison of the specimens in terms of bond strength leads to a surprising observation, where the bond strength of the specimen with no duct is actually higher than that of the specimens with plastic duct. Reductions in bond strength relative to the steel duct specimen are 17% for the specimen with no duct, 23% for the specimen with polyethylene duct, and 27% for the specimen with polypropylene duct. Plastic ducts do not provide confinement to the connector and grout, and appear to have a negative effect on the frictional resistance of the connection.

The variation in stress distribution along connectors embedded in different duct materials is shown in Figure 7.8. The propagation of stress along connectors is directly related to the initial stiffness (or slip) of the connectors. At applied stress levels of 20 and 40 ksi, the connector with no duct has the highest stress at a depth of 12 in.; connectors housed inside both types of plastic duct follow. At an applied stress of 60 ksi, the stress at 12 in. in the connector housed inside the polyethylene duct is the highest.

When no duct is provided, cracks that form in the grout can propagate more easily into the concrete. Ducts made of the plastic materials interrupt the cracks that form in the grout, but at higher load levels, slip of the grout/bar out of the duct becomes significant. Spacing between the ribs of the polyethylene ducts is larger than that of the polypropylene ducts. Shorter spacing between duct ribs increases the grout plug bond strength of the connection and influences the initial stiffness of the connection. Based on the limited available data, the geometrical properties of the ducts (the spacing between the ribs and the height of the ribs), rather than the material properties of the plastic duct, appear to govern the behavior of the connectors.

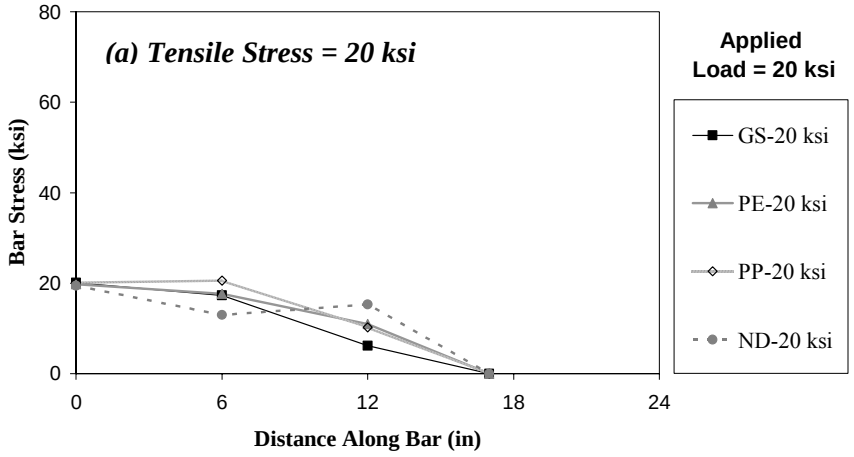

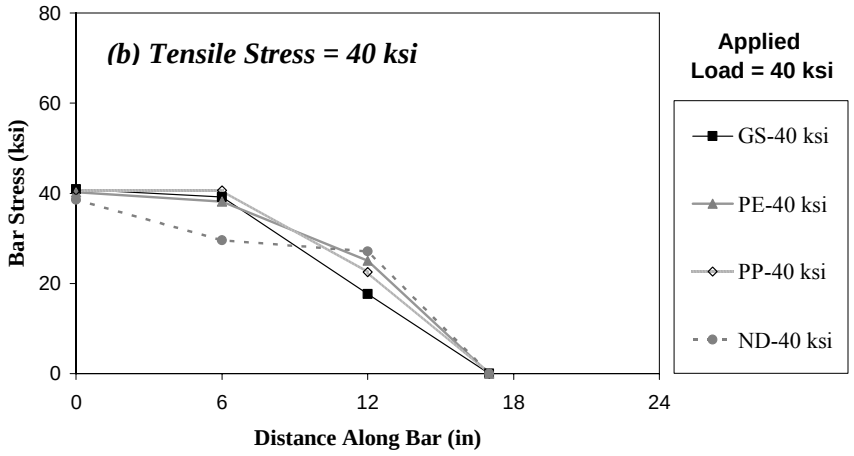

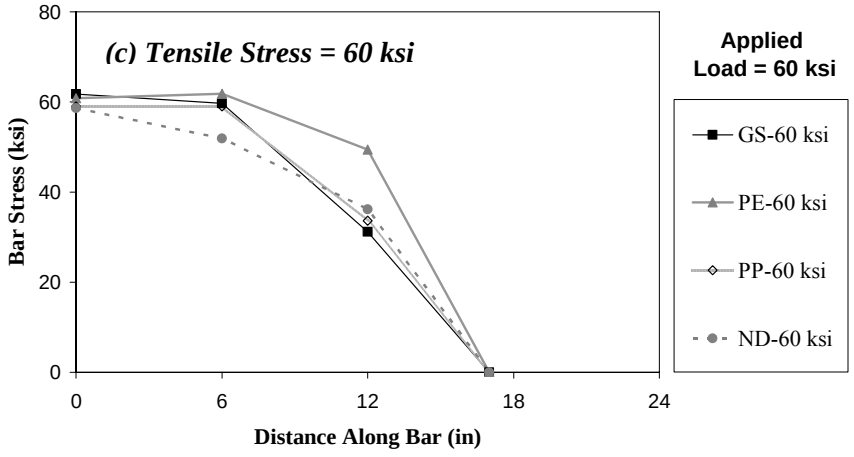

GS = Test 3 PE = Test 7 PP = Test 30 ND = Test 12

Figure 7.8 Effect of Duct Material on Stress Distribution along Connector (Single Connectors, $12d_b$ Embedment)

Figure 7.9 shows the bond-stress response of specimens with double connectors and an embedment of $12d_b$. Comparison is made only between specimens with galvanized steel (GS) and polyethylene (PE) duct. Higher initial stiffness and bond strength are again associated with the specimens with steel duct. The bond strength of the specimen containing polyethylene ducts is approximately 27% lower than that of the steel duct specimen. This reduction level is similar to that shown in Figure 7.7 for single connectors with the same embedment depth.

Figure 7.10 compares the bond stress-slip response of specimens with double connectors and an embedment of $16d_b$. The specimen with steel duct again has the highest initial stiffness, followed by the polypropylene duct specimen. With respect to bond strength relative to the specimen with steel duct, a reduction of 27% was again observed in the specimen containing polyethylene ducts. The specimen with polypropylene duct shows a smaller reduction in bond strength of 17%.

Figure 7.11 compares the bond stress-slip response of the two specimens tested with three connectors. The embedded depth was $16d_b$. Following the established trend, initial stiffness and strength are higher for the specimen with galvanized steel duct. The strength of the specimen with polypropylene duct was approximately 10% less than the strength of the specimen with steel duct.

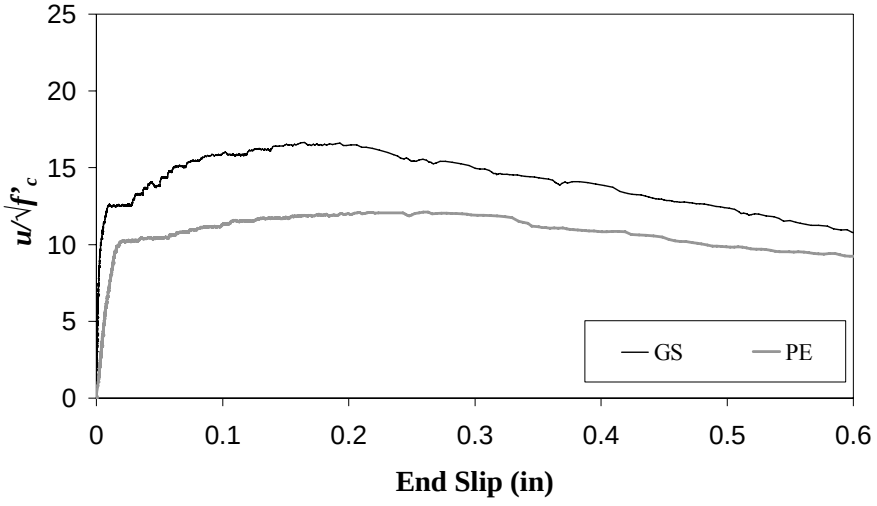

GS = Test 17 PE = Test 18

Figure 7.9 Influence of Duct Material (Double Connectors, $12d_b$ Embedment)

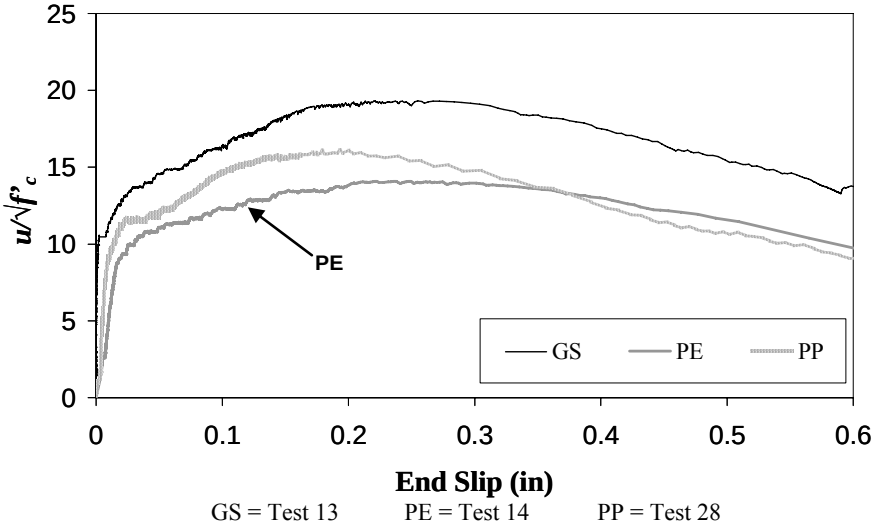

GS = Test 13 PE = Test 14 PP = Test 28

Figure 7.10 Influence of Duct Material (Double Connectors, 16d_b Embedment)

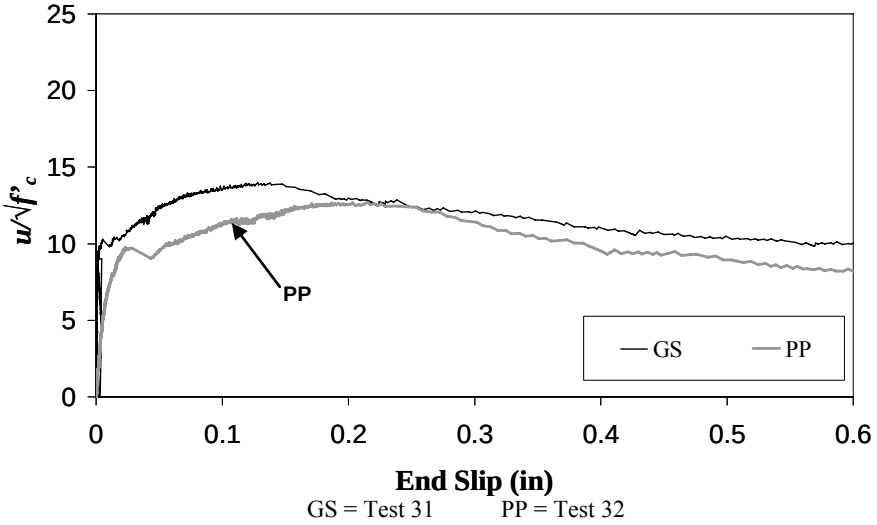

GS = Test 31 PP = Test 32

Figure 7.11 Influence of Duct Material (Triple Connectors, 16d_b Embedment)

7.4 INFLUENCE OF EMBEDMENT DEPTH

The effect of embedment depth on connection behavior is evaluated by comparing the bond stress response of test specimens with one and two connectors. The comparisons are made separately for specimens constructed with different duct materials. For tests with two connectors, the average response of the individual connectors is shown.

Embedment depth appears to have a negligible effect on initial stiffness and strength of single connectors in galvanized steel ducts (Figure 7.12). The initial stiffness of double connectors also appears to be independent of the embedment depth (Figure 7.13), but the specimen with the deeper embedment achieved higher bond stresses.

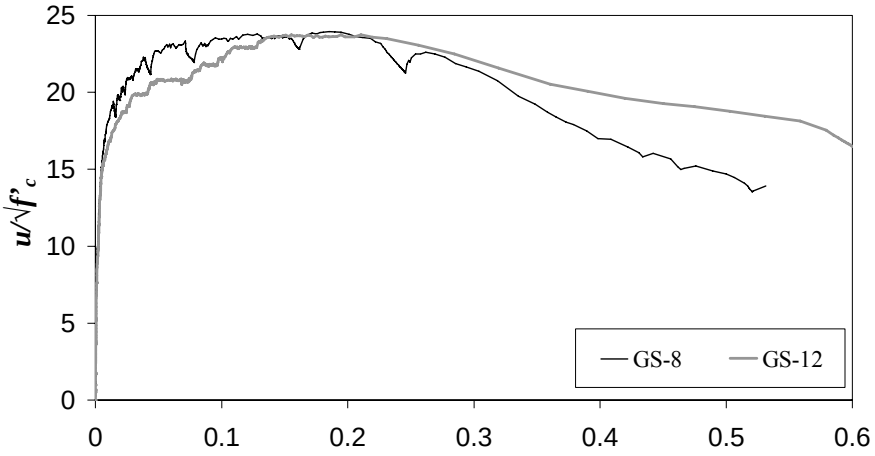

GS-8 = Test 1 GS-12 = Test 3

Figure 7.12 Influence of Embedment Depth (Single Connectors, Galvanized Steel Duct)

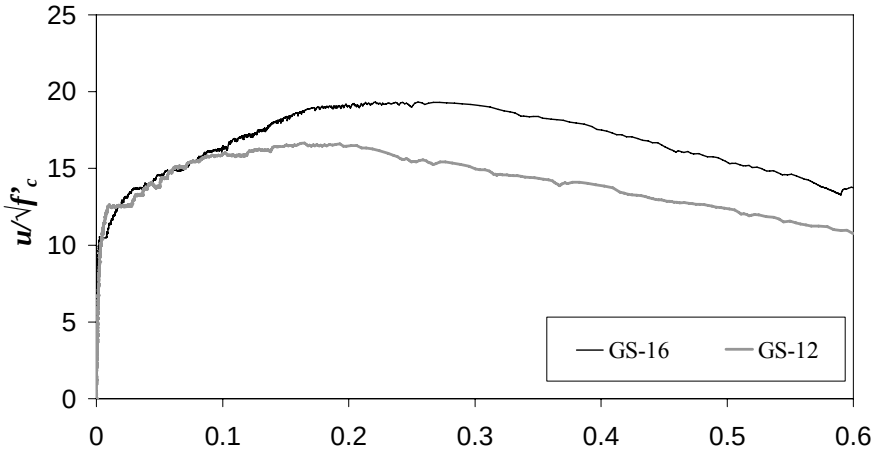

GS-16 = Test 13 GS-12 = Test 17

Figure 7.13 Influence of Embedment Depth (Double Connectors, Galvanized Steel Duct)

The response of single and double connectors in polyethylene (PE) ducts is shown in Figure 7.14 and Figure 7.15, respectively. Embedment depth appears to have a minor influence on the initial stiffness and bond strength of the single connectors. The connector embedded $16d_b$ show an increase in toughness (area under the curve) with respect to the specimens with shorter embedment depths. When two connectors were tested, the initial stiffness was independent of the embedment depth, but the connectors with the deeper embedment achieved approximately 15% higher maximum bond stress.

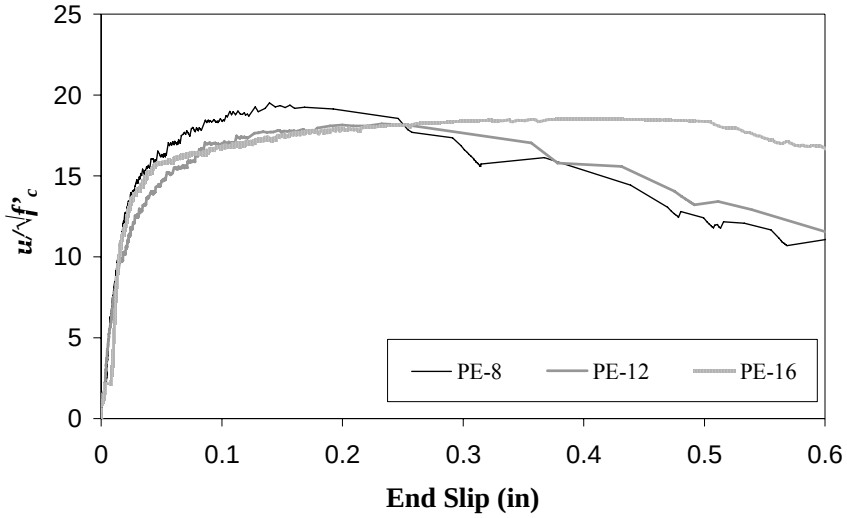

PE-8 = Test 5 PE-12 = Test 7 PE-16 = Test 22

Figure 7.14 Influence of Embedment Depth (Single Connectors, Polyethylene Duct)

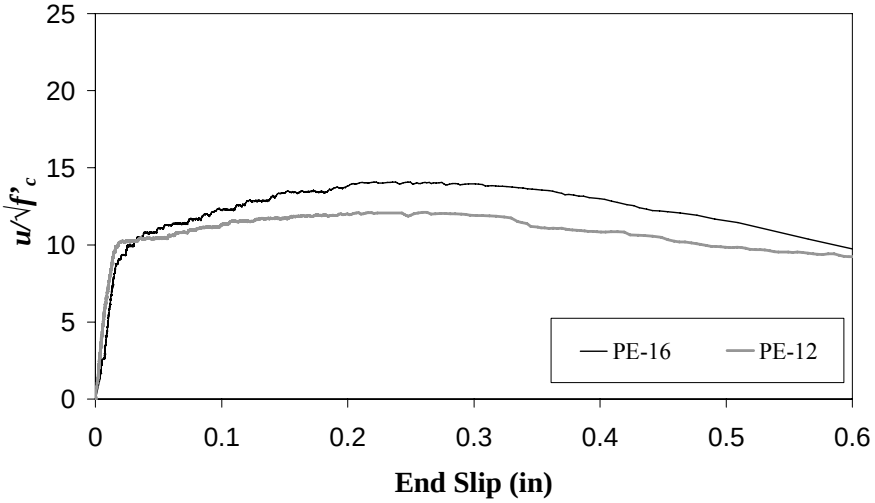

PE-16 = Test 14 PE-12 = Test 18

Figure 7.15 Influence of Embedment Depth (Double Connectors, Polyethylene Duct)

The effect of embedment depth on behavior of specimens containing polypropylene (PP) duct specimens is shown in Figure 7.16. A minor reduction in strength is observed in the specimen with the shorter embedment.

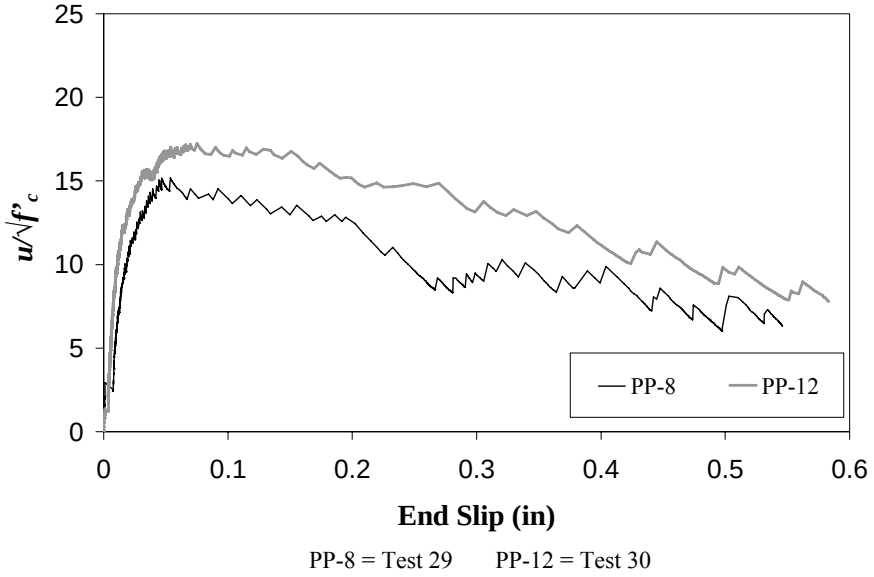

PP-8 = Test 29 PP-12 = Test 30

Figure 7.16 Influence of Embedment Depth (Single Connector, Polypropylene Duct)

7.5 INFLUENCE OF NUMBER OF CONNECTORS

The influence of the number of connectors on bond strength is evaluated in this section. All specimens considered were constructed with closely-spaced ducts – the clear spacing between ducts is approximately equal to the diameter of the duct. The comparisons are made separately for specimens constructed with different duct materials. For tests with multiple connectors, the average response of the individual connectors is shown.

Figure 7.17 compares the response of single and double connectors embedded $12d_b$ in galvanized steel ducts. While the initial stiffness is not affected by the number of connectors, a substantial reduction in bond strength was observed. The maximum stress resisted by the double connectors was approximately 25% less than the maximum stress resisted by the single connector. Similar behavior was observed for double and triple connectors embedded $16d_b$ in galvanized steel ducts (Figure 7.18).

Figure 7.19 shows the effect of increasing the number of connectors from two to three on stress distribution along the connectors. At small loads, the shape of the stress distribution is independent of the number of connectors. At higher loads, increasing the number of connectors affects the stress distribution.

The effect of number of connectors on the behavior of connections containing polyethylene ducts is shown in Figure 7.20 and Figure 7.21. Again, the bond strength is reduced as the number of connectors is increased. For the polyethylene ducts, the reduction was approximately 30% for connectors embedded $12d_b$ and approximately 25% for connectors embedded $16d_b$.

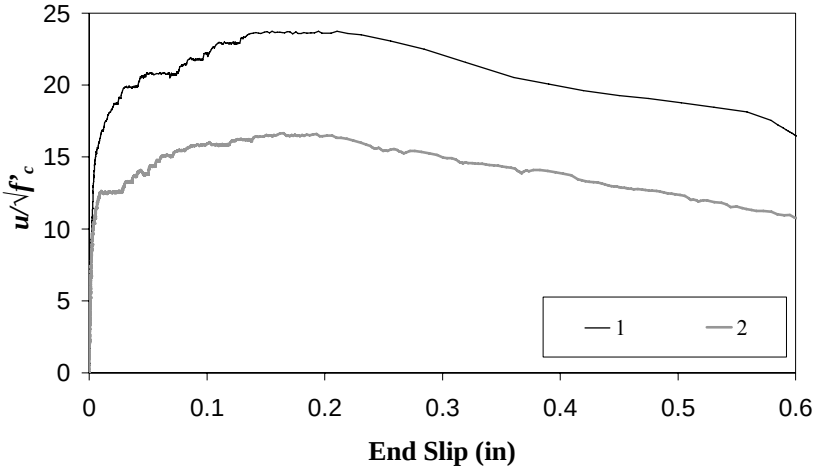

1 = Test 3 2 = Test 17

Figure 7.17 Influence of Number of Connectors (Galvanized Steel Duct, 12d_b Embedment)

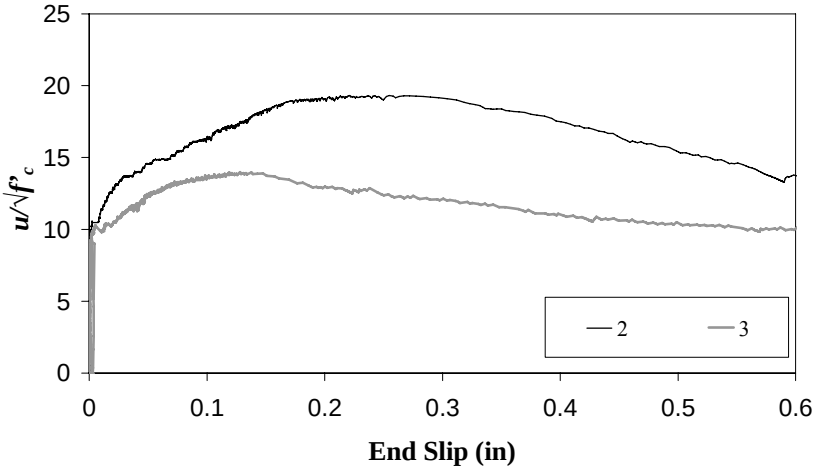

2 = Test 13 3 = Test 31

Figure 7.18 Influence of Number of Connectors (Galvanized Steel Duct, 16d_b Embedment)

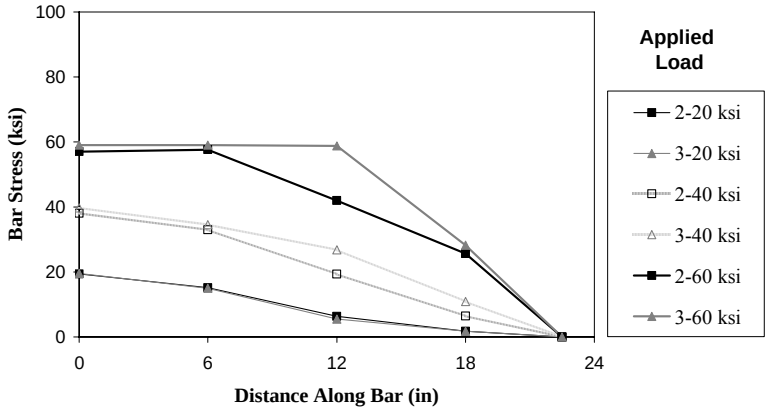

2 = Test 13 3 = Test 31

Figure 7.19 Influence of Number of Connectors on Stress Distribution along Connectors (Galvanized Steel Duct, 16d_b Embedment)

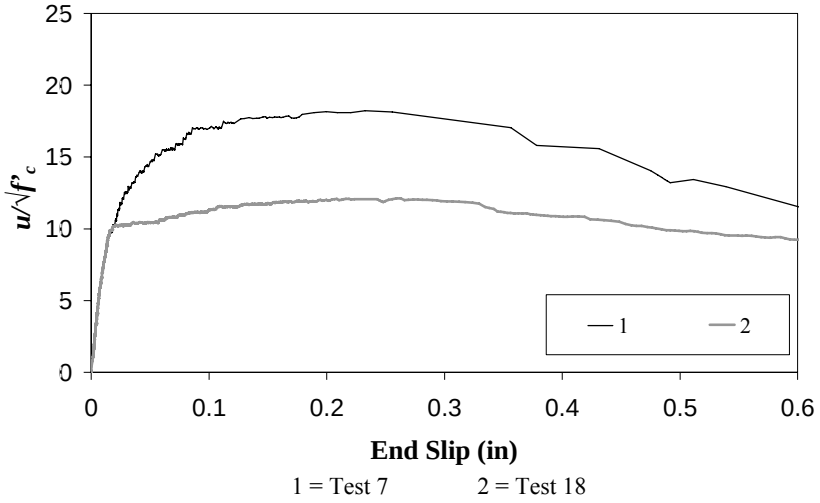

1 = Test 7 2 = Test 18

Figure 7.20 Influence of Number of Connectors (Polyethylene Duct, 12d_b Embedment)

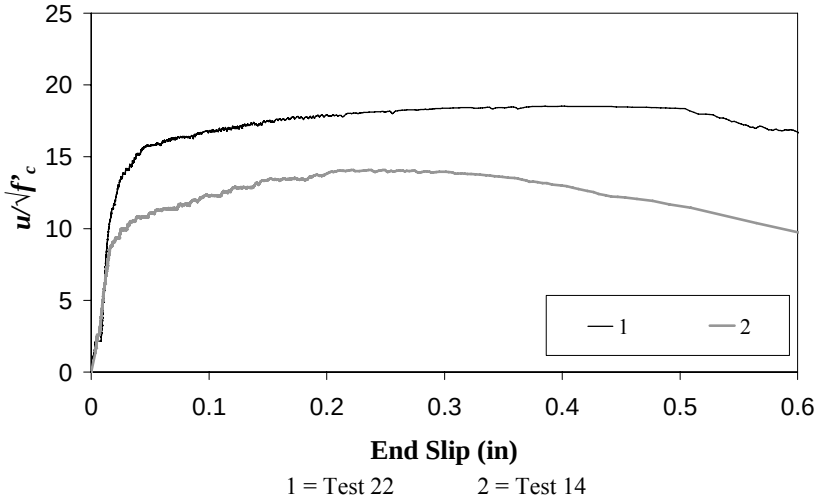

1 = Test 22 2 = Test 14

Figure 7.21 Influence of Number of Connectors (Polyethylene Duct, 16d_b Embedment)

The effect of increasing the number of connectors from one to two on the stress distribution along the length of connectors is shown in Figure 7.22. At low levels of applied load, the axial stress distribution along connectors is independent of the number of connectors. At high load levels (and after splitting of the concrete has occurred), increasing the number of connectors affects the stress distribution, and a larger portion of the load is anchored deep in the embedment.

Figure 7.23 shows the effect of number of connectors on behavior of connection specimens containing polypropylene ducts. An increase in the number of connectors from two to three leads to a decrease in bond strength of 21%. Initial connection stiffness is affected very little by an increase in number of connectors. The stress distribution along connectors in polypropylene ducts is affected by an increase in the number of connectors in a manner similar to that described for specimens with galvanized steel and polyethylene duct (Figure 7.24).

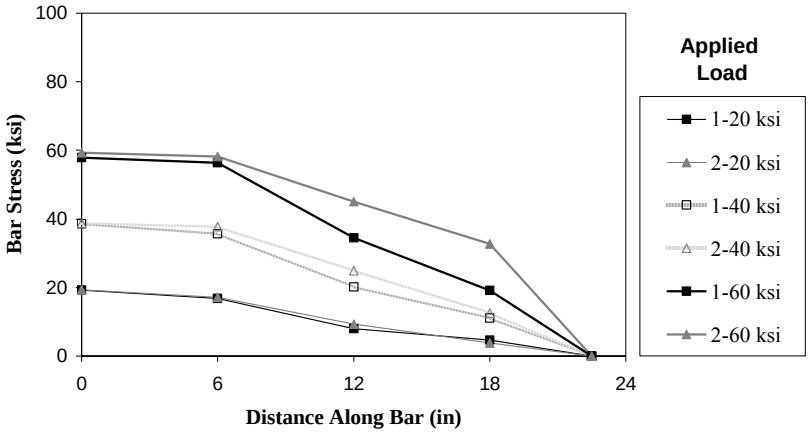

1 = Test 22 2 = Test 14

Figure 7.22 Effect of Number of Connectors on Stress Distribution along Connectors (Polyethylene Duct, 16d_b Embedment)

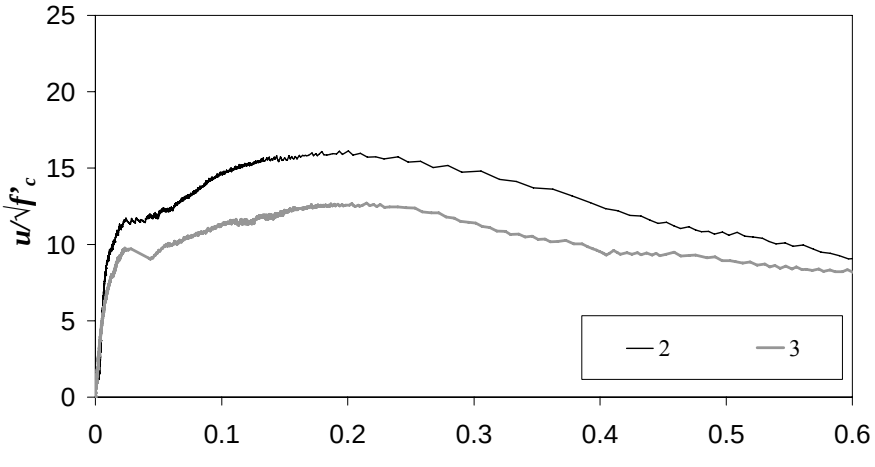

2 = Test 28 3 = Test 32

Figure 7.23 Influence of Number of Connectors (Polypropylene Duct, 16d_b Embedment)

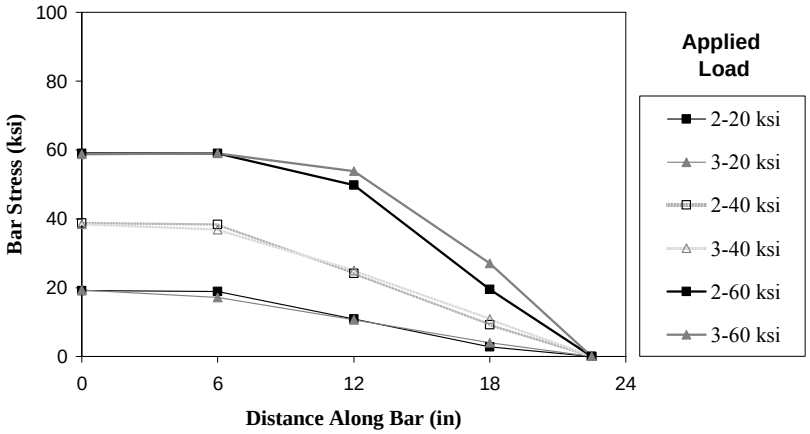

2 = Test 28 3 = Test 32

Figure 7.24 Effect of Number of Connectors on Stress Distribution along Connectors (Polypropylene Duct, 16d_b Embedment)

7.6 INFLUENCE OF DUCT SPACING

A limited number of tests were conducted to evaluate the influence of duct spacing. Two connectors were tested in all comparisons. In most cases, the clear spacing of the duct was 1*D*, where *D* is the nominal diameter of the duct. Two specimens in Test Series 5 were constructed with a clear spacing of 2*D*.

The response of the specimens constructed with galvanized steel duct is shown in Figure 7.25. The response of the specimens was nearly the same, but a very small increase in bond strength was observed for the specimen with the larger duct spacing. In contrast, the specimen with the closer duct spacing achieved slightly higher bond stresses when polyethylene duct was used (Figure 7.26). This result was not expected, and additional tests are required to investigate this trend further. However, the specimen strength and stiffness does not appear to be sensitive to the spacing of the ducts.

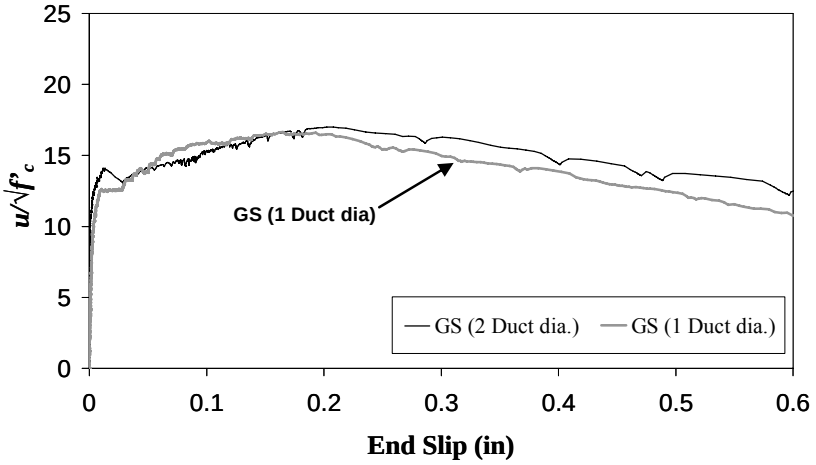

GS (2 Duct dia.) = Test 23 GS (1 Duct dia.) = 13

Figure 7.25 Influence of Duct Spacing (Steel Duct, 12d_b Embedment)

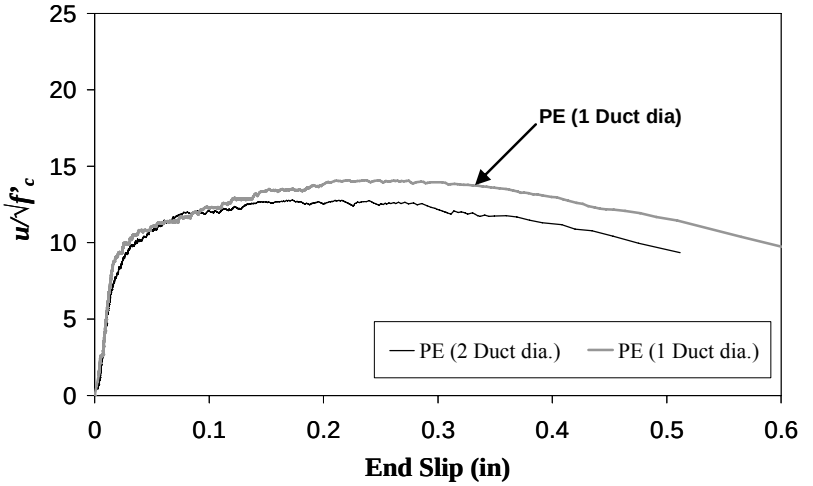

PE (2 Duct dia.) = Test 24 PE (1 Duct dia.) = 26

Figure 7.26 Influence of Duct Spacing (Polyethylene Ducts, 16d_b Embedment)

7.7 INFLUENCE OF BAR ECCENTRICITY

Eccentric placement of the connectors inside the duct was investigated in Test Series 4. Figure 7.27 shows the response of specimens with single connectors embedded $8d_b$ in galvanized steel and polyethylene ducts. Bar eccentricity has a small influence on the initial stiffness and reduces the capacity by approximately 17%. The same trends may be observed for specimens with single connectors embedded $12d_b$ (Figure 7.28).

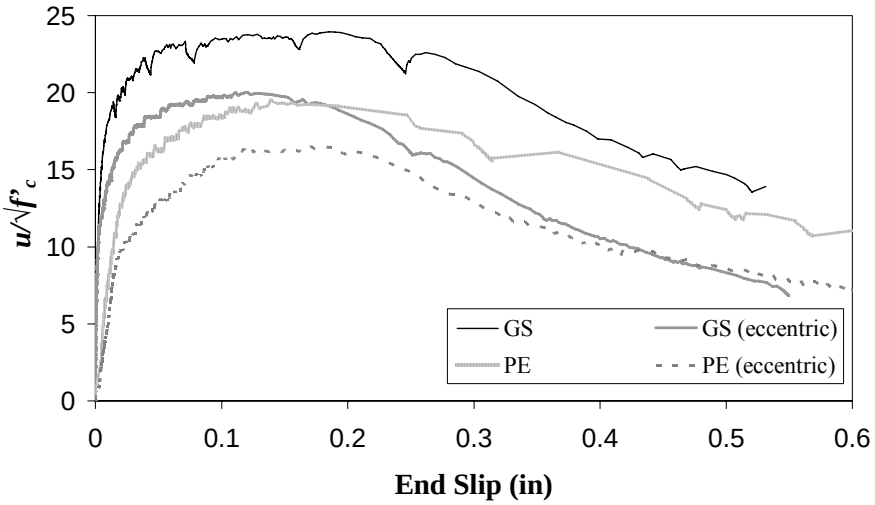

GS = Test 1 PE = Test 5
GS (eccentric) = Test 19 PE (eccentric) = Test 20

Figure 7.27 Influence of Connector Eccentricity ($8d_b$ Embedment)

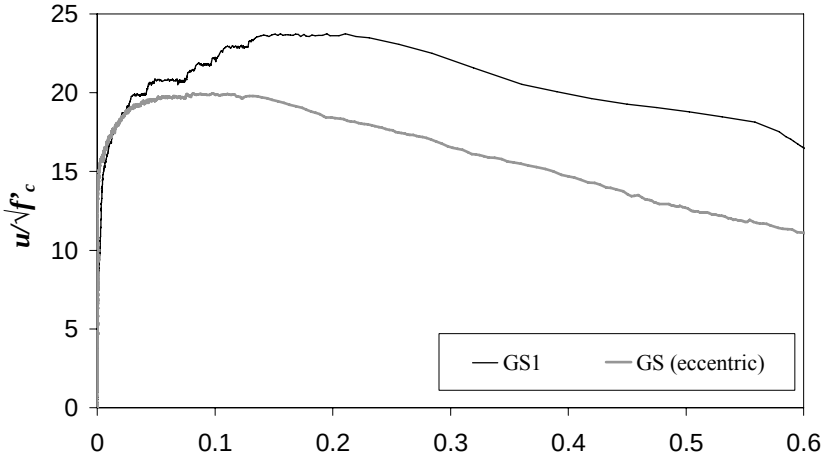

GS1 = Test 3 GS (eccentric) = Test 21

Figure 7.28 Influence of Connector Eccentricity ($12d_b$ Embedment)

Figure 7.29 shows the effect of bar eccentricity on the stress distribution along the connector. The stresses in the connector placed eccentrically in the duct at depths of 6 and 12 in. are equal to or smaller than those of the connector placed concentrically. At high levels of applied stresses, a larger portion of the load is anchored deeper in the connector placed eccentrically.

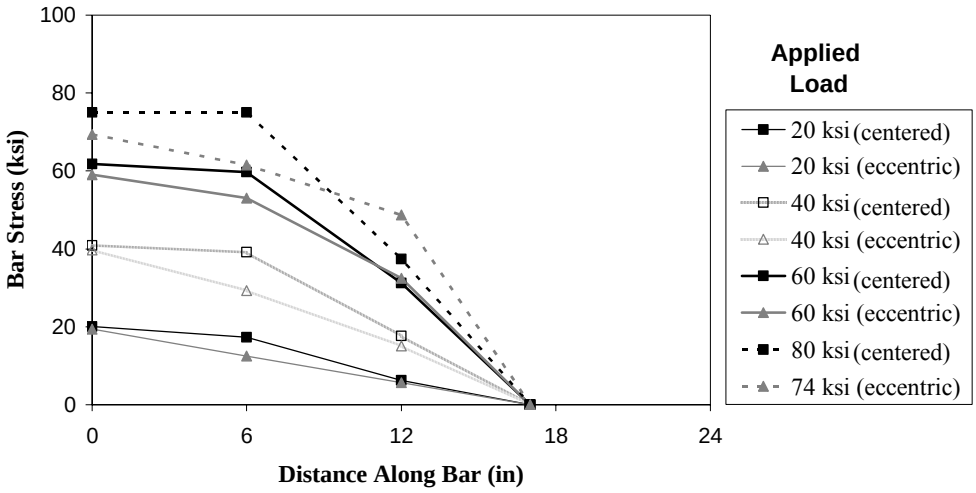

(centered) = Test 3 GS (eccentric) = Test 21

Figure 7.29 Effect of Bar Eccentricity on Stress Distribution along Connector ($12d_b$ Embedment)

7.8 INFLUENCE OF TRANSVERSE REINFORCEMENT

Two types of transverse reinforcement were investigated: a large spiral around a group of ducts and smaller spirals around individual ducts. Specimens were also tested without any form of spiral reinforcement.

Figure 7.30 shows the response of specimens with two connectors in galvanized steel ducts. One of the specimens was constructed with a large spiral around the group of four connectors, while no transverse reinforcement was used in the other specimen. The transverse reinforcement (group spiral) seems to have a negligible influence on the behavior of the connections.

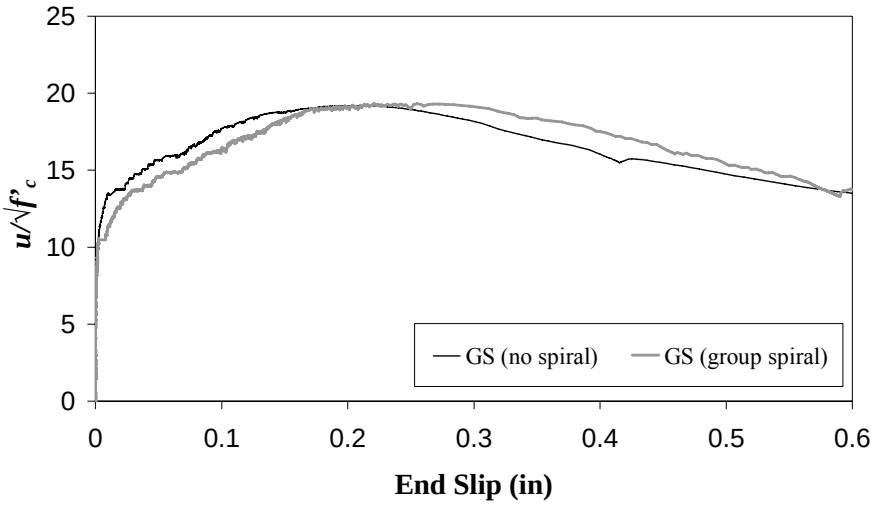

GS (no spiral) = Test 15 GS (group spiral) = Test 15

Figure 7.30 Effect of Transverse Reinforcement (Steel Ducts, $16d_b$ Embedment)

The influence of transverse reinforcement on the behavior of connections containing polyethylene ducts is evaluated in Figure 7.31 and Figure 7.32. Specimens with single connectors and embedment depths of $8d_b$ and $12d_b$ indicate that the presence of the individual spirals around ducts degraded the performance of the connection (Figure 7.31). Although the spiral reinforcement was somewhat effective in restraining the upward movement (slip) of the duct, failure occurred as the bar/grout slipped out of the polyethylene duct.

The response of specimens with two connectors and an embedment depth of $16d_b$ is shown in Figure 7.32. The specimen constructed with a large spiral around the group of four connectors exhibited a slightly higher bond strength than the specimen constructed with no transverse reinforcement. In this case, the use of small spirals around individual ducts did not improve the performance of the connectors, but had a modest negative impact on the response. The small pitch of the individual spirals, and the small clearance between spirals and the ducts probably interfered with placement of the concrete, which could lead to lower strength concrete in the vicinity of the duct. This is only a hypothesis, because the strength of the concrete in the vicinity of the ducts was not investigated experimentally.

The response of strain gages bonded to the spiral reinforcement is not presented because there is no meaningful data to report. Significant strains are possible only at locations where radial splitting cracks formed, and these did not coincide with the location of strain gages. Because crack widths were not measured, no evaluation is made of the effectiveness of the transverse reinforcement in controlling the opening of cracks.

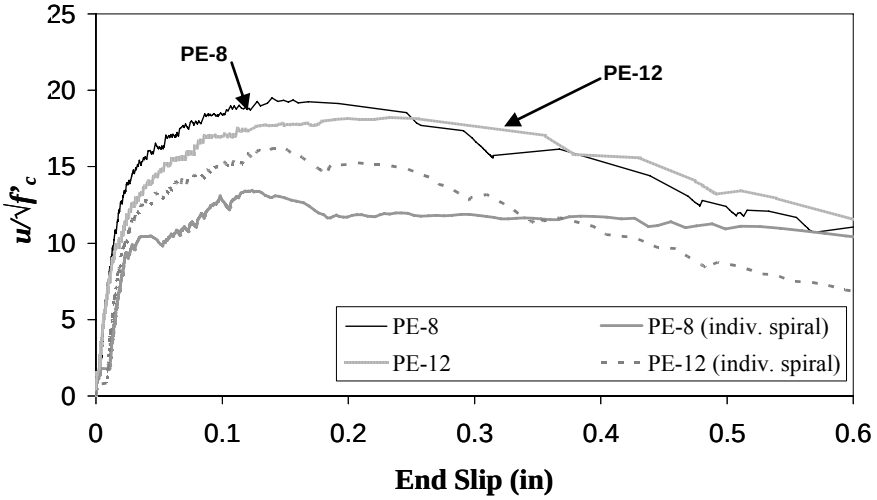

PE-8 = Test 5 PE-8 (indiv. spiral) = Test 25
PE-12 = Test 7 PE-12 (indiv. Spiral) = Test 27

Figure 7.31 Influence of Transverse Reinforcement (Single Connectors, Polyethylene Duct)

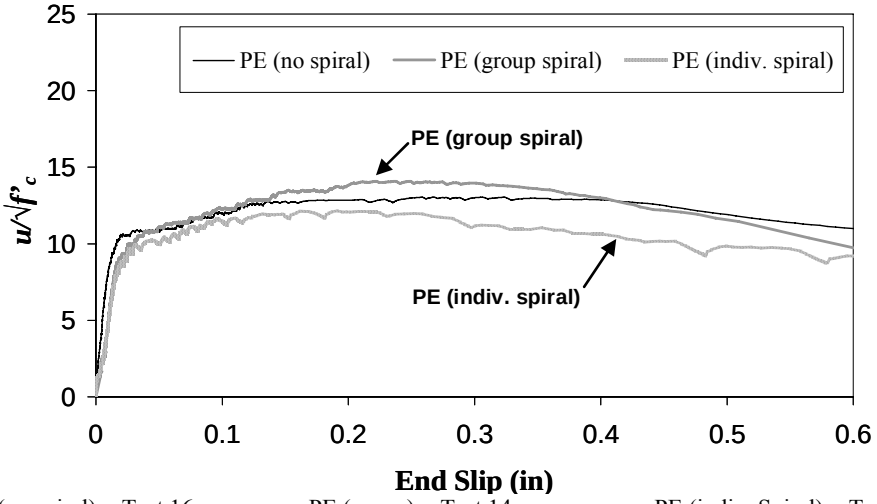

PE (no spiral) = Test 16 PE (group) = Test 14 PE (indiv. Spiral) = Test 26

Figure 7.32 Influence of Transverse Reinforcement (Double-Connectors, Polyethylene Duct, 16d_b Embedment)

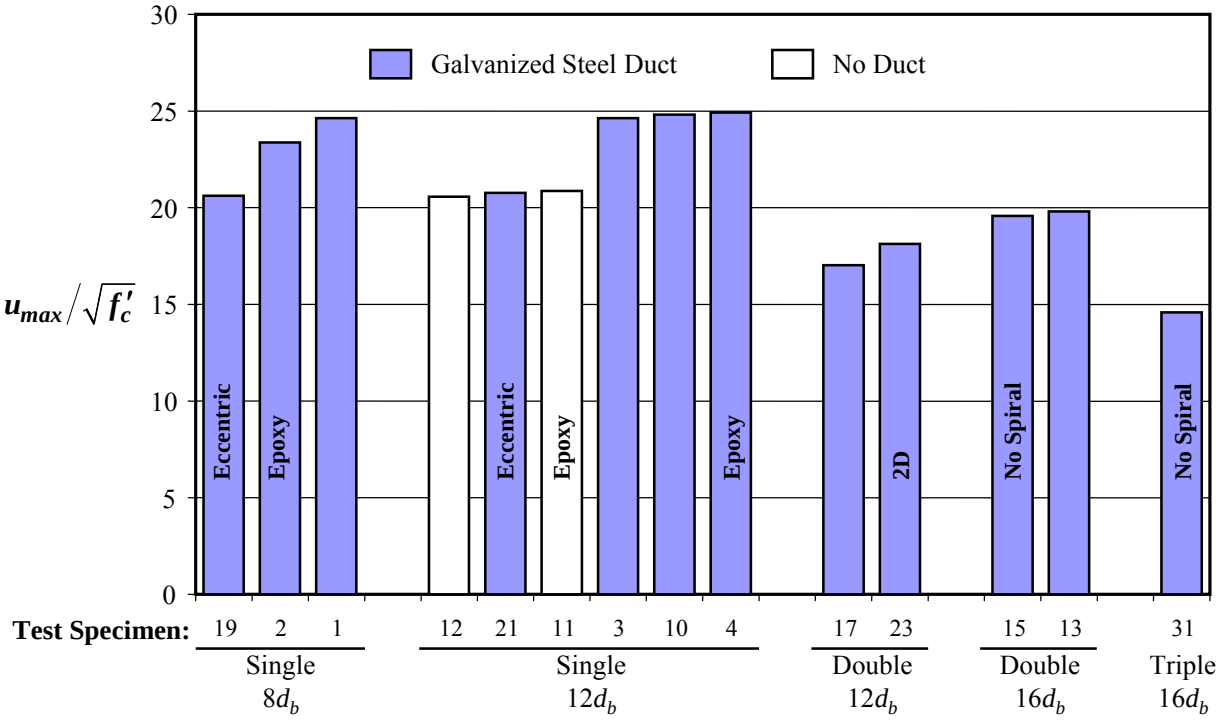

Figure 7.33 Capacity of All Specimens with Galvanized Steel Duct

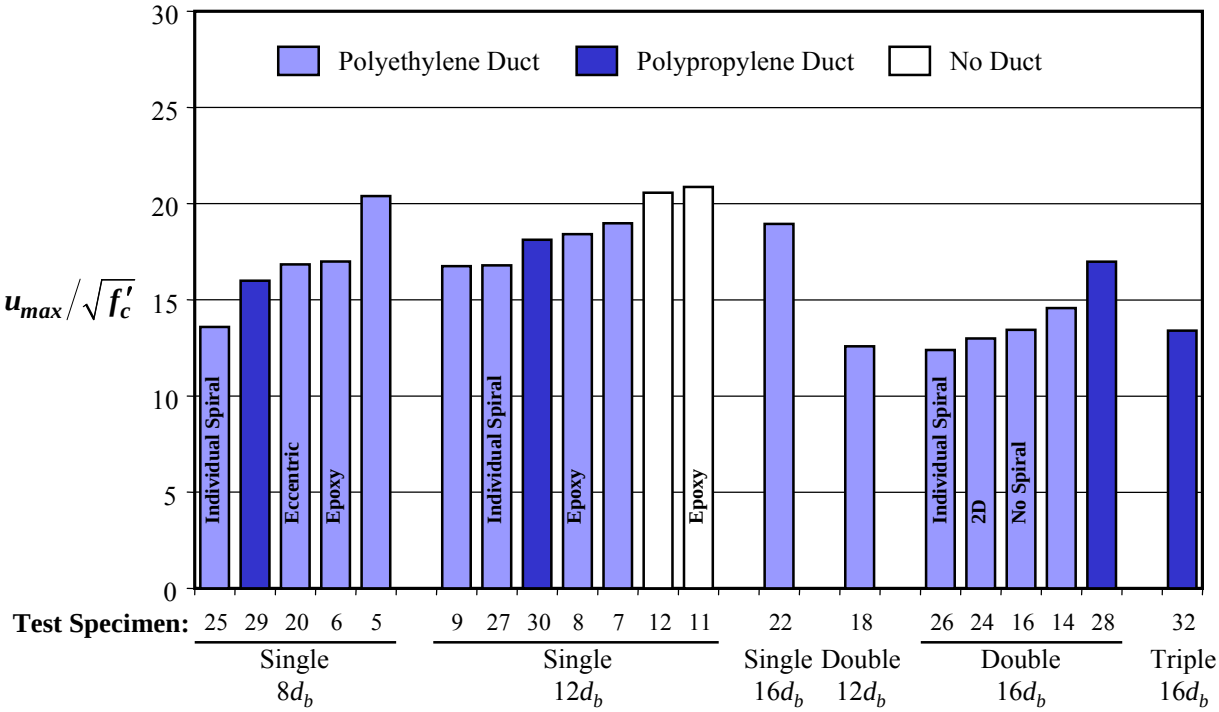

Figure 7.34 Capacity of All Specimens with Plastic Duct

7.9 SUMMARY

Based on the results of the experimental program, the average bond stress resisted by the grouted vertical connectors was found to be most sensitive to the type of duct, the number of connectors tested simultaneously in tension, and the eccentricity of the connector within the duct. The response was found to be insensitive to the presence of epoxy coating, the embedded depth of the connector, the clear spacing between ducts, and the presence of transverse reinforcement.

The bond strengths of all specimens are compared in Figure 7.33and Figure 7.34. The test number, the number of connectors tested simultaneously and the embedded length are indicated below the horizontal axes. The type of duct is indicated by the color of the bars. Most of the specimens were constructed with plain bars, a single spiral around the entire group of ducts, with the connectors centered within the ducts, and with a clear spacing between ducts of 1*D*. Specimens that were constructed with different configurations are indicated.

The twelve specimens with galvanized steel duct and the two specimens with no duct are plotted in Figure 7.33. Although the specimens with no duct do not represent a practical configuration, the data are shown to highlight the influence of the duct. The capacities of specimens with single connectors centered in galvanized steel duct and embedded $12d_b$ are consistently higher than similar specimens with no duct. This observation highlights the influence of the passive confinement provided by the galvanized steel duct (Figure 7.1b). In contrast, the capacities of specimens with single connectors centered in polyethylene or polypropylene duct and embedded $12d_b$ are consistently less than similar specimens with no duct (Figure 7.34). This observation highlights the reduction of strength that may be attributed to slip of the connector and grout relative to the surrounding concrete due to the presence of the plastic duct (Figure 7.1c).

Grouted vertical connectors in galvanized steel duct resisted consistently higher average bond stresses than connectors in polyethylene or polypropylene ducts. Differences were in the range of 15 to 35%. Reductions in the average bond strength were observed when multiple connectors were tested. Comparing specimens with one and two connectors, a 25 to 30% reduction was observed. Additional reductions were observed when the number of connectors increased from two to three. Eccentric placement of the connector within the duct reduced the capacity between 15 and 20%.

Epoxy coating did reduce the average bond strength of connectors with short embedded lengths by 5 to 15%. However, when the embedded length was increased to $12d_b$, the influence of the coating was negligible.

In most cases, the average bond strength varied by less than 10% for embedded depths of 8, 12, and 16 d_b. This result was not expected, because the average bond stress developed in deformed

reinforcement is very sensitive to ℓ_e/d_b in this range (Orangun et al. 1977). The differences in the response of the grouted vertical connectors are attributed to the confinement provided by the duct, which restrains the development of splitting cracks in the concrete.

Varying the clear spacing of the duct from 2*D* to 1*D* had only a negligible influence on the average bond strength. The presence of transverse reinforcement, as currently used by TxDOT, also had a negligible influence on the response. A single spiral around a group of connectors did not increase the average bond strength. Placing small spirals around individual connectors reduced the bond strength slightly, and is not recommended.

CHAPTER 8
Requirements for Embedded Length

As discussed in Chapter 7, the average bond response of grouted vertical connectors is sensitive to the type of duct, the number of connectors tested simultaneously in tension, and the eccentricity of the connector within the duct. Therefore, each of these factors was considered explicitly during the development of the design recommendations. Other parameters, such as epoxy coating and transverse reinforcement, were considered to have a negligible influence on the response of the connectors and are not discussed in this chapter.

Because dead loads tend to dominate the design of bridge substructures, a two-level approach was adopted for grouted vertical-duct connectors. Design moments in the cap-to-column connections for typical multi-column bents are usually small, and the tensile demand on the connectors is quite low. In these cases, the connectors must be embedded a minimum depth, $\ell_{e,min}$. The design provisions for this limit state are tied to the measured tensile stress at the onset of widespread splitting cracks in the concrete. This stress level was selected for two reasons: (1) the stiffness of the connector does not change appreciably until after widespread splitting cracks form, and (2) the durability of the connection will be improved by limiting cracking of the concrete.

In contrast, the design moments in cap-to-column connections can be large if the bents are asymmetric, if the superstructure is supported by a single column, if the bent experiences significant unbalanced dead loads during construction, or if the lateral design loads are large. In these cases, the connectors must be embedded a sufficient distance, ℓ_d, to develop the calculated tensile stresses corresponding to the design load combinations. The design equations for this limit state are tied to the maximum measured tensile stress in the connectors.

Design equations are developed, discussed, and evaluated in this chapter. Five factors were used to develop these equations. The two modification factors related to the type of duct, β, and layout of the connectors, γ, are considered explicitly in the final design equations. Values for the other three factors – which are related to connector eccentricity, ξ; the design basis tensile stress, α; and material variability, ϕ – are embedded in the design equations and the values do not change with the configuration of the grouted vertical-duct connectors. Each of these parameters is described in Section 8.1. The design equations for development length, ℓ_d, and minimum embedded length, $\ell_{e,min}$, are proposed in Section 8.2. Representative values of embedded length for precast substructure construction in Texas are calculated in Section 8.3.

8.1 MODIFICATION FACTORS

The design equations include three modification factors which represent the type of duct, β; the number and layout of connectors subjected to simultaneous tensile stresses, γ; and the eccentricity of the connector within the duct, ξ. The equations also depend on the design basis stress for the connectors – the measured stress level that is used to calculate the average available bond stress. The term α is used to represent this stress level. In addition, a strength reduction factor, ϕ, was selected to represent the variability of material properties.

Values of β, γ, ξ, and α were selected based on the available experimental data. In contrast, the value of ϕ was selected to be consistent with current codes and specifications for the design of structural concrete elements.

The comparisons discussed in this section are made for two levels of tensile stress in the connectors: the onset of widespread cracking in the concrete and the capacity of the connector. Because not all the parameters considered in the experimental program represented practical and/or recommended configurations, not all experimental results were used to develop the design equations. For example, specimens constructed with individual spirals around the ducts and specimens constructed with no ducts were excluded from consideration. In addition, the three specimens with eccentric connectors were considered only in Section 8.1.3.

The factors related to duct material, connector layout, connector eccentricity, design basis tensile stress, and material variability for grouted vertical-duct connectors are discussed in Sections 8.1.1 through 8.1.5, respectively. Key response parameters for specimens with a single connector are summarized in Table 8.1 and the same information is listed in Table 8.2 for specimens with multiple connectors.

8.1.1 Duct Material

As discussed in Chapter 7, the connector response is sensitive to the type of duct. Connectors embedded in galvanized steel ducts were able to achieve higher tensile stresses, and therefore higher average bond stresses, than connectors embedded in plastic ducts. Insufficient data were available to determine if the observed differences between the performance of connectors embedded in polyethylene and polypropylene ducts were attributable to the duct material or to the geometry of the duct. Therefore, specimens with both types of plastic ducts are considered together in this section.

The responses of the thirteen specimens with single connectors are compared in Figure 8.1 and Figure 8.2. Data in Figure 8.1 correspond to the measured tensile stress at the onset of widespread splitting in the concrete, while data in Figure 8.2 correspond to the capacity of the connectors. The tensile stress in the connectors at each stress level is normalized by the square root of the compressive strength of

the concrete and the embedded length, ℓ_e/d_b . Although some scatter is observed within each group of specimens, the data appear to be well represented by the average values.

The difference in strength attributable to the choice of duct material is obvious from these two plots. The average strength of the specimens with galvanized steel ducts is clearly larger than the average strength of the specimens with plastic ducts. In addition, the lowest normalized tensile stress for the specimens with galvanized steel duct exceeded the highest normalized tensile stress for the specimens with plastic duct at both stress levels.

It is also interesting to note that the average tensile stress in the specimens with galvanized steel ducts increased 22% between the onset of widespread splitting in the concrete and the capacity of the connector. In contrast, the average tensile stress in the specimens with plastic duct increased only 11% for the same stress levels.

Table 8.1 Specimens with Single Connectors
(a) Galvanized Steel Ducts

Test	ℓ_e (d_b)	γ	f'_c (psi)	f_g (psi)	f_{ws} (ksi)	f_{max} (ksi)	$\frac{f_{ws}d_b}{\gamma\sqrt{f'_c}\ell_e}$	$\frac{f_{max}d_b}{\gamma\sqrt{f'_c}\ell_e}$
1	8	0.98	5400	5000	48	58	82.9	100.2
2*	8	0.98	5400	6100	48	55	82.9	95.0
3	12	0.98	5400	6400	72	87	82.9	100.2
4*	12	0.98	5400	6400	76	88	87.5	101.4
10	12	0.98	4500	5600	57	80	71.9	100.9
						Average:	81.6	99.5

(b) Plastic Ducts

Test	ℓ_e (d_b)	γ	f'_c (psi)	f_g (psi)	f_{ws} (ksi)	f_{max} (ksi)	$\frac{f_{ws}d_b}{\gamma\sqrt{f'_c}\ell_e}$	$\frac{f_{max}d_b}{\gamma\sqrt{f'_c}\ell_e}$
5	8	0.98	5400	4700	41	48	70.8	82.9
6*	8	0.98	5400	5500	40	40	68.2	69.1
7	12	0.98	5400	5900	58	67	66.8	77.2
8*	12	0.98	5400	5800	60	65	69.1	74.9
9	12	0.98	4500	5100	50	54	63.1	68.1
22	16	0.98	5500	5400	74	90	63.3	77.0
29†	8	0.98	6100	7100	40	40	63.4	65.0
30†	12	0.98	6100	7100	68	68	65.0	73.7
						Average:	66.2	73.5

Notes:
* Epoxy-coated connector
† Polypropylene duct

Table 8.2 Specimens with Multiple Connectors
(a) Galvanized Steel Ducts

Test	ℓ_e (d_b)	γ	f_c' (psi)	f_g (psi)	f_{ws} (ksi)	f_{max} (ksi)	$\frac{f_{ws} d_b}{\gamma\sqrt{f_c'}\ell_e}$	$\frac{f_{max} d_b}{\gamma\sqrt{f_c'}\ell_e}$
13	16	0.68	4700	5200	57	87	76.6	116.9
15	16	0.68	4700	5400	54	86	72.6	115.5
17	12	0.68	5200	4800	45	59	76.6	100.5
23	12	0.77	6100	6000	53	68	73.3	94.0
31	16	0.56	6100	5800	50	73	71.2	103.9
						Average:	74.0	102.9

(b) Plastic Ducts

Test	ℓ_e (d_b)	γ	f_c' (psi)	f_g (psi)	f_{ws} (ksi)	f_{max} (ksi)	$\frac{f_{ws} d_b}{\gamma\sqrt{f_c'}\ell_e}$	$\frac{f_{max} d_b}{\gamma\sqrt{f_c'}\ell_e}$
14	16	0.68	4700	5300	49	64	65.8	86.0
16	16	0.68	4700	5400	42	49	65.8	79.3
18	12	0.68	5300	4900	37	44	62.4	74.2
24	16	0.77	6100	6300	52	65	53.9	67.4
28†	16	0.68	6100	6800	53	85	62.5	100.2
32†	16	0.56	6100	5800	47	67	66.9	95.4
						Average:	66.2	73.5

Note:
† Polypropylene duct

The modification factor β is used in the design equations to represent the influence of the duct material. Because the relative strength of the two types of duct was not the same at the two stress levels, it is not possible to represent all trends in the experimental data exactly. However, β is assumed to be 1.0 for galvanized steel duct and 1.3 for plastic duct. These values overestimate the differences between the two types of duct at the onset of widespread cracking and underestimate the differences at capacity, but the differences are relatively modest.

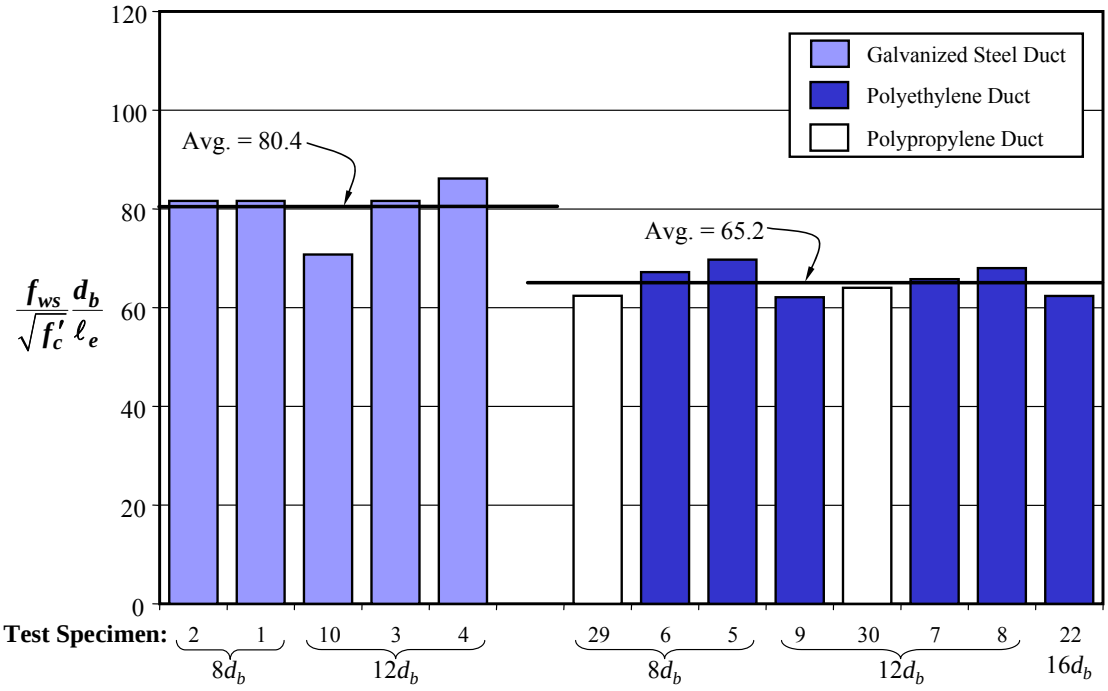

Figure 8.1 Normalized Tensile Stress at the Formation of Widespread Splitting Cracks in the Concrete for Specimens with a Single Connector

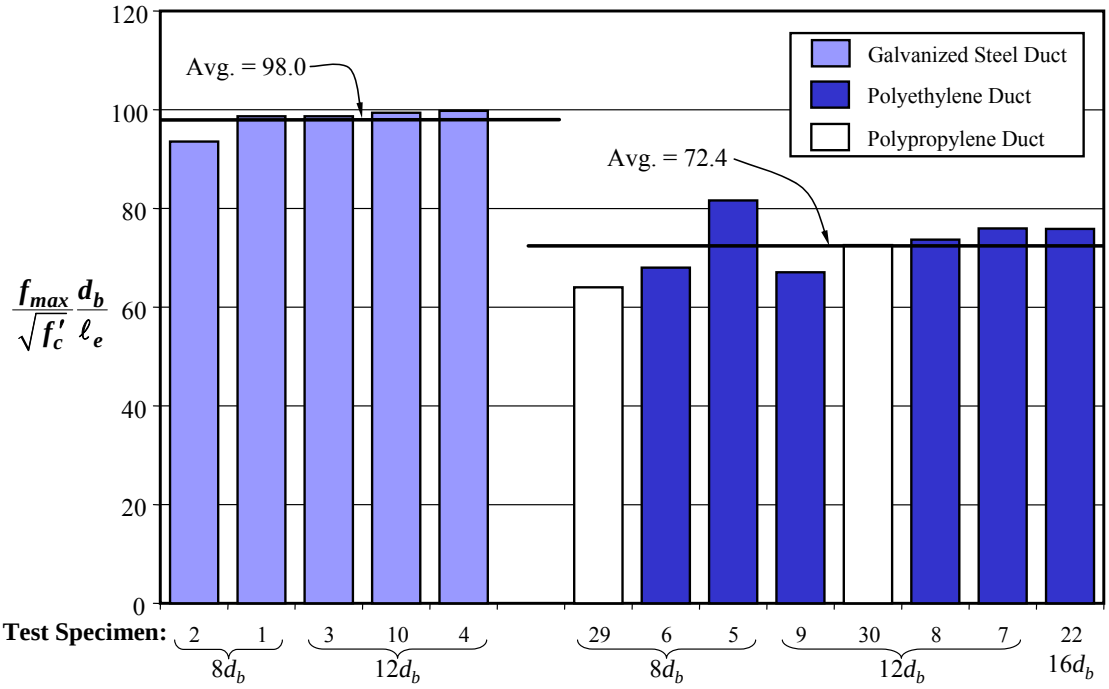

Figure 8.2 Normalized Tensile Stress at Capacity for Specimens with a Single Connector

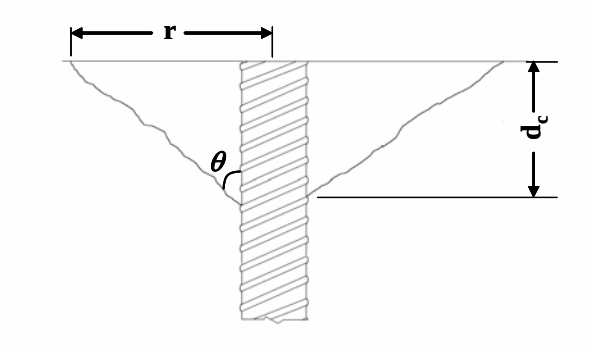

Figure 8.3 Cone-Shaped Break-Out in Concrete around Connector

8.1.2 Connector Layout

Observed crack patterns and concrete cone breakouts in the test specimens (Chapter 6) indicate that the zone of influence around an individual connector extends a radial distance, r, of approximately 11 in. from the axis of the connector (Figure 8.3). For a #11 bar, this distance corresponds to $7.8d_b$. Measured depths of the concrete cone breakout, d_c, ranged between 4 and 6 in. for specimens with single connectors and between 6 and 10 in. for specimens with multiple connectors.

In cases where the zones of influence for adjacent connectors overlap, the capacity of each connector is reduced compared with that of a companion specimen with a single connector. This trend was expected and the variations in the bond response due to the number of connectors were discussed in Chapter 7. The variations of the normalized tensile stresses for specimens with single and multiple connectors are shown in Figure 8.4 for galvanized steel duct and Figure 8.5 for plastic duct. At both stress levels considered, the average tensile stress in the specimens with multiple connectors is significantly less than the average tensile stress in the specimens with single connectors.

The modification factor γ is used to account for group effects among the connectors. The factor is based on the approach used by Miltenberger (2001) to determine the nominal tensile strength of anchors in concrete and incorporates both the Concrete Capacity Design (CCD) and the Uniform Bond Stress (UBS) models. The same approach is the basis for the design approach in Appendix D of ACI 318 (2005).

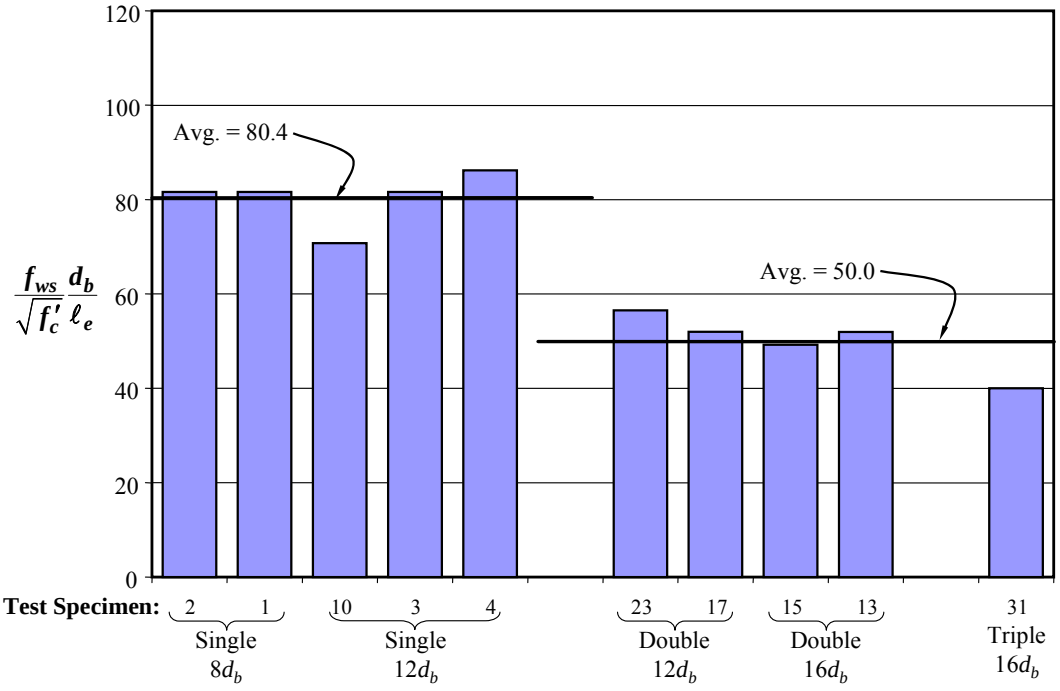

(a) Onset of Widespread Splitting in the Concrete

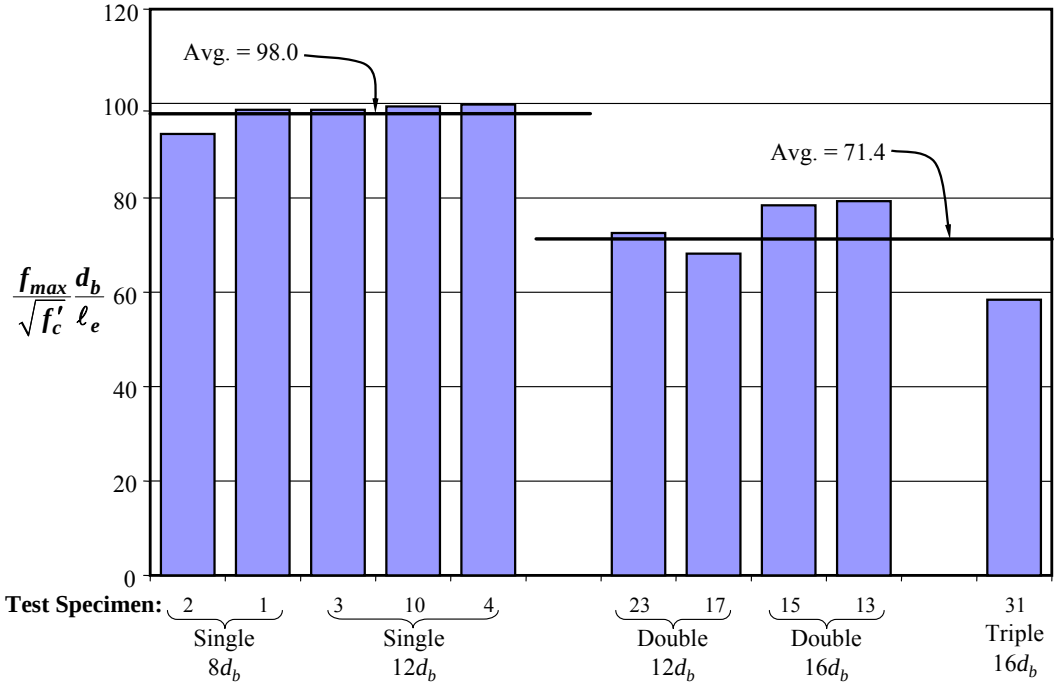

(b) Capacity of Connector

Figure 8.4 Normalized Tensile Stresses in Specimens with Galvanized Steel Duct

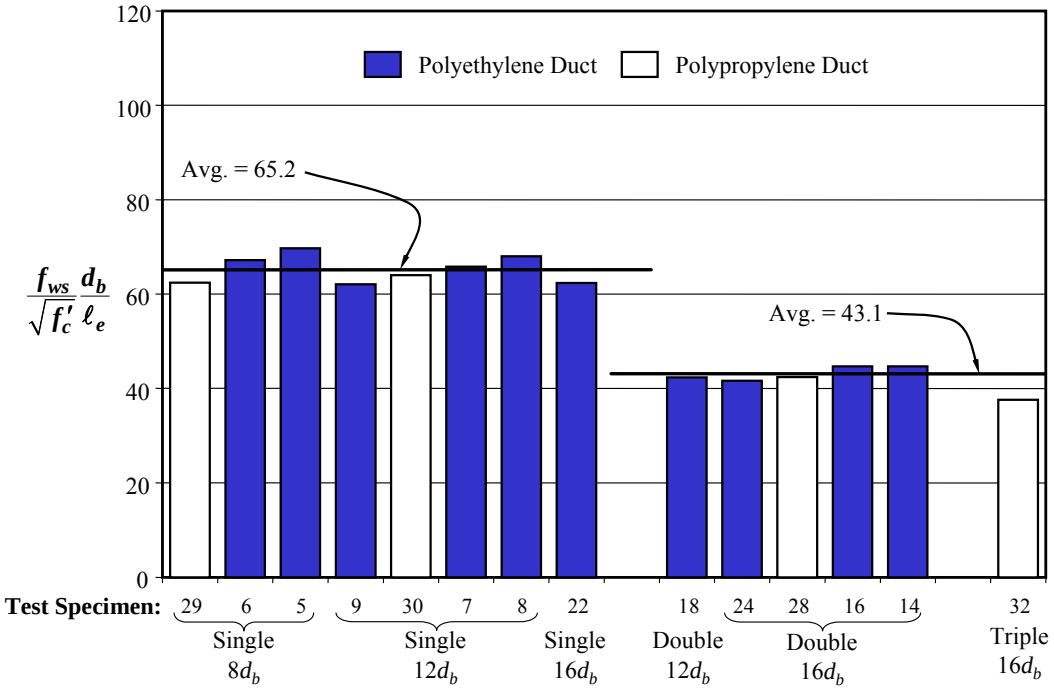

(a) Onset of Widespread Splitting in the Concrete

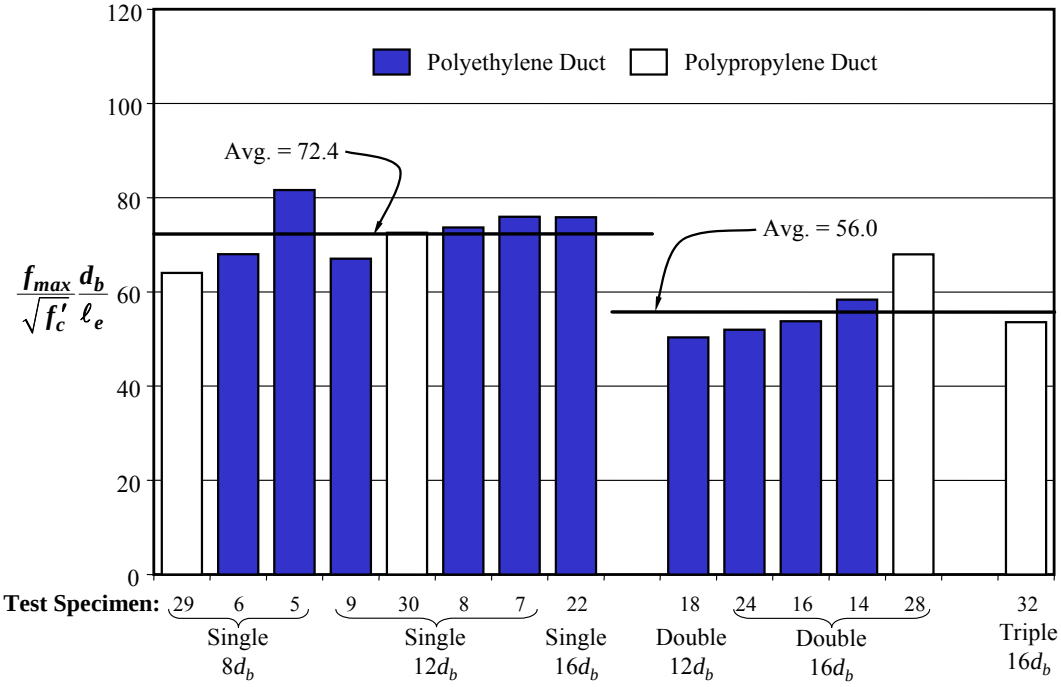

(b) Capacity of Connector

Figure 8.5 Normalized Tensile Stresses in Specimens with Plastic Duct

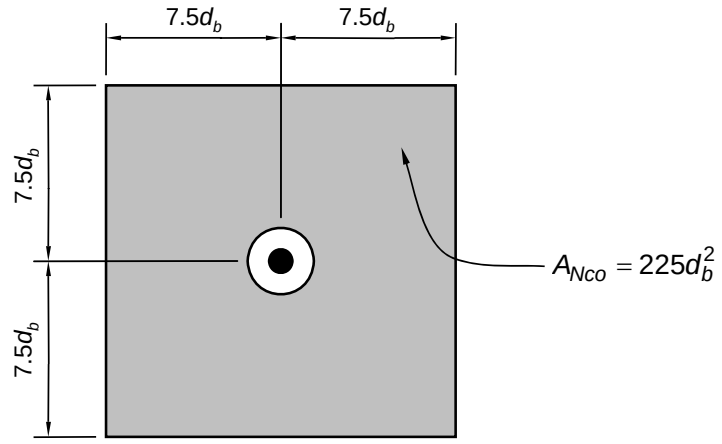

Figure 8.6 Idealized Projected Failure Surface for an Individual Connector

The configuration of the grouted vertical-duct connectors that are subjected to simultaneous tensile stresses is used to define the modification factor γ:

$$\gamma = \frac{A_{Nc}}{nA_{Nco}} \tag{8.1}$$

where A_{Nc} is the projected failure surface of the group of connectors in tension (in.^{2}), A_{Nco} is the maximum projected failure surface for an individual connector (in.^{2}), and n is the number of connectors subjected to simultaneous tensile stresses. As will be discussed in Section 8.3, it is conservative to calculate γ using all the connectors in the group, rather than just the connectors that are calculated to be in tension.

Based on the observed response of the test specimens, the projected failure surface of an individual connector, A_{Nco}, was assumed to be a square with sides equal to $15d_b$ (Figure 8.6). While the actual failure surface more closely represents a circle than a square, the square was selected to simplify the calculations. The surface area proposed by Miltenberger (2001) is also square, but the sides are slightly larger (Figure 2.17).

The projected failure surface for a group of connectors, A_{Nc}, is limited by the distance between adjacent connectors and the distance from the connectors to the nearest edge of the concrete beam. The four connector layouts tested in this program are shown in Figure 8.7 and the projected failure surfaces for each configuration are shown in grey. The corresponding values of γ are listed in Table 8.3. The values of x correspond to the horizontal dimension of the projected failure surface (Figure 8.7) and the values of y correspond to the vertical dimension.

Table 8.3 Modification Factors for Group Effects

Number of Connectors	Duct Spacing	x (in.)	y (in.)	A_{Nc} (in.^{2})	γ^*
1	–	21.15	20.83	440.4	0.98
2	1*D*	29.15	20.83	607.0	0.68
2	2*D*	33.15	20.83	690.3	0.77
3	1*D*	29.15 21.15	15.00 15.00	754.5	0.56

Note:
* A_{Nco} = 447.3 in.^{2}

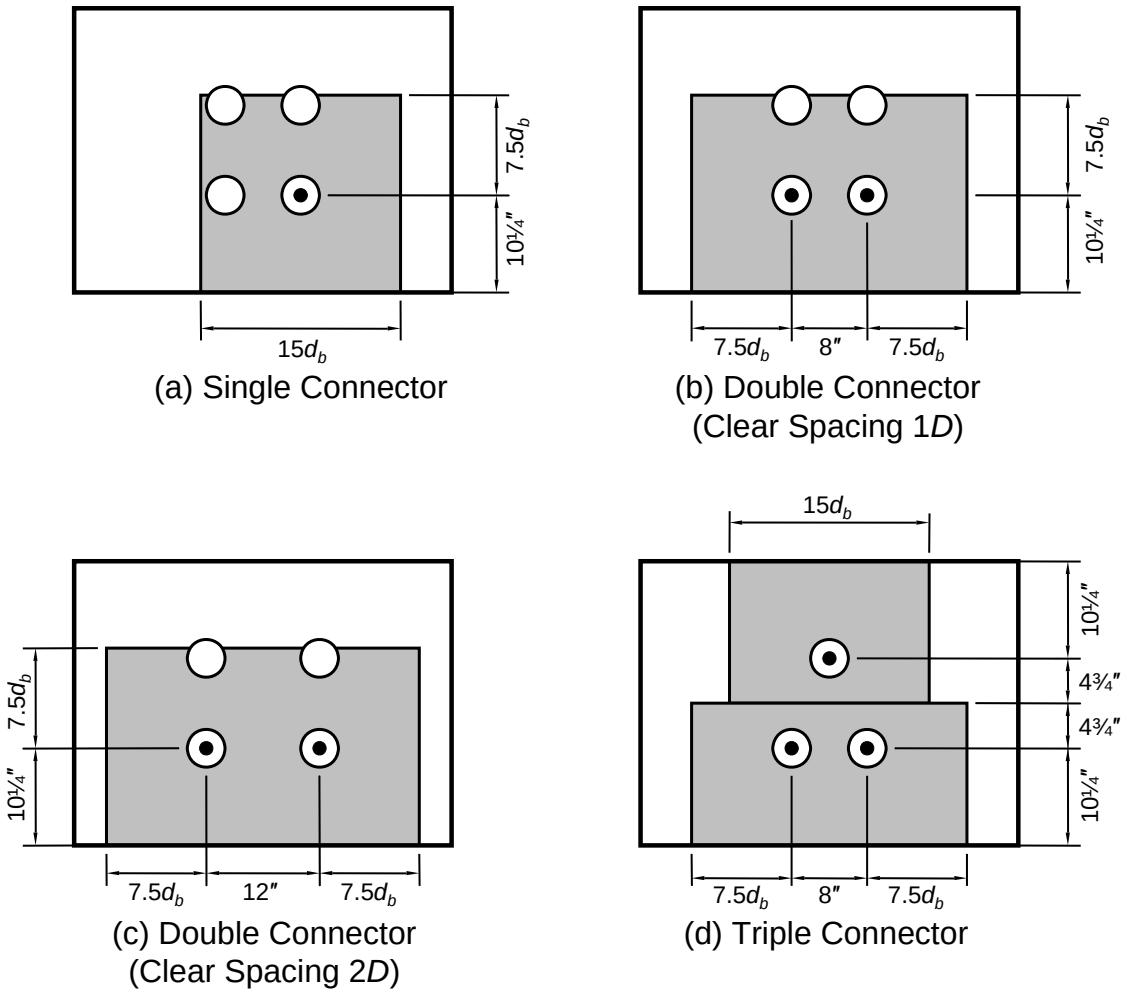

(a) Single Connector

(b) Double Connector (Clear Spacing 1*D*)

(c) Double Connector (Clear Spacing 2*D*)

(d) Triple Connector

Figure 8.7 Idealized Projected Failure Surfaces for Groups of Connectors

The normalized stress data shown in Figure 8.4 and Figure 8.5 are modified to include group effects in Figure 8.8 and Figure 8.9, respectively. The calculated values of γ are not sufficient for the modified normalized tensile stress data for specimens with multiple connectors to equal those for specimens with single connectors. However, introducing the γ factor represents a significant improvement at both stress levels. The averages of the normalized tensile stresses modified for group effects are within 10% for specimens with single and multiple connectors.

8.1.3 Connector Eccentricity

Only three specimens were tested with the connectors placed eccentrically within the duct (Table 8.4). The results from those tests are plotted in Figure 8.10 along with the results of four companion specimens with concentric connectors. In all cases, the tensile strength resisted by the eccentric connectors was less than 85% of the average tensile strength of the companion specimens.

The modification factor ξ was used to represent the influence of connector eccentricity, and a value of 0.8 was selected for all cases. The horizontal lines in Figure 8.10 represent ξ times the average normalized tensile strength of the companion specimens.

Table 8.4 Influence of Connector Eccentricity

Test	Duct	Location	ℓ_e (d_b)	f_c' (psi)	f_g (psi)	f_{max} (ksi)	$\frac{f_{max} d_b}{\sqrt{f_c'}\ell_e}$
1	Steel	Centered	8	5400	5000	58	98.7
19	Steel	Eccentric	8	5500	5100	49	82.6
3	Steel	Centered	12	5400	6400	87	98.7
10	Steel	Centered	12	4500	5600	80	99.4
21	Steel	Eccentric	12	5500	5400	74	83.2
5	PE	Centered	8	5400	4700	48	81.6
20	PE	Eccentric	8	5500	5100	40	67.4

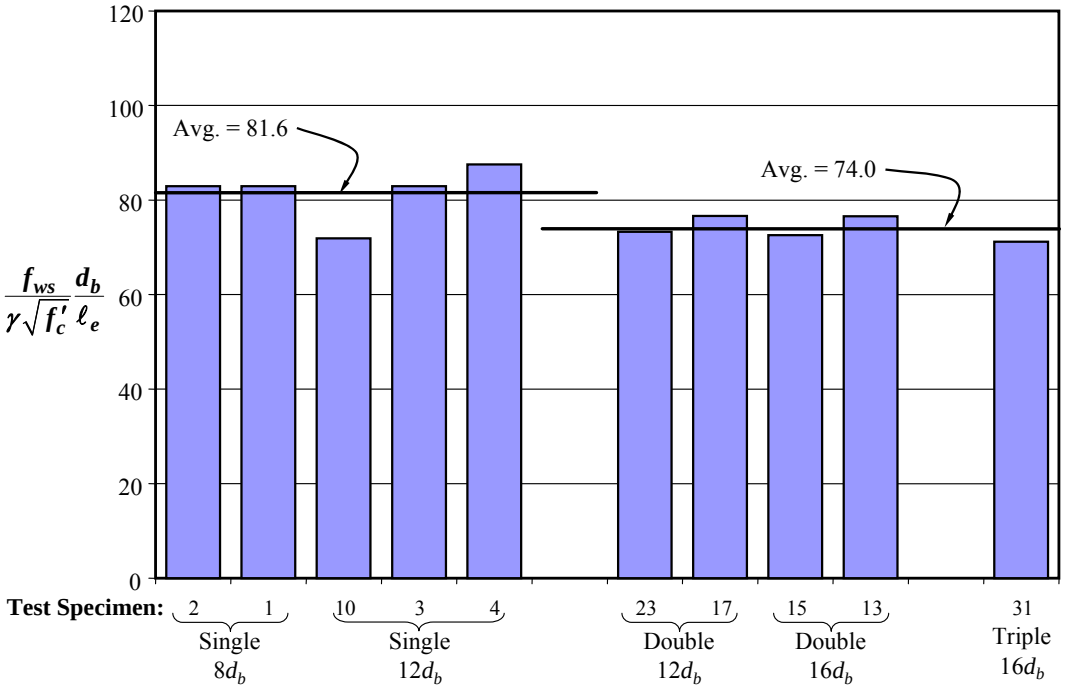

(a) Onset of Widespread Splitting in the Concrete

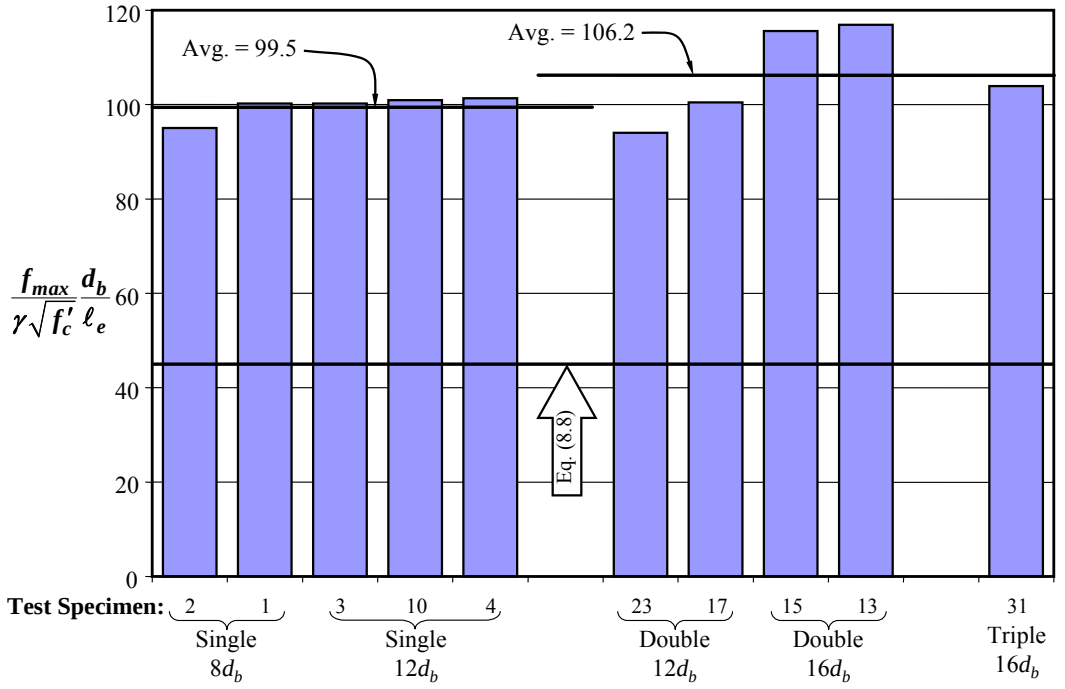

(b) Capacity of Connector

Figure 8.8 Normalized Tensile Stresses Modified to Include Group Effects in Specimens with Galvanized Steel Duct

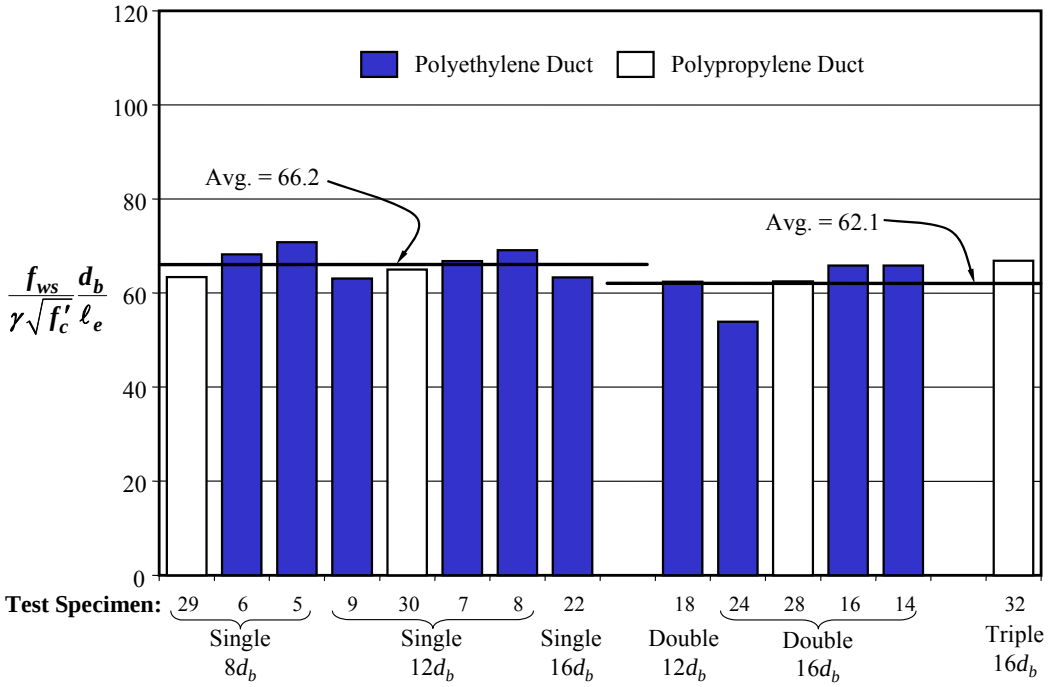

(a) Onset of Widespread Splitting in the Concrete

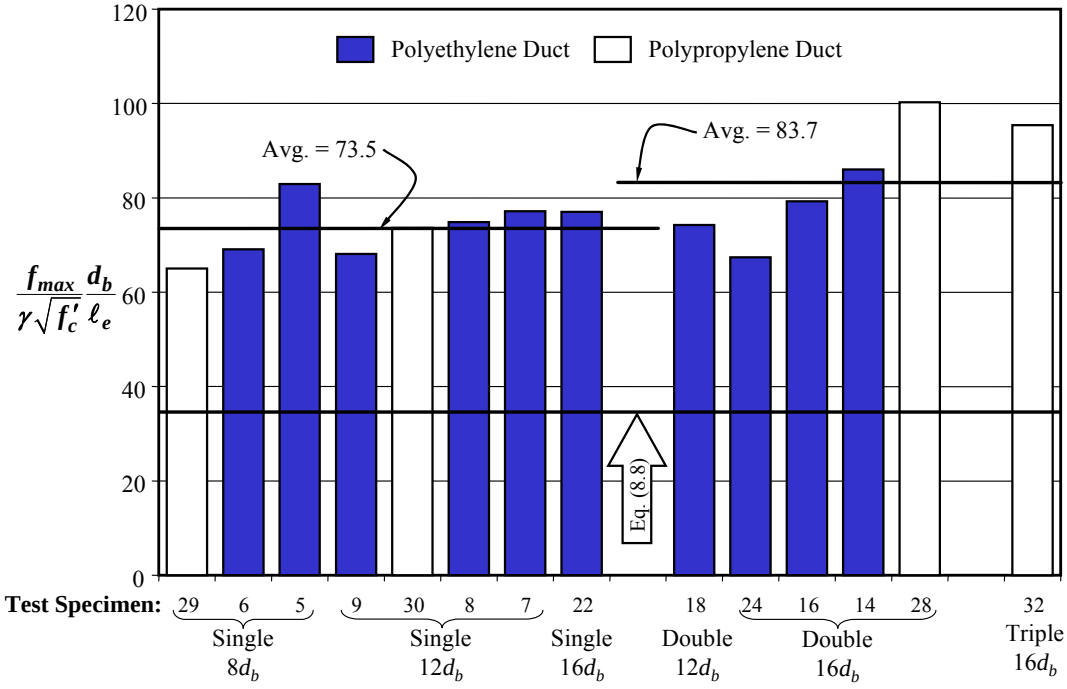

(b) Capacity of Connector

Figure 8.9 Normalized Tensile Stresses Modified to Include Group Effects in Specimens with Plastic Duct

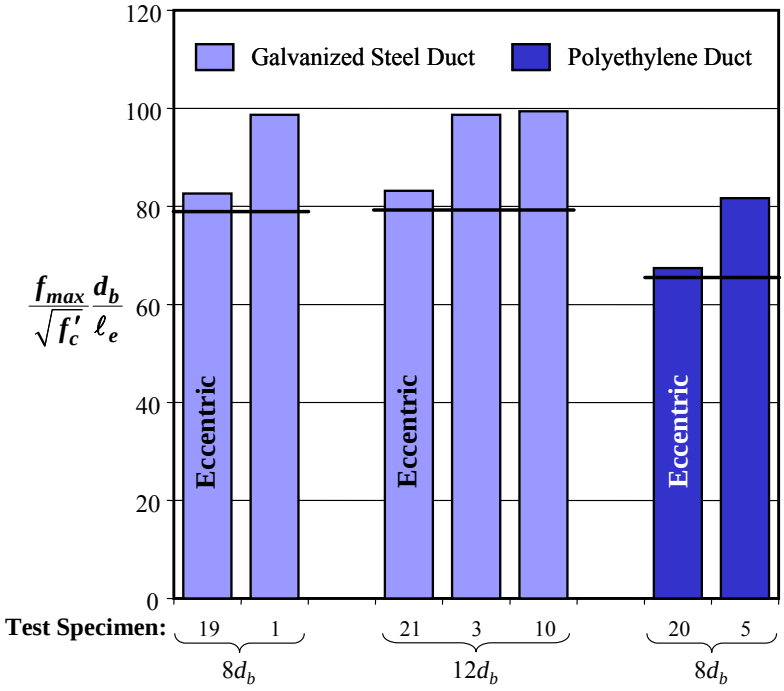

Figure 8.10 Influence of Connector Eccentricity

8.1.4 Design Basis Tensile Stress

Two different approaches are used in ACI 318 (2005) to determine the stress level in the test specimens that serves as the basis for the design equations. The mean bond stress achieved in experimental tests is used as the basis for the development length equations in Chapter 12. In contrast, the stress corresponding to the five percent fractile is used as the basis for determining the nominal strength of cast-in-place and post-installed anchors in Appendix D.

Due to the limited amount of data regarding the tensile response of grouted vertical-duct connectors, neither of these approaches was considered appropriate. Rather, the design basis tensile stress, α, was taken as the mean minus the standard deviation of the available data. In addition, the calculated tensile stress in the connectors under the factored loads is multiplied by 1.25. This amplification level has traditionally been used in Chapter 12 of ACI 318 (2005) to ensure that the actual yield stress in the reinforcement can be developed (Orangun, et al. 1977).

8.1.5 Strength Reduction Factor for Tension

Appendix D of ACI 318 (2005) specifies a strength reduction factor, ϕ, of 0.75 for cast-in-place and post-installed anchors in tension. A strength reduction factor of 0.8 is embedded in the development length equations in Chapter 12 (ACI 318-05). Due to the similarities of the shape of the concrete cone breakouts for anchors and connectors, a value of 0.75 was used for the grouted vertical-duct connectors.

8.2 DESIGN EQUATIONS FOR EMBEDDED LENGTH

The data presented in Section 8.1 are used to develop design equations for the required embedded length of grouted vertical-duct connectors. Two conditions are considered:

- All connectors must be designed to resist the maximum calculated tensile stress, $f_{s,cr}$, corresponding to the critical load combinations, for both strength and extreme event limit states, from the AASHTO *LRFD Design Specifications* (2004). In the following discussion, the term ℓ_d will be used to represent this development length in tension.
- All connectors must be embedded a sufficient distance such that widespread splitting cracks do not form in the concrete. In the following discussion, the term $\ell_{e,min}$ will be used to represent this minimum embedded length.

Design equations for development lengths in tension and minimum embedded lengths are presented in Sections 8.2.1 and 8.2.2, respectively. The equations are compared in Section 8.2.3.

The mean and standard deviation of the normalized tensile stresses resisted by the test specimens at both the onset of widespread cracking of the concrete and the tensile capacity of the connectors are summarized in Table 8.5. Separate values are reported for galvanized steel and plastic duct.

8.2.1 Development Length in Tension

As discussed in Chapter 7, bond stresses are typically assumed to be constant along the embedded length of the reinforcement. While this assumption is not true (Fig. 2.14), it does provide a convenient idealization for design because the maximum tensile stress that can be developed in a reinforcing bar is proportional to the embedded length of the bar:

$$f_s A_b = u \pi d_b \ell_e \tag{8.2}$$

where f_s is the tensile stress in the bar (psi), A_b is the area of the bar (in.^{2}), u is the average bond stress (psi), d_b is the diameter of the bar (in.), and ℓ_e is the embedded length (in.).

Table 8.5 Normalized Tensile Response of Grouted Vertical Connectors

Duct	$\frac{f_{ws}}{\gamma\sqrt{f_c'}}\frac{d_b}{\ell_e}$			$\frac{f_{max}}{\gamma\sqrt{f_c'}}\frac{d_b}{\ell_e}$		
	Mean	Standard Deviation	Design Basis	Mean	Standard Deviation	Design Basis
Galvanized Steel*	77.8	5.8	72.0	102.9	7.6	95.2
Plastic†	64.8	4.1	60.7	77.9	10.3	67.6

Notes:

* Statistics based on results of Tests 1, 2, 3, 4, 10, 13, 15, 17, 23, and 31.
† Statistics based on results of Tests 5, 6, 7, 8, 9, 14, 16, 18, 22, 24, 28, 29, 30, and 32.

The average normalized tensile stress reported in Table 8.5; therefore, is proportional to the average bond stress that can be developed in the connectors. The design basis for the normalized tensile stress in the connector, α, was taken as the mean minus the standard deviation of the experimental data (α = 95.2 for grouted vertical connectors in galvanized steel ducts and α = 67.6 for connectors in plastic ducts).

The tensile stress, f_s, that can be developed in a connector that is embedded a length ℓ_e can, therefore, be written as:

$$f_s = \alpha\gamma\sqrt{f_c'}\,\frac{\ell_e}{d_b} \tag{8.3}$$

where α is the design basis stress (Section 8.1.4), γ is the modification factor for group effects (Section 8.1.2), f_c' is the specified compressive strength of the concrete (psi), and d_b is the nominal diameter of the connector (in.). When calculating the required development length, ℓ_d, the calculated tensile stress in the connector under the critical load combination, $f_{s,cr}$, is multiplied by 1.25 (8.1.4). Although the yield stress is the only stress level considered in ACI 318 (2005), the same factor is used for all stress levels for the grouted vertical-duct connectors.

The right side of Eq. (8.3) is multiplied by $(\phi\xi)$ to account for variability of the strength of the concrete and connector eccentricity. Because connectors are likely to be eccentric relative to the ducts in the field (Figure 4.4), the modification factor for connector eccentricity is used in all cases. Substituting values of ϕ = 0.75 (Section 8.1.5) and ξ = 0.8 (Section 8.1.3) into Eq. (8.3) leads to:

$$1.25\,f_{s,cr} = (\phi\xi)\alpha\gamma\sqrt{f_c'}\,\frac{\ell_d}{d_b} = 0.6\alpha\gamma\sqrt{f_c'}\,\frac{\ell_d}{d_b} \tag{8.4}$$

Rearranging, Eq. (8.4):

$$\ell_d = \frac{1.25\,f_{s,cr}\,d_b}{0.6\alpha\gamma\sqrt{f_c'}} \tag{8.5}$$

Substituting the appropriate values of the design basis stress, α, into Eq. (8.5) yields Eq. (8.6) for connectors in galvanized steel ducts and Eq. (8.7) for connectors in plastic ducts:

$$\ell_d = \frac{1.25\,f_{s,cr}\,d_b}{0.6(95.2)\gamma\sqrt{f_c'}} = \frac{f_{s,cr}\,d_b}{45.7\gamma\sqrt{f_c'}} \tag{8.6}$$

$$\ell_d = \frac{1.25\,f_{s,cr}\,d_b}{0.6(67.6)\gamma\sqrt{f_c'}} = \frac{f_{s,cr}\,d_b}{32.4\gamma\sqrt{f_c'}} \tag{8.7}$$

Finally, a single equation for development of a grouted vertical-duct connector is developed by introducing the modification factor β (Section 8.1.1):

$$\ell_d = \frac{\beta f_{s,cr} d_b}{45\gamma\sqrt{f_c'}} \tag{8.8}$$

where β=1.0 for galvanized steel duct and 1.3 for plastic duct. The resulting development lengths in Eq. (8.8) are 2% larger than those from Eq. (8.6) for galvanized steel duct and 7% larger than those from Eq. (8.7) for plastic duct.

The constant in the denominator of Eq. (8.8) divided by β may be compared directly with the design basis stress in Table 8.5 and the vertical axes in Figure 8.8(b) and Figure 8.9(b). For galvanized steel duct, the design level, 45, is approximately half the design basis, 95.2. Similarly, the design value for plastic duct is 34.6, while the design basis is 67.6. These differences are consistent with the assumptions discussed in this section: ϕ=0.75, ξ=0.8, and a stress amplification factor of 1.25.

8.2.2 Minimum Embedded Length

All connectors must be embedded a sufficient distance to prevent the formation of widespread splitting cracks in the concrete. As before, the design basis stress in the connectors was taken as the mean minus the standard deviation of the measured data. However, the normalized tensile stress corresponding to the formation of widespread splitting cracks in the concrete was used in this case. Therefore, the design basis, α, is 72.0 for connectors in galvanized steel ducts and 60.7 for connectors in plastic ducts.

When calculating the minimum embedded length, $\ell_{e,min}$, the tensile stress in the connector is taken as 0.25 f_y. The strength reduction factor, ϕ, and the connector eccentricity factor, ξ, are the same as before:

$$0.25 f_y = (\phi\xi)\alpha\gamma\sqrt{f_c'}\frac{\ell_{e,min}}{d_b} = 0.6\alpha\gamma\sqrt{f_c'}\frac{\ell_{e,min}}{d_b} \tag{8.9}$$

The corresponding minimum embedded length for connectors in galvanized steel ducts and plastic ducts are given in Eq. (8.10) and (8.11), respectively.

$$\ell_{e,min} = \frac{0.25 f_y d_b}{0.6(72.0)\gamma\sqrt{f_c'}} = \frac{f_y d_b}{172.8\gamma\sqrt{f_c'}} \tag{8.10}$$

$$\ell_{e,min} = \frac{0.25 f_y d_b}{0.6(60.7)\gamma\sqrt{f_c'}} = \frac{f_y d_b}{145.7\gamma\sqrt{f_c'}} \tag{8.11}$$

Combining Eq. (8.10) and (8.11) into a single design equation leads to:

$$\ell_{e,min} = \frac{\beta f_y d_b}{180\gamma\sqrt{f_c'}} \tag{8.12}$$

where β = 1.0 for galvanized steel duct and 1.3 for plastic duct. The minimum embedded lengths calculated using Eq. (8.12) are 6% smaller than those from Eq. (8.10) for galvanized steel duct and 5% larger than those from Eq. (8.11) for plastic duct. The choice of 180 as the coefficient in Eq. (8.12) is slightly less conservative than the approach used to determine the equation for development length, but it provides a smooth transition between the two design equations.

Two additional points are worth considering: (1) it is appropriate to take γ = 1.0, regardless of the layout of the connectors, if the calculated stresses in the connectors are compressive under the critical design load combinations, and (2) in addition to satisfying Eq. (8.12), the value of $\ell_{e,min}$ should not be less than the smaller of $8d_b$ and 12 in.

8.2.3 Evaluation of Design Equations

Using the proposed design equations, the minimum embedded length controls the design of the grouted vertical-duct connectors when the critical calculated tensile stress is low or if the connector is subjected to only compressive stresses. The development length will control for higher values of the critical calculated tensile stress. The boundary between these two requirements depends on the type of duct, the group modification factor, and the strength of the concrete.

If the product of $\gamma\sqrt{f_c'}$ is low (less than 39 for galvanized steel duct and less than 51 for plastic duct when #11 bars are used as connectors), the minimum embedded length given in Eq. (8.12) will control for values of $f_{s,cr}$ less than 0.25 f_y (Figure 8.11a). In contrast, if the product of $\gamma\sqrt{f_c'}$ exceeds these limits, the minimum embedded length will be the larger of 12 in. and $8d_b$ and the threshold tensile stress where the development length controls the design will be larger (Figure 8.11b). In this second case, the threshold tensile stress will be larger for connectors in galvanized steel ducts than for connectors in plastic ducts.

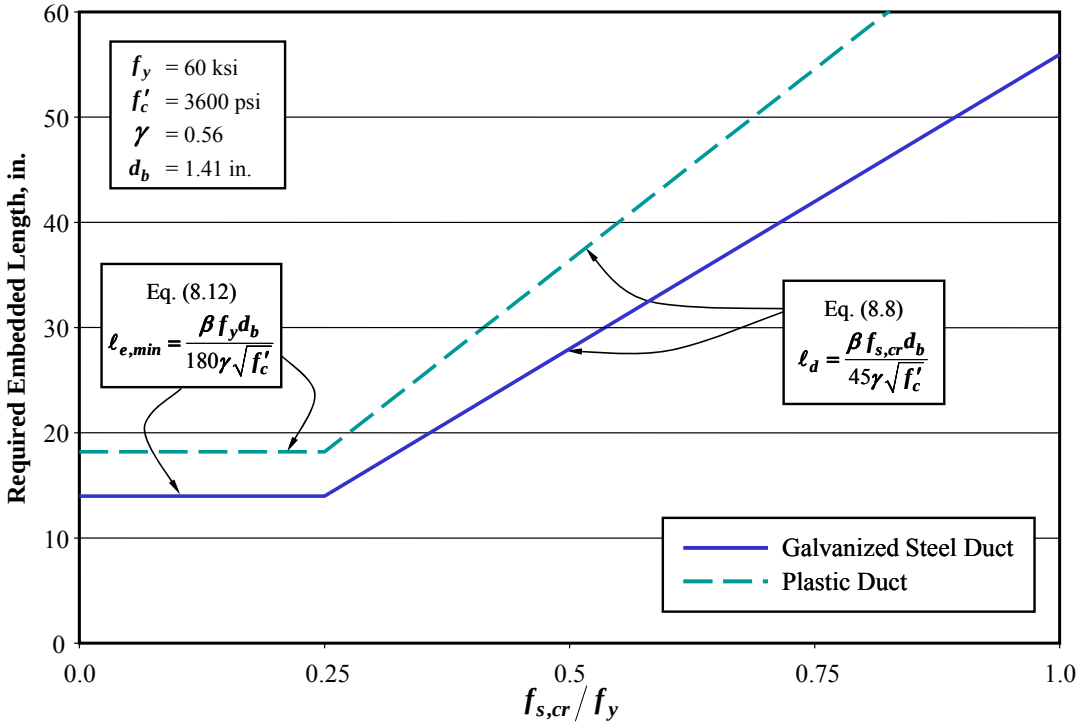

(a) Minimum Embedded Length Controlled by Eq. 8.12

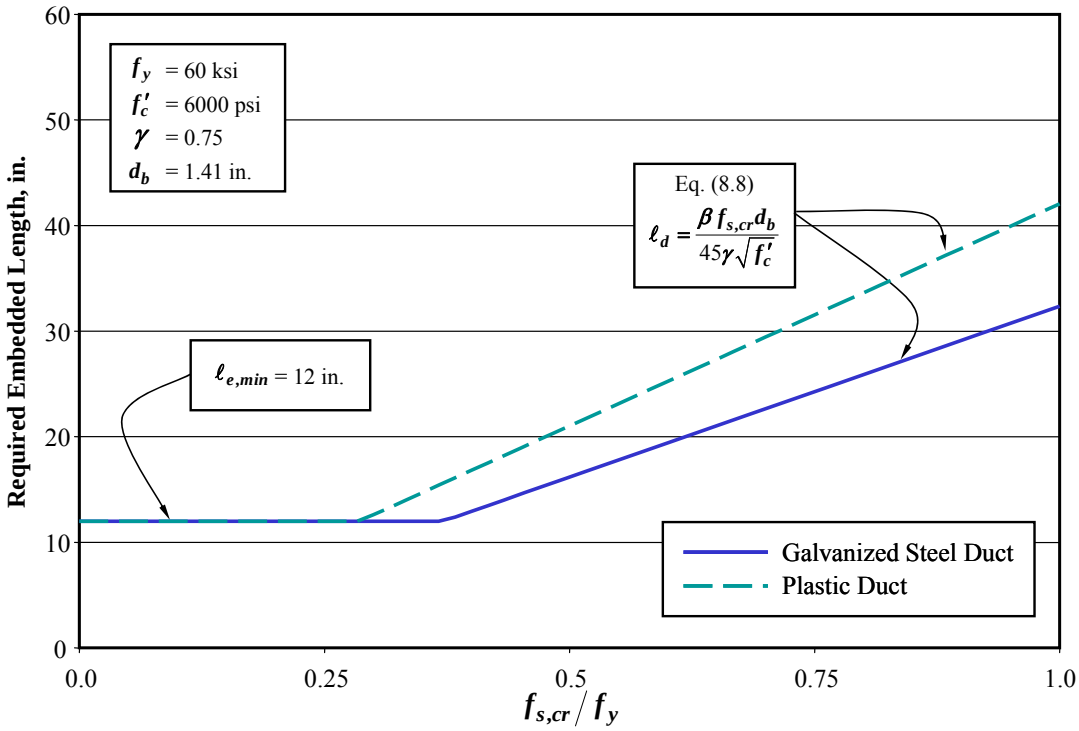

(b) Minimum Embedded Length Controlled by Lower Limit

Figure 8.11 Required Embedded Lengths

8.3 REPRESENTATIVE DESIGN EXAMPLES

The geometries of the Lake Ray Hubbard and Lake Belton precast bent caps (Freeby et al. 2003) will be used as examples to determine representative values for the required embedded length of grouted vertical-duct connectors. The examples discussed in this section are based on the configurations of the connectors only, and no attempt has been made to determine the critical calculated tensile stresses that governed the design of these structures.

Layouts with six and twelve connectors are shown in Figure 8.12 and Figure 8.13, respectively. The precast bent caps extend beyond the limits shown in these figures in the horizontal direction, but the vertical dimension represents the width of the bent cap. Number 11 reinforcing bars are assumed for both cases.

The design moments in the transverse direction of the bridge are expected to govern the design of the connectors. Therefore, the neutral axis for the group of connectors is assumed to be parallel to the y axis in both cases. Representative values of the modification factor for group effects, γ, were calculated for both configurations assuming that different numbers of connectors experience tensile stresses under the critical load combination for design. All calculations are based on the projected failure surface of a single #11 connector, $A_{Nco} = 447.3$ in.^{2}

Table 8.6 Calculated Modification Factors for Group Effects for Connector Layouts Representative of Precast Construction in Texas

Total Number of Connectors	Number of Connectors in Tension	x (in.)	y (in.)	A_{Nc} (in.^{2})	γ
6	2	21.15	37.15	786	0.88
6	4	29.15	37.15	1083	0.61
6	6	37.15	37.15	1380	0.51
12	6	28.15	42.15	1186	0.44
12	12	55.15	42.15	2325	0.43

The values of γ reported in Table 8.6 vary from 0.88 for two of six connectors in tension to 0.43 for twelve of twelve connectors in tension. As discussed in Section 8.1.2, conservative values of γ are obtained if all the connectors in a group are assumed to experience tension. When the spacing between the connectors in tension and the connectors in compression is close to $15d_b$, the linear projection of the idealized failure surface for a single connector (Figure 8.6), the calculated values of γ using the two approaches are similar. This observation is confirmed by comparing the values of γ calculated with 6 of 12 and 12 of 12 connectors are in tension. However, when the spacing between the connectors in tension

and the connectors in compression is considerably less than $15d_b$, using all the connectors to calculate γ may be overly conservative. The value calculated with 6 of 6 connectors is tension is approximately 60% of the value calculated for 2 of 6 connectors in tension.

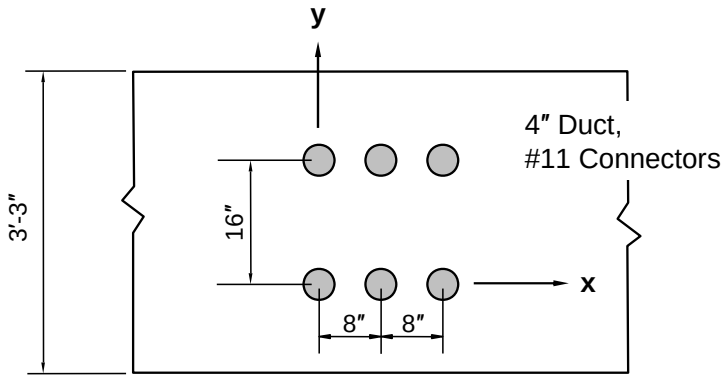

Figure 8.12 Layout with Six #11 Connectors

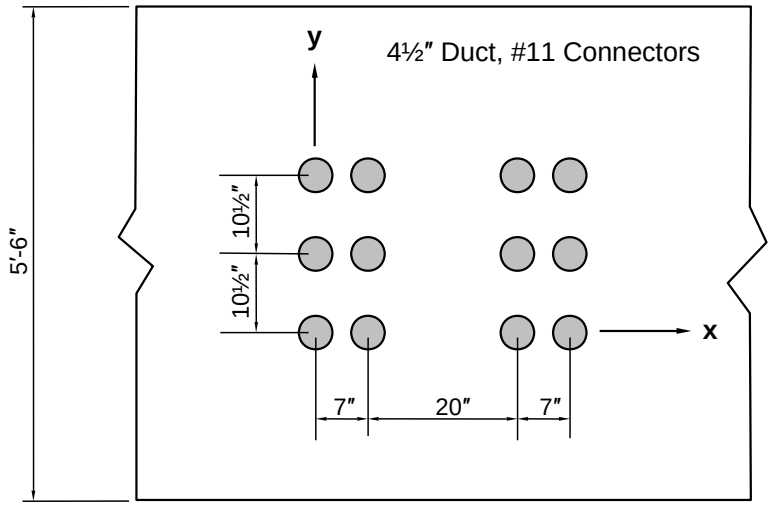

Figure 8.13 Layout with Twelve #11 Connectors

Based on the calculations summarized in Table 8.6, four values of γ (0.45, 0.60, 0.75, and 0.90) were used to calculate representative embedded lengths for #11 connectors. Results are presented in Table 8.7 for connectors in galvanized steel ducts and in Table 8.8 for connectors in plastic ducts. Three values of the calculated critical tensile stress in the connectors were used: 0.5 f_y, 0.75 f_y, and f_y. All calculations were based on a nominal yield stress of 60 ksi for the reinforcement. Two values of concrete compressive strength were also considered: 3600 and 6000 psi.

In these calculations, it is assumed that all connectors in the group will be embedded the same depth, regardless of the location of the neutral axis. This assumption is based on the practical desire to

minimize errors during construction. For a bent cap supported on multiple columns, however, it may be appropriate to use longer embedded lengths for the exterior groups of connectors, which experience higher design tensile forces, than for the interior groups of connectors.

Table 8.7 Required Embedded Length for #11 Connectors in Galvanized Steel Ducts

(a) f_c' = 3600 psi

γ	$\ell_{e,min}$ (in.)	ℓ_d (in.)		
		$f_{s,cr} = 0.5 f_y$	$f_{s,cr} = 0.75 f_y$	$f_{s,cr} = f_y$
0.45	17.4	34.8	52.2	69.6
0.60	13.1	26.1	39.2	52.2
0.75	12.0	20.9	31.3	41.8
0.90	12.0	17.4	26.1	34.8

(b) f_c' = 6000 psi

γ	$\ell_{e,min}$ (in.)	ℓ_d (in.)		
		$f_{s,cr} = 0.5 f_y$	$f_{s,cr} = 0.75 f_y$	$f_{s,cr} = f_y$
0.45	13.5	27.0	40.5	53.9
0.60	12.0	20.2	30.3	40.5
0.75	12.0	16.2	24.3	32.4
0.90	12.0	13.5	20.2	27.0

Table 8.8 Required Embedded Length for #11 Connectors in Plastic Ducts

(a) f_c' = 3600 psi

γ	$\ell_{e,min}$ (in.)	ℓ_d (in.)		
		$f_{s,cr} = 0.5 f_y$	$f_{s,cr} = 0.75 f_y$	$f_{s,cr} = f_y$
0.45	22.6	45.3	67.9	90.5
0.60	17.0	33.9	50.9	67.9
0.75	13.6	27.2	40.7	54.3
0.90	12.0	22.6	33.9	45.3

(b) f_c' = 6000 psi

γ	$\ell_{e,min}$ (in.)	ℓ_d (in.)		
		$f_{s,cr} = 0.5 f_y$	$f_{s,cr} = 0.75 f_y$	$f_{s,cr} = f_y$
0.45	17.5	35.1	52.6	70.1
0.60	13.1	26.3	39.4	52.6
0.75	12.0	21.0	31.6	42.1
0.90	12.0	17.5	26.3	35.1

The values of the minimum required embedded length ranged from 12 in. to 22.6 in. for the range of parameters considered. The minimum of 12 in. controlled for most cases with galvanized steel duct, while Eq. (8.12) controlled for most cases with plastic duct. The values for the development length required to resist the full yield stress in the connector varied by more than a factor of 3 (27.0 in. to 90.5 in.).

For calculated tensile stresses up to 0.5 f_y, the required embedded length is less than 36 in. for almost all combinations of duct, connector layout, and concrete compressive strength. Most precast bent caps used in Texas are at least this deep. If the calculated tensile stress exceeds 0.5 f_y, it may be necessary to increase the spacing between connectors (and thereby increase γ) or increase the depth of the bent cap to accommodate a larger development length to satisfy the recommended design provisions.

8.4 SUMMARY

The design provisions presented in this chapter provide an approach for determining the required embedded length of a grouted vertical-duct connector based on the type of duct, the configuration of the connectors, and the level of calculated tensile stress in the connector under the design load combinations. The recommended design provisions are based on the observed response of 32 grouted vertical connectors tested as part of the experimental phase of this project.

The minimum embedded length for all connectors was established using the serviceability state at the onset of widespread splitting cracks in the concrete. The development length represents the embedded length necessary to resist the maximum tensile stress calculated using the strength and extreme event limits states in the AASHTO *LRFD Design Specifications* (2004). Design equations for development length are based on the measured tensile capacities of the connectors.

In an earlier TxDOT report, Matsumoto et al. (2001) recommended the embedded length in Eq. 8.13 to develop the full yield stress for grouted vertical-duct connectors in galvanized steel ducts:

$$\ell_d = \frac{0.024 f_y d_b}{\sqrt{f_c'}} \tag{8.13}$$

Group effects and plastic duct were not considered in the development of Eq. (8.13). The previous design recommendations can be compared with the results from this investigation by substituting $f_{s,cr} = f_y$, β =1.0, and γ =1.0 into Eq. (8.8):

$$\ell_d = \frac{f_y d_b}{45\sqrt{f_c'}} = \frac{0.022 f_y d_b}{\sqrt{f_c'}} \tag{8.14}$$

As indicated by comparing Eq. (8.13) and Eq. (8.14), the development lengths proposed in this research are approximately 10% less than those recommended by Matsumoto et al. (2001) for this ideal case. The advantage of the current approach is that group effects and plastic duct may be considered explicitly in the design of the precast bent cap.

It should be noted, however, that the design equations have been developed from a rather small data set comprising a single size of connectors and a single size of duct. Caution is urged when extrapolating beyond the range of parameters tested. For example, the compressive strength of the concrete used to construct the test specimens ranged from 4500 psi to 6100 psi. Further testing is required to determine if the development length provisions are applicable with high-strength concrete. In addition, the specified compressive strength of the grout must increase if high-strength concrete is used to avoid premature plug failures of the connectors. This mode of failure will not control for the range of grout strengths (4700 psi to 7100 psi) considered.

Damage to concrete bridges along the Gulf Coast during recent hurricanes highlights an extreme event that is not considered in the AASHTO *LRFD Design Specifications* (2004). During the tidal surge, the superstructure is lifted off the supports due to wave forces. This loading condition would induce significant tensile stresses in the grouted vertical-duct connectors if the superstructure is attached to the substructure. For bridges along the Texas coast, it may be necessary to design the connectors to resist higher tensile stresses than calculated using the AASHTO *LRFD Design Specifications* (2004) or to elevate the bridge so that the connectors are above the tidal surge.

CHAPTER 9
Design Provisions

The design provisions for grouted vertical connectors are summarized in this chapter and provide engineers with practical design guidelines. The provisions address the design approach and detailing of connections, but are not intended to include all aspects of the design of precast bent caps.

1. Scope

1.1 The provisions in this chapter are applicable to the design of grouted vertical connectors for precast bent caps. Equations for anchorage of connectors are developed based on experimental data. Practical details for connecting bent caps to columns and piles using grouted vertical duct connections are suggested.

1.2 The provisions are not intended to be used to design bent structures of unusual proportions or bents subjected to seismic loads.

2. Definitions

Bent Cap – A concrete beam of rectangular or inverted-T cross-section that transfers loads from the bridge superstructure to columns or piles.

Bedding Layer – A thin layer of grout that is formed at the interface of the top of the column and the bottom of the bent cap.

Connector – A straight or headed reinforcing bar that is used to join together the bent cap to columns or piles.

Grouted Vertical Duct – Corrugated galvanized steel or plastic duct that is precast in the bent cap to serve later as a sleeve to house a connector, and then filled with grout.

Embedded Length – The length the connector extends into the bent cap within the grouted vertical duct.

Transverse Reinforcement – Reinforcement used to resist shear, torsion, or to confine concrete in a structural member.

3. Notation

A_{Nc} = the projected failure surface of a group of connectors, which is limited by the distance between the connectors and the nearest edge (in.^{2}).

A_{Nco} = the maximum projected failure surface of an individual connector, defined as a square with sides equal to $15\,d_b$ (in.^{2}).

d_b = nominal diameter of connector (in.)

f'_c = specified compressive strength of concrete (psi)

$f_{s,cr}$ = calculated tensile stress in connector corresponding to the critical load combination (psi)

f_y = specified yield stress of connector (psi)

ℓ_d = development length for connector in tension (in.)

$\ell_{e,min}$ = minimum required embedded length of connector (in.)

n = number of connectors in group

β = modification factor for duct material, taken as 1.0 for galvanized steel duct and 1.3 for plastic duct

γ = modification factor for group effects, calculated based on the number of ducts subjected to simultaneous tension under the design load combinations

4. Material Properties

4.1 Concrete

4.1.1 Concrete used in precast bent caps shall be normal-weight concrete with a specified 28-day compressive strength of at least 3600 psi.

4.1.2 The value of concrete compressive strength used in anchorage design equations shall not exceed 6000 psi, regardless of the specified compressive strength, f'_c.

4.2 Grout

4.2.1 Grout material used in grouted vertical duct connections must satisfy the TxDOT Grout Performance Specification.

4.2.2 Prepackaged grout material shall not be used after the expiration date.

4.3 Reinforcing Steel and Connectors

4.3.1 Both straight and headed connectors are permitted.

4.3.2 Reinforcing bars used as connectors shall conform to ASTM A615 or A706. The specified yield strength for connectors shall be 60 ksi.

4.3.3 Epoxy-coated connectors shall conform to ASTM A775.

4.4 Ducts

4.4.1 Ducts must be corrugated.

4.4.2 Corrugated strip steel ducts must be galvanized and conform to ASTM A653. The minimum wall thickness is 0.45 mm (26 gage) for duct diameters up to 4 in., and 0.65 mm (24 gage) for duct diameters larger than 4.5 in. Corrugation (rib) height of steel ducts must be at least 0.12 in.

4.4.3 Ducts made of high-density polyethylene or polypropylene are permitted. In lieu of a standard specification, plastic ducts must comply with fib technical bulletin 7, "Corrugated Plastic Ducts for Internal Bonded Post-Tensioning" (2000). In addition, the following restrictions apply:

- Minimum wall thickness of plastic duct is 3 mm (0.118 in.).
- Minimum corrugation (rib) height of plastic duct is 0.2 in.
- Maximum spacing between ribs (corrugations) is 2.5 in.

5. General Connection Design Approach

5.1 Determination of Connection Actions following AASHTO *LRFD Design Specifications* (2004)

5.1.1 The forces acting on the connections are determined by frame analysis of the bent, considering the connection at the top of the columns to be capable of resisting moments. The load combination that controls the design consists of the most severe combination of simultaneous transverse and longitudinal actions.

5.2 Selection of Connector Configuration

5.2.1 The trial connector configuration is selected based on spacing and minimum connection reinforcement requirements.

5.2.2 Reinforcement crossing the joint must be at least 0.7% of the gross area of the column, or 1.0% of the gross area of the pile. To provide redundancy, a minimum of four connectors must be provided in columns, whereas a minimum of three connectors must be provided in trestle piles.

5.3 Analysis of Connector Configuration

5.3.1 The selected trial configuration must be analyzed by evaluating strength and serviceability requirements.

5.3.2 Strength requirements must include:

- Determination of the connector area of steel required to resist factored axial load and moments.
- Estimation of the shear friction at the bedding layer using the AASHTO *LRFD Design Specifications* (2004).

5.3.3 Serviceability checks must include:

- Determination of potential opening at the bedding layer by estimating the location of the neutral axis.
- Control of concrete cracking in the connection area following the AASHTO *LRFD Design Specifications* (2004) [2, Section 5.7.3.4].
- Control of bent deflections.

5.3.4 Sectional analysis based on the factored forces calculated in 5.3.2 shall be used to determine which connectors are expected to experience tension. These connectors are then used to calculate the projected failure surface of the connector group, A_{Nc}, used in the calculation of the modification factor for group effects, γ. A conservative value of γ is obtained using all the connectors in the group.

The connector with the highest calculated tensile stress, $f_{s,cr}$, controls the design of the connection group. The group modification factor, γ, is calculated from Eq. 9.1:

$$\gamma = \frac{A_{Nc}}{nA_{co}} \tag{9.1}$$

If sectional analysis of a particular connection indicates that connectors experience only compressive stresses, then the group modification factor may be taken as 1.0.

5.3.5 The required embedded length of connectors is determined using the provisions in Sections 7.1 and 7.2.

5.4 Selection of Transverse Reinforcement

5.4.1 Providing spiral transverse reinforcement around the connector group over the depth of the cap has no influence on response.

5.4.2 Use of spirals around individual ducts is discouraged.

6. Detailing of Connections

6.1 The duct diameter shall be selected so that a horizontal clearance of at least 1 in. exists around the periphery of the connector. For connections involving more than six connectors, a minimum horizontal clearance of 1.5 in. should be provided.

6.2 Reinforcing bars used as connectors shall be no smaller than #9 and no larger than #14.

6.3 Minimum clear spacing between ducts shall be at least 2 in. to permit adequate placement of concrete around ducts. The minimum recommended clear spacing between ducts is one duct diameter.

6.4 Minimum clear cover to ducts is 6 in.

7. Embedded Length of Connectors

7.1 The minimum embedded length for a connector, $\ell_{e,min}$, is given in Eq. (9.2), but shall not be less than the larger of $8d_b$ and 12 in.

$$\ell_{e,min} = \frac{\beta f_y d_b}{180\gamma\sqrt{f_c'}} \tag{9.2}$$

7.2 The development length in tension for a connector, ℓ_d, is given in Eq. (9.3). The value of $f_{s,cr}$ used for design is calculated in 5.3.4.

$$\ell_d = \frac{\beta f_{s,cr} d_b}{45\gamma\sqrt{f_c'}} \tag{9.3}$$

7.3 In 7.1 and 7.2, the modification factor β is taken as 1.0 for galvanized steel duct and 1.3 for plastic duct.

7.4 Regardless of the number of connectors that are calculated to resist tension under the design load combination, all connectors in a group should be embedded the same length to minimize installation errors.

7.5 Equations (9.2) and (9.3) may be used without modification for both plain and epoxy-coated connectors.

7.6 The embedded lengths calculated using Eq. (9.2) and (9.3) may not be reduced due to the presence of transverse reinforcement.

7.7 It is recommended that the embedded length of the connectors be at least ¾ of the cap depth, even for cases where anchorage design provisions indicate that a much shorter embedment length is acceptable.

8. Durability

8.1 For designs where durability is a primary concern, the designer is encouraged to consider the following options:

- Use of epoxy-coated connectors
- Use of plastic ducts
- Terminate the vertical ducts before reaching the top of the cap
- Embedding the column (or pile) in the cap
- Use an external sealant

CHAPTER 10
Summary and Conclusions

The Texas Department of Transportation (TxDOT) has used prefabricated bridge elements for many years. Prefabrication of key components of bridges has provided efficiency by accelerating the construction schedule and has provided a safer working environment in congested urban areas and over water.

Bridge projects constructed in Texas utilizing precast bent caps typically employ grouted vertical ducts in the cap-to-column connections. Contractors and TxDOT engineers prefer this type of precast connection due to the simple geometry and because the volume of grout needed to complete the connections is minimized. Many uncertainties related to the configuration and details of grouted vertical connectors were identified during the design and construction of these bridges.

Researchers at the University of Texas conducted TxDOT Project 0-4176 to learn more about the behavior of grouted vertical-duct connectors constructed using both galvanized steel and plastic ducts. A second objective was to develop appropriate design provisions for grouted vertical-duct connectors. The research project has accomplished both of these primary objectives. A brief summary of the project is provided in Section 10.1, and the major conclusions are summarized in Section 10.2. Five suggestions for future research are proposed in Section 10.3.

10.1 SUMMARY

The aim of the experimental program was to understand how different connector configurations and duct materials influence the behavior of precast bent cap connections constructed using grouted vertical-duct connectors. The primary parameters selected for study were bar coating, duct material, connector embedment depth, number of connectors, bar eccentricity, and configuration of transverse reinforcement. Thirty-two, large-scale specimens with one to three connectors were tested. A single connector size (#11) and duct diameter (4 in.) were used in all experiments. Embedded lengths of connectors ranged from $8d_b$ to $16d_b$ (11.3 in. to 22.6 in.).

The measured response of the test specimens was sensitive to the duct material and the embedded depth of the connectors. Connector strength also tended to decrease as the number of connectors tested simultaneously in tension increased. In addition, eccentric placement of the connector within the duct reduced the capacity of the connector. The measured response was not sensitive to bar coating or the configuration of transverse reinforcement.

Anchorage design provisions were developed for connectors based on the level of calculated tensile stress in the connectors for the design load combinations. Load combinations corresponding to

both strength and extreme event limit states were considered. The measured tensile stresses at the capacity of the test specimens were used to establish the design provisions for development length in tension, ℓ_d. The measured tensile stresses at the onset of widespread cracking in the concrete were used to determine the minimum embedded depths of grouted vertical-duct connectors, $\ell_{e,min}$. The final design equations include two modification factors: β represents the influence of the duct material and γ represents the configuration of the connectors. The complete recommendations for design of grouted vertical-duct connectors are given in Chapter 9.

10.2 CONCLUSIONS

Conclusions from this investigation related to the behavior of grouted vertical connectors are presented below:

1. *The duct material has an important influence on the behavior and mode of failure of connections.* The initial stiffness and strength of connectors constructed using galvanized steel ducts were higher than those of the test specimens constructed using plastic ducts. Reductions in strength relative to the specimens with galvanized steel duct specimens averaged 30 to 35%. In all cases, specimens constructed using galvanized steel ducts failed by pullout of the connector from the surrounding grout. In many instances, specimens constructed using plastic ducts failed when the connector and the surrounding plug of grout pulled out of the duct. The modification factor β is included in the design equations for ℓ_d and $\ell_{e,min}$ to include the influence of the duct material. The value of β is 1.0 for galvanized steel duct and 1.3 for plastic duct.
2. *The formation of widespread splitting cracks in the concrete represents a critical stage of response.* The axial stiffness of connectors and the stress distribution along connectors changed considerably after the formation of widespread splitting cracks in the concrete. Galvanized steel ducts provided passive confinement of the connector, which mobilized after the splitting cracks formed. Plastic ducts did not provide confinement and the tensile strength did not increase appreciably after the splitting cracks formed.
3. *Increasing the number of connectors reduces the tensile capacity of each connector.* As the number of connections subjected to simultaneous tensile stresses was increased, the tensile stress at the onset of widespread cracking in the concrete and the tensile capacity of the connectors decreased. Reductions on the order of 30 to 40% were observed. The modification factor γ is included in the design equations for ℓ_d and $\ell_{e,min}$ to include the influence of connector configuration. Values of γ range from 0.45 to 0.9 for typical configurations of grouted vertical-duct connectors.

4. *Bar eccentricity reduces the tensile capacity of the connectors.* Based on a limited number of tests of single connectors, placement of the connector within the duct influenced the strength of the connector. The bond strengths were reduced an average of 17% when the connector was located near the duct, rather than centered within the duct. The modification factor ξ is embedded in the design equations for ℓ_d and $\ell_{e,min}$ to include the influence of connector eccentricity. Because eccentric placement of connectors is expected in the field, ξ is taken as 0.8 in the design of all connectors.
5. *The presence of transverse reinforcement in the connection zone did not improve connection behavior.* The inclusion of a large spiral around a group of ducts had no influence on connection behavior. Results indicated that placing individual spirals around polyethylene ducts degraded the performance of the connection. Although the individual spirals were somewhat effective in restraining the upward movement of the duct, failure occurred as the connector/grout plug slipped out of the duct. Therefore, the use of small spirals around individual ducts is not recommended.
6. *Design equations for development lengths are based on the level of the calculated tensile stress*. Because dead loads dominate the design of most precast substructure systems, designing all connectors to resist the full yield stress of the connector in tension was considered to be overly conservative. Therefore, the maximum calculated tensile stress, $f_{s,cr}$, is used to determine the required embedded length of the connector. For design tensile stresses up to 0.5 f_y, the required embedded lengths for #11 connectors are less than 3 ft for most practical combinations of connector layout and duct material. For design stress levels of f_y, the required development lengths for closely-spaced #11 connectors exceeds 5 ft in some cases.

10.3 SUGGESTIONS FOR FURTHER RESEARCH

The demand for precast bent caps is expected to increase as TxDOT continues to incorporate rapid construction techniques as an option to conventional construction in upcoming bridge projects. This research has provided experimental data to clarify many of the uncertainties that had been identified regarding the design of grouted vertical duct connections. Additional research is needed to extend the use of the anchorage design provisions to other design situations. Some suggestions for further research are given below:

1. *Duct materials and geometric properties* – Although two types of plastic ducts were included in this investigation, the available data were insufficient to determine if the type of plastic or the geometry of the ducts has a larger influence on the connector response. Additional tests are

required to determine the influence of rib spacing, variations in duct wall thickness and rib height on connector behavior.

2. *Grout materials* – Other types of grout materials should also be investigated experimentally. Brands of prepackaged grout that meet the grout performance specifications should be identified and pullout tests should be conducted to assess variability in connection behavior. Durability properties of grout materials that are of interest to grouted vertical duct connections should also be investigated further.
3. *Influence of a compressive stress field in the connection zone* – The effects of varying the geometry of the compressive stress field in the connection zone should be studied to approximate different load conditions in the field. Tests of column-bent cap subassemblies and/or connector pullout tests that incorporate movable test frame reaction supports can be conducted to further evaluate serviceability stress limits, and differences in crack patterns and load resisting mechanisms of grouted vertical duct connections.
4. *Ratio of duct to connector diameter* – All tests were conducted using one bar diameter and one duct diameter. Tests are needed to determine if the ratio of duct to connector diameter influences the susceptibility to plug failures of the grout.
5. *Design load combinations* – Currently the AASHTO *LRFD Design Specifications* (2004) do not consider tidal surges due to hurricanes. This loading condition may lead to tensile stresses that are critical for bridge construction with precast substructures along the Gulf Coast.

APPENDIX A
Measured Properties of Concrete and Grout

A.1 CONCRETE

The concrete used to fabricate the test specimens was provided by a local ready-mix supplier. The standard TxDOT Class C mixture was specified. The maximum coarse aggregate size was ¾ in. and the specified compressive strength at 28 days was 3600 psi. The mixture proportions are summarized in Table A.1. The average measured slump was 4 in.

Table A.1 Concrete Mixture Proportions

Cement (lb/yd^3)	Coarse Aggregate (lb/yd^3)	Fine Aggregate (lb/yd^3)	Water (lb/yd^3)	Retarder (oz)
564	1882	1191	250	24

Six by twelve-in. cylinders were tested regularly to assess the strength of the concrete. The measured compressive strength on the days that the connectors were tested is summarized in Table A.2.

Table A.2 Measured Compressive Strength of Concrete

Beam ID	Connector Test	Age of Concrete at Test (day)	f_c' (psi)
1	1-4	90 (approx.)	5400
2	5-8	120 (approx.)	5500
3	9	42	4500
	10	49	4500
4	11-12	64 (approx.)	4600
5	13-14	48 (approx.)	4700
6	15-16	54 (approx.)	4700
7	17	34	5200
	18	41	5300
8	19-20	51	5500
	21-22	58	5500
9	23-24	58 (approx.)	6100
10	25-27	74 (approx.)	6100
11	28-30	36 (approx.)	6100
12	31-32	42 (approx.)	6100

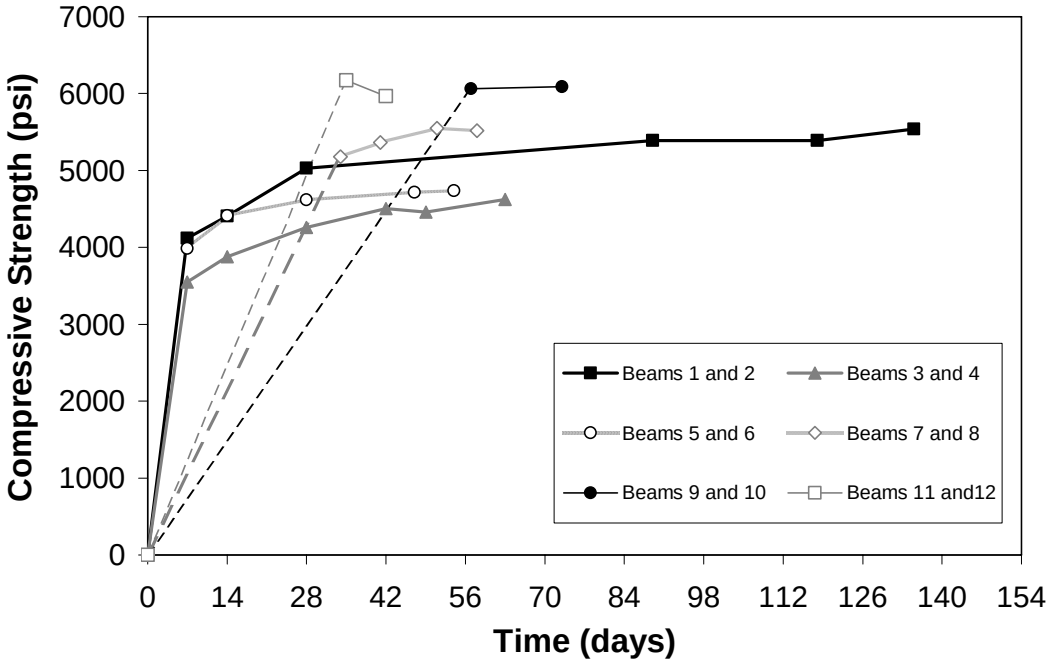

Figure A.1 Concrete Compressive Strengths for Beam Specimens

For the first three pairs of beams, cylinders were tested 3, 7, 14, and 28 days after casting, in addition to the day of the test. Cylinders were only tested on the day of the connector tests for Beams 7 through 12. The variation of compressive strength with age is shown in Figure A.1.

A.2 GROUT

Masterflow 928, prepackaged grout was used in the experiments. This product is a high-precision, non-shrink, natural aggregate grout that meets ASTM C 1107, Grades B and C, and satisfies the TxDOT Grout Performance Specification (Table 4.3). A series of trial batches were conducted to determine the optimal amount of water to be added per bag to obtain the fluidity necessary in the grout to complete the connections within the established working time of the mixture.

Figure A.2 shows the equipment used during the grouting operations: mortar mixer, flow cone, funnels, plastic hoses, and cube forms.

a. Mortar Mixer Used to Mix Grout

b. Flow Cone

Figure A.2 Equipment Used during Grout Operations

For the grouting operations, the amount of water added varied between 1.27 to 1.37 gallons (10.45 to 11.25 lb) per 55 lb bag of grout material (Table A.3). These were within the fluid consistency range provided by the manufacturer for an efflux time of 25 to 35 sec using the ASTM C 939 flow cone standard test. Water amounts were adjusted depending on the temperature at the time of grouting. Efflux times measured using the flow cone were always larger than 35 sec and did not appear to be related to the amount of water in the mixture or the air temperature.

The compressive strength of the grout was inspected regularly by testing 2-in. grout cubes in accordance with ASTM C 109. Table A.4 summarizes the measured compressive strength of the grout on the days that the connectors were tested.

The variation of the compressive strength of the grout cubes with time is shown in Figure A.3 through Figure A.5.

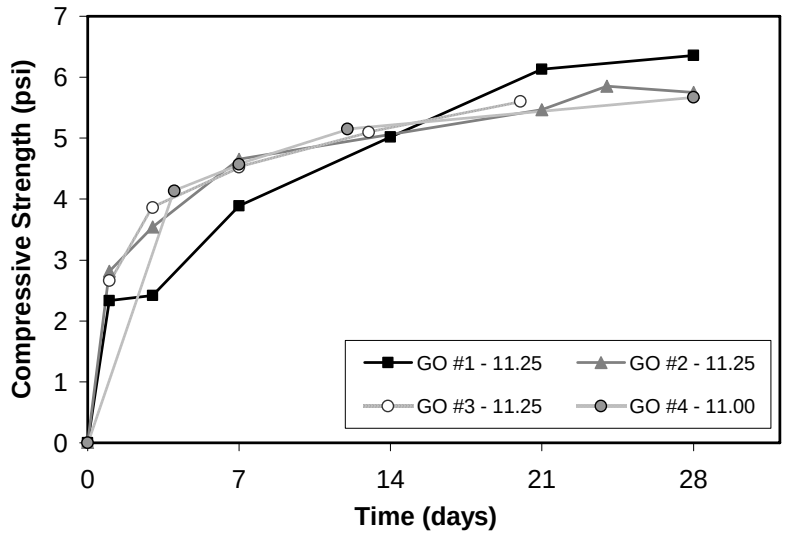

Figure A.3 Grout Strength – Beam Specimens 1 through 4

Table A.3 Properties of Grout

Beam ID	Weight of Water (lb/bag)	Air Temperature (°F)	Efflux Time (sec)	Comments
1	11.25	85	44	Minimal clumps
2	11.25	86	65	No clumps
3	11.25	81	77	No clumps
4	11.00	69	60	Few clumps
5	10.75	70	81	Few clumps
6	10.75	70	83	Few clumps
7	11.25	66	56	Minimal clumps
8	11.00	76	86	Few clumps
9	11.00	91	68	Minimal clumps
10	10.45	85	101	Few clumps
11	10.45	76	96	Low workability
12	11.00	67	81	Low workability

Table A.4 Measured Compressive Strength of Grout

Beam ID	**Connector Test**	**Age of Grout at Test (days)**	f_g **(psi)**
1	1	14	5000
	2	21	6100
	3	27	6400
	4	31	6400
2	5	7	4700
	6	21	5500
	7	24	5900
	8	28	5800
3	9	13	5100
	10	20	5600
4	11	12	5100
	12	12	5100
5	13	13	5200
	14	14	5300
6	15	13	5400
	16	14	5400
7	17	14	4800
	18	21	4900
8	19	14	5100
	20	14	5100
	21	21	5400
	22	21	5400
9	23	27	6000
	24	33	6300
10	25	20	6500
	26	23	6500
	27	29	6500
11	28	14	6800
	29	16	7100
	30	16	7100
12	31	14	5800
	32	14	5800

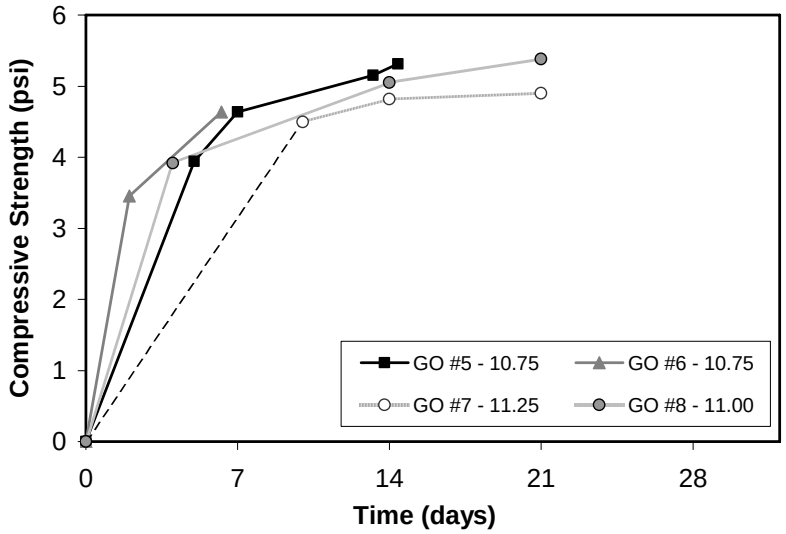

Figure A.4 Grout Strength – Beam Specimens 5 through 8

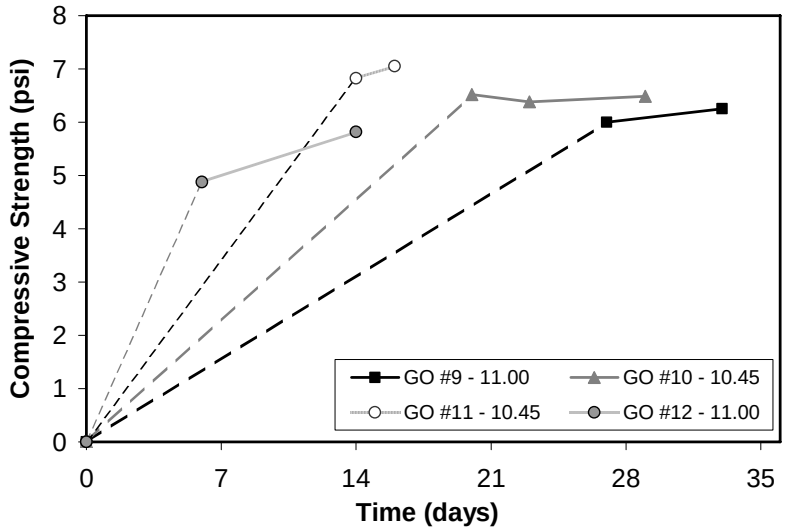

Figure A.5 Grout Strength – Beam Specimens 9 through 12

APPENDIX B
Strain Gages

B.1 APPLICATION OF STRAIN GAGES

Two types of strain gages were used in the experiments. Strains in the reinforcement and and galvanized steel ducts were measured using 5-mm strain gages, which had a grid area of 7.5 mm^2 and a resistance of 120 ohm. As discussed in Section B.2, strain gages used to measure strains on the polyethylene and polypropylene ducts had a length of 6 mm, a grid area of 16.2 mm^2, and a resistance of 350 ohm. The larger resistance and grid area were selected due to the poor thermal conductivity of the plastic duct materials. The strain gages attached to the plastic duct also had a very flexible backing material, which is specially suited for plastic applications.

Surfaces of the materials were carefully prepared and cleaned before strain gages were applied. In the case of the reinforcing bars, a small portion of a bar lug was ground away to leave a flat surface, which was long enough to bond the gage and apply the water-proofing and protective coatings. Care was taken to grind only the amount of metal necessary to achieve this flat surface. Figure B.1 shows the surface preparation of the rebar.

Figure B.1 Surface Preparations on a Connector for Bonding a Strain Gage

The adhesive used to bond gages to the metal surfaces was a cyanoacrylate-type adhesive, commonly used in structural experiments. The plastic surfaces had to be pre-treated with a poly-primer compound before bonding the gage using the same cyanoacrylate adhesive. After visually confirming that the bonding procedure was successful, a series of water-proofing and protective coatings was applied to the gages.

For the case of the strain gages bonded to metal surfaces, the first water-proofing coating consisted of an acrylic-based solvent. This solvent, once dry, forms a hard, but tough coating over the gage. Two coats of this solvent were applied within a 45-minute interval. This acrylic-based solvent was not used on the gages bonded to plastic materials because it could provide sufficient stiffness to constrain the gage. Therefore, a more flexible water-proofing coating was used over the gages installed on plastic materials. Two coats of a silicone rubber compound were applied over the gages, also within a 45-minute interval.

Additional coatings were the same for both metal and plastic surfaces. A second water-proofing coating consisting of a layer of butyl rubber was applied over the first coating, as shown in Figure B.2. Then, a pad of neoprene rubber was placed over the butyl-rubber to give some mechanical protection to the gage, which was followed by application of aluminum foil tape to completely cover the gage, as shown in Figure B.3. Following these procedures, none of the gage installations were damaged due to moisture penetration or placement of concrete.

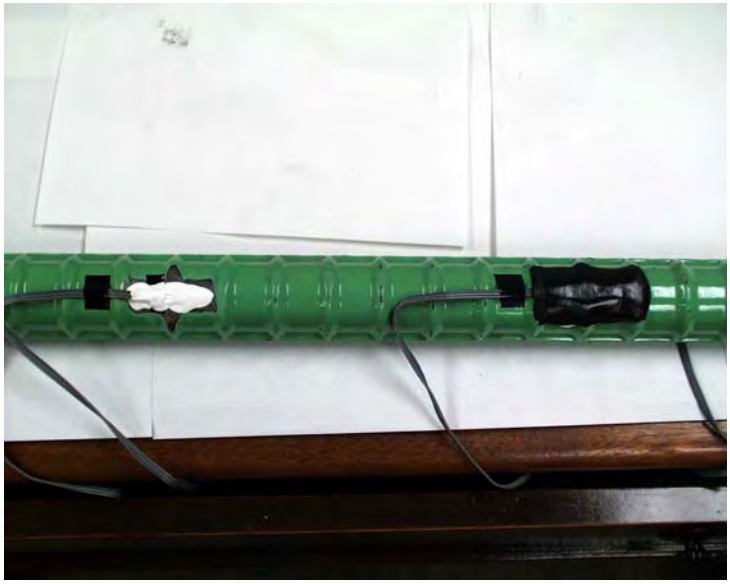

Figure B.2 Layers of Waterproofing Protection on Gage Installations Bonded to Metal Surfaces

Figure B.3 Two Completed Strain Gage Installations

B.2 BONDING STRAIN GAGES TO PLASTIC

The heat generated within a strain gage must be transferred by conduction to the mounting surface. The heat flow through the specimen causes a temperature rise in the substrate, which is a function of its heat-sink capacity and the gage power level (Measurements Group 2000). Strain measurement on plastic requires special consideration. Most plastics act as thermal insulators rather than heat sinks. Very low values of excitation are required to avoid serious self-heating effects.

The elastic moduli of common plastic materials are typically two or more orders of magnitude lower than those for metals (Measurements Group 2001). Strains measured on plastics tend to be considerably larger than on metals, and can normally exceed 1 percent. The presence of the gage installation may reinforce the material locally, leading to large measurement errors. Gages having very flexible backing material should be used in plastic applications.

Strain gages used to measure strains on the polyethylene and polypropylene ducts had a larger resistance and a larger grid area because of the poor thermal conductivity of these materials. Based on recommendations given by Measurements Group (2001), a value of power grid density, P_G, of 0.1 watts/in.^{2} was considered appropriate during the selection of the strain gage size. Based on an excitation voltage, E_B, of 2 volts, the gages selected for use on the plastic materials had a length of 6 mm (0.236 in.), a grid area, A_G, of 16.2 mm^2 (0.025 in.^{2}), and a resistance, R_G, of 350 ohm. The power grid density of the strain gages selected is determined by the following equation:

$$P_G = \frac{E_B^2}{4 A_G R_G} \tag{B.1}$$

where the value of power grid density calculated using Eq. (B.1) is 0.11 watt/in^2.

Gages having a larger area or a higher resistance could have been selected to obtain an even smaller value of power grid density in order to increase the accuracy of measurements. Increasing the resistance of the gage was not possible because of limitations in the electronic equipment available in the laboratory. Larger gage sizes were not desired because of possible fitting problems in the areas of gage installation in the ducts.

The degree of uncertainty involved in strain gage applications on plastic materials is rather high because very limited information is available. In this investigation, strain measurements in the ducts were required in order to assess the mobilization of confinement by the ducts. There is substantial variability in material properties for many common plastics. The guide by Measurements Group (2001) is a very useful guide to be used in the process of selecting strain gages for applications involving plastic materials.

APPENDIX C
Detailed Response of Connectors

The overall response of the connectors was presented in Chapter 6 by discussing observed crack patterns, stress-slip response, and observed modes of failure. Additional information about the performance of the connectors is provided in this appendix. The distribution of measured strains along the connectors is presented in Section C.1 and the corresponding distribution of stress along the connectors is presented in Section C.3. The procedure used to convert strain to stress is described in Section C.2. The slip of the connector relative to the grout is discussed in C.4 and the strain measured in the ducts is presented in Section C.5.

C.1 DISTRIBUTION OF STRAIN

The strain in the connectors was measured directly using strain gages. As mentioned in Section 5.2, strain was measured at the lead end of the connector, and at 6 in. intervals along the embedded portion of each connector. The results show the measured bar strain at the different gage locations, for a series of applied stress levels. The strain values shown in the results at the lead end of each connector correspond to the calculated average of the two lead gage readings.

The gages and adhesive used in the experiments were not designed to measure post-yield strain measurements; therefore, several gage readings at strains above 10,000 με were not reliable. These unreliable data points are shown in the plotted results with a broken line. In a few occasions, gages in the embedded portion of the connectors were damaged during a test. Strain readings at these bar locations are thus not available for subsequent levels of applied stress.

C.1.1 Galvanized Steel Duct

The strain distribution along the length of connectors housed inside galvanized steel ducts is illustrated by a representative set of tests consisting of one and two connectors.

Test 3 consisted of a single uncoated connector embedded at $12d_b$. The strain distribution along the length of the connector is shown in Figure C.1. For applied stresses between 20 and 60 ksi, the strain readings show that the entire length of the connector was reacting to the applied load. The strain measured at a depth of 6 in. was approximately equal to the strain measured at the lead. Since the strain readings at a depth of 12 in. were small compared to the readings at the other gage locations, it is clear that at stress levels between 20 and 60 ksi, the applied load was being resisted mostly by the portion of the connector closest to the surface. The strain distribution corresponding to an applied stress of 80 ksi shows that the

connector was experiencing post-yield strains at the lead, and even at a depth of 6 in. below the surface. These measured strains are corroborated given that the yield strength of the connector used in Test 3 was 75 ksi. Failure of the connector occurred at an applied stress level of 87 ksi. At this stress level, the dashed line in Figure C.1 indicates that the measured strains in the connector at the lead and at 6 in. below the surface were not reliable. Furthermore, there is no strain reading available for the bar location 12 in. below the surface, since the gage suffered damage.

Figure C.2 shows a similar strain distribution diagram, this time corresponding to Test 4. This test consisted of one epoxy-coated connector embedded at $12d_b$. While the strain distribution diagram corresponding to Test 3 had an approximate trapezoidal shape for applied stress levels between 20 and 60 ksi, the diagram shown for Test 4 has a more dominant triangular shape. The connector portion located closest to the surface was not effective at resisting most of the applied load, and the load had to be resisted more uniformly along the entire length of the connector. This difference in the strain distribution patterns of Tests 3 and 4 can be attributed to the detrimental effect of the epoxy-coating on friction resistance. The strain distribution at 70 ksi shows that post-yield strains were recorded at the bar lead and at 6 in. below the surface of the specimen. These measured strains are corroborated since the yield strength of the connector used in Test 4 was 68 ksi. At an applied stress of 80 ksi, the recorded strain at the lead was unreliable, as shown by the dashed line. The failure load for this test corresponded to an applied stress of 88 ksi. Strain distribution data at this stress level were unreliable.

Figure C.3 shows the strain distribution along the length of one of the connectors (left) tested in Test 13. Both of the connectors in this test had a similar strain distribution, hence only the results for one connector are shown. A first thing to notice by looking at the diagram in Figure C.3 is that at a load level of 20 ksi, the gage located at a depth of 18 in. was recording a strain value close to zero. This means that at this stress level, the load was mainly being resisted by the top portion of the connector. As loading progressed, the gage located at a depth of 18 in. did begin to measure more significant strains. At a stress level of 60 ksi, the diagram shows that the bar was straining appreciably along its length. The strain recorded at a depth of 6 in. was approximately equal to the measured strain at the lead. At 80 ksi, 5 ksi above the connector's yield strength, the measured strains are in the post-yield range at the lead and at a depth of 6 in. At failure, at an applied stress of 87 ksi, the recorded strain at the lead was unreliable, as shown by the dashed line.

The strain distribution diagram for one of the connectors tested in Test 17 is shown in Figure C.4. The two connectors in this test behaved similarly, as in the case of Test 13, hence only the results for the left connector are presented. The embedment depth provided for the connectors in Test 17 was $12d_b$. The connectors failed by pullout at an applied stress of 59 ksi. The strain distribution along the connector length is similar for stress levels of 20 and 40 ksi. The only difference lies in the overall magnitude of the

measured strains. However, as the load increased, widespread radial splitting in the concrete occurred and the load was redistributed along the connector length, with more of the load being anchored deep at the end portion of the connector.

C.1.2 Polyethylene Duct

The strain distribution along the length of connectors housed inside polyethylene ducts is illustrated by a representative set of tests consisting of one and two connectors.

Test 7 consisted of a single connector embedded at $12d_b$. The strain distribution along the length of the connector is shown in Figure C.5. Throughout the test, the strains recorded at the gage located 6 in. below the surface of the specimen were approximately equal than the ones recorded at the lead of the connector. Appreciable values of strain were also measured at the location 12 in. below the surface. The strain reading corresponding to a depth of 12 in. at failure was not available.

Figure C.6 shows the strain distribution diagram for Test 22. Even at an applied stress as small as 20 ksi, a noticeable value of strain was recorded at a depth of 18 in. below the surface. At stress levels equal and smaller than 60 ksi, the strains measured 6 in. below the surface of the specimen were approximately equal than the ones recorded at the lead end of the connector. A post-yield strain value was recorded at the lead of the connector when the applied stress was 80 ksi. At this load stage, the strain gage located at 6 in. below the surface indicated that the bar at this location was beginning to experience yield deformations as well. The connector failed at a load corresponding to 90 ksi. The strain record at a depth of 6 in. indicates that considerable yielding occurred in the connector as deep as 6 in. below the surface. The strain measured at the connector lead at this applied stress was unreliable.

The strain distribution diagram of Test 14 is shown in Figure C.7. The results for the left connector are presented. Throughout the test, the strain values measured 6 in. below the surface were roughly equal to those measured at the lead. This is a phenomenon observed in all tests involving the polyethylene duct, and occurred independent of the embedment depth provided or the number of connectors. The diagram in Figure C.7 shows that at stress levels of 60 and 64 ksi, the load was being redistributed along the length of the connector and the anchorage of the bar was essentially taking place very near the end portion of the connector.

For comparison purposes, a similar strain distribution diagram, corresponding to Test 24, is presented in Figure C.8. The only difference between Test 14 and Test 24 was that the duct clear spacing in Test 24 was twice that of Test 14. The capacities of both tests were, nonetheless very similar. The results presented here correspond to the left connector of Test 24 tested up to the connection failure load, and do not include the data obtained upon reloading of the connector. The strain distribution data for this connector, up to the failure load, appear to be similar to that obtained for the connector of Test 22.

C.1.3 Polypropylene Duct

The strain distribution along the length of connectors placed inside polypropylene ducts is illustrated by a representative set of tests consisting of one, two, and three connectors.

Test 30 consisted of a single connector embedded at $12d_b$. The strain distribution along the length of the connector is shown in Figure C.9. At applied stresses between 20 and 60 ksi, the strain readings corresponding to a depth of 6 in. were equivalent to the strain values measured at the lead. At a stress level of 68 ksi, post-yield strains were measured at a depth of 6 in. and at the lead. However, the strain value at the lead was unreliable, since it is suspected that, at this point, the gage installation was damaged. In general, for loads lower than the connector yield strength of 59 ksi, the strain distribution diagram has a trapezoidal shape, similar to that exhibited by Test 3, which involved galvanized steel ducts.

The strain distribution for one of the connectors of Test 28 is shown in Figure C.10. Radial splitting in the concrete started to occur at a load of 66 kip (44 ksi). The strains measured along the length of the connector show that the strain recorded by the gage located 12 in. below the surface increased somewhat between applied stresses of 40 and 60 ksi. The change in the pattern of strain distribution indicates that due to extensive splitting in the concrete, the load along the connector was redistributed and more of it was being transferred deep into the end portion of the connector. An intermediate load step corresponding to an applied stress of 70 ksi shows that considerable yielding is occurring in the connector, even at 6 in. below the surface. Moreover, the strain measured at a load corresponding to 80 ksi at a depth of 12 in. indicates that yielding was progressing along the length of the connector. The strain readings at the lead associated with the ultimate load stages were not reliable.

For comparison purposes, the strain distribution diagram for one of the three connectors of Test 32 is presented in Figure C.11. In the case of Test 32, splitting in the concrete began at a low connector stress of 20 ksi. However a general widespread pattern of splitting did not develop until the load reached 46 ksi (70 kip). The event of significant concrete splitting and its effects on the pattern of strain distribution along the connector length can be seen in the diagram as the applied stress increased from 40 to 60 ksi. The load along the connector was redistributed and more of it was being transferred deep into the end portion of the connector. At failure, the strain measurements indicate that yielding in the connector extended to a depth of 12 in. below the surface.

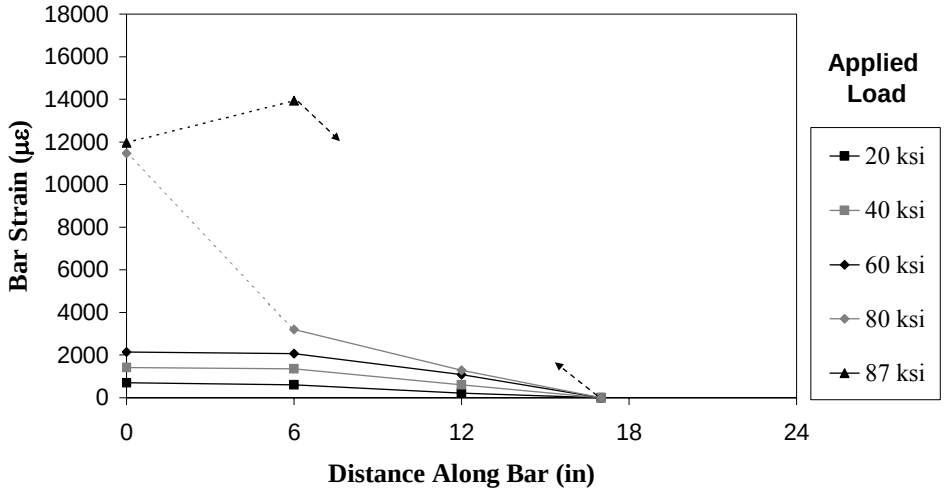

Figure C.1 Strain Distribution along Connector (Test 3)

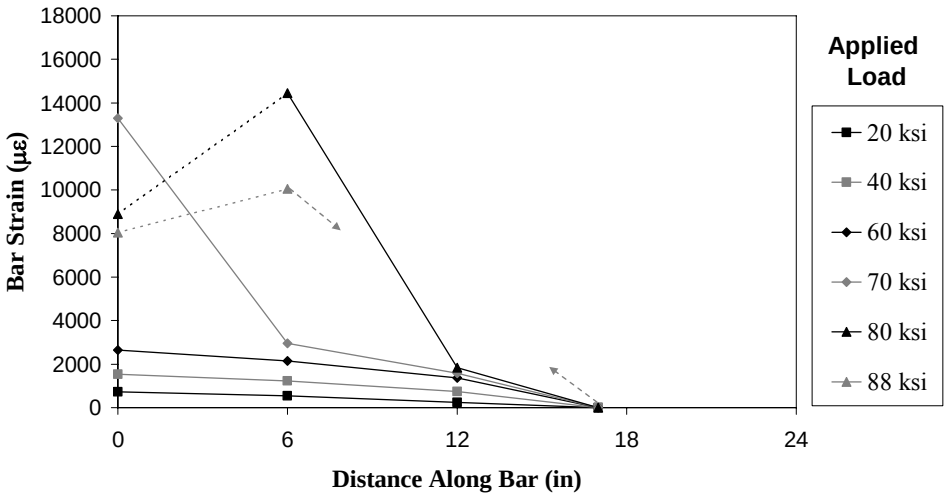

Figure C.2 Strain Distribution along Connector (Test 4)

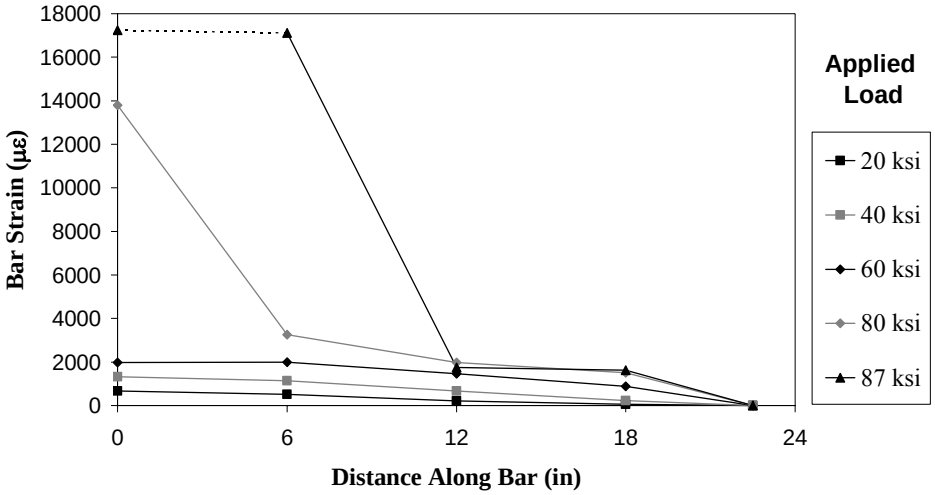

Figure C.3 Strain Distribution along Connector (Test 13, Left Bar)

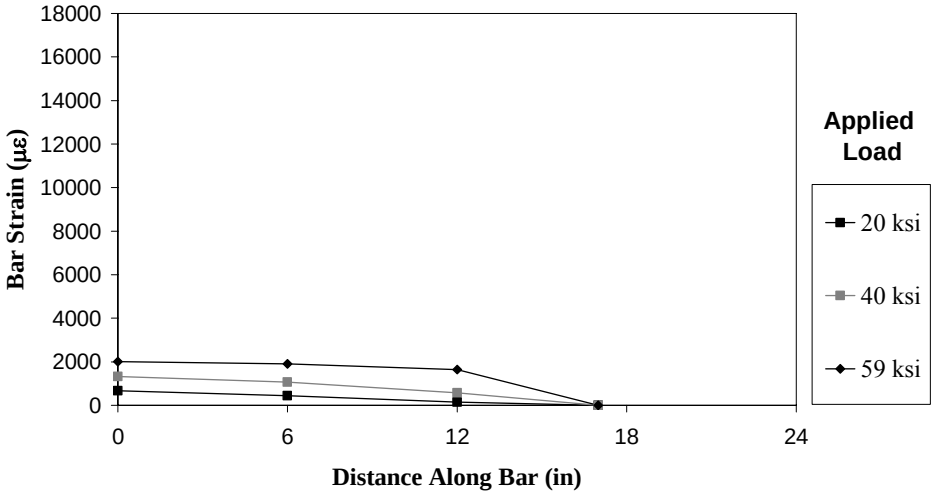

Figure C.4 Strain Distribution along Connector (Test 17, Left Bar)

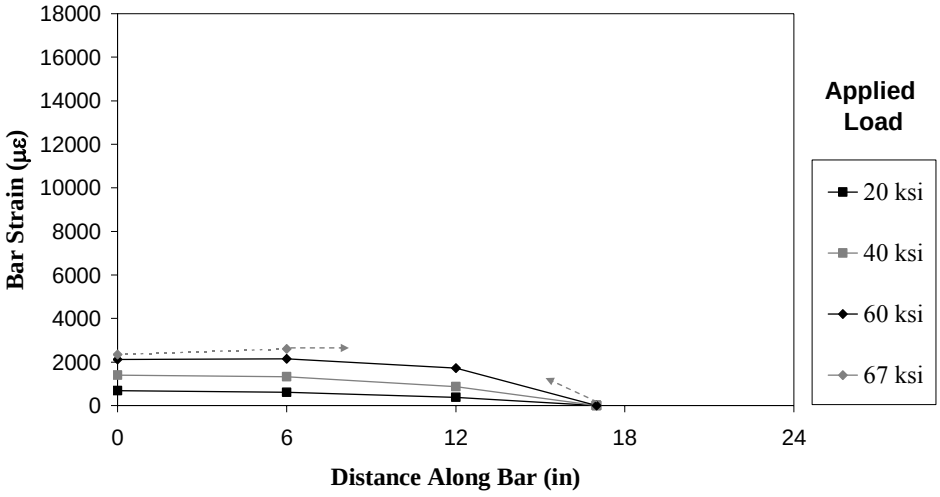

Figure C.5 Strain Distribution along Connector (Test 7)

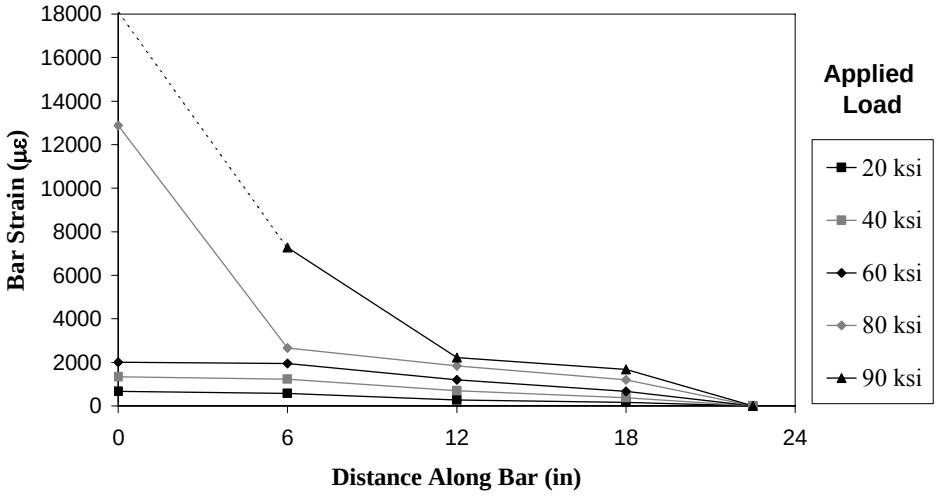

Figure C.6 Strain Distribution along Connector (Test 22)

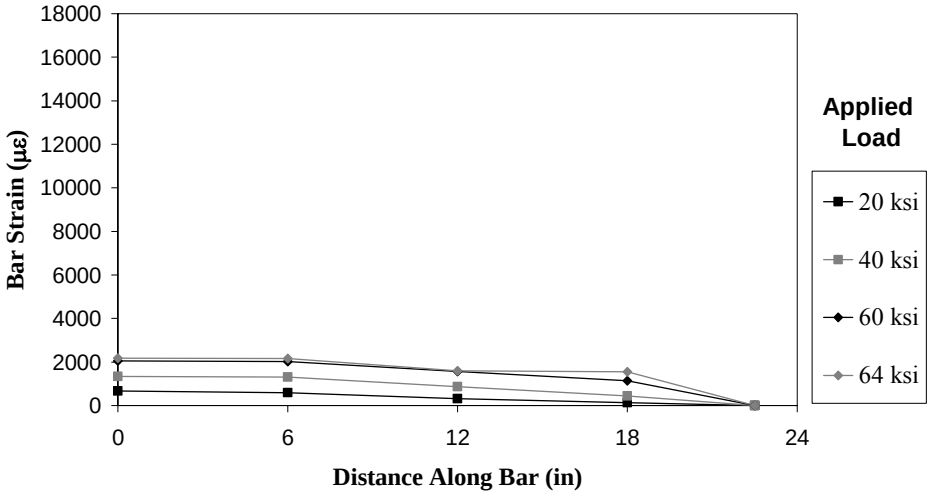

Figure C.7 Strain Distribution along Connector (Test 14, Left Bar)

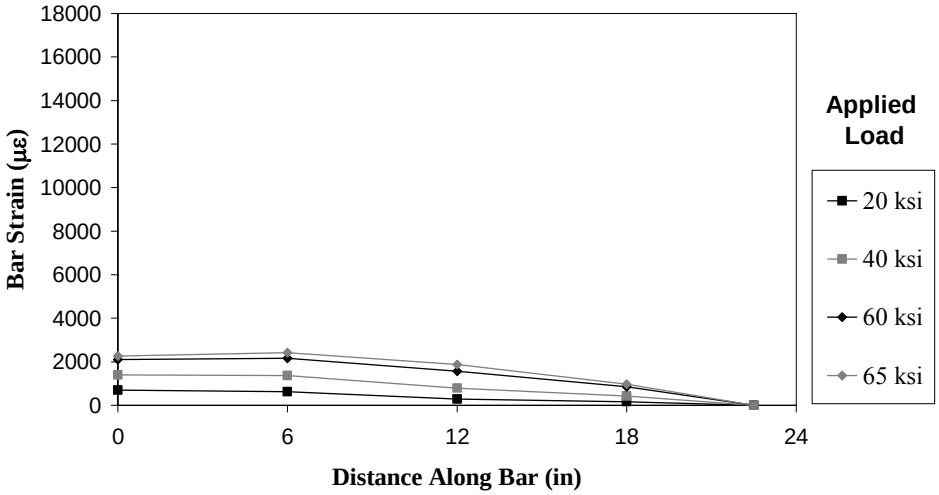

Figure C.8 Strain Distribution along Connector (Test 24, Left Bar)

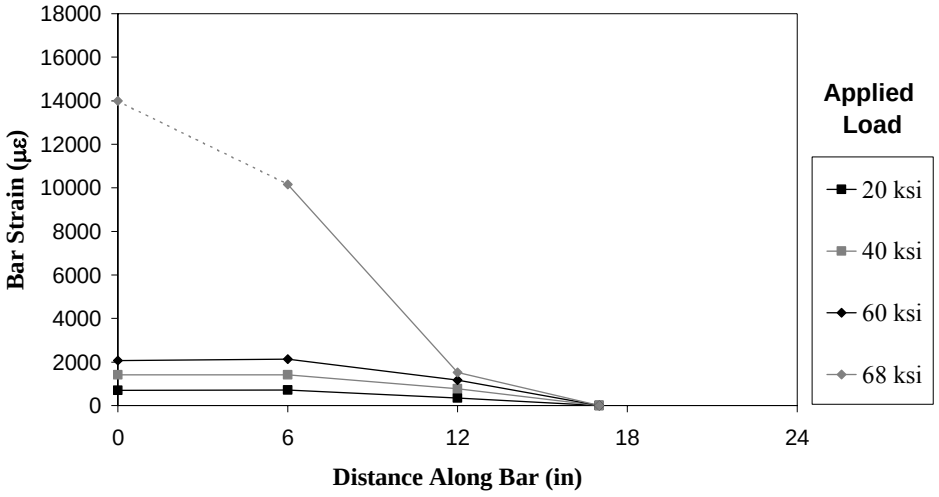

Figure C.9 Strain Distribution along Connector (Test 30)

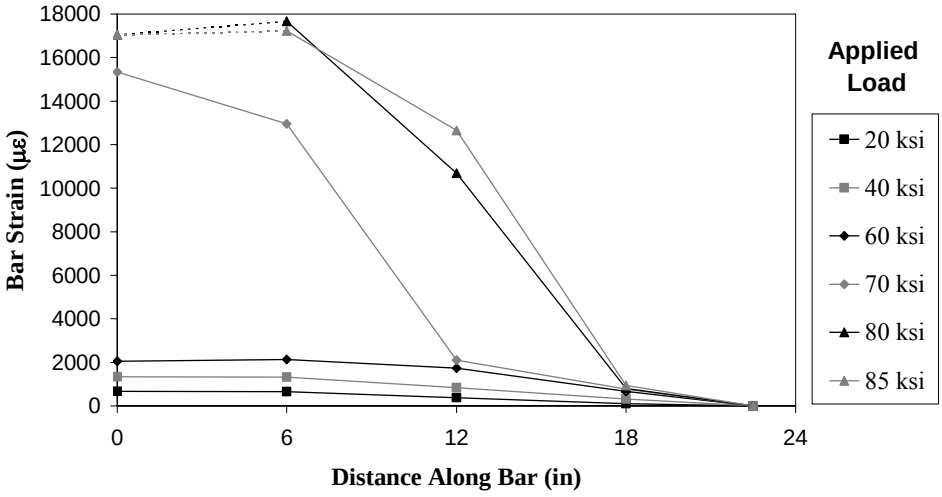

Figure C.10 Strain Distribution along Connector (Test 28, Right Bar)

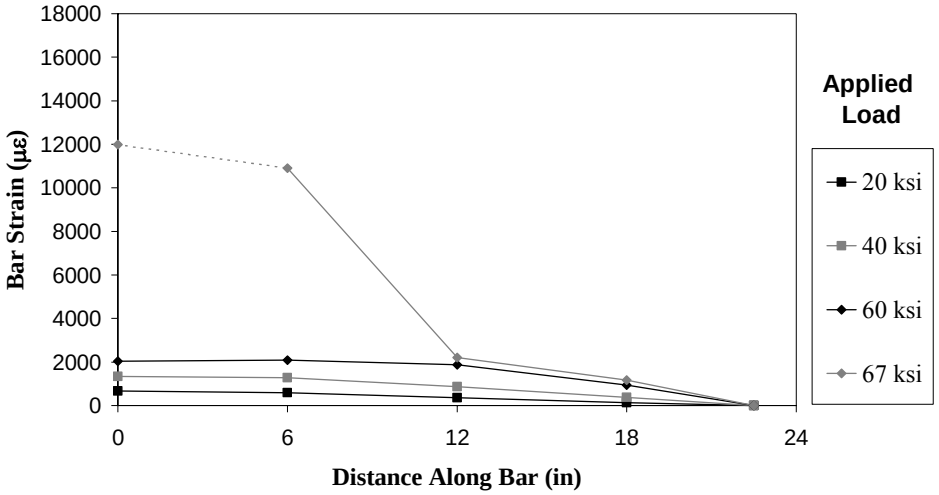

Figure C.11 Strain Distribution along Connector (Test 32, Right Bar)

C.2 CALCULATION OF STRESS IN CONNECTORS

Strains in the connectors were measured during tests using strain gages. In order to obtain values for stress, strains were converted to stresses using the model described in this section. The model consists of three different stress-strain relationships, which correspond to the three different types of reinforcing bars used as connectors:

- Epoxy-coated (f_y = 68 ksi)
- Uncoated Type I (f_y = 75 ksi)
- Uncoated Type II (f_y = 59 ksi)

The model is based on the work of Viwathanatepa et al. (1979) and is idealized in Figure C.12.

In the strain hardening region, (BC in Figure C.12), the stress in the steel is calculated using a cubic polynomial:

$$f_s = \left[E_{sh} r - 2\left(f_{s\,max} - f_y \right) \right] \left(\frac{s}{r} \right)^3 + 3 \left[\left(f_{s\,max} - f_y \right) - \frac{2}{3} E_{sh} r \right] \left(\frac{s}{r} \right)^2 + E_{sh} s + f_y \qquad \text{(C-1)}$$

where

$$r = \varepsilon_{s\,max} - \varepsilon_{sh} \qquad \text{(C-2)}$$

$$s = \varepsilon_s - \varepsilon_{sh} \qquad \text{(C-3)}$$

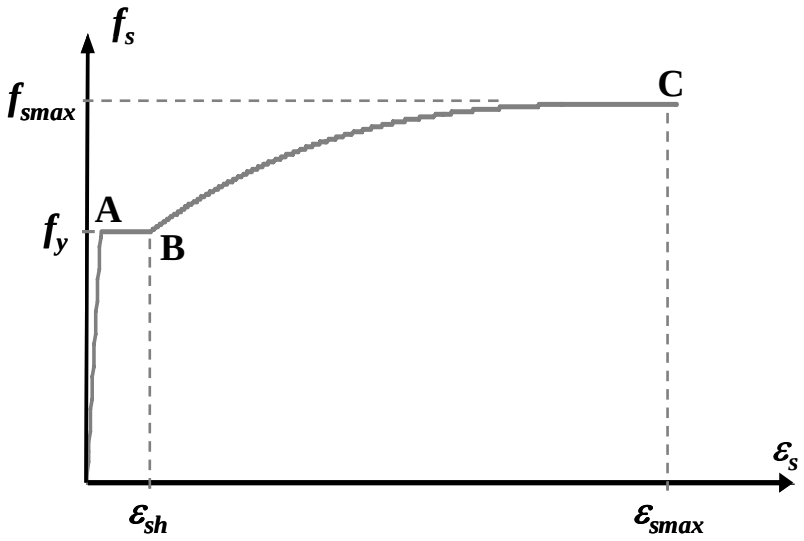

Figure C.12 Idealized Stress-Strain Model for Reinforcement

At the onset of strain hardening (point B in Figure C.12), $f(\varepsilon_{sh}) = f_y$. At the maximum stress (point C), $f(\varepsilon_{s\,max}) = f_{s\,max}$. E_{sh} is the tangent stiffness in the strain hardening region, ε_{sh} is the strain at the onset of strain hardening, f_y is the yield stress, and f_{smax} and ε_{smax} are the stress and strain at maximum stress.

Table C.1 Parameters for Stress-Strain Idealized Model

Parameter	#11 Epoxy Coated	#11 Uncoated Type I	#11 Uncoated Type II
E_{sh} (ksi)	1150	1200	1200
ε_{sh}	0.011	0.012	0.0105
f_y (ksi)	68	75	59
f_{smax} (ksi)	102	106	95
ε_{smax}	0.09	0.10	0.10

Table C.1 shows the values of E_{sh}, ε_{sh}, f_y, f_{smax}, and ε_{smax} for the three kinds of reinforcement used as connectors in the tests. The value of the elastic modulus, E, was taken as 29000 ksi.

The model was calibrated to tensile tests of actual connectors. Figure C.13, Figure C.14, and Figure C.15 show a comparison between the stress-strain curves obtained using the model and those obtained in connector tensile tests (gage length of 8 in.). As seen in Figure C.15, slight discrepancies between the measured stress-strain curve for a given connector and the idealized model used for converting strains to stresses can lead to some error. These discrepancies are relevant only at the strain-hardening region, and the margin of error is estimated to be plus or minus 5%.

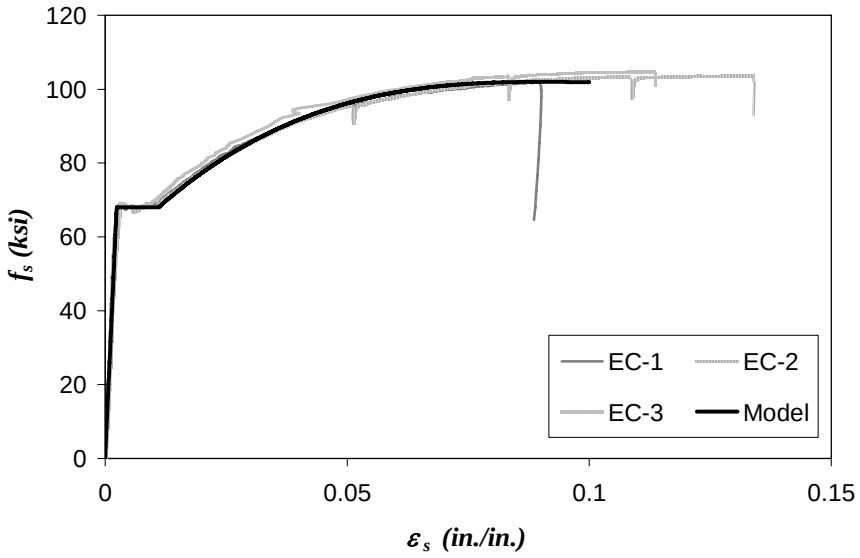

Figure C.13 Stress-Strain Curves for Epoxy-coated Connectors

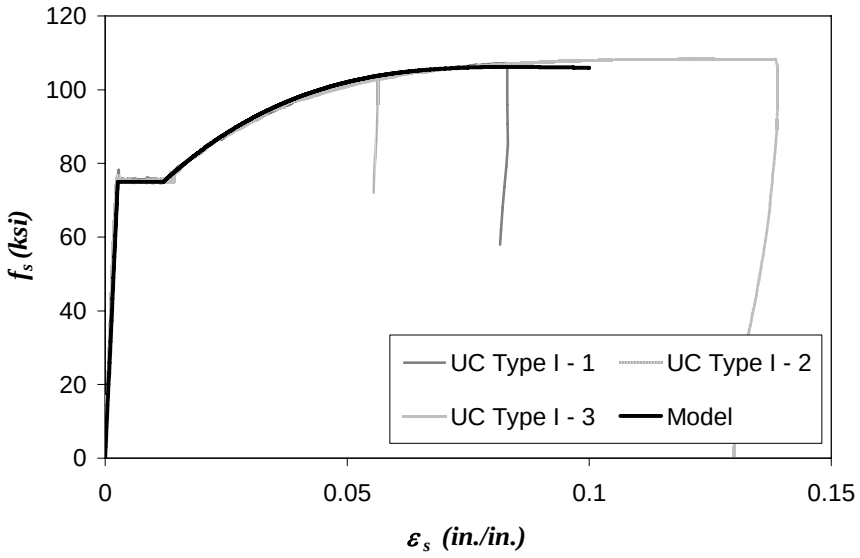

Figure C.14 Stress-Strain Curves for Uncoated Type I Connectors

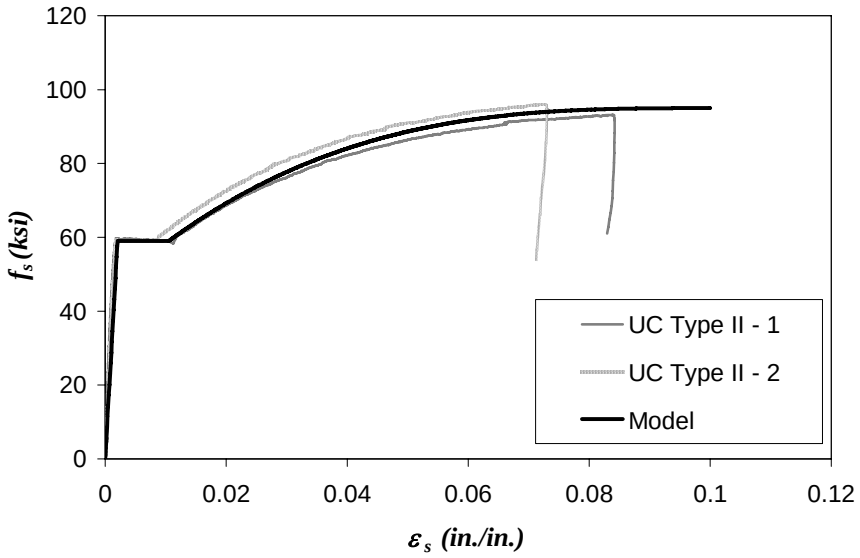

Figure C.15 Stress-Strain Curves for Uncoated Type II Connectors

C.3 DISTRIBUTION OF STRESS

The stress distribution diagrams for the same set of representative tests presented in Section C.1 are shown in this section. Stress distribution diagrams provide a means of illustrating the load distribution along the connectors, especially at stresses larger than the yield strength of the connectors. Whereas connector strain was measured directly during the tests using strain gages, to obtain the values for stress, the strain values needed to be converted to stresses using the model discussed in Section C.2. The model was calibrated to tensile tests of actual connectors. Still, slight discrepancies between the real stress-strain curve for a given connector and the model used for converting strain to stress can lead to some error. The range for errors is larger for converted stresses in the strain-hardening region.

The results show the stress at the different connector locations, for a series of applied stress levels. The stress values shown in the results at the lead end of each connector correspond to the strains recorded by the strain gages. Sometimes, the converted stress values differed slightly with respect to the applied stress. The discrepancies in the readings can be attributed to signal noise during the tests. Because the gage installations were not specially suited to withstand large deformations, several gage readings at strains above 10,000 με were not reliable. Consequently, the converted stress values are not reliable either, but are still shown and indicated by dashed lines. In a few occasions, gages in the embedded portion of the connectors were damaged during a test. Stress values are thus not available at those locations for subsequent levels of applied stress.

The stress distribution diagrams include an indication of the yield strength of the connector, represented by a horizontal dashed line. The figures also show the stress level at which radial concrete splitting started (first splitting) in the connection specimens.

C.3.1 Galvanized Steel Duct

The stress distribution along the length of connectors housed inside galvanized steel ducts is illustrated by a representative set of tests consisting of one and two connectors.

The stress distribution along the length of the connector of Test 3 is shown in Figure C.13. As the applied stress level increased from 20 to 60 ksi, the stress in the connector at a depth of 12 in. increased in relation to the applied stress from a ratio of 30 percent to 50 percent. The stress in the connector at a depth of 6 in. was approximately equal to the applied stress at all load stages. Since the stress at a depth of 12 in. was in all cases small compared to the stress near the lead portion of the connector, it is clear that the applied load was being resisted mostly by the portion of the connector closest to the surface. Considerable concrete splitting, which occurred at stresses higher than 66 ksi, did not cause a change in the stress distribution along the connector, as shown by the stress results for an applied stress of 80 ksi. At this load, the value of stress at the lead, obtained by conversion from the strain gage reading is 75 ksi, instead of the known stress level present of 80 ksi. As shown in Figure C.1, the strain reading corresponding to this data point had a value in excess of 10,000 με; this particular strain gage was damaged, and the strain value recorded is deemed unreliable. The data points are thus shown in both the strain and stress distribution diagrams with a dashed line. Failure of the connector occurred at an applied stress level of 87 ksi. At this stress level, the dashed line in Figure C.16 indicates that the stress values obtained at the lead and at 6 in. below the surface were not reliable. Moreover, there is no strain reading available at a depth of 12 in. below the surface, since the gage suffered damage, hence there is no converted stress value to show.

Figure C.17 shows the stress distribution diagram for Test 4. As the applied stress level increased from 20 to 60 ksi, the stress in the connector at a depth of 12 in. increased in relation to the applied stress from a ratio of 36 percent to 66 percent. Additionally, for applied stress levels of 40 and 60 ksi, the ratio of stress in the connector at a depth of 6 in. to the applied stress increased from 79 percent to 89 percent. The stress values obtained at the lead of the connector diverged with respect to the known applied stresses. It is possible that the source for this error was signal noise during the test. In comparison to the results for Test 3, the stress at a depth of 12 in. was not small compared to the stress near the lead portion of the connector. This meant that the applied load was being resisted more uniformly along the entire length of the connector. This difference in behavior between Tests 3 and 4 can be attributed to the detrimental effect of the epoxy-coating on friction resistance. Concrete splitting, which occurred at stresses higher than 60 ksi, did not cause a change in the stress distribution along the connector, as shown by the stress

results for an applied stress of 70 ksi. At an applied stress of 80 ksi, an erroneous stress value of 68 ksi was obtained at the lead; the strain reading from which it was determined was deemed unreliable. No reliable stress distribution information was available for an applied stress of 88 ksi.

The stress distribution along the length of one of the connectors tested in Test 13 is presented in Figure C.18. At stresses smaller than 40 ksi, most of the applied load was being resisted by the top portion of the connector. This last statement can be verified by the low connector stresses observed at a depth of 18 in. below the surface. As loading increased from 40 to 60 ksi, the stress in the connector at a depth of 18 in. increased from 16 percent to 43 percent of the applied stress. At 60 ksi, the stress in the connector at a depth of 6 in. was approximately equal to the applied stress. The first concrete splitting cracks developed at a stress level of 38 ksi. However, a widespread pattern of radial cracking developed until a load of 86 kip (57 ksi). Extensive cracking in the concrete caused the load to be redistributed down the connector. The pattern of stress distribution corresponding to an applied stress of 80 ksi was similar to that at 60 ksi; the ratio of the stress in the connector at a depth of 18 in. to the applied stress increased to 54 percent. At failure (87 ksi), the converted value of stress at the lead end of the connector was not reliable.

Figure C.19 shows the stress distribution diagram for one of the connectors tested in Test 17. As the load was increased from a stress level of 20 to 40 ksi, the ratio of the stress in the connector at a depth of 12 in. to the applied stress increased significantly. This ratio was 22 percent at 20 ksi, and 42 percent at 40 ksi. Although radial cracks in the concrete emerged at a stress level of 33 ksi, significant cracking did not occur until the stress increased to 45 ksi. After severe cracking, the load redistributed along the connector length, and a larger portion of the load was anchored deep at the end portion of the connector. The ratio of stress in the connector at a depth of 12 in. to the applied stress increased to 79 percent by the time the connection failed at 59 ksi.

C.3.2 Polyethylene Duct

The stress distribution along the length of connectors placed inside polyethylene ducts is illustrated by a representative set of tests consisting of one and two connectors.

The stress distribution along the length of the connector of Test 7 is shown in Figure C.20. The data show that even at the low stress level of 20 ksi, a large share of the load was being resisted deep down in the connector. As the applied stress level increased from 20 to 60 ksi, the stress in the connector at a depth of 12 in. increased in relation to the applied stress from a ratio of 55 percent to a ratio of 82 percent. No reliable stress data were available at the failure stress of 67 ksi.

Figure C.21 shows the stress distribution diagram for Test 22. The entire length of the connector was reacting to the applied load even at low stress levels. At a stress level of 20 ksi, a stress equal to 40

percent of the applied stress was measured at 12 in. below the surface. Six in. deeper, the stress in the connector was 23 percent of the applied stress. Following the initial splitting cracks that formed at 45 ksi, the expansion of radial splitting cracks in the concrete between applied stresses of 60 and 80 ksi triggered a progressive redistribution of the load down the connector. The results at 80 ksi show that the connector was undergoing yielding as deep as 6 in. below the surface. At failure, the ratios of connector stress to applied stress were 71 percent for the 12 in. depth, and 53 percent for the 18 in. depth. The erroneous stress value at the lead was obtained from an unreliable strain reading. Throughout the test, the stress values obtained at the lead of the connector diverged with respect to the known applied stresses. As in Test 4, it is suspected that the source for this error was signal noise.

The stress distribution diagram of the left connector of Test 14 is shown in Figure C.22. As the connector of Test 22, the entire length of the connector responded to the applied load even at low stress levels. At a stress level of 40 ksi, the stress in the connector 12 in. below the surface was 62 percent of the applied stress. Six inches below, the ratio of stress in the connector to applied stress was 31 percent. The development of radial splitting cracks in the concrete changed the pattern of stress distribution in the connector. A larger proportion of the load was now being resisted deeper down the connector. At 60 ksi and at a depth of 12 in., the connector stress to applied stress ratio was 76 percent; at 18 in., the ratio was 54 percent. As the connection reached its capacity, the stress in the connector 18 in. below the specimen's surface was 70 percent of the applied stress of 64 ksi.

The stress distribution diagram for the left connector of Test 24 is shown in Figure C.23. The diagram includes the data up to the connection failure load, and does not include the data obtained upon reloading of the connector. The entire length of the connector reacted to the applied load even at low stress levels. At a stress level of 40 ksi, the stress in the connector 12 in. below the surface was 56 percent of the applied stress. Six inches below, the ratio of stress in the connector to applied stress was 31 percent. The development of radial splitting cracks in the concrete changed the pattern of stress distribution in the connector. The share of the load that was being resisted deep down the connector increased. At 60 ksi and at a depth of 12 in., the connector stress to applied stress ratio increased to 75 percent; at 18 in., the ratio increased to 41 percent. As the connection reached its capacity, the stress in the connector 12 in. below the surface was 83 percent of the applied stress; while the stress at the 18 in. depth had only increased to 43 percent of the applied stress.

C.3.3 Polypropylene Duct

The stress distribution along the length of connectors housed inside polypropylene ducts is illustrated by a representative set of tests consisting of one, two, and three connectors.

The stress distribution along the length of the connector of Test 30 is shown in Figure C.24. For stress levels between 20 and 60 ksi, the stress in the connector at a depth of 6 in. was equivalent to the applied stress. The percentage of the load that was being transferred down the connector, based on observed stress values at a depth of 12 in., varied from 51 percent at 20 ksi to 64 percent at failure. At the failure stress of 68 ksi, the incorrect stress obtained at the connector lead indicated that the strain gage reading at that location was not reliable.

The stress distribution for one of the connectors of Test 28 is shown in Figure C.25. Radial splitting in the concrete started to occur at a load of 66 kip (44 ksi). The stress in the connector 12 in. below the surface increased substantially between applied stresses of 40 and 60 ksi. The ratio of stress in the connector to the applied stress rose from 60 percent to 83 percent. At a depth of 18 in., the ratio only rose from 23 to 32 percent. The change in the pattern of strain distribution indicates that due to extensive splitting in the concrete, the load along the connector was redistributed down into the connector. The data for an applied stress of 70 ksi show that yielding was occurring in the connector at depths greater than 6 in. below the surface. At an applied stress of 85 ksi, the stress in the connector at a depth of 12 in. indicates that yielding had progressed down the length of the connector further. The stresses at the lead associated with the ultimate load stages, shown in the diagram with dashed lines, were obtained from unreliable strain gage readings.

Figure C.26 shows the stress distribution diagram for one of the three connectors of Test 32. Although splitting in the concrete began at a low connector stress of 20 ksi, a general widespread pattern of splitting did not develop until the load reached 46 ksi (70 kip). After 46 ksi, the splitting cracks continued to grow, and at 50 ksi, V-shaped cracks also developed on the specimen's side that was loaded more heavily. The effect on the connector of extensive cracking in the concrete between the applied stresses of 40 and 60 ksi can be seen in the stress distribution diagram. The ratio of stress in the connector at a depth of 12 in. to applied stress increased from 62 to 90 percent. At 18 in., the ratio increased from 27 to 45 percent. At failure, the stress obtained at a depth of 12 in., indicates that yielding was progressing even to this depth.

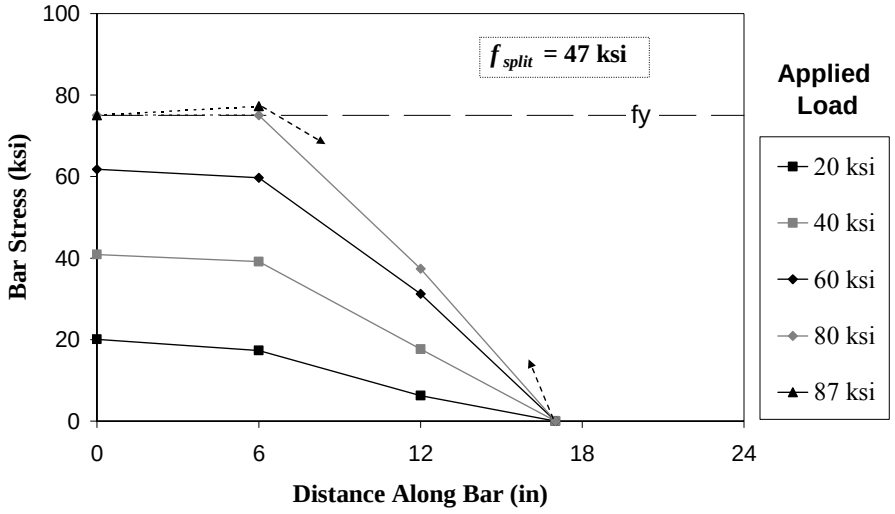

Figure C.16 Stress Distribution along Connector (Test 3)

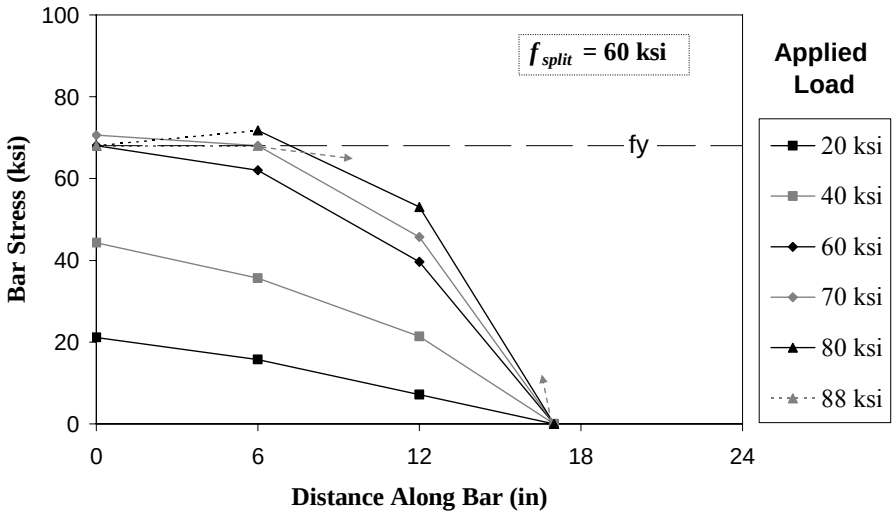

Figure C.17 Stress Distribution along Connector (Test 4)

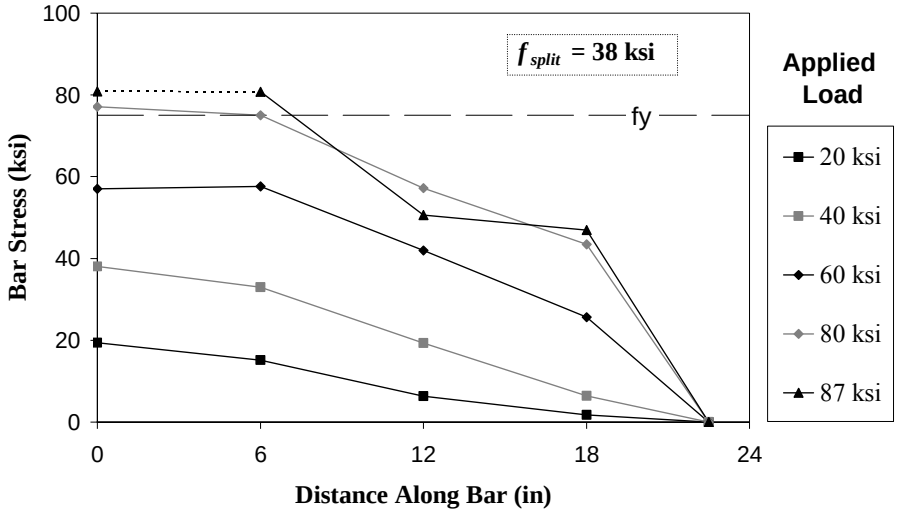

Figure C.18 Stress Distribution along Connector (Test 13, Left Bar)

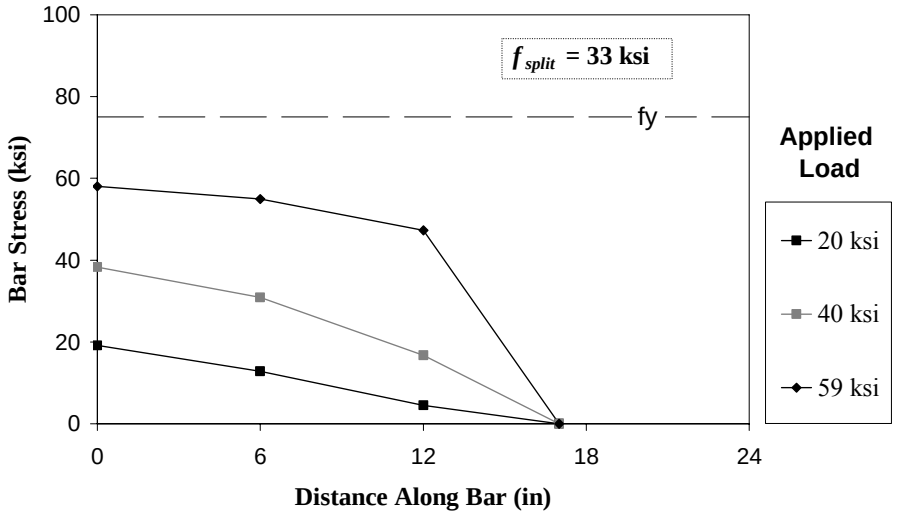

Figure C.19 Stress Distribution along Connector (Test 17, Left Bar)

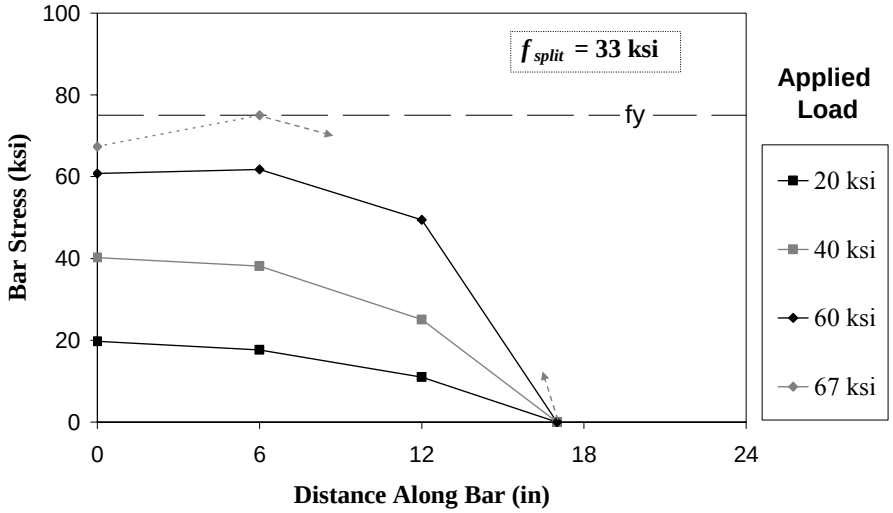

Figure C.20 Stress Distribution along Connector (Test 7)

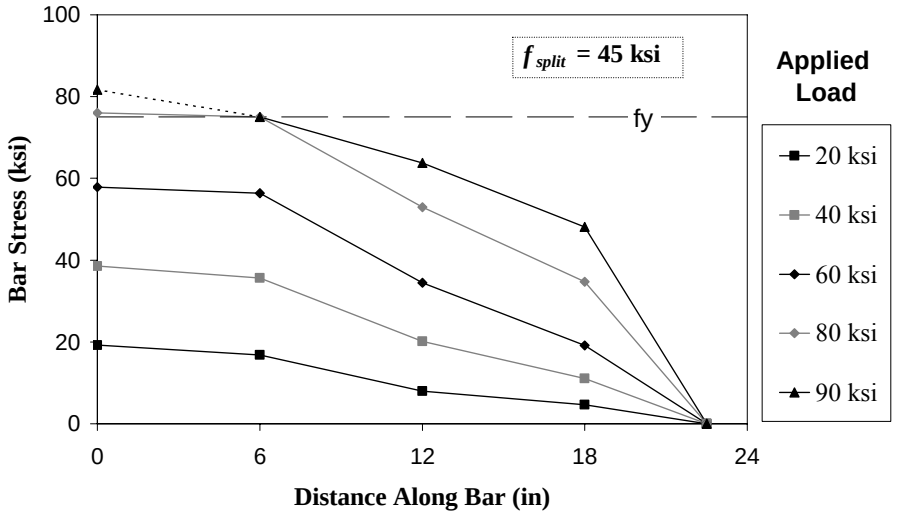

Figure C.21 Stress Distribution along Connector (Test 22)

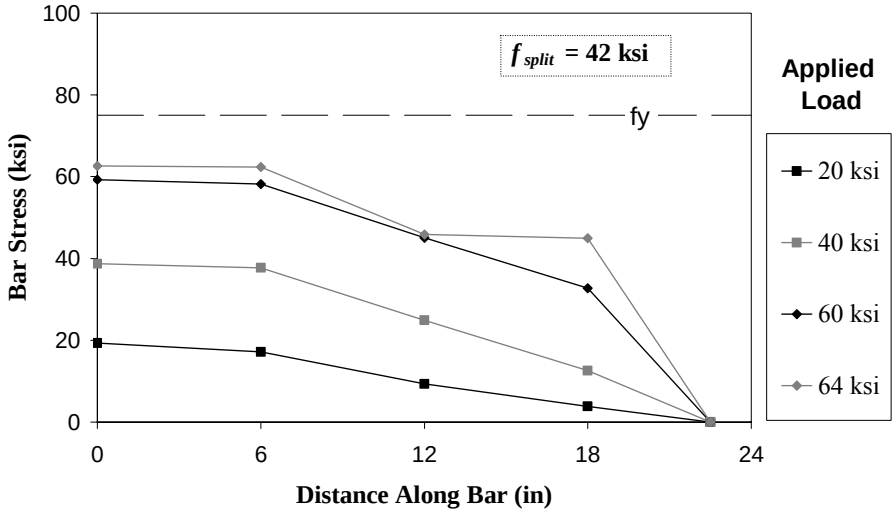

Figure C.22 Stress Distribution along Connector (Test 14, Left Bar)

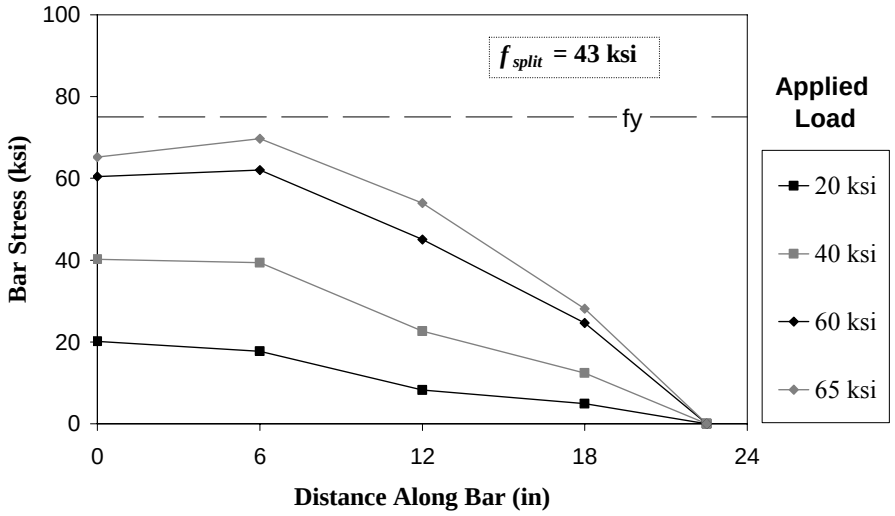

Figure C.23 Stress Distribution along Connector (Test 24, Left Bar)

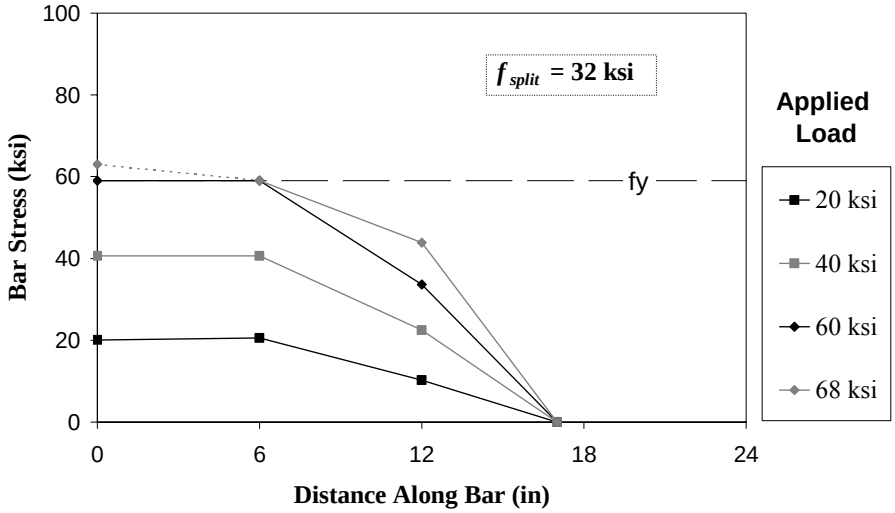

Figure C.24 Stress Distribution along Connector (Test 30)

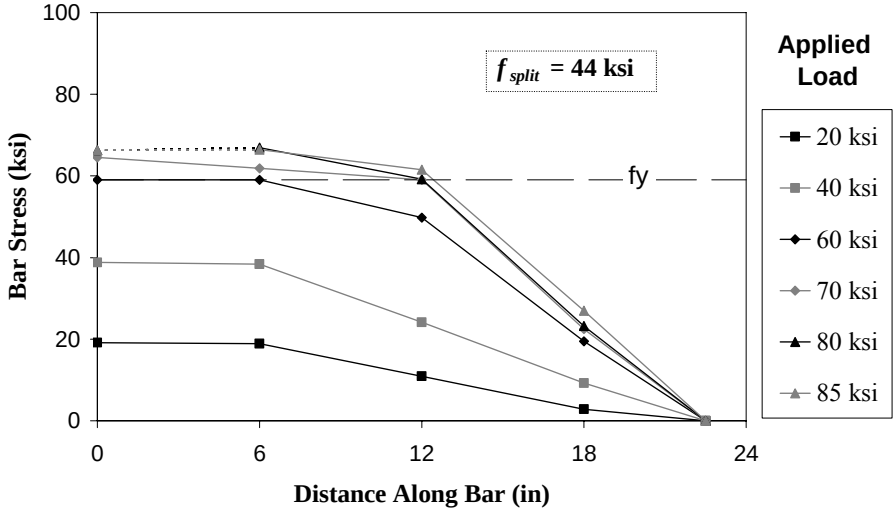

Figure C.25 Stress Distribution along Connector (Test 28, Right Bar)

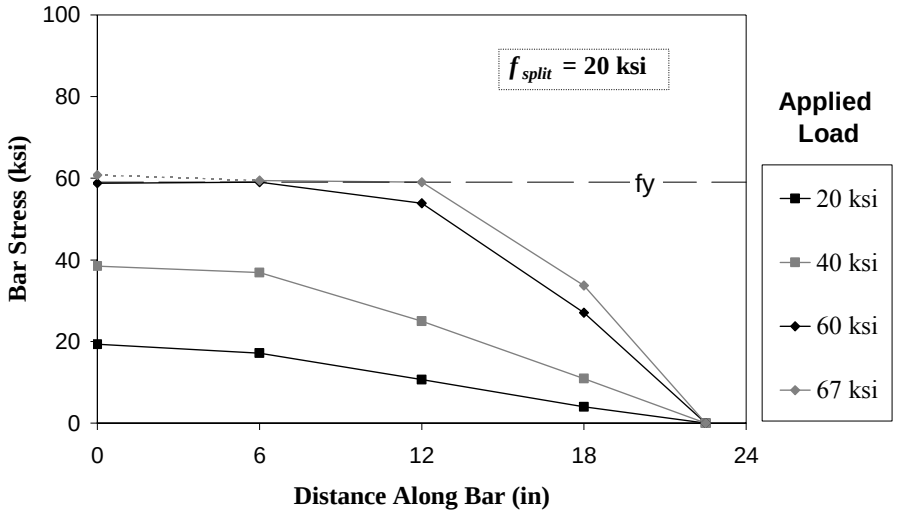

Figure C.26 Stress Distribution along Connector (Test 32,Right Bar)

C.4 SLIP OF CONNECTOR RELATIVE TO GROUT

As mentioned in Chapter 5, the relative displacement between the grout and the concrete specimen was monitored during the tests using a linear potentiometer. The grout displacement data were useful in acquiring information about the slip of the connectors and about the anchorage of the grout inside the ducts.

The data collected by the grout instrumentation were reliable until extensive cracking occurred in the connection specimens during the tests. The spreading and widening of radial cracks emanating from the ducts together with the development of cracks on the sides of the specimens led to the formation of concrete breakouts. The breakouts involved a large area of the top surface of the specimens, and often disturbed the concrete zone beneath the epoxy-glued metal stands that supported the grout instrumentation. The accuracy of the grout displacement data was lost after cracking occurred underneath the instrumentation stands. Cracking caused an upward shift of the instrumentation, and the loss of the top concrete surface of the specimen as a reference point to measure grout displacement. The grout displacement data that are presented in the results exclude those portions of data that were considered unreliable due to extensive cracking in the specimen. Typically, grout displacement data were not available after connection failure.

Figure 6.24 showed the relationship between the grout displacement, δ_g, and the connector end displacement, δ_e. Three main scenarios of behavior were described in the figure: (1) δ_e equals δ_g, which suggests that the entire connector and the grout are pulling outward together as a unit (plug), (2) δ_e is

smaller than δ_g, suggesting that the top portion of the grout is moving upward together with the lead end of the connector, while the end portion of the connector is moving upward a smaller amount, and (3) δ_e is greater than δ_g, implying that the connector, as a whole, is slipping out of the grout. The slip of the connector relative to the grout was calculated as the difference between δ_e and δ_g.

Whereas the connector end displacements provide general information about the overall slip of the connectors inside the grout-duct-concrete system, the stress-slip relative to grout diagrams provide more detailed information about the interaction between the connector and the grout.

A series of stress-slip relative to grout diagrams are presented in this section to illustrate the connector displacement relative to the grout for a representative set of tests. The results are presented again in three groups, determined by the type of duct material.

C.4.1 Galvanized Steel Duct

The stress-slip relative to grout behavior of connectors placed inside galvanized steel ducts is illustrated by a set of representative tests consisting of one and two connectors.

For each of the representative tests, two curves are shown: (1) stress-end slip curve and (2) stress-slip relative to grout curve. The curve that displays the connector end slip is analogous to the curve displaying the slip of the connector relative to the grout. The first curve shows the displacement of the connector relative to the concrete specimen, while the second one shows the displacement of the connector relative to the grout. This, and ensuing, sections concentrate on examining the slip of the connector with respect to the grout.

It is possible to determine the relationship between the connector and the grout by examining the stress-slip relative to grout diagrams. If the direction of the curve is to the right, this means that the connector is slipping out of the grout. If the direction of the curve is to the left, this suggests that a portion of the grout near the lead of the connector has separated and is moving upward at a faster rate that the end of the connector. Then, if the direction of the curve is such that there is no increase or decrease of slip with a corresponding change in applied stress, this indicates that the connector and the grout are displacing upward together as a unit.

Figure C.27 shows the stress-slip relative to grout diagram for Test 3. In general, the data reveal that the connector and the grout were displacing upward together up to an applied stress of around 66 ksi. This stress level coincided with the occurrence of splitting cracks in the concrete. The effect of proliferating splitting cracks in the concrete can be seen in the diagram as the connector's slip increased relative to the grout. At a stress level of 75 ksi, the connector experienced yielding. The formation of V-shaped cracks also occurred at a stress of 75 ksi, which caused additional slip of the connector relative to the grout. The data associated with applied stresses between 76 and 83 ksi show that the value of slip

between the connector and the grout underwent a series of cycles, where the connector and the grout moved upward at different rates. The first cycle, where the relative slip between the connector and the grout decreased, can be attributed to yielding occurring in the connector at the lead and at a shallow depth beneath the surface. The connector elongation can subject the grout located near the surface to large strains, leading to a series of cracks that would allow the top surface of the grout to rise. Nonetheless, the overall slip between the connector and the grout at a stress of 83 ksi was almost equal to the observed value at 76 ksi. At a stress of 83 ksi, a horizontal crack began to form on the side of the specimen at a depth corresponding to the location of the beam's top longitudinal reinforcement. The formation of this horizontal crack, and its subsequent growth observed at 86 ksi led to additional slip of the connector relative to the grout.

Figure C.28 shows the stress-slip relative to grout diagram for the epoxy-coated connector of Test 4. In general, the data show that the connector and the grout were moving upward together up to an applied stress of around 77 ksi. However, the data show that at stress levels between 30 and 58 ksi, the connector did slip temporarily relative to the grout. Splitting cracks in the concrete emerged at an applied stress of 60 ksi. The data show that the connector was slipping relative to the grout when it began experiencing yielding at 68 ksi. Soon after yielding, the slip of the connector relative to the grout decreased, and at 75 ksi, both the connector and the grout were displacing upward together again at the same rate. At a stress of 77 ksi, V-shaped cracks formed on the side of the specimen; the connector slip relative to the grout then increased. At larger stresses of 85 and 88 ksi, the V-shaped cracking pattern intensified and the connector continued to slip relative to the grout. At a stress of 89 ksi, the connector failed by pullout and a concrete breakout formed at the specimen's surface. Grout displacement data were not available after failure.

The stress-slip relative to grout diagram for the left connector of Test 13 is shown in Figure C.29. The connector and the grout were moving upward together until the applied stress was around 63 ksi. At this point during the test, the concrete underneath the grout instrumentation was affected significantly by radial splitting cracks. The data after this point were thus considered unreliable and are not shown. In spite of this, data for the other connector of Test 13 were available, and since the behavior of both connectors was very similar, it is possible to deduce that the grout displacement data for both connectors were similar. The data collected for the other connector show that at a stress of 63 ksi, the connector slipped with respect to the grout. V-shaped cracks formations were observed on the loaded side of the specimen at this stress level. The connector continued to slip relative to the grout until the yield strength of the connector was reached. Then both the connector and the grout slipped together at the same rate up to failure.

Figure C.30 shows the stress-slip relative to grout diagram for the left connector of Test 17. The data show that the connector and the grout were moving upward together until the applied stress was around 33 ksi. At this stress level, splitting cracks in the concrete were detected. Immediately after concrete splitting, the grout displaced upward an amount larger than the displacement measured at the connector end. Then both the connector and the grout continued to move upward together, at the same rate, until a widespread radial crack pattern developed around each connector at a stress of 45 ksi. At this stress level, the connector slipped relative to the grout. Later, at a stress of 48 ksi, V-shaped cracks formed on the side of the specimen, and the slip of the connector relative to the grout increased. At a stress of 57 ksi, a horizontal crack formed on the side of the specimen at a depth corresponding to the location of the beam's top longitudinal reinforcement. The slip of the connector relative to the grout kept increasing until failure of the connection.

C.4.2 Polyethylene Duct

The stress-slip relative to grout behavior of connectors placed inside polyethylene ducts is illustrated by a set of representative tests consisting of one and two connectors.

Figure C.31 shows the stress-slip relative to grout diagram for Test 7. The diagram shows that the connector slipped temporarily a small amount relative to the grout between applied stresses of 8 and 33 ksi. The first splitting crack in the concrete was detected at a stress of 33 ksi. As splitting cracks continued to emerge around the connector, the connector and the grout displaced together until a stress of 53 ksi was reached. Then, the connector slipped relative to the grout as the stress approached 57 ksi. At this stress, a widespread pattern of splitting cracks developed. The connector and the grout now moved upward together as a unit until the applied stress was 63 ksi and a horizontal crack formed on the side of the specimen at a depth corresponding to the location of the beam's top reinforcement. Following the formation of the crack, the slip of the connector relative to the grout increased until failure was reached.

The stress-slip relative to grout diagram for Test 22 is displayed in Figure C.32. After an initial slip of the connector relative to the grout at low stress levels, the displacement of the grout increased in relation to the connector end displacement. At a stress of 45 ksi, when the first splitting cracks were detected in the concrete, the data show a sudden increase in displacement for the grout. For stresses between 45 and 62 ksi, the connector and the grout were displacing upward at the same rate. Then, when additional splitting cracks emerged at 63 ksi, another sudden increase in displacement was observed in the grout. For stresses between 63 ksi and 77 ksi, the connector and the grout moved upward together again as a unit. The bar experienced yielding at a stress of 76 ksi; this coincided with the development of a widespread pattern of radial splitting around the connector. At this stress, the connector slipped a small amount relative to the grout, but a subsequent increase in grout displacement followed. The increase in

grout displacement can be attributed to the effect of yielding in a portion of the connector below the surface. When the stress reached 81 ksi, a horizontal crack formed on the side of the specimen at a depth corresponding to the location of the beam's top reinforcement. Further loading extended the length of the horizontal crack; the slip of the connector relative to the grout increased until failure was reached.

Figure C.33 shows the stress-slip relative to grout diagram for the left connector of Test 14. In general, the data show that the connector and the grout were moving upward together until the applied stress was around 25 ksi. As loading progressed, the data show a series of sudden changes in grout displacement. At stresses between 33 and 50 ksi, the value of connector slip relative to the grout is negative, indicating that the top surface of the grout has displaced a larger distance than the connector end. At a stress of 51 ksi, the first V-shaped cracks formed on the side of the specimen, and the connector slipped relative to the grout. As more V-shaped cracks developed, at 55 and 58 ksi, the slip of the connector relative to the grout increased.

The stress-slip relative to grout diagram for the left connector of Test 24 is shown in Figure C.34. By and large, the connector and the grout were displacing at the same rate until the formation of V-shaped cracks on the loaded side of the specimen at a stress of 61 ksi. The connector slip with respect to the grout increased at this point. When another crack appeared on the side of the specimen at a stress of 64 ksi; the connector slip with respect to the grout increased even further. Shortly after this, the connection failed, but only the connector on the right pulled-out. The connector on the left was reloaded, but grout displacement data is not available for the latter portion of the test.

C.4.3 Polypropylene Duct

The stress-slip relative to grout behavior of connectors housed inside polypropylene ducts is illustrated by a set of representative tests consisting of one, two, and three connectors.

Figure C.35 shows the stress-slip relative to grout diagram for Test 30. The diagram shows that after a sudden initial slip of the connector at a very low stress of 5 ksi, the connector and the grout displaced upward together as a unit. This was the case until the applied stress reached the yield strength of the connector. At this point, the data show that the top surface of the grout began to move upward, while the end of the connector continued to move but at a smaller rate. No grout displacement data were available for stresses above 66 ksi.

The stress-slip relative to grout diagram for the right connector of Test 28 is shown in Figure C.36. At first loading, the connector showed signs of slip relative to the grout. However, after a stress of 18 ksi, the general trend observed was that of the grout surface displacing upward relative to the end of the connector. This can be seen in the diagram, as the relative displacement of the connector end relative to the grout decreased and went from positive values to negative values. When the stress reached 53 ksi, a

widespread pattern of radial splitting developed, and the connector and the grout now moved upward together as a unit. At a stress of 59 ksi, the connector experienced yielding. Shortly after, the connector slip relative to the grout increased; this was followed by an equal decrease in connector slip relative to the grout. V-shaped cracks formed on the side of the specimen when the stress reached 63 ksi. At this point, the grout surface continued to displace upward relative to the connector end, but at a decreasing rate as more V-shaped cracks formed on the side of the specimen at stresses of 67 and 74 ksi. At 79 ksi, V-shaped cracks formed on the unloaded side of the specimen, and failure of the connection was imminent; the relative displacement of the connector end relative to the grout increased until the connection failed.

Figure C.37 shows the stress-slip relative to grout for the right connector of Test 32. The data show that the connector and the grout displaced together until the first splitting cracks emerged in the concrete at 20 ksi. Then, the grout temporarily displaced a small amount relative to the connector end. However, at a stress of 29 ksi, the connector and the grout were again moving upward at the same rate. When the stress reached 45 ksi, a widespread pattern of radial splitting developed around the connectors. The connector slipped relative to the grout a small amount. At a stress of 50 ksi, V-shaped cracks formed on the more heavily loaded side of the specimen, and a drop in connection resistance was recorded; a corresponding increase in connector slip relative to the grout was also recorded. Loading of the connection continued, and additional V-shaped crack formations emerged on both sides of the specimen at stresses of 53 and 57 ksi. The rate of connector slip relative to the grout increased. At a stress of 59, the connector underwent yielding. Immediately after, the connector displacement relative to the grout increased, but a decrease was also observed shortly after. As has been mentioned before, this increase in grout displacement can be attributed to yield elongation occurring in the connector a short distance beneath the surface of the grout. When the stress reached 63 ksi, one of the connectors (third bar) showed signs of failure after a shallow horizontal crack developed on the less heavily loaded side of the specimen. At failure, some additional slip of the connector relative to the grout was observed.

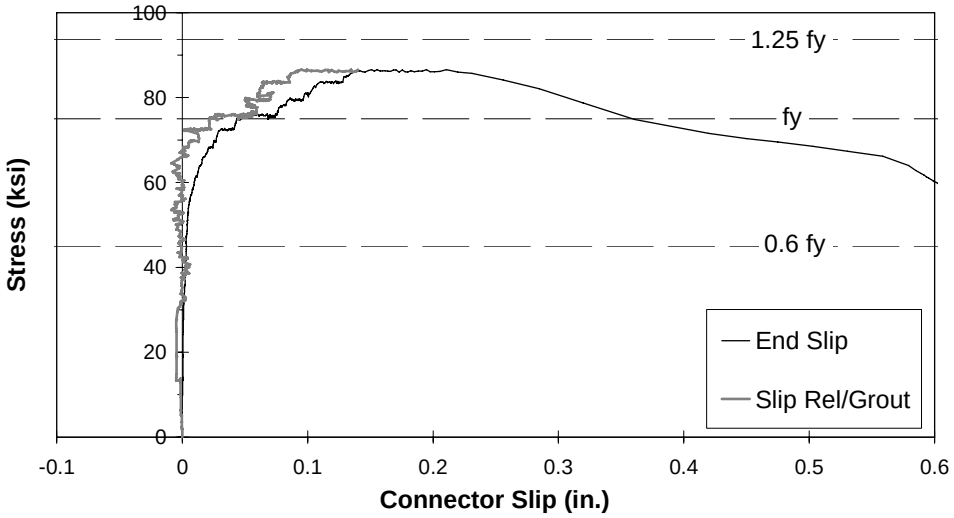

Figure C.27 Connector Slip Relative to Grout (Test 3)

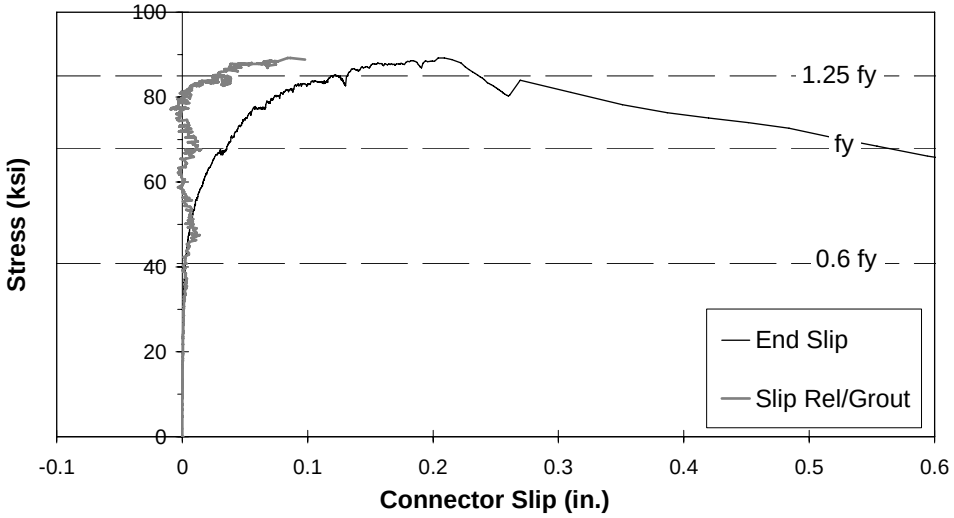

Figure C.28 Connector Slip Relative to Grout (Test 4)

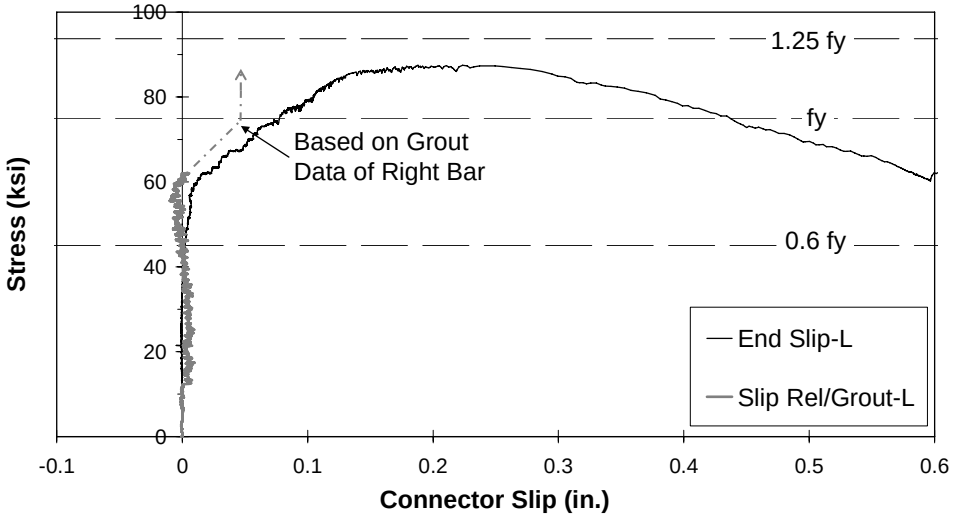

Figure C.29 Connector Slip Relative to Grout (Test 13, Left Connector)

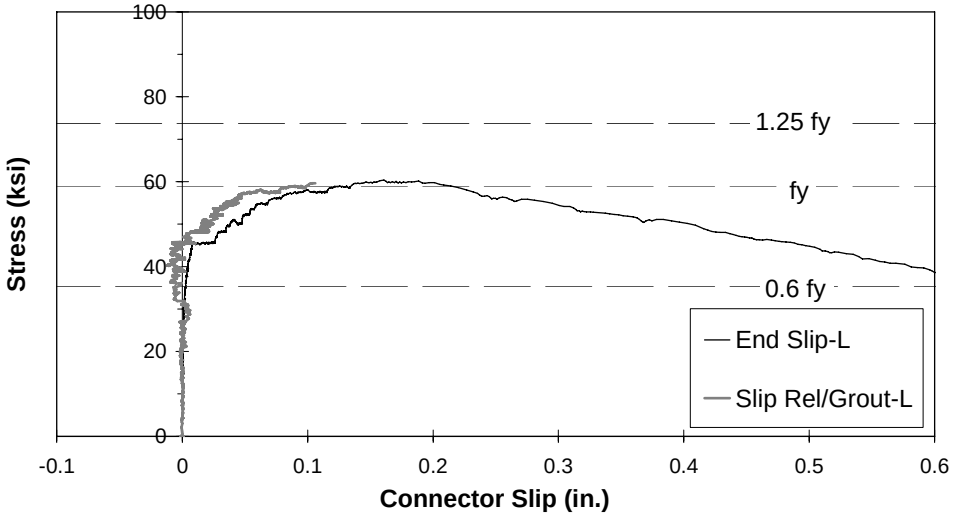

Figure C.30 Connector Slip Relative to Grout (Test 17, Left Connector)

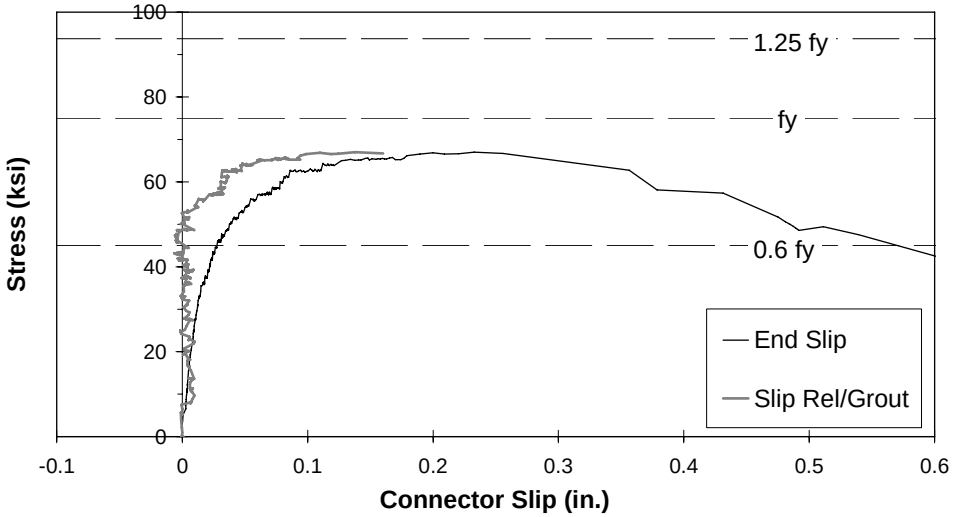

Figure C.31 Connector Slip Relative to Grout (Test 7)

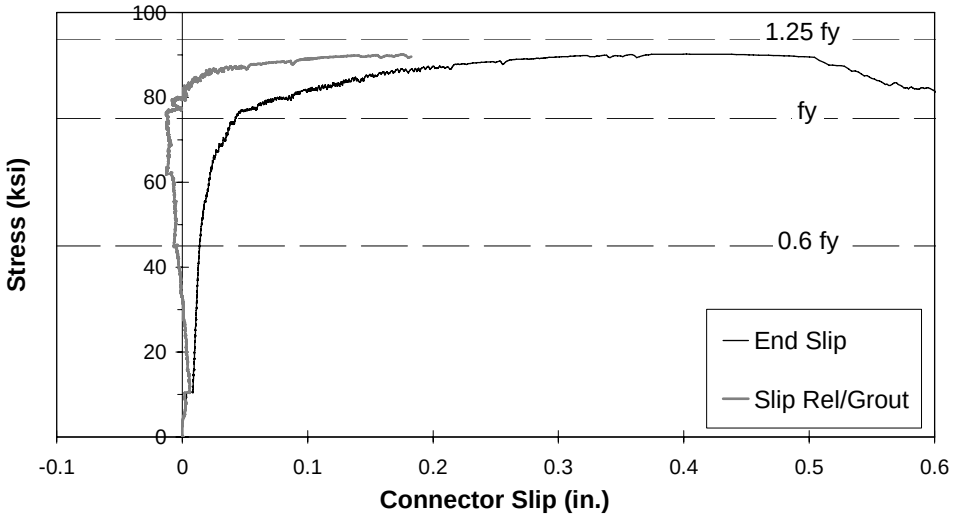

Figure C.32 Connector Slip Relative to Grout (Test 22)

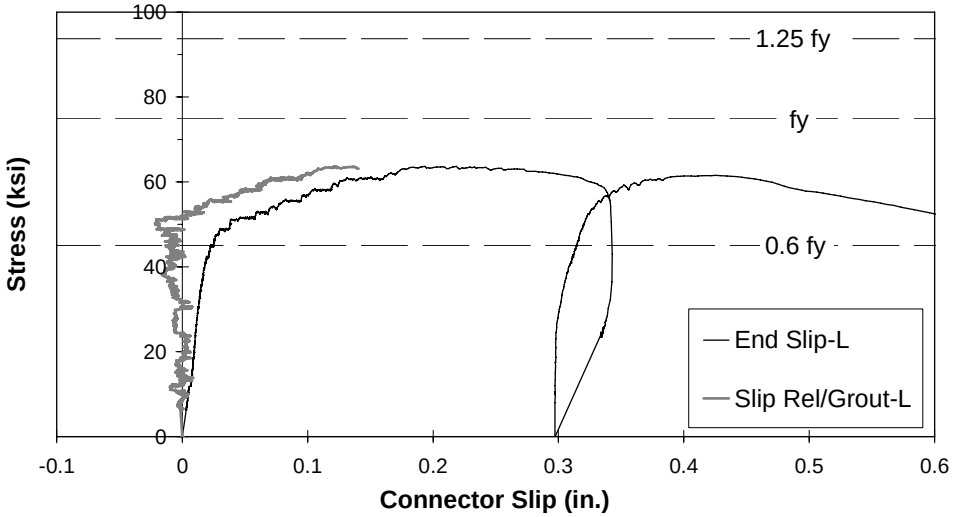

Figure C.33 Connector Slip Relative to Grout (Test 14, Left Connector)

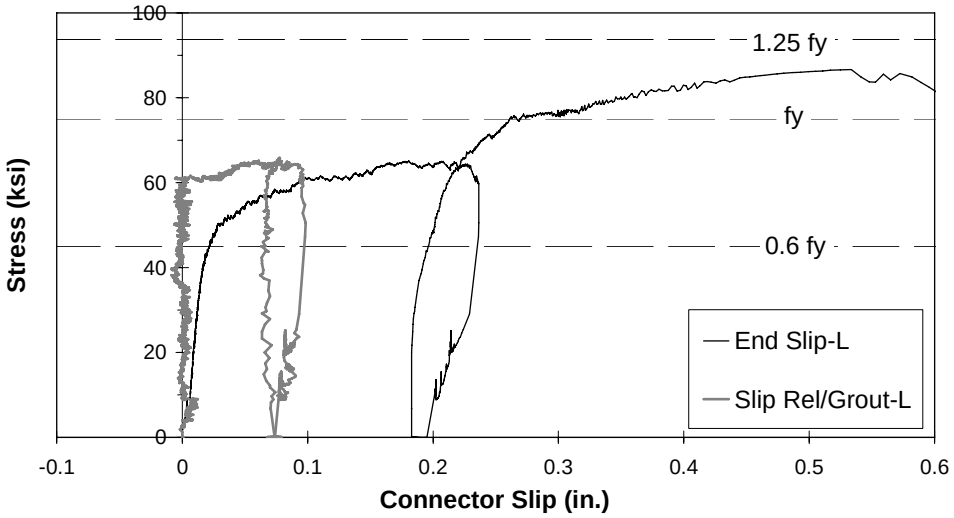

Figure C.34 Connector Slip Relative to Grout (Test 24, Left Connector)

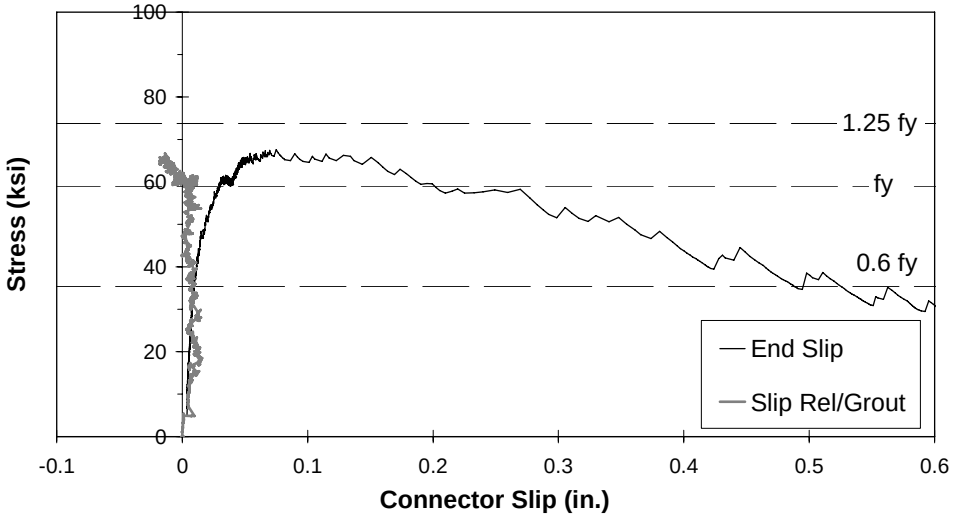

Figure C.35 Connector Slip Relative to Grout (Test 30)

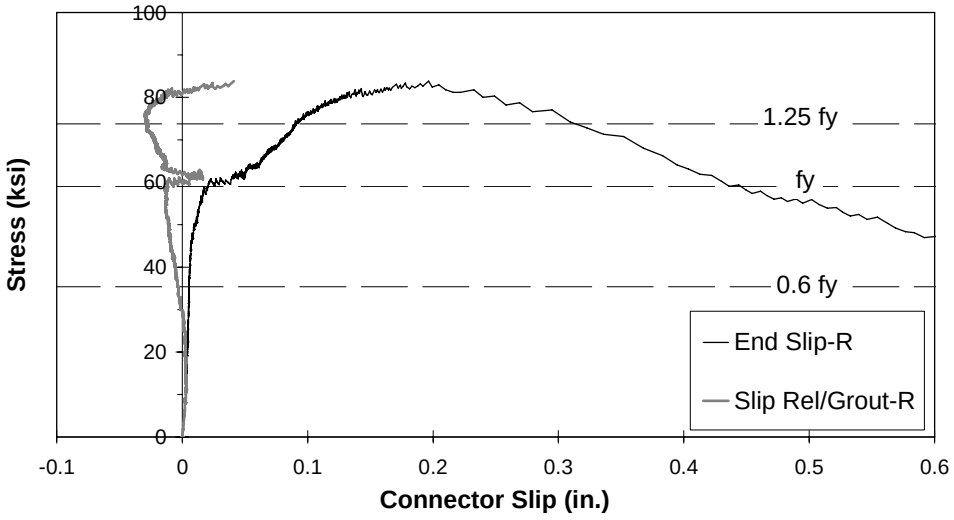

Figure C.36 Connector Slip Relative to Grout (Test 28, Right Connector)

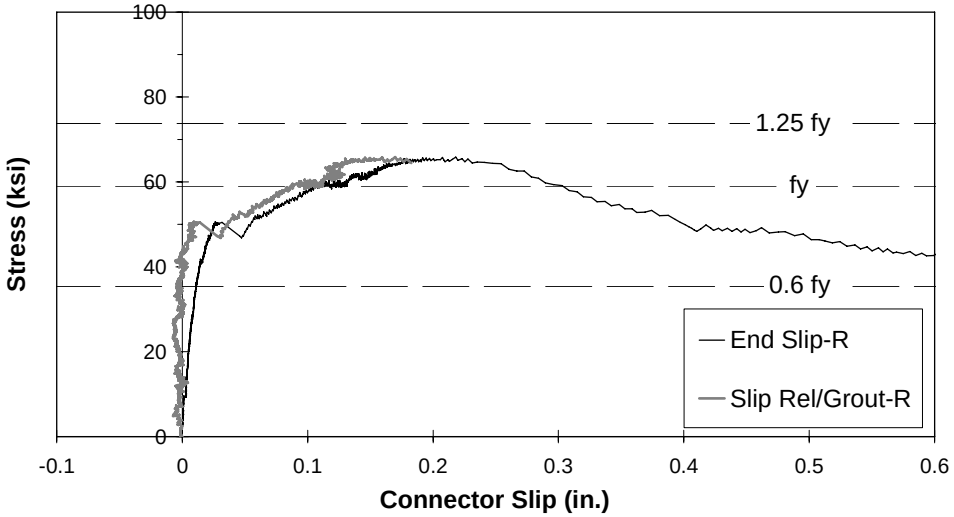

Figure C.37 Connector Slip Relative to Grout (Test 32, Right Connector)

C.5 STRAIN IN DUCT

As discussed in Chapter 5, the strain in the ducts was monitored during the tests using strain gages. Measurements of strain in the ducts can provide an indication of the degree of confinement provided to the connector at different load stages. The duct gages were generally oriented in the circumferential direction to measure tensile stresses in the duct.

The function of the duct as part of the force resisting mechanism is to transfer the force applied on the connector to the surrounding concrete. This transfer of force includes enhancing the bond between the connector and the grout by providing confinement to the grout. The duct must also be able to resist the axial tension that is being transferred by friction between its surface and the grout and the concrete; the duct corrugation pattern plays a very important role here. The state of stress in the duct is therefore very complex, and may involve tensile stresses in many directions.

A series of stress-duct strain diagrams are presented in this section that show the strains in the duct at different depths for a representative set of tests. The results are presented once again in three groups determined by the duct type.

C.5.1 Galvanized Steel Duct

The stress-duct strain behavior of connectors placed inside galvanized steel ducts is illustrated by a set of representative tests consisting of one and two connectors.

Figure C.38 shows the stress-duct strain diagram for Test 3. The strain readings in the duct increased slightly as loading began. Somewhat larger strains were observed at a depth of 4 in. than at other depths. At a stress of 47 ksi, the first splitting crack emerged in the concrete. Additional splitting cracks developed as the stress applied increased. As a result of splitting, the strain in the duct at a depth of 13 in. increased. The duct readings corresponding to the connector's yield strength of 75 ksi stayed constant for the most part. For stress values between 76 and 83 ksi, comparison of the duct strain data to the stress-slip relative to grout data for the connector (Figure C.27) shows that increases in duct strain were observed for a corresponding increase in connector slip relative to the grout. The strains mobilized in the ducts show that they were confining the grout and the connector as the latter was slipping out of the grout. At maximum load, the strains in the duct down to a depth of 8 in. increased significantly. Comparison of strain data collected at a depth of 8 in. for both the strain gage oriented in the circumferential direction, and the one aligned with the duct seams, shows small differences. The gage aligned with the duct seams measured larger strains for stress values higher than 75 ksi.

The stress-duct strain diagram for Test 4 is shown in Figure C.39. The strain readings in the duct increased slightly as loading began. A sudden increase in strain was observed at a depth of 4 in. at a stress of 34 ksi, attributed to minor slip of the connector relative to the grout. At a stress of 60 ksi, the first splitting crack emerged in the concrete. Additional splitting cracks developed as the stress applied increased. As a result of splitting, the strain in the duct at a depth of 13 in. increased somewhat. Soon after the yield strength of the connector was reached, the strains in the duct at a depth of 4 in. decreased. This can be attributed to the development of horizontal cracks in the grout near the surface, and connector yield elongation. At a stress of 77 ksi, V-shaped cracks developed on the side of the specimen, and the slip of the connector relative to the grout increased (Figure C.28). The connector slipping out of the grout incited the confining action of the ducts, demonstrated by an increase in the duct strain readings at all gage locations. Comparison of strain data collected at a depth of 8 in. for both the strain gage oriented in the circumferential direction, and the one aligned with the duct seams, shows small differences. The gage aligned with the duct seams measured larger strains for stress values higher than 85 ksi, the stress when an additional V-shaped crack formed on the side of the specimen.

Figure C.40 shows the stress-duct strain diagram for the left connector of Test 13. The diagram shows small increases in duct strain at very low stresses. Many radial cracks in the grout were noticed at stresses between 13 and 16 ksi. The stress-slip relative to grout diagram for the same connector showed

an increase in slip at these stresses (Figure C.29). Splitting cracks in the concrete were detected at a stress of 38 ksi. Duct strains increased as splitting cracks continued to develop, especially at a depth 8 in. below the surface. The duct readings at 8 in. in the seam or spiral orientation between stresses of 53 and 66 ksi involved a series of cycles where the strain was increasing and decreasing alternately. The stress-slip relative to grout diagram for the connector (Figure C.29) revealed that within this stress range, the upward displacement of the grout was larger to that of the connector end. It is possible that horizontal cracks in the grout were forming at a depth of 8 in. and the duct was experiencing axial tension. This would explain the reductions in duct strain. When V-shaped cracks developed at a stress of 63 ksi, confining action at a depth of 13 in. was mobilized, indicated by the increase in the duct strain at this location. The connector was slipping out of the grout at this time. At a stress of 74 ksi, a significant number of cracks had developed on the side of the specimen. The connector then experienced yielding, and shortly after, the connector and the grout were displacing together upward confined by the steel duct. The strain readings at a depth of 8 in. show that a duct strain reversal occurred at a stress of 77 ksi. This reversal in duct strain can also be explained as the duct experiencing axial tension due to upward movement of the portion of grout located just above that particular gage location. With increased slip of the connector, increases in duct strain were observed at a depth of 13 in.; whereas increases in duct strain at a depth of 4 in. can be attributed to yield elongation as well as slip of the connector. Comparison of the circumferential and the seam oriented strain gage readings at 8 in. shows that, aside from the series of strain reversals observed in the spirally oriented gage, the strain values recorded up to the failure load were very similar.

The stress-duct strain diagram for the left connector of Test 17 is shown in Figure C.41. The strain readings in the duct increased slightly as loading began. Somewhat larger strains were observed at a depth of 4 in. than at other depths. At a stress of 33 ksi, the first splitting crack emerged in the concrete. Additional splitting cracks developed as the stress applied increased. No significant increases in duct strain were observed until the stress reached 45 ksi. At this stress level, a widespread pattern of radial cracks surrounded the connectors. The duct readings increased a small amount, and then continued to increase until the connection reached its capacity. At failure, the gages located 8 in. below the surface recorded the largest values of strain.

C.5.2 Polyethylene Duct

The stress-duct strain behavior of connectors housed inside polyethylene ducts is illustrated by a set of representative tests consisting of one and two connectors.

Figure C.42 shows the stress-duct strain diagram for Test 7. As loading began, the strains recorded in the duct remained small; the gages located deeper in the duct recorded strains of negative value. At a stress of 33 ksi, the first splitting cracks were detected in the concrete. Additional splitting

cracks developed as the stress applied increased. As a result of splitting, the strains in the duct gradually increased. The stress-slip relative to grout diagram for the connector showed that between stresses of 45 and 49 ksi, the grout was displacing upward at a faster rate relative to the connector end (Figure C.31). The strain measured in the duct at a depth of 8 in. decreased after the stress reached 49 ksi. The decrease in strain is attributed to axial tension in the duct, which led to corresponding negative Poisson strains in the circumferential direction. At an applied stress of 57 ksi, extensive radial splitting has developed in the concrete; as the connector and the grout are moving upward together, increases in duct strain were observed at a depth of 4 and 13 in. below the surface. When the stress reached 63 ksi, a horizontal crack developed on the side of the specimen, and the connector slip relative to the grout increased (Figure C.31). Increases in duct strain were then observed at all gage locations as loading continued. Shortly before failure, there was another strain reversal in the duct 8 in. below the surface; a strain reversal was also simultaneously recorded by the gage located 4 in. below the surface. These strain reversals can also be attributed to Poisson effects related to axial tension in the duct.

The stress-duct strain diagram for Test 22 is shown in Figure C.43. The strain increased very slowly in the duct during the beginning of the test. The gage located 4 in. below the surface experienced an increase in negative strain, but steadily the strain readings shifted to positive values when the connector slipped a small distance relative to the grout. When the stress applied was 45 ksi, the first splitting crack emerged in the concrete. At this point, all duct gages were measuring small, but positive increases in strain. Shortly after, at a stress of 57 ksi, a second splitting crack developed, and larger changes in duct strain were observed. When the stress reached 63 ksi, the stress-slip relative to grout diagram showed that the grout displacement increased relative to the connector end (Figure C.32). As loading progressed, the negative strain readings in the duct at a depth of 4 in. indicate that at this depth the duct was experiencing significant axial tension. Soon after the yield strength of the connector was achieved, duct strains reversed at depths of 8 in. and 18 in. At a stress of 81 ksi, a horizontal crack formed on the side of the specimen. This crack extended at 83 ksi, and led to a steady increase in slip of the connector relative to the grout. Strain measurements in the duct indicate that the duct was experiencing axial tension along its entire length, caused by upward movement of the grout, possibly out of the duct.

Figure C.44 shows the stress-duct strain diagram for the left connector of Test 14. As loading began, the strains recorded in the duct remained small. At a stress of 42 ksi, the first splitting cracks were detected in the concrete. Additional splitting cracks developed as the stress applied increased. As a result of splitting, the strains in the duct increased. When the stress reached 51 ksi, V-shaped cracks formed on the loaded side of the specimen. The duct strain values at a depth of 8 in. indicate that the duct was experiencing significant axial tension at this depth. At a stress of 64 ksi, the connection failed, and the other connector involved pulled-out. As loading resumed, this time only the left connector, strains in the

duct came close to their values before the connection failed. At a stress of 61 ksi, the left connector failed; the strain recorded by the gage at a depth of 8 in. increased as the bar was pulling out of the grout.

The stress-duct strain diagram for the left connector of Test 24 is shown in Figure C.45. The first splitting cracks in the concrete were detected at a stress of 43 ksi, and splitting was widespread when the stress reached 58 ksi. Duct strain measurements increased at depths of 4, 8, and 13 inches. At 61 ksi, V-shaped cracks formed on the loaded side of the specimen and the connector slipped relative to the grout. Duct strain reversals were observed at depths of 8 and 13 in., indicating that the duct was experiencing significant axial tension at these locations just before failure. The strain in the duct at a depth of 18 in. increased as the connector's slip relative to the grout increased.

C.5.3 Polypropylene Duct

The stress-duct strain behavior of connectors placed inside polypropylene ducts is illustrated by a set of representative tests consisting of one, two, and three connectors.

Figure C.46 shows the stress-duct strain diagram for Test 30. As loading began, the strains recorded in the duct remained small; two of the gages recorded strains of negative value. At a stress of 32 ksi, the first splitting crack was detected in the concrete. No appreciable change was seen in the strain measurements. At a stress of 42 ksi, the stress-slip relative to grout diagram showed a slight increase in grout displacement relative to the connector end (Figure C.35). The strain in the ducts decreased and switched into negative values as loading progressed. After the stress reached the connector yield strength, the gage located 4 in. below the surface recorded small increases in strain. The stress-slip relative to grout diagram also showed that the grout displacement was increasing in relation to the connector end (Figure C.35). The upward movement of the grout coincided with significant axial tension in the duct, indicated by the strain readings at depths of 8 and 13 inches. At the failure stress of 65 ksi, and as the bar pulled out, increases in strain were observed in the duct at 4 and 13 inches. The gage at 8 in. continued to measure negative strains even after failure.

The stress-duct strain diagram for the right connector of Test 28 is shown in Figure C.47. Radial splitting in the concrete first developed at a stress of 44 ksi. No appreciable changes were seen directly in the duct strain readings. The gage located at a depth of 4 in., followed by the one located at 8 in., recorded the largest strains, as splitting in the concrete continued. Yielding of the connector was a large event in the duct strain history. Shortly after yielding, V-shaped cracks developed on the loaded side of the specimen. After these successive events, strain increases were observed along the duct, except at a depth of 18 in.; here, the strain remained negative. At a stress of 81 ksi, the slip of the connector relative to the grout increased (Figure 5.63); the slip of the connector appeared to affect the gage readings at 8 and 13 in. in contrasting ways.

Figure C.48 shows the stress-duct strain diagram for the right connector of Test 32. Radial splitting in the concrete first developed at a stress of 20 ksi. Strains in the duct remained small, except at 4 in. below the surface. As loading continued, and additional splitting cracks formed, increases in duct strain were eventually observed at the 8 in. depth. At a stress level of 50 ksi, a V-shaped crack formed on the side of the specimen. The connector slip relative to the grout increased (Figure C.37). Strains increased in the duct at depths of 4, 8, and 13 in.; the gage located at a depth of 18 in. recorded negative strain values. At 59 ksi, the connector experienced yielding; the duct strains continued to increase at the shallow depths, but a strain reversal was observed at a depth of 13 inches. This indicates that following the yielding event, the duct was experiencing significant axial strains at depths of 13 and 18 inches.

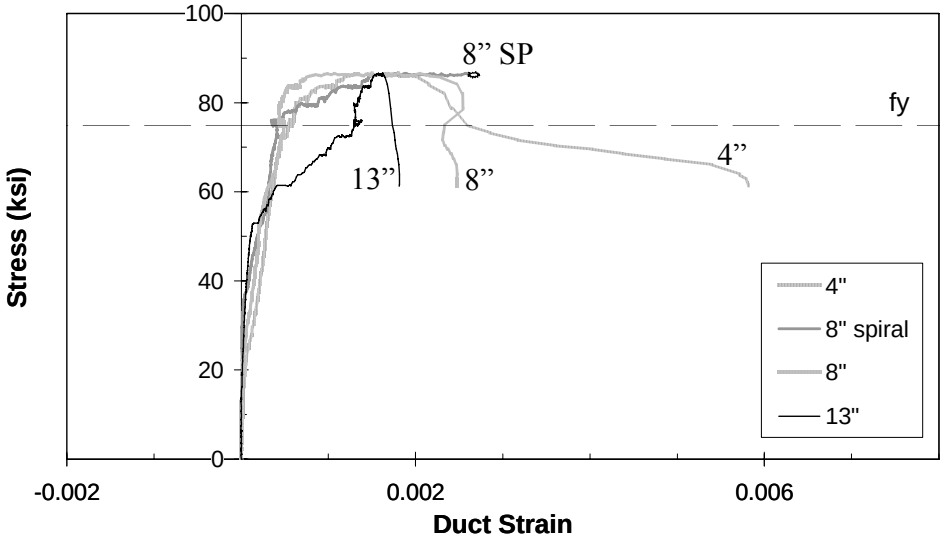

Figure C.38 Strain in Duct (Test 3)

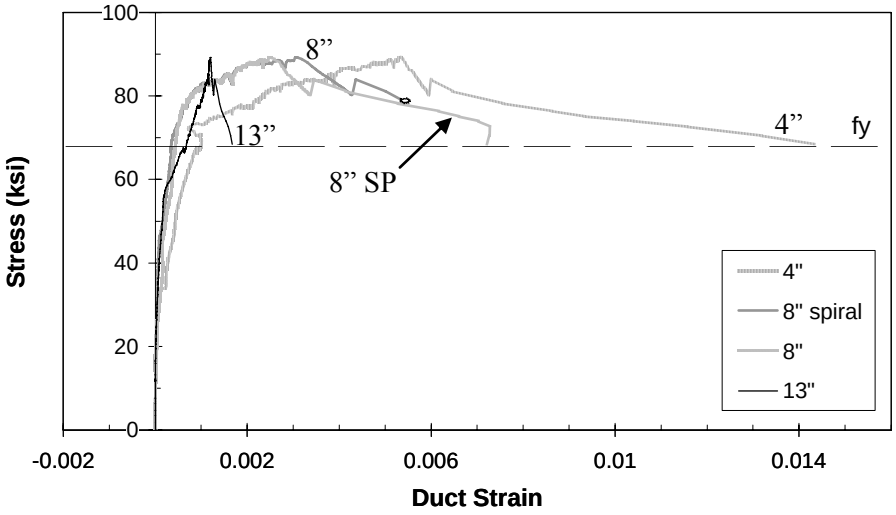

Figure C.39 Strain in Duct (Test 4)

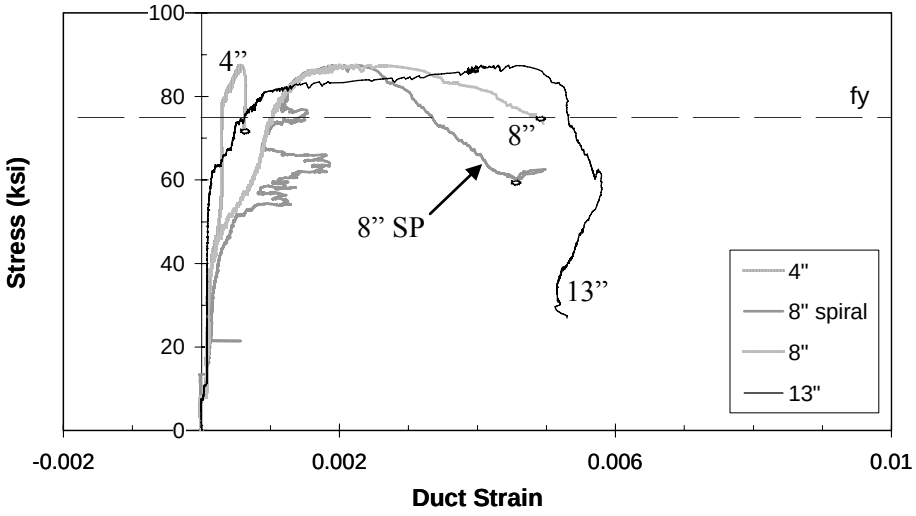

Figure C.40 Strain in Duct (Test 13, Left Connector)

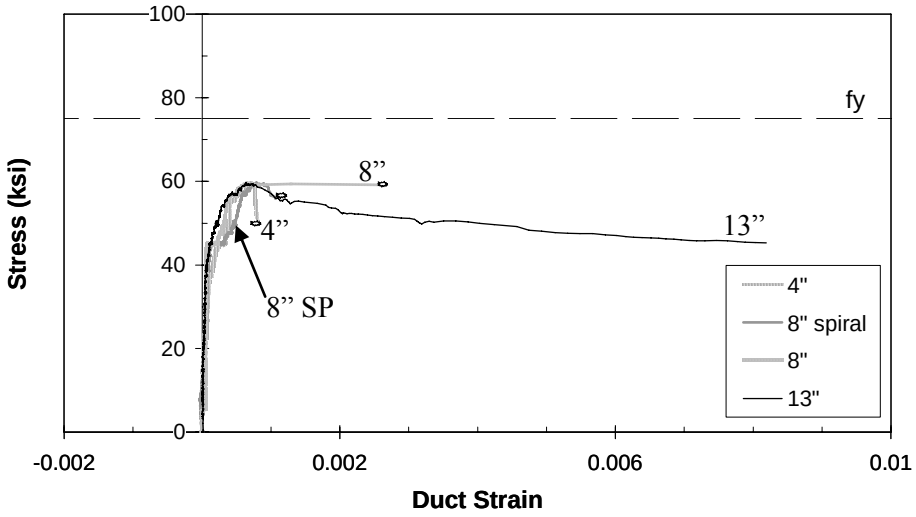

Figure C.41 Strain in Duct (Test 17, Left Connector)

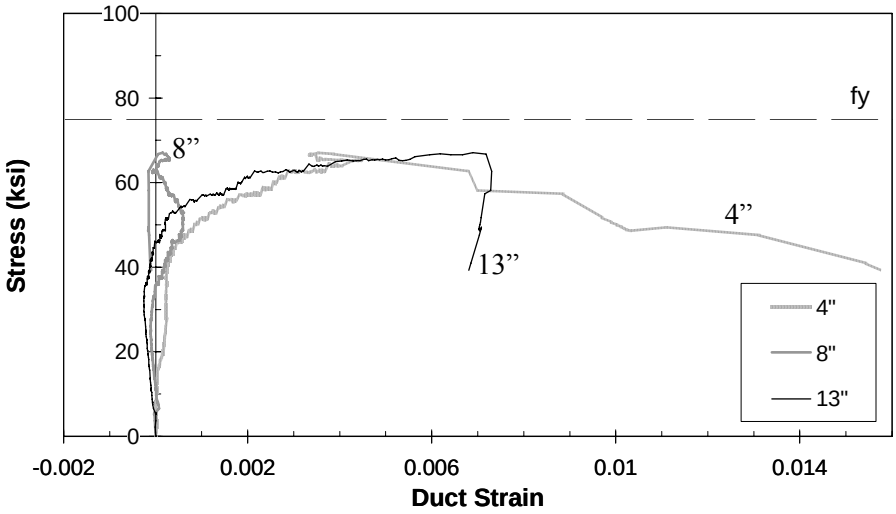

Figure C.42 Strain in Duct (Test 7)

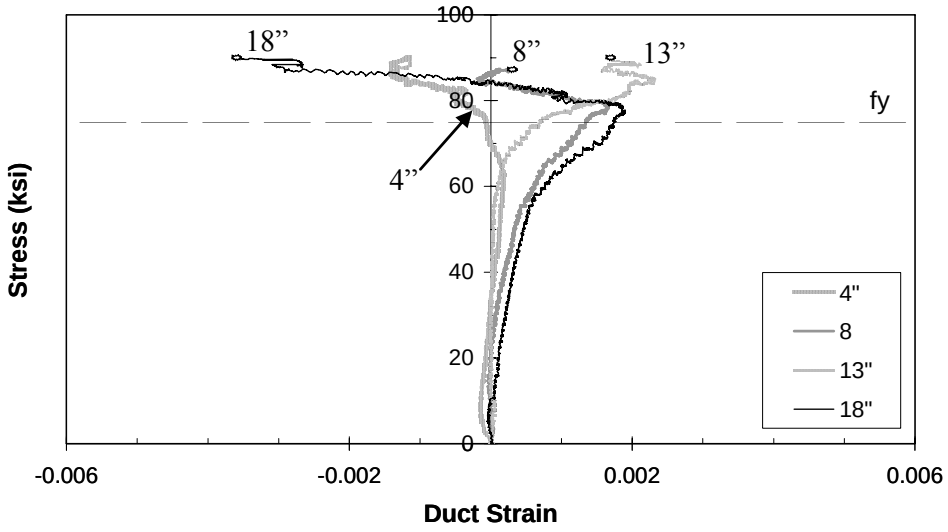

Figure C.43 Strain in Duct (Test 22)

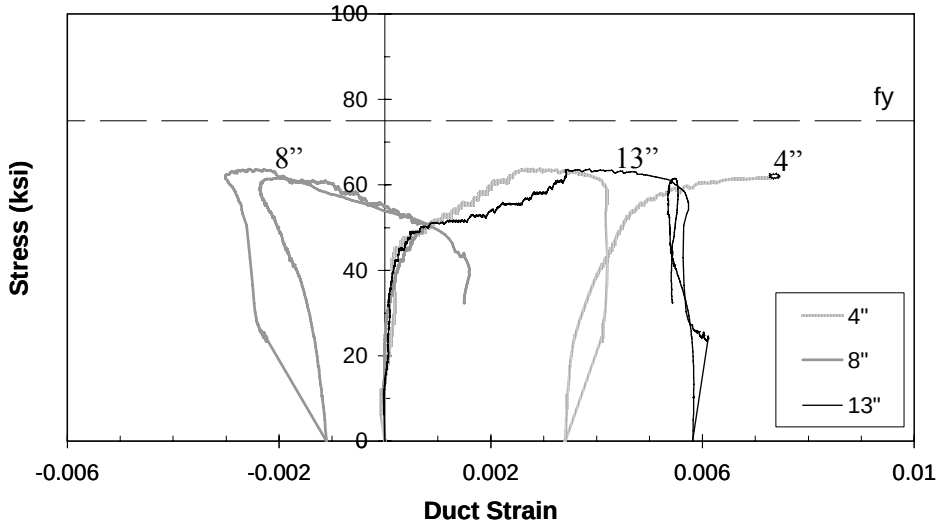

Figure C.44 Strain in Duct (Test 14, Left Connector)

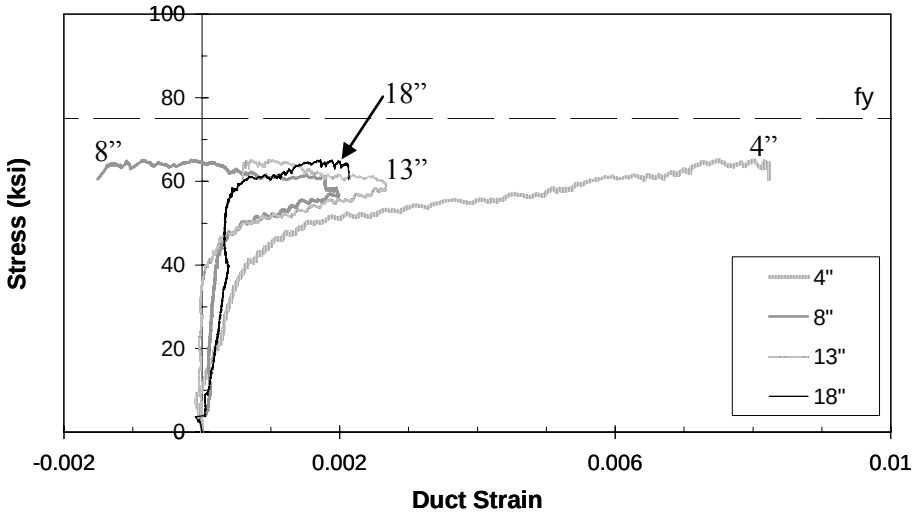

Figure C.45 Strain in Duct (Test 24, Left Connector)

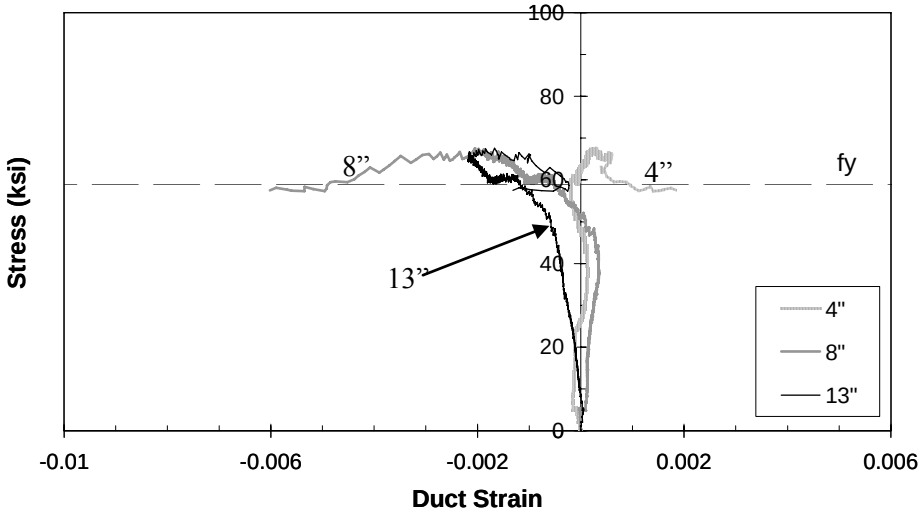

Figure C.46 Strain in Duct (Test 30)

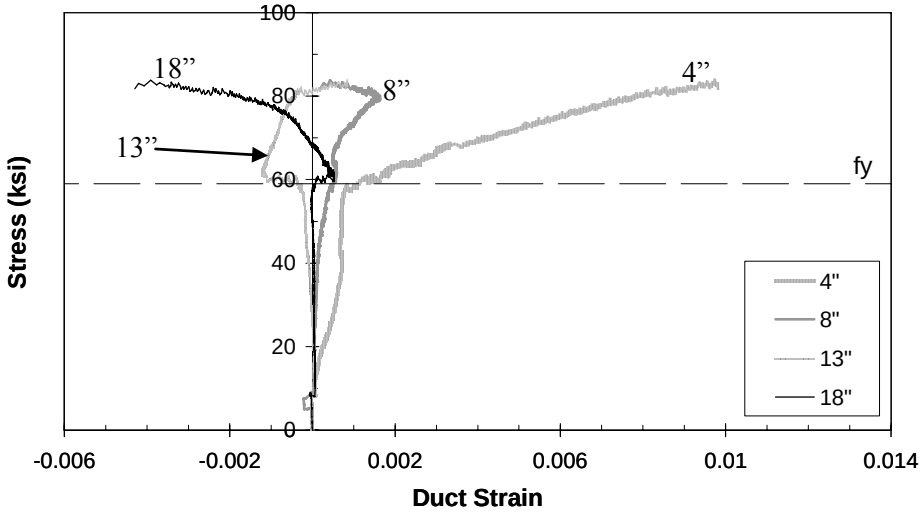

Figure C.47 Strain in Duct (Test 28, Right Connector)

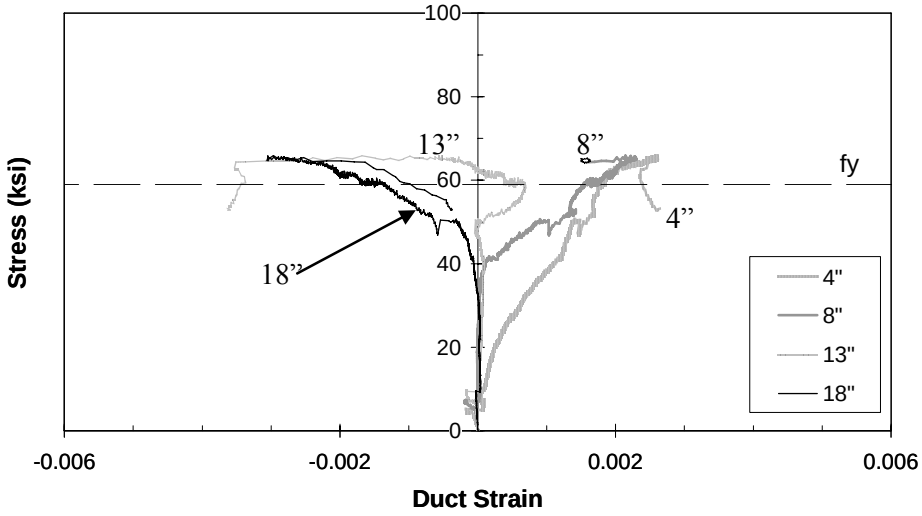

Figure C.48 Strain in Duct (Test 32, Right Connector)

REFERENCES

ACI Committee 318 (1971) "Building Code Requirements for Reinforced Concrete," *ACI 318-71*, American Concrete Institute, Detroit, MI.

ACI Committee 318 (2002). "Building Code Requirements for Structural Concrete and Commentary," *ACI 318-02/ACI 318R-02*, American Concrete Institute, Farmington Hills, MI.

ACI Committee 318 (2005). "Building Code Requirements for Structural Concrete and Commentary," *ACI 318-05/ACI 318R-05*, American Concrete Institute, Farmington Hills, MI.

ACI Committee 550 (2001). "Emulating Cast-in-Place Detailing in Precast Concrete Structures," *ACI 550.1R-01*, American Concrete Institute, Farmington Hills, MI.

AASHTO (2004). *LRFD Bridge Design Specifications*, 3rd ed., Association of State Highway and Transportation Officials, Washington, DC.

Astrova, T. I., Dmitriev, S. A., and Mulin, N. M. (1961). "The Anchorage of Deformed Reinforcing Bars in Ordinary and Prestressed Reinforced Concrete," *Transactions*, Scientific-Research Institute, Concrete and Reinforced Concrete, Academy of Building and Architecture, Issue 23, Moscow.

Brenes, F.J. (2005). "Anchorage of Grouted Vertical Duct Connectors for Precast Bent Caps," Dissertation, University of Texas, Department of Civil, Architectural and Environmental Engineering, Austin, TX.

Cook, R. A. (1998). "Grouted and Adhesive Anchor Tests of Master Builders Products," Structures and Materials Research Report No. 98-4, University of Florida.

Cook, R. A., Kunz, J., Fuchs, W., and Konz, R. C. (1998). "Behavior and Design of Single Adhesive Anchors Under Tensile Load in Uncracked Concrete," *Structural Journal*, American Concrete Institute, Vol. 95, No. 1.

Darwin. D., and Zavaregh, S. S. (1996). "Bond Strength of Grouted Reinforcing Bars," *Structural Journal*, American Concrete Institute, Vol. 93, No. 4.

Einea, A., Yamane, T., and Tadros, M. K. (1995). "Grout-Filled Pipe Splices for Precast Concrete Construction," *PCI Journal*, Precast/Prestressed Concrete Institute, Vol. 40, No. 1.

Eligehausen, R., Popov, E. P., and Bertero, V. V. (1983). "Local Bond Stress-Slip Relationship of Deformed Bars Under Generalized Excitations," Report No. UCB/EERC-83/23, Earthquake Engineering Research Center, University of California, Berkeley, CA.

Ferguson, P. M., Breen, J. E., and Jirsa, J. O. (1988). *Reinforced Concrete Fundamentals*, 5th edition, John Wiley and Sons, Inc., New York, NY.

fib Commission 9 (2000). "Corrugated Plastic Ducts for Internal Bonded Post-Tensioning," *Bulletin No. 7*, Task Group 9.6 Plastic Ducts, International Federation for Structural Concrete ***fib***, Lausanne, Switzerland, 2000.

FHWA (2003). *2002 Study of the Nation's Highways, Bridges, and Transit: Conditions and Performance*, U.S. Department of Transportation, Federal Highway Administration.

FHWA (2005a). "Prefabricated Bridge Elements and Systems: Beaufort and Morehead Railroad Trestle Bridge Project Photos," Federal Highway Administration, http://www.fhwa.dot.gov/bridge/prefab/beauphot.htm.

FHWA (2005b). "Prefabricated Bridge Elements and Systems-Substructures: Bent Caps," Federal Highway Administration, http://www.fhwa.dot.gov/bridge/prefab/bentcaps.htm.

Freeby, G., Hyzak, M., Medlock, R. D., Ozuna, K., Vogel, J., and Wolf, L. (2003). "Design and Construction of Precast Bent Caps at TxDOT," *Proceedings*, 82nd Transportation Research Board Annual Meeting, Washington, D. C.

Friggle, T. (2002). "State Highway 66 Lake Ray Hubbard Bridge Construction with Precast Bent Caps," *Lake Ray Hubbard Bridge-Precast Concrete Bent Cap Demonstration Workshop*, FHWA/AASHTO/TxDOT, Mesquite, TX.

Ganz, H. R. (1991). "PT-Plus Plastic Duct System," Report No. 241 e, VSL International Ltd, Berne, Switzerland.

Goto, Y. (1971). "Cracks Formed in Concrete around Deformed Tension Bars," *Journal*, American Concrete Institute, Vol. 68, No. 4.

Holt, J., and Medlock, R. (2004). "Standardized Concrete Bridges in Texas," *Proceedings*, Post-Tensioning Institute/National Concrete Bridge Council Concrete Bridge Conference, Charlotte, NC.

Hyzak, M. (2002). "Lake Ray Hubbard Bridge: Structural Design," *Lake Ray Hubbard Bridge-Precast Concrete Bent Cap Demonstration Workshop*, FHWA/AASHTO/TxDOT, Mesquite, TX.

Hyzak, M. (2003). "Lake Belton: Precast Bent Cap Design," *Lake Belton Bridge-Precast Concrete Bent Cap Demonstration Workshop*, FHWA/AASHTO/TxDOT, Temple, TX, July 2003.

Josten, M. G., Painter, W. L., and Guarre, J. S. (1995). "Precast Prestressed Concrete Structure Provides Solution for Getty Center Tram Guideway," *PCI Journal*, Precast/Prestressed Concrete Institute, Vol. 40, No. 3.

LoBuono, Armstrong, and Associates, (1996). "Development of Precast Bridge Substructures," Report for the Florida Department of Transportation.

Lutz, L. A., and Gergely, P. (1967). "Mechanics of Bond and Slip of Deformed Bars in Concrete," *Journal*, American Concrete Institute, Vol. 64, No. 11.

Mandawe, J., Mislinski, S., and Matsumoto, E. E. (2002). "Reinforcement Anchorage in Grouted Duct Connections for a Precast Bent Cap System in Seismic Regions," *Proceedings*, PCI/Federal Highway Administration/National Concrete Bridge Council Concrete Bridge Conference, Nashville, TN.

Marti, P. (1993). "Pull-out Tests with PT-Plus Plastic Ducts," Report No. 92.205-1, VSL International Ltd., Berne, Switzerland.

Matsumoto, E. E. (2003). "Development of a Precast Bent Cap System for Seismic Regions," *Lake Belton Bridge-Precast Concrete Bent Cap Demonstration Workshop*, FHWA/AASHTO/TxDOT, Temple, TX.

Matsumoto, E. E., Waggoner, M. C., Sumen, G., Kreger, M. E., Wood, S. L., and Breen, J. E. (2001). "Development of a Precast Bent Cap System," Research Report 1748-2, Center for Transportation Research, University of Texas at Austin.

Measurements Group, Inc. (2000). "Optimizing Strain Gage Excitation Levels," Tech Note TN-502, Raleigh, NC.

Measurements Group, Inc. (2001). "Strain Gage Measurements on Plastics and Composites," http://www.measurementsgroup.com/guide/ta/pc/pcindex.htm

Medlock, R., Hyzak, M., Wolf, L. (2002). "Innovative Prefabrication in Texas Bridges," *Proceedings*, American Society of Civil Engineers, Texas Section, Spring Meeting, Austin, TX.

Miltenberger, M. (2001). "Capacity Design of Grouted Anchors," *Transactions*, 16th International Conference on Structural Mechanics in Reactor Technology (SMiRT 16) *Transactions*, Washington DC.

Nicholas, D. G., Solis, P. M., and Brown, D. K. (2001). "Airport on the Move," *Civil Engineering Magazine*, American Society of Civil Engineers, September.

Orangun, C. O., Jirsa, J. O., and Breen, J. E. (1977). "Reevaluation of Test Data on Development Length and Splices," *Journal*, American Concrete Institute, Vol. 74, No. 3.

Park, R. (1995). "A Perspective on the Seismic Design of Precast Concrete Structures in New Zealand," *PCI Journal*, Precast/Prestressed Concrete Institute, Vol. 40, No. 3, May-June 1995.

PCI (2005). "Bridges: Precast Concrete Bridges Aid Environment, Seismic Design," Precast/Prestressed Concrete Institute, http://www.pci.org/markets/markets.cfm?path=bridges&id=wolf_river.cfm.

PCI Design Handbook-Precast and Prestressed Concrete (1992). 4th edition, Precast/Prestressed Concrete Institute, Chicago, IL.

PCI Design Handbook-Precast and Prestressed Concrete (1999). 5th edition, Precast/Prestressed Concrete Institute, Chicago, IL.

PTI Committee on Grouting Specifications (2001). "Specification for Grouting of Post-Tensioned Structures," Post-Tensioning Institute, First Edition.

Restrepo, J. I., Park, R., and Buchanan, A. H. (1993). "The Seismic Behavior of Connections Between Precast Concrete Elements," Research Report No. 93-3, Department of Civil Engineering, University of Canterbury, Christchurch, New Zealand.

Salas, R. M., Kotys, A. L., West, J. S., Shocker, A. J., Breen, J. E., and Kreger, M. E. (2003). "Long-Term Post-Tensioned Beam Exposure Test Specimens: Final Evaluation," Research Report 0-1405-7, Center for Transportation Research, University of Texas at Austin.

Stanton, J. F., Anderson, R. G., Dolan, C. W., and McCleary, D. E. (1986). "Moment Resistant Connections and Simple Connections," Research Project No. 1/4, Precast/Prestressed Concrete Institute, Chicago, IL.

Tepfers, R. (1973). "A Theory of Bond Applied to Overlapped Tensile Reinforcement Splices for Deformed Bars," Publication No. 73:2, Division of Concrete Structures, Chalmers University of Technology, Göteborg, Sweden.

Untrauer, R. E., and Henry, R. L. (1965). "Influence of Normal Pressure on Bond Strength," *Journal*, American Concrete Institute, Vol. 62, No. 5.

Viwathanatepa, S., Popov, E. P., and Bertero, V. V. (1979). "Effects of Generalized Loadings on Bond of Reinforcing Bars in Confined Concrete Blocks," Report No. UCB/EERC-79/22, Earthquake Engineering Research Center, University of California, Berkeley, CA.

Wigington, N. (1997). "Pierce Elevated Draws Rave Reviews," *Transportation News*, Texas Department of Transportation, Houston, TX.

Wolf, L. M., and Friedman, N. K. (1994). "Redfish Bay and Morris & Cummings Cut: Innovations on Bridge Construction and Durability," *Technical Quarterly*, Texas Department of Transportation, Vol. 9, No. 2, Austin, TX.

Wolf, L. M., and Hyzak, M. D. (2004). "Design of Precast Bent Cap to Column Connections," *Post-Tensioning Institute (PTI)/National Concrete Bridge Council Concrete Bridge Conference Proceedings*, Charlotte, NC.